Efficient multivariate approximation with transformed rank-1 lattices

Inauguraldissertation

zur Erlangung des Akademischen Grades
Doktor eines Wissenschaftszweiges
doctor rerum naturalium

vorgelegt der
Fakultät für Mathematik
der
Technischen Universität Chemnitz

von
Robert Nasdala, M.Sc.
geboren am 11. Juni 1990
in Chemnitz

Chemnitz, 29. Juni 2021

Contents

Chapter 1

Introduction

In applied mathematics - especially in numerical analysis - a variety of interesting topics emerge from the problem of approximating high-dimensional functions. A main objective is the approximation of functions f in a Hilbert space $L_2(\Omega)$ by a partial sum

$$f(\mathbf{x}) \approx S_I f(\mathbf{x}) := \sum_{\mathbf{k}\in I} \hat{f}_{\mathbf{k}} \varphi_{\mathbf{k}}(\mathbf{x}), \quad I \subset \mathbb{Z}^d, \mathbf{x} \in \Omega,$$

with respect to an $L_2(\Omega)$-orthonormal system $\{\varphi_{\mathbf{k}}\}_{\mathbf{k}\in I}$ and coefficients $\hat{f}_{\mathbf{k}} := (f, \varphi_{\mathbf{k}})_{L_2(\Omega)}$. Under the assumption that the function f is either continuous or has a continuous representative, approximation approaches are usually concerned with at least one of the following problems:

- estimating the approximation error $\|f - S_I f\|$, measured in (weighted) $L_\infty(\Omega)$- or $L_2(\Omega)$-norms,
- minimizing the number of coefficients $|I|$, when the indices of the largest Fourier coefficients $\hat{f}_{\mathbf{k}}$ might be unknown,
- reducing the computation time to evaluate functions values $\{f(\mathbf{x}_j)\}_{j=1}^M$ or to reconstruct coefficients $\hat{f}_{\mathbf{k}}$,
- minimizing the number $M \in \mathbb{N}$ of necessary sampling nodes $\{\mathbf{x}_j\}_{j=1}^M, \mathbf{x}_j \in \Omega$, to reconstruct the coefficients $\hat{f}_{\mathbf{k}}$ of a fixed or unknown frequency set I of finite cardinality $|I| < \infty$.

Various authors developed techniques and algorithms to improve different aspects of the approximation of periodic functions that are defined on the torus $\Omega = \mathbb{T}^d$ and many results are known for the multivariate periodic case. The main objective of this work is to study the above listed problems for the approximation of functions on $\Omega = \mathbb{R}^d$ and $\Omega = \left[-\frac{1}{2}, \frac{1}{2}\right]^d$. In particular, we investigate which results and techniques of the approximation theory on the torus $\mathbb{T}^d$ can be transfered or adapted to these other domains.

In the following, we summarize important milestones and publications concerned with the approximation on the torus $\mathbb{T}^d$. Often, it is assumed that we are given samples of a multivariate periodic function f, whose Fourier coefficients $\hat{f}_{\mathbf{k}} \in \mathbb{C}$ are absolutely or square summable and decay at a certain rate, for which there is a well-studied approximation error

analysis [Tem86, KPV15, BKUV17, Vol17, KMNN21]. However, generally the exact values of the Fourier coefficients $\hat{f}_{\mathbf{k}}$ are not known and can not be calculated analytically. Instead a fast Fourier transform (FFT), see [CT65], can be applied to a set of given equispaced function samples which yields approximated Fourier coefficients $\hat{f}_{\mathbf{k}}^{\Lambda} \in \mathbb{C}$. Then the corresponding approximated Fourier partial sum $S_I^{\Lambda} f$ is formed and used as an approximant of the function f whose samples were initially provided. At the same time, the discretizion of high-dimensional problems usually leads to a large amount of data in form of sampling values and Fourier matrices that have to be processed numerically. The exponential growth of necessary samples to construct a reasonably good approximant is a common problem refered to as the *curse of dimensionality* [Bel61]. Especially in higher dimensions, rank-1 lattices $\Lambda(\mathbf{z}, M)$ with a generating vector $\mathbf{z} \in \mathbb{Z}^d$ and the lattice size $M \in \mathbb{N}$ provide sampling schemes that are simply structured and can be used to evaluate a d-dimensional Fourier approximation by a single one-dimensional FFT. An introduction to lattice rules can be found in [Nie78, SJ94] and a detailed overview is provided in [DKS13, KNP18]. These cubature rules were used for the approximation of functions on the torus [Tem93], and high-dimensional integrals have been computed by efficient algorithms based on component-by-component methods [CN04, CKN10]. For the approximation of high-dimensional functions there are efficient algorithms - see [Käm14b, Algorithm 3.1 and 3.2] or [KPV15, KMNN21] - based on rank-1 lattice sampling schemes that reduce the evaluation and reconstruction of high-dimensional trigonometric polynomials supported on some frequency set $I \subset \mathbb{Z}$ to a single one-dimensional FFT.

Under mild assumptions, the lattice size M is bounded by $|I| \leq M \leq |I|^2$ for a non-empty frequency set $I \subset \mathbb{Z}$ of finite cardinality $|I| < \infty$, see [Käm14a], [KPV15, Theorem 2.1]. By using multiple rank-1 lattices [Käm19], the upper bound is improved to $M \lesssim |I| \log |I|$. Furthermore, there are dimension incremental algorithms [Vol15, PV16] - the *sparse FFT algorithms* - for the reconstruction of sparse multivariate trigonometric polynomials with an unknown frequency domain $I \subset \mathbb{Z}$. Additionally, sublinear-time compressive sensing algorithms have been developed in [CIK21] for rapidly learning functions of many variables that admit sparse representations in arbitrary Bounded Orthonormal Product bases. Recently, dimension incremental algorithms were adapted for multiple rank-1 lattices [KPV20, KKV20]. We note, that there are various other sampling strategies for periodic signals such as sparse grids [GH14, BDuSU16, GH19], or interlaced scrambled polynomial lattice rules [GD15, DGSY17]. Randomized least square sampling approaches were discussed in [DTU18, Chapter 5] and [KUV19, KU20], and [NW12, p. 55 ff.] additionally investigates Monte Carlo methods. In total, approximation methods on the torus $\mathbb{T}^d$ have the advantage that there are

- fast algorithms based on rank-1 lattice sampling for the efficient evaluation and stable reconstruction of multivariate trigonometric polynomials,
- worst case upper L_∞- and L_2-approximation error bounds for functions in the Sobolev space $\mathcal{H}^m(\mathbb{T}^d)$,
- dimension incremental construction methods to approximate functions with an unknown index set I.

A long-standing problem has been to transfer these properties to the approximation of functions defined on $\mathbb{R}^d$ or the cube $\left[-\frac{1}{2}, \frac{1}{2}\right]^d$. In the last decade, various authors used periodization strategies to set up transformed rank-1 lattices for the numerical integration and approximation of non-periodic functions in order to make use of the efficiency of the

component-by-component construction methods used for the approximation of periodic signals. Chebyshev transformed lattices have been used in weighted Lebesgue spaces [PV15] and tent-transformed lattice rules were used in half-periodic cosine spaces and in Korobov spaces [DNP14, CKNS16, IKP18, GSY19, KMNN21]. While those two approaches extend the original function evenly, a periodization strategy using an odd extension was suggested in [GKL13] which requires exact information about the original function at the boundary points of its domain. The numerical integration of periodized integrands on the cube [SSO83, BH92, NUU17] have been recently discussed with regards to digital nets [DP21]. Periodized integrands on $\mathbb{R}^d$ have also been investigated from different angles, e.g. by using randomly shifted lattice rules [KWW06], in terms of Hermite spaces [IKLP15, DILP18] and with the goal to achieve exponential convergence rates [NN17]. In [KSW07] the approximation of transformed integrands is investigated and various special cases of transformations and generating lattice vectors $\mathbf{z} \in \mathbb{Z}^d$ are discussed to showcase setups in which such an approach can fail when $d \to \infty$. Extended orthonormal systems and frames have also been considered to handle certain types of boundary singularities of non-periodic functions, cf. [AH20]. In [KPPW20] a periodization approach is developed for the approximation of functions defined on $\mathbb{R}^d$ and $\mathbb{R}^d_+$ with bounded L_p-norms of mixed first order partial derivatives with $p \in \{1, \infty\}$, whereas we're going to be concerned with functions on $\mathbb{R}^d$ or $[-\frac{1}{2}, \frac{1}{2}]^d$ with weighted L_2-norms and bounded higher order mixed partial derivatives. An excellent general overview on the versatility of changes of variables can be found in [Boy00, Chapter 16 and 17], where many practical aspects are discussed.

The aim of this work is to derive two general frameworks for the approximation of non-period functions defined on $\mathbb{R}^d$ and on the cube $\left[-\frac{1}{2}, \frac{1}{2}\right]^d$ by means of a specific periodization strategy. We generalize the idea of applying a change of variables to periodize a function, approximating it on the torus $\mathbb{T}^d \simeq \left[-\frac{1}{2}, \frac{1}{2}\right)^d$ with respect to the Fourier system and finally reverting the change of variables to obtain an orthonormal system for functions on $\mathbb{R}^d$ or on the cube $\left[-\frac{1}{2}, \frac{1}{2}\right]^d$, respectively. To this end, we introduce new parameterized transformation mappings and investigate the possibility to transfer the important properties and results from the classical Fourier approximation methods on the torus $\mathbb{T}^d$ to other domains.

At first, we consider parameterized measure functions $\omega(\cdot, \boldsymbol{\mu}), \boldsymbol{\mu} \in \mathbb{R}^d_+$ and functions $h \in L_2(\mathbb{R}^d, \omega(\cdot, \boldsymbol{\mu})) \cap H^m_{\text{mix}}\left(\mathbb{R}^d\right)$ with dominating mixed smoothness of order $m \in \mathbb{N}_0$. We define parameterized, invertible torus-to-$\mathbb{R}^d$ transformations

$$\psi(\cdot, \boldsymbol{\eta}) = (\psi_1(\cdot, \eta_1), \ldots, \psi_d(\cdot, \eta_d)) : \left(-\frac{1}{2}, \frac{1}{2}\right)^d \to \mathbb{R}^d, \quad \boldsymbol{\eta} \in \mathbb{R}^d_+$$

so that $\|h\|_{L_2(\mathbb{R}^d, \omega(\cdot, \boldsymbol{\mu}))} = \|f\|_{L_2(\mathbb{T}^d)}$ with

$$f(\mathbf{x}, \boldsymbol{\eta}, \boldsymbol{\mu}) = h(\psi(\mathbf{x}, \boldsymbol{\eta})) \sqrt{\omega(\psi(\mathbf{x}, \boldsymbol{\eta}), \boldsymbol{\mu}) \prod_{j=1}^{d} \psi_j'(x_j, \eta_j)}, \quad \mathbf{x} \in \mathbb{R}^d.$$

We prove sufficient L_∞-conditions on the transformation $\psi(\cdot, \boldsymbol{\eta})$ and the measure function $\omega(\cdot, \boldsymbol{\mu})$ so that the transformed function f inherits a guaranteed minimal degree of Sobolev smoothness from the initally chosen function h. Furthermore, we're able to calculate the parameter ranges for $\boldsymbol{\eta}, \boldsymbol{\mu} \in \mathbb{R}^d_+$ for which the periodized function f inherits a specific minimal degree $\tilde{m} = \tilde{m}(\boldsymbol{\eta}, \boldsymbol{\mu}) \leq m$ of Sobolev smoothness from the given function h. By applying the inverse torus-to-$\mathbb{R}^d$ transformation $\psi^{-1}(\cdot, \boldsymbol{\eta})$, the approximation of functions $f \in L_2(\mathbb{T}^d)$ with respect to the Fourier system $\left\{\mathrm{e}^{2\pi \mathrm{i} \mathbf{k}(\cdot)}\right\}_{\mathbf{k} \in \mathbb{Z}^d}$ by a Fourier partial sum $S_I f := \sum_{\mathbf{k} \in I} \hat{f}_{\mathbf{k}} \, \mathrm{e}^{2\pi \mathrm{i} \mathbf{k}(\cdot)}$

translates into the approximation of functions $h \in L_2\left(\mathbb{R}^d, \omega\right)$ by a transformed Fourier partial sum of the form $\sum_{\mathbf{k}\in I} \hat{h}_{\mathbf{k}}\, \varphi_{\mathbf{k}}$, with the system $\left\{\varphi_{\mathbf{k}} := \sqrt{\frac{(\psi^{-1})'(\cdot,\boldsymbol{\eta})}{\omega(\cdot,\boldsymbol{\mu})}}\, \mathrm{e}^{2\pi \mathrm{i}\mathbf{k}\cdot\psi^{-1}(\cdot,\boldsymbol{\eta})}\right\}_{\mathbf{k}\in\mathbb{Z}^d}$ being orthonormal with respect to the $L_2\left(\mathbb{R}^d, \omega(\cdot,\boldsymbol{\mu})\right)$-scalar product. Consequently, we denote the transformed trigonometric functions on $\mathbb{R}^d$ by $\Pi_{I,\psi} := \operatorname{span}\{\varphi_{\mathbf{k}} : \mathbf{k} \in I\}$. The $\mathbf{k}$-th Fourier coefficient of h is given by $\hat{h}_{\mathbf{k}} := (h, \varphi_{\mathbf{k}})_{L_2\left(\mathbb{R}^d,\omega(\cdot,\boldsymbol{\mu})\right)}$. Due to the definition of the torus-to-$\mathbb{R}^d$ transformations ψ, their first derivatives $\{\psi_j'\}_{j=1}^d$ are always unbounded. Therefore, we must consider a non-constant measure function ω that counteracts the unboundedness of the first derivatives $\{\psi_j'\}_{j=1}^d$ of the transformation ψ, so that the transformed function f is continuously extendable regardless of the particular choice of the transformation ψ. Therefore, the resulting transformed Fourier system $\{\varphi_{\mathbf{k}}\}_{\mathbf{k}\in\mathbb{Z}^d}$ is always an unbounded orthonormal system on $\mathbb{R}^d$. Consequently, L_∞- and L_2-approximation errors are measured in weighted L_∞- and L_2-norms, respectively. This derivation highlights the duality of either having a working periodization strategy or being able to construct bounded orthonormal systems on $\mathbb{R}^d$. At the same time, this framework allows us to figure out exactly what kinds of transformations $\psi(\cdot,\boldsymbol{\eta})$ are suitable for any given measure function $\omega(\cdot,\boldsymbol{\mu})$ to have a working periodization approach for functions originally defined on $\mathbb{R}^d$. A big advantage of this framework is the availability of fast algorithms for the evaluation and reconstruction of transformed trigonometric functions on $\mathbb{R}^d$ by means of transformed rank-1 lattices $\Lambda_{\psi(\cdot,\boldsymbol{\eta})}(\mathbf{z}, M)$ and considering a specific type of a transformed Fourier matrix. As with the fast algorithms for trigonometric polynomials on the torus $\mathbb{T}^d$, we determine transformed reconstructing rank-1 lattice $\Lambda_{\psi(\cdot,\boldsymbol{\eta})}(\mathbf{z}, M, I), I \subset \mathbb{Z}^d$ so that the evaluation and the reconstruction algorithms reduce a d-variate Fourier problem into a single one-dimensional FFT. In total, for the approximation on $\mathbb{R}^d$ we have

- fast algorithms based on transformed rank-1 lattices $\Lambda_{\psi(\cdot,\boldsymbol{\eta})}(\mathbf{z}, M)$ for the efficient evaluation and stable reconstruction of transformed trigonometric functions $h \in \Pi_{I,\psi}$ on $\mathbb{R}^d$,

- worst case upper weighted L_∞- and L_2-approximation error bounds for functions in the Sobolev space $\mathcal{H}^m(\mathbb{R}^d, \omega(\cdot,\boldsymbol{\mu}))$,

- adapted dimension incremental construction methods to approximate functions with an unknown frequency domain.

The presented framework is tested in numerical experiments in up to dimension $d = 8$ for transformations of algebraic and exponential type. Especially the tests with the algebraic transformation showcase the great utility of the dimension incremental construction methods, which we have to rely on in higher dimensions to figure out the distribution of the largest Fourier coefficients in order to obtain good approximation results without sacrificing too much computation time on frequencies with very small Fourier coefficients.

Secondly, forming invertible maps of the form $\psi^{-1}(\boldsymbol{\eta}\,\psi(\cdot)) : \left(-\frac{1}{2}, \frac{1}{2}\right)^d \to \left(-\frac{1}{2}, \frac{1}{2}\right)^d, \boldsymbol{\eta} \in \mathbb{R}_+^d$ based on torus-to-$\mathbb{R}^d$ transformations $\psi : \left(-\frac{1}{2}, \frac{1}{2}\right)^d \to \mathbb{R}^d$ immediately leads to a periodization strategy on the cube $\left[-\frac{1}{2}, \frac{1}{2}\right]^d$ that has a lot of fundamental similarities with the previous periodization approach on $\mathbb{R}^d$. We consider parameterized measure functions $\omega(\cdot,\boldsymbol{\mu}), \boldsymbol{\mu} \in \mathbb{R}_+^d$ and functions $h \in L_2\left(\left[-\frac{1}{2}, \frac{1}{2}\right]^d, \omega(\cdot,\boldsymbol{\mu})\right) \cap \mathcal{C}_{\mathrm{mix}}^m\left(\left[-\frac{1}{2}, \frac{1}{2}\right]^d\right)$ of mixed continuous differentiability order $m \in \mathbb{N}_0$ and proceed analogously as with the torus-to-$\mathbb{R}^d$ transformations. We

define invertible torus-to-cube transformations

$$ {}_{\square}\psi(\cdot,\boldsymbol{\eta}) = ({}_{\square}\psi_1(\cdot,\eta_1),\ldots,{}_{\square}\psi_d(\cdot,\eta_d)) : \left[-\frac{1}{2},\frac{1}{2}\right]^d \to \left[-\frac{1}{2},\frac{1}{2}\right]^d, \quad \boldsymbol{\eta}\in\mathbb{R}_+^d, $$

so that $\|h\|_{L_2\left(\left[-\frac{1}{2},\frac{1}{2}\right]^d,\omega(\cdot,\boldsymbol{\mu})\right)} = \|f\|_{L_2(\mathbb{T}^d)}$ with

$$ f(\mathbf{x},\boldsymbol{\eta},\boldsymbol{\mu}) = h({}_{\square}\psi(\mathbf{x},\boldsymbol{\eta}))\sqrt{\omega({}_{\square}\psi(\mathbf{x},\boldsymbol{\eta}),\boldsymbol{\mu})\prod_{j=1}^d {}_{\square}\psi_j'(x_j,\eta_j)}, \quad \mathbf{x}\in\mathbb{T}^d. $$

We prove sufficient L_∞-conditions on the transformation ${}_{\square}\psi(\cdot,\boldsymbol{\eta})$ and the measure function $\omega(\cdot,\boldsymbol{\mu})$ so that the transformed function f inherits a guaranteed minimal degree of smoothness from the initally chosen function h. By means of the inverse torus-to-cube transformation ${}_{\square}\psi^{-1}(\cdot,\boldsymbol{\eta})$, the approximation of functions $f\in L_2(\mathbb{T}^d)$ with respect to the Fourier system $\left\{\mathrm{e}^{2\pi\mathrm{i}\mathbf{k}(\cdot)}\right\}_{\mathbf{k}\in\mathbb{Z}^d}$ by a Fourier partial sum $S_I f := \sum_{\mathbf{k}\in I}\hat{f}_{\mathbf{k}}\,\mathrm{e}^{2\pi\mathrm{i}\mathbf{k}(\cdot)}$ is rewritten as the approximation of functions $h\in L_2\left(\left[-\frac{1}{2},\frac{1}{2}\right]^d,\omega(\cdot,\boldsymbol{\mu})\right)$ by a transformed Fourier partial sum of the form $\sum_{\mathbf{k}\in I}\hat{h}_{\mathbf{k}}\,\varphi_{\mathbf{k}}$ with respect to the orthonormal system $\left\{\varphi_{\mathbf{k}} := \sqrt{\frac{({}_{\square}\psi^{-1})'(\cdot,\boldsymbol{\eta})}{\omega(\cdot,\boldsymbol{\mu})}}\,\mathrm{e}^{2\pi\mathrm{i}\mathbf{k}\cdot{}_{\square}\psi^{-1}(\cdot,\boldsymbol{\eta})}\right\}_{\mathbf{k}\in\mathbb{Z}^d}$. Consequently, we denote the transformed trigonometric functions on the cube by $\Pi_{I,{}_{\square}\psi} := \operatorname{span}\{\varphi_{\mathbf{k}} : \mathbf{k}\in I\}$. The $\mathbf{k}$-th Fourier coefficient of h is given by $\hat{h}_{\mathbf{k}} := (h,\varphi_{\mathbf{k}})_{L_2\left(\left[-\frac{1}{2},\frac{1}{2}\right]^d,\omega(\cdot,\boldsymbol{\mu})\right)}$. In contrast to the torus-to-$\mathbb{R}^d$ transformations ψ torus-to-cube transformations ${}_{\square}\psi(\cdot,\boldsymbol{\eta})$ are defined in such a way, that their first derivatives $\{{}_{\square}\psi_j'(\cdot,\eta_j)\}_{j=1}^d$ are bounded and have to decay to 0 towards each boundary point. Therefore, the density $({}_{\square}\psi^{-1})'(\cdot,\boldsymbol{\eta})$ will automatically be unbounded and yields once again unbounded transformated Fourier systems $\{\varphi_{\mathbf{k}}\}_{\mathbf{k}\in\mathbb{Z}^d}$ unless the unboundedness is counteracted by a non-constant measure function $\omega(\cdot,\boldsymbol{\mu})$. So, this time it is feasible to consider constant measure functions $\omega\equiv 1$ and still obtain valid periodizations that are continuously extendable to the torus $\mathbb{T}^d$. In specific cases it is also a good choice to put $\omega = ({}_{\square}\psi^{-1})'$, for example to extract the Chebyshev system from this framework of generalized transformed Fourier systems. Nevertheless, L_∞- and L_2-approximation errors are measured in weighted L_∞- and L_2-norms, respectively. There are setups in which one of these errors ends up being unweighted. For example, for a constant measure function $\omega\equiv 1$ we have an unweighted L_2-approximation error. Once again, this framework determines the variety of feasible torus-to-cube transformations ${}_{\square}\psi(\cdot,\boldsymbol{\eta})$ for any previously fixed measure function $\omega(\cdot,\boldsymbol{\mu})$ to obtain a working periodization strategy for functions defined on the cube $\left[-\frac{1}{2},\frac{1}{2}\right]^d$. A big advantage of this periodization strategy is that it is easy to set up fast algorithms for the evaluation and reconstruction of transformed trigonometric functions on the cube $\Pi_{I,{}_{\square}\psi}$ by means of transformed rank-1 lattices $\Lambda_{{}_{\square}\psi(\cdot,\boldsymbol{\eta})}(\mathbf{z},M)$ and specifically transformed Fourier matrices. As with the fast algorithms for polynomials on the torus $\mathbb{T}^d$, we determine transformed reconstructing rank-1 lattice $\Lambda_{{}_{\square}\psi(\cdot,\boldsymbol{\eta})}(\mathbf{z},M,I), I\subset\mathbb{Z}^d$ so that the evaluation and the reconstruction algorithms reduce a d-variate Fourier problem into a single one-dimensional FFT. In total, for the approximation on the cube $\left[-\frac{1}{2},\frac{1}{2}\right]^d$ we have

- fast algorithms for the efficient evaluation and stable reconstruction of transformed trigonometric functions on the cube $h\in\Pi_{I,{}_{\square}\psi}$ based on transformed rank-1 lattices $\Lambda_{{}_{\square}\psi(\cdot,\boldsymbol{\eta})}(\mathbf{z},M)$,
- worst case upper weighted L_∞- and L_2-approximation error bounds for functions in the Sobolev space $\mathcal{H}^m\left(\left[-\frac{1}{2},\frac{1}{2}\right]^d,\omega(\cdot,\boldsymbol{\mu})\right)$,

- adapted dimension incremental construction methods to approximate functions with an unknown frequency domain.

In preparation for the numerics, we compare the structure of our transformed Fourier orthonormal systems with the half-periodic cosine system using tent-transformed samples and the Chebyshev polynomials using Chebyshev transformed samples. We note that both the tent-transformation and the Chebyshev transformation are not torus-to-cube transformations. In numerical tests in up to dimension $d = 7$ we compare the approximation results of all previously considered orthonormal systems on the cube $\left[-\frac{1}{2}, \frac{1}{2}\right]^d$. For these applications we use B-splines of first and second order to limit the smoothness degrees that could possibly be preserved by a torus-to-cube transformation ${}_{\square}\psi$. For the first order B-spline, specific transformed Fourier systems are able to produce better approximation results than the Chebyshev system. For the slightly smoother second order B-spline we found torus-to-cube transformations so that the transformed Fourier systems are able to match the approximation quality of the Chebyshev system at least in lower dimensions $d \leq 4$. In a specific example we again show the utility of the dimension incremental construction method used in the adapted sparse FFT method and the resulting improvements on the approximation errors in dimension $d = 7$.

Parts of this work were already published in [NP20, NP21a, NP21b].

Outline of the thesis

We provide an overview of the other chapters in this thesis.

Chapter 2: Preliminaries and notations

We introduce notations that will be used repeatedly throughout the rest of this work, such as the bold notation of constant multi-indices $\mathbf{1} := (1, \ldots, 1)^\top$. We define certain function spaces, such as the space of mixed continuous differentiability $\mathcal{C}^m_{\text{mix}}(\Omega)$ and the Sobolev space $H^m_{\text{mix}}(\Omega)$ of dominating mixed smoothness m simultaneously on $\Omega \in \left\{\mathbb{R}^d, \mathbb{T}^d, \left[-\frac{1}{2}, \frac{1}{2}\right]^d\right\}$. We also fix the notation for some finite-dimensional vector spaces. Additionally, we recall the Leibniz rule and the Faá di Bruno formula for calculating higher derivatives of the product or composition of two functions, cf. (2.0.1) and (2.0.3).

We refer to the index at the end of this work for a complete list of all occurring objects and their respective symbols.

Chapter 3: Fourier approximation on the torus

In this section, we summarize crucial objects and properties from the literature concerned with the theory of approximating periodic functions by classical Fourier methods. At first, we reflect the definition of functions spaces, whose elements have absolutely summable Fourier coefficients and we define rank-1 lattice sampling sets. Then, we recall some major worst-case upper bounds for L_∞- and L_2-approximation errors. Afterwards, we describe two efficient algorithms for the evaluation and reconstruction of multivariate trigonometric polynomials. Furthermore, we outline the ideas of sampling at multiple rank-1 lattices and the idea of not being given a set of frequencies and the task to detect the most important frequencies of any given function. Finally, we present combinatorial arguments for the adequate discretization of the previously mentioned L_∞- and L_2-approximation errors.

Chapter 4: Torus-to-$\mathbb{R}^d$ transformation mappings

We define invertible torus-to-$\mathbb{R}^d$ mappings $\psi(\cdot,\boldsymbol{\eta}) : \left(-\frac{1}{2},\frac{1}{2}\right)^d \to \mathbb{R}^d, \boldsymbol{\eta} \in \mathbb{R}_+^d$ and list important examples. For a given measure function $\omega(\cdot,\boldsymbol{\mu}), \boldsymbol{\mu} \in \mathbb{R}_+^d$ and a class of functions $h \in L_2(\mathbb{R}^d,\omega(\cdot,\boldsymbol{\mu})) \cap H_{\text{mix}}^m(\mathbb{R}^d)$, we prove a set of conditions on these transformations $\psi(\cdot,\boldsymbol{\eta})$ for which we obtain a bounded periodization mapping of the form

$$\begin{aligned}
&h \in L_2(\mathbb{R}^d,\omega(\cdot,\boldsymbol{\mu})) \cap H_{\text{mix}}^m(\mathbb{R}^d)\\
&\downarrow\\
&f := h(\psi(\cdot,\boldsymbol{\eta})) \sqrt{\omega(\psi(\cdot,\boldsymbol{\eta}),\boldsymbol{\mu}) \prod_{j=1}^d \psi_j'(\cdot,\eta_j)} \in \mathcal{H}^m(\mathbb{T}^d),
\end{aligned}$$

so that $\|h\|_{L_2(\mathbb{R}^d,\omega(\cdot,\boldsymbol{\mu}))} = \|f\|_{L_2(\mathbb{T}^d)}$, where the Sobolev spaces $H_{\text{mix}}^m(\mathbb{R}^d)$ and $\mathcal{H}^m(\mathbb{T}^d)$ are given in (2.0.8) and (3.1.7). For a particular torus-to-$\mathbb{R}^d$ mapping we calculate the parameter values $\boldsymbol{\eta},\boldsymbol{\mu}$, so that the Sobolev smoothness m of the original function h is fully transfered to its periodization f under the particular transformation. We apply the approximation techniques for smooth periodic function on the torus $\mathbb{T}^d$ from Chapter 3 and transfer the orthonormality of the Fourier system, important upper approximation error bounds and the efficient algorithms based on rank-1 lattices by means of the inverse torus-to-$\mathbb{R}^d$ transformation $\psi^{-1}(\cdot,\boldsymbol{\eta})$ to the considered non-periodic function class defined on $\mathbb{R}^d$. In particular, we investigate the structure of the resulting weighted exponential functions $\left\{\sqrt{\frac{\varrho(\cdot,\boldsymbol{\eta})}{\omega(\cdot,\boldsymbol{\mu})}}\,\mathrm{e}^{2\pi\mathrm{i}\mathbf{k}\cdot\psi^{-1}(\cdot,\boldsymbol{\eta})}\right\}_{\mathbf{k}\in\mathbb{Z}^d}$ that form an $L_2(\mathbb{R}^d,\omega(\cdot,\boldsymbol{\mu}))$-orthonormal system. Furthermore, we prove weighted upper $L_2\left(\mathbb{R}^d,\omega(\cdot,\boldsymbol{\mu})\right)$- and $L_\infty\left(\mathbb{R}^d,\sqrt{\frac{\omega(\cdot,\boldsymbol{\mu})}{\varrho(\cdot,\boldsymbol{\eta})}}\right)$-approximation error bounds. We propose two efficient algorithms using transformed rank-1 lattices $\Lambda_{\psi(\cdot,\boldsymbol{\eta})}(\mathbf{z},M)$ that adapt the idea of reducing a d-dimensional Fourier transformation into a single one-dimensional FFT from Algorithms 3.4.1 and 3.4.2. Finally, we compare the discrete approximations errors $\varepsilon_\infty^M(h)$ and $\varepsilon_2^M(h)$ in up to dimension $d=7$ for a torus-to-$\mathbb{R}^d$ transformation of exponential type. We showcase the varying approximation quality of the transformation for a fixed parameter $\boldsymbol{\mu} \in \mathbb{R}_+^d$ and different parameter values $\boldsymbol{\eta} \in \mathbb{R}_+^d$ and apply adapted multiple rank-1 lattice methods as well as an adjusted sparse FFT algorithm.

Chapter 5: Torus-to-cube transformation mappings

We switch from the domain $\mathbb{R}^d$ to the cube $\left[-\frac{1}{2},\frac{1}{2}\right]^d$ and for the most part follow the line of the previous chapter. We define torus-to-cube mappings ${}_\square\psi(\cdot,\boldsymbol{\eta}) : \left[-\frac{1}{2},\frac{1}{2}\right]^d \to \left[-\frac{1}{2},\frac{1}{2}\right]^d$ and list important examples. For a given measure function $\omega(\cdot,\boldsymbol{\mu}), \boldsymbol{\mu} \in \mathbb{R}_+^d$ and a class of functions $h \in L_2\left(\left[-\frac{1}{2},\frac{1}{2}\right]^d,\omega(\cdot,\boldsymbol{\mu})\right) \cap \mathcal{C}_{\text{mix}}^m\left(\left[-\frac{1}{2},\frac{1}{2}\right]^d\right)$, we prove a set of conditions on these transformations $\psi(\cdot,\boldsymbol{\eta})$ for which we obtain a bounded periodization mapping of the form

$$\begin{aligned}
&h \in L_2\left(\left[-\frac{1}{2},\frac{1}{2}\right]^d,\omega(\cdot,\boldsymbol{\mu})\right) \cap \mathcal{C}_{\text{mix}}^m\left(\left[-\frac{1}{2},\frac{1}{2}\right]^d\right)\\
&\downarrow\\
&f := h({}_\square\psi(\cdot,\boldsymbol{\eta})) \sqrt{\omega({}_\square\psi(\cdot,\boldsymbol{\eta}),\boldsymbol{\mu}) \prod_{j=1}^d {}_\square\psi_j'(\cdot,\eta_j)} \in \mathcal{H}^m(\mathbb{T}^d),
\end{aligned}$$

so that $\|h\|_{L_2\left(\left[-\frac{1}{2},\frac{1}{2}\right]^d,\omega(\cdot,\boldsymbol{\mu})\right)} = \|f\|_{L_2(\mathbb{T}^d)}$, with the function space $\mathcal{C}^m_{\text{mix}}\left(\left[-\frac{1}{2},\frac{1}{2}\right]^d\right)$ given in (2.0.6). For several torus-to-cube transformations ${}_{\square}\psi(\cdot,\boldsymbol{\eta})$ we calculate the parameter values $\boldsymbol{\eta},\boldsymbol{\mu}$, so that the Sobolev smoothness m of the original function h is fully preserved by its periodization f under the particular transformation. We apply the approximation techniques for smooth periodic function on the torus $\mathbb{T}^d$ from Chapter 3 and transfer the orthonormality of the Fourier system, important upper approximation error bounds and the efficient algorithms based on rank-1 lattices by means of the inverse torus-to-cube transformation ${}_{\square}\psi^{-1}(\cdot,\boldsymbol{\eta})$ to the considered function classes in $L_2\left(\left[-\frac{1}{2},\frac{1}{2}\right]^d,\omega(\cdot,\boldsymbol{\mu})\right)$. We investigate the structure of the weighted exponential functions $\left\{\sqrt{\frac{{}_{\square}\varrho(\cdot,\boldsymbol{\eta})}{\omega(\cdot,\boldsymbol{\mu})}}\,\mathrm{e}^{2\pi\mathrm{i}\mathbf{k}\cdot{}_{\square}\psi^{-1}(\cdot,\boldsymbol{\eta})}\right\}_{\mathbf{k}\in\mathbb{Z}^d}$ that form an $L_2\left(\left[-\frac{1}{2},\frac{1}{2}\right]^d,\omega(\cdot,\boldsymbol{\mu})\right)$-orthonormal system. Furthermore, we prove weighted worst-case upper $L_2\left(\left[-\frac{1}{2},\frac{1}{2}\right]^d,\omega(\cdot,\boldsymbol{\mu})\right)$- and $L_\infty\left(\left[-\frac{1}{2},\frac{1}{2}\right]^d,\sqrt{\frac{\omega(\cdot,\boldsymbol{\mu})}{{}_{\square}\varrho(\cdot,\boldsymbol{\eta})}}\right)$-approximation error bounds. We propose two efficient algorithms using transformed rank-1 lattices $\Lambda_{{}_{\square}\psi(\cdot,\boldsymbol{\eta})}(\mathbf{z},M)$ that adapt the idea of reducing a d-dimensional Fourier transformation into a single one-dimensional FFT from Algorithms 3.4.1 and 3.4.2. We compare the transformed Fourier systems with classical orthonormal systems used for the approximation of functions defined on the cube $\left[-\frac{1}{2},\frac{1}{2}\right]^d$ in the form of the half-periodic cosine system which uses tent-transformed rank-1 lattice points as samples and the Chebyshev polynomials which use Chebyshev transformed rank-1 lattice sampling nodes. We showcase that the transformed Fourier system provides a generalized framework to create orthonormal systems on the cube. Finally, in two numericals tests we compare the discrete approximation errors $\varepsilon^M_\infty(h)$ and $\varepsilon^M_2(h)$ in up to dimension $d=7$ for multiple torus-to-cube transformations. We showcase the varying approximation quality of all considered transformations for different parameter values $\boldsymbol{\eta}\in\mathbb{R}^d_+$ and apply adapted multiple rank-1 lattice methods as well as an adjusted sparse FFT algorithm.

Chapter 6: Conclusion

We briefly summarize the discussed topics and main results within this work.

Acknowledgements

First of all, I have to thank Prof. Dr. Daniel Potts for his guidance, support and constant encouragement over the past years, which ultimately enabled me to write this thesis. Additionally, I'm grateful for the friendly environment within the whole working group in all these years and for the fruitful discussions especially with Dr. Lutz Kämmerer, Dr. Toni Volkmer and Prof. Dr. Tino Ullrich.

This work was partly supported by funds of the European Union and the Free State of Saxony (ESF).

Chapter 2

Preliminaries and notations

We establish various notations that will be used throughout the rest of this work. More definitions will be made within this work when necessary. All appearing symbols are listed in an index at the end of this work.

Let $\Omega \in \left\{\mathbb{R}^d, \mathbb{T}^d, \left[-\frac{1}{2}, \frac{1}{2}\right]^d\right\}$ with $\mathbb{T}^d \simeq [-\frac{1}{2}, \frac{1}{2})^d$ being the d-dimensional torus. The space $\big(\mathcal{C}(\Omega), \|\cdot\|_{L_\infty(\Omega)}\big)$ denotes the collection of all continuous multivariate functions $f : \Omega \to \mathbb{C}$. Furthermore, by $(\mathcal{C}_0(\mathbb{R}^d), \|\cdot\|_{L_\infty(\mathbb{R}^d)})$ we denote the space of all continuous functions defined on $\mathbb{R}^d$ that vanish at infinity in every direction and $\left(\mathcal{C}_0\left(\left[-\frac{1}{2}, \frac{1}{2}\right]^d\right), \|\cdot\|_{L_\infty\left(\left[-\frac{1}{2}, \frac{1}{2}\right]^d\right)}\right)$ denotes the space of all continuous functions defined on the cube $\left[-\frac{1}{2}, \frac{1}{2}\right]^d$ that vanish at the boundary points $\left[-\frac{1}{2}, \frac{1}{2}\right]^d \setminus \left(-\frac{1}{2}, \frac{1}{2}\right)^d$.

For a given dimension $d \in \mathbb{N}$, we use the bold notation $\mathbf{x} := (x_1, \ldots, x_d)^\top$, $\mathbf{k} := (k_1, \ldots, k_d)^\top$ as well as $\mathbf{k} \cdot \mathbf{x} := k_1 x_1 + \ldots + k_d x_d$ and we also fix the sets

$$\mathbb{N}_0^d := \left\{\mathbf{k} \in \mathbb{N}^d : k_j \in \mathbb{N} \cup \{0\}, j \in \{1, \ldots, d\}\right\},$$
$$\mathbb{R}_+^d := \left\{\mathbf{x} \in \mathbb{R}^d : 0 < x_j \in \mathbb{R}, j \in \{1, \ldots, d\}\right\}.$$

For numbers $k, \ell \in \mathbb{R}$ the Kronecker delta $\delta_{k,\ell}$ is defined as

$$\delta_{k,\ell} := \begin{cases} 1 & \text{for} \quad k = \ell, \\ 0 & \text{for} \quad k \neq \ell. \end{cases}$$

For the multi-indices $\boldsymbol{\alpha} := (\alpha_1, \ldots, \alpha_d)^\top \in \mathbb{N}_0^d$ we define the differential operator

$$D^{\boldsymbol{\alpha}}[f](\mathbf{x}) = D^{(\alpha_1, \ldots, \alpha_d)}[f](x_1, \ldots, x_d) := \frac{\partial^{\alpha_1}}{\partial x_1^{\alpha_1}} \cdots \frac{\partial^{\alpha_d}}{\partial x_d^{\alpha_d}}[f](x_1, \ldots, x_d).$$

In the univariate case, we denote the k-th derivative of a function $f(x)$ with respect to x by one of the equivalent expressions $f^{(k)}(x) = \frac{\mathrm{d}^k}{\mathrm{d}x^k}[f](x)$, and for $k = 1$ we most commonly just write $f'(x)$.

The n-th derivative of a product of two function $f, g \in \mathcal{C}^n(\Omega)$ is expressed by the *generalized Leibniz rule*

$$(fg)^{(n)}(x) = \sum_{k=0}^{n} \binom{n}{k} f^{(k)}(x)\, g^{(n-k)}(x). \tag{2.0.1}$$

The k-th derivative of the composition of functions $h, \psi \in \mathcal{C}^k(\Omega)$ is expressed by the *Faá di Bruno* formula

$$(h \circ \psi)^{(k)}(x) = \sum_{\ell=1}^{k} h^{(\ell)}(\psi(x))\, B_{k,\ell}(\psi'(x), \psi^{(2)}(x), \dots, \psi^{(k-\ell+1)}(x)) \tag{2.0.2}$$

with the well-known Bell polynomials $B_{k,\ell}(\mathbf{z})$ for $k, \ell \in \mathbb{N}_0$ and $\mathbf{z} = (z_1, \dots, z_{k-\ell+1})^\top$ given by

$$B_{k,\ell}(\mathbf{z}) := \sum_{\substack{j_1+j_2+\dots+j_{k-\ell+1}=\ell,\\ j_1+2j_2+\dots+(k-\ell+1)j_{k-\ell+1}=k}} \frac{\ell!}{j_1! \cdot \dots \cdot j_{k-\ell+1}!} \prod_{r=1}^{k-\ell+1} \left(\frac{z_r}{r!}\right)^{j_r}. \tag{2.0.3}$$

For $0 < p \leq \infty$ we define the finite-dimensional sequence spaces

$$\ell_p^d := \{\mathbf{x} = (x_j)_{j=1}^d, x_j \in \{\mathbb{R}, \mathbb{C}\} : \|\mathbf{x}\|_{\ell_p^d} < \infty\} \tag{2.0.4}$$

with the sequence norm

$$\|\mathbf{x}\|_{\ell_p^d} := \begin{cases} \left(\sum_{j=1}^d |x_j|^p\right)^{\frac{1}{p}} & \text{for } 0 < p < \infty, \\ \sup_{j \in \{1,\dots,d\}} |x_j| & \text{for } p = \infty, \end{cases}$$

which is a quasi-norm for $0 < p < 1$. Accordingly, the d-dimensional unit ball of the sequence space ℓ_p^d is given by

$$I_1^{\ell_p^d} := \{\mathbf{x} \in \ell_p^d : \|\mathbf{x}\|_{\ell_p^d} \leq 1\} \tag{2.0.5}$$

and for scaled ℓ_p^d-balls we put we put $I_N^{\ell_p^d} := N \cdot I_1^{\ell_p^d}$ for any $N \in \mathbb{N}$. Additionally, for sequences there is the zero-norm given by

$$\|\mathbf{x}\|_0 := |\{j \in \{1, \dots, d\} : x_j \neq 0\}|,$$

that quantifies the number of non-zero entries in any given sequence.

We define the *function space of mixed continuous differentiability* of order $m \in \mathbb{N}$, see [ST87, p. 132], as

$$\mathcal{C}_{\text{mix}}^m(\Omega) := \left\{ f \in \mathcal{C}(\Omega) : \|f\|_{\mathcal{C}_{\text{mix}}^m(\Omega)} := \sum_{\|\boldsymbol{\alpha}\|_{\ell_\infty^d} \leq m} \|D^{\boldsymbol{\alpha}}[f]\|_{L_\infty(\Omega)} < \infty \right\}. \tag{2.0.6}$$

The corresponding univariate space of m-times continuously differentiable functions are denoted by $\mathcal{C}^m(\Omega)$. The weighted function spaces $L_p(\Omega, \omega)$ with $1 \leq p < \infty$ an integrable measure function $\omega : \Omega \to [0, \infty)$ are defined as

$$L_p(\Omega, \omega) := \left\{ h \in L_p(\Omega) : \|h\|_{L_p(\Omega,\omega)} < \infty \right\}. \tag{2.0.7}$$

with the norm

$$\|h\|_{L_p(\Omega,\omega)} := \begin{cases} \left(\int_\Omega |h(\mathbf{x})|^p\, \omega(\mathbf{x})\, \mathrm{d}\mathbf{x}\right)^{\frac{1}{p}} & \text{for } 1 \leq p < \infty, \\ \operatorname{ess\,sup}_{\mathbf{x} \in \Omega} \left(|h(\mathbf{x})|^p\, \omega(\mathbf{x})\right) & \text{for } p = \infty. \end{cases}$$

For the constant measure function $\omega(\mathbf{x}) \equiv 1$ we have $L_2(\Omega, \omega) = L_2(\Omega)$.

Finally, we define the *Sobolev spaces of dominating mixed natural smoothness* of $L_2(\Omega)$-functions with smoothness order $m \in \mathbb{N}_0$, see [ST87, Ull07, Vyb05], as

$$H^m_{\text{mix}}(\Omega) := \left\{ f \in L_2(\Omega) : \|f\|_{H^m_{\text{mix}}(\Omega)} := \left(\sum_{\|\boldsymbol{\alpha}\|_{\ell^d_\infty} \leq m} \|D^{\boldsymbol{\alpha}}[f]\|^2_{L_2(\Omega)} \right)^{1/2} < \infty \right\}. \tag{2.0.8}$$

The corresponding univariate spaces are denoted by $H^m(\Omega)$.

For a matrix $\mathbf{A} = (a_{ij})_{i=1,j=1}^{m,n} \in \mathbb{C}^{m \times n}$, the adjoint matrix $\mathbf{A}^* := (\overline{a_{ji}})_{j=1,i=1}^{n,m} \in \mathbb{C}^{n \times m}$ is obtained by replacing each complex element a_{ij} with its complex conjugate $\overline{a_{ij}}$ and forming the transpose of the resulting matrix.

On a different note, we will repeatedly fix certain multivariate parameter vectors that will have the same number in each entry. We define that any bold number represents a d-dimensional vector containing itself in each coordinate, e.g. $\mathbf{4} = (4, \ldots, 4)^\top$. If an argument in a function remains unspecified, we use a single dot as a place holder, e.g. $f(\cdot)$, that is not to be confused with the multiplication dot as for example in $\mathbf{k} \cdot \mathbf{x}$.

Chapter 3

Fourier approximation on the torus

We reflect on the notation and major results for the approximation of multivariate continuous functions defined on $\mathbb{T}^d$ by trigonometric polynomials.

In Section 3.1 we introduce the Fourier system $\left\{\mathrm{e}^{2\pi\mathrm{i}\mathbf{k}(\cdot)}\right\}_{\mathbf{k}\in\mathbb{Z}^d}$ that is orthonormal in $L_2\left(\mathbb{T}^d\right)$, cf. (3.1.1). We define the hyperbolic cross I_N^d based on the measure function ω_{hc} as an alternative frequency set, whose cardinality is growing much slower than the scaled ℓ_p^d-balls $I_N^{\ell_p^d}, p > 0$ given in (2.0.5). Afterwards, we introduce function spaces $\mathcal{A}^\beta(\mathbb{T}^d)$ and $\mathcal{H}^\beta(\mathbb{T}^d)$ of $L_2\left(\mathbb{T}^d\right)$-functions with absolutely or square summable Fourier coefficients $\hat{f}_{\mathbf{k}}$, cf. (3.1.6) and (3.1.7), and reflect on equivalence and embedding properties.

In Section 3.2 we define rank-1 lattices $\Lambda(\mathbf{z}, M)$ in (3.2.2) and state the reconstructing rank-1 lattice property, for which we have the exact integration property (3.2.3) of multivariate trigonometric polynomials. Considering arbitrary functions $f \in \mathcal{H}^\beta(\mathbb{T}^d)$, we define *approximated Fourier coefficients* $\hat{f}_{\mathbf{k}}^\Lambda$, cf. (3.2.5), as well as the approximated Fourier partial sum $S_I^\Lambda f$.

Afterwards in Section 3.3 we recall two worst case $L_\infty(\mathbb{T}^d)$- and $L_2(\mathbb{T}^d)$-approximation error bounds, cf. (3.3.1) and (3.3.2).

In Section 3.4 we reflect the Algorithms 3.4.1 and 3.4.2 based on a single rank-1 lattice for the efficient evaluation and stable reconstruction of multivariate trigonometric polynomials. We also highlight the advantages of using multiple rank-1 lattices $\Lambda(\mathbf{z}_1, M_1, \ldots, \mathbf{z}_s, M_s)$, cf. (3.4.5), and discuss the basic idea behind the dimension incremental construction of frequency sets $I \subset \mathbb{Z}^d$ to algorithmically determine a fixed number of the largest frequencies within a predefined search space in $\mathbb{Z}^d$.

Finally in Section 3.5 we provide combinatorial arguments to obtain suitable discretized relative ℓ_∞-approximation errors ε_∞^M and ℓ_2-approximation errors ε_2^M, cf. (3.5.1) and (3.5.4).

3.1 Fourier analysis on the torus

For $\mathbf{x} = (x_1, \ldots, x_d)^\top \in \mathbb{T}^d$ and frequencies $\mathbf{k} = (k_1, \ldots, k_d)^\top \in \mathbb{Z}^d$, we consider the Fourier system

$$\left\{\mathrm{e}^{2\pi\mathrm{i}\mathbf{k}\cdot\mathbf{x}} = \prod_{j=1}^d \mathrm{e}^{2\pi\mathrm{i}k_j x_j}\right\}_{\mathbf{k}\in\mathbb{Z}^d}, \tag{3.1.1}$$

that is orthonormal with respect to the scalar product

$$(f,g)_{L_2(\mathbb{T}^d)} := \int_{\mathbb{T}^d} f(\mathbf{x})\,\overline{g(\mathbf{x})}\,\mathrm{d}\mathbf{x},$$

so that for $\mathbf{k}_1, \mathbf{k}_2 \in \mathbb{Z}^d$ we have

$$(\mathrm{e}^{2\pi\mathrm{i}\mathbf{k}_1(\cdot)}, \mathrm{e}^{2\pi\mathrm{i}\mathbf{k}_2(\cdot)})_{L_2(\mathbb{T}^d)} := \delta_{\mathbf{k}_1,\mathbf{k}_2}.$$

For any frequency set $I \subset \mathbb{Z}^d$ of finite cardinality $|I| < \infty$ we denote the space of all multivariate trigonometric polynomials supported on I by

$$\Pi_I := \operatorname{span}\{\mathrm{e}^{2\pi\mathrm{i}\mathbf{k}(\cdot)} : \mathbf{k} \in I\}. \tag{3.1.2}$$

For all $\mathbf{k} \in \mathbb{Z}^d$, we define the *Fourier coefficients* $\hat{f}_{\mathbf{k}}$ as

$$\hat{f}_{\mathbf{k}} := (f, \mathrm{e}^{2\pi\mathrm{i}\mathbf{k}(\cdot)})_{L_2(\mathbb{T}^d)} = \int_{\mathbb{T}^d} f(\mathbf{x})\,\mathrm{e}^{-2\pi\mathrm{i}\mathbf{k}\cdot\mathbf{x}}\,\mathrm{d}\mathbf{x}, \tag{3.1.3}$$

and the corresponding *Fourier partial sum* is given by $S_I f(\cdot) = \sum_{\mathbf{k}\in I} \hat{f}_{\mathbf{k}}\,\mathrm{e}^{2\pi\mathrm{i}\mathbf{k}(\cdot)}$. For all $f \in L_2(\mathbb{T}^d)$, we have

$$\|f - S_I f\|_{L_2(\mathbb{T}^d)} \to 0 \quad \text{for} \quad |I| \to \infty, \tag{3.1.4}$$

where $|I| \to \infty$ means $\min(|k_1|, \dots, |k_d|) \to \infty$ for $\mathbf{k} = (k_1, \dots, k_d)^\top \in I$, see [Wei12, Theorem 4.1].

We define the *hyperbolic cross* I_N^d as

$$I_N^d := \left\{\mathbf{k} \in \mathbb{Z}^d : \mathrm{w_{hc}}(\mathbf{k}) \le N\right\} \quad \text{with} \quad \mathrm{w_{hc}}(\mathbf{k}) := \prod_{j=1}^d \max(1, |k_j|), \tag{3.1.5}$$

which is illustrated alongside two scaled ℓ_p^d-balls $I_N^{\ell_p^d}$ with $p \in \{\frac{1}{2}, 1\}$ as defined in (2.0.5) for $N = 16$ in two dimensions in Figure 3.1.1.

Remark 3.1.1. *The size of the frequency set $I \subset \mathbb{Z}^d$ will factor in the overall computation time. At first, we will focus on hyperbolic cross sets I_N^d. Later on, we consider functions f for which the optimal choice for a frequency set $I \subset \mathbb{Z}^d$ of finite cardinality $|I| < \infty$ that corresponds to the largest Fourier coefficients $\hat{f}_{\mathbf{k}}$ is unknown. The approach of switching to scaled ℓ_p^d-balls $I_N^{\ell_p^d}$ is not feasible in higher dimensions d, because the cardinality $|I_N^{\ell_p^d}|$ grows asymptotically like N^d whereas the cardinality $|I_N^d|$ grows only like $N\log(N)^{d-1}$. Eventually, we reflect on a dimension incremental construction method [Vol15, PV16] that determines the $|I_N^d|$ largest Fourier coefficients in a fixed search space $[-N, N]^d \cap \mathbb{Z}^d$.* □

For $\beta \ge 0$, we define the space

$$\mathcal{A}^\beta(\mathbb{T}^d) := \left\{ f \in L_1(\mathbb{T}^d) : \|f\|_{\mathcal{A}^\beta(\mathbb{T}^d)} := \sum_{\mathbf{k}\in\mathbb{Z}^d} \mathrm{w_{hc}}(\mathbf{k})^\beta |\hat{f}_{\mathbf{k}}| < \infty \right\} \subset \mathcal{C}(\mathbb{T}^d) \tag{3.1.6}$$

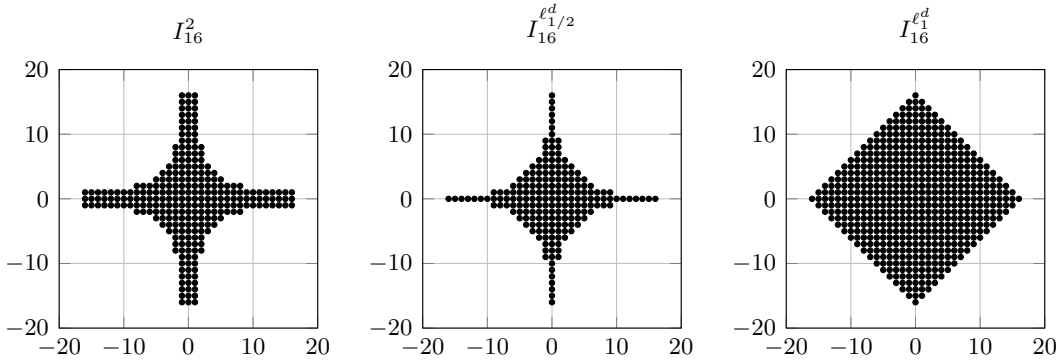

Figure 3.1.1: The hyperbolic cross I_N^d as in (3.1.5), two scaled ℓ_p^d-balls $I_N^{\ell_p^d}, p \in \{\frac{1}{2}, 1\}$ as in (2.0.5) for $N = 16, d = 2$.

and the Hilbert space

$$\mathcal{H}^\beta(\mathbb{T}^d) := \left\{ f \in L_2(\mathbb{T}^d) : \|f\|_{\mathcal{H}^\beta(\mathbb{T}^d)} := \left(\sum_{\mathbf{k}\in\mathbb{Z}^d} \mathrm{w}_{\mathrm{hc}}(\mathbf{k})^{2\beta} |\hat{f}_{\mathbf{k}}|^2 \right)^{\frac{1}{2}} < \infty \right\} \subset \mathcal{C}(\mathbb{T}^d). \tag{3.1.7}$$

For $\beta = 0$ and the constant measure function $\mathrm{w}_{\mathrm{hc}}(\mathbf{k}) \equiv 1$, we call the space $\mathcal{A}(\mathbb{T}^d) := \mathcal{A}^0(\mathbb{T}^d)$ the *Wiener Algebra*. For all $m \in \mathbb{N}$, it was shown in [KSU15] that

$$\|\cdot\|_{\mathcal{H}^m(\mathbb{T}^d)} \sim \|\cdot\|_{H^m_{\mathrm{mix}}(\mathbb{T}^d)}. \tag{3.1.8}$$

As shown in [KPV15, Lemma 2.2], for $\beta \geq 0, \lambda > \frac{1}{2}$ and fixed $d \in \mathbb{N}$ there are the continuous embeddings

$$\mathcal{H}^{\beta+\lambda}(\mathbb{T}^d) \hookrightarrow \mathcal{A}^\beta(\mathbb{T}^d) \hookrightarrow \mathcal{A}(\mathbb{T}^d) \tag{3.1.9}$$

and for $f \in \mathcal{H}^{\beta+\lambda}(\mathbb{T}^d)$ we have

$$\|f\|_{\mathcal{A}^\beta(\mathbb{T}^d)} \leq C_{d,\lambda} \|f\|_{\mathcal{H}^{\beta+\lambda}(\mathbb{T}^d)} \tag{3.1.10}$$

with a constant $C_{d,\lambda} := C(d,\lambda) > 1$. Additionally, for each function in $\mathcal{A}(\mathbb{T}^d)$ there exists a continuous representative, as proven in [Käm14b, Lemma 2.1]. Later on, when we sample functions $f \in \mathcal{H}^{\beta+\lambda}(\mathbb{T}^d)$ we identify them with their continuous representatives given by their Fourier series $\sum_{\mathbf{k}\in\mathbb{Z}^d} \hat{f}_{\mathbf{k}} \, \mathrm{e}^{2\pi \mathrm{i} \mathbf{k}(\cdot)}$.

3.2 Fourier approximation with rank-1 lattices

We collect some objects and observations from [SK87, CKN10, Käm14b] to discuss the approximation of functions $f \in \mathcal{H}^\beta(\mathbb{T}^d)$. For each frequency set $I \subset \mathbb{Z}^d$ there is the *difference set*

$$\mathcal{D}(I) := \{\mathbf{k} \in \mathbb{Z}^d : \mathbf{k} = \mathbf{k}_1 - \mathbf{k}_2 \text{ with } \mathbf{k}_1, \mathbf{k}_2 \in I\}. \tag{3.2.1}$$

The set

$$\Lambda(\mathbf{z}, M) := \left\{ \mathbf{x}_j := \left(\frac{j}{M} \mathbf{z} \bmod \mathbf{1} \right) \in \mathbb{T}^d : j = 0, 1, \ldots M-1 \right\} \tag{3.2.2}$$

is called *rank-1 lattice* with the *generating vector* $\mathbf{z} \in \mathbb{Z}^d$ and the *lattice size* $M \in \mathbb{N}$. A *reconstructing rank-1 lattice* $\Lambda(\mathbf{z}, M, I)$ is a rank-1 lattice $\Lambda(\mathbf{z}, M)$ for which the condition

$$\mathbf{t} \cdot \mathbf{z} \not\equiv 0 \,(\mathrm{mod}\, M) \quad \text{for all } \mathbf{t} \in \mathcal{D}(I) \setminus \{\mathbf{0}\}$$

holds. Given a reconstructing rank-1 lattice $\Lambda(\mathbf{z}, M, I)$, we have exact integration for all multivariate trigonometric polynomials $g \in \Pi_{\mathcal{D}(I)}$, see [SK87], so that

$$\int_{\mathbb{T}^d} g(\mathbf{x})\,\mathrm{d}\mathbf{x} = \frac{1}{M} \sum_{j=0}^{M-1} g(\mathbf{x}_j), \quad \mathbf{x}_j \in \Lambda(\mathbf{z}, M, I). \tag{3.2.3}$$

In particular, for $f \in \Pi_I$ and $\mathbf{k} \in I$ we have $f(\cdot)\,\mathrm{e}^{-2\pi \mathrm{i}\mathbf{k}(\cdot)} \in \Pi_{\mathcal{D}(I)}$ and

$$\hat{f}_{\mathbf{k}} = \int_{\mathbb{T}^d} f(\mathbf{x})\,\mathrm{e}^{-2\pi \mathrm{i}\mathbf{k}\cdot\mathbf{x}}\,\mathrm{d}\mathbf{x} = \frac{1}{M} \sum_{j=0}^{M-1} f(\mathbf{x}_j)\,\mathrm{e}^{-2\pi \mathrm{i}\mathbf{k}\cdot\mathbf{x}_j}, \quad \mathbf{x}_j \in \Lambda(\mathbf{z}, M, I). \tag{3.2.4}$$

For an arbitrary function $f \in \mathcal{H}^\beta(\mathbb{T}^d)$ we lose the former mentioned exactness and define the *approximated Fourier coefficients* $\hat{f}^\Lambda_{\mathbf{k}}$ of the form

$$\hat{f}_{\mathbf{k}} \approx \hat{f}^\Lambda_{\mathbf{k}} := \frac{1}{M} \sum_{j=0}^{M-1} f(\mathbf{x}_j)\,\mathrm{e}^{-2\pi \mathrm{i}\mathbf{k}\cdot\mathbf{x}_j}, \quad \mathbf{x}_j \in \Lambda(\mathbf{z}, M, I), \tag{3.2.5}$$

leading to the *approximated Fourier partial sum* $S^\Lambda_I f$ given by

$$S_I f(\mathbf{x}) \approx S^\Lambda_I f(\mathbf{x}) := \sum_{\mathbf{k}\in I} \hat{f}^\Lambda_{\mathbf{k}}\,\mathrm{e}^{2\pi \mathrm{i}\mathbf{k}\cdot\mathbf{x}}.$$

3.3 Approximation error bounds on the torus

For functions f in $\mathcal{A}^\beta(\mathbb{T}^d)$ and $\mathcal{H}^\beta(\mathbb{T}^d)$ we reflect certain upper bounds for approximation errors of the form $\left\| f - S^\Lambda_{I^d_N} f \right\|$. First of all, the existence of reconstructing rank-1 lattices is secured by the arguments provided in [Käm14a, Corollary 1] and [KPV15, Theorem 2.1]:

Lemma 3.3.1. *Let $I \subset \mathbb{Z}^d$ be a frequency set of finite cardinality $4 \le |I| < \infty$ and with $I \subset \mathbb{Z}^d \cap \left(-\frac{M}{2}, \frac{M}{2}\right)^d, M \in \mathbb{N}$. For all multivariate trigonometric polynomials $f \in \Pi_I$ there exists a reconstructing rank-1 lattice $\Lambda(\mathbf{z}, M, I)$ where the lattice size M is bounded by $|I| \le M \le |\mathcal{D}(I)| \le |I|^2$, such that $\hat{f}_{\mathbf{k}} = \hat{f}^\Lambda_{\mathbf{k}}$. The generating vector $\mathbf{z} \in \mathbb{Z}^d$ can be constructed using a component-by-component approach.*

Now, there are worst case upper bounds for the L_∞-approximation error of functions in $\mathcal{A}^\beta(\mathbb{T}^d)$, as proven in [KPV15, Theorem 3.3]:

Theorem 3.3.2. *Let $f \in \mathcal{A}^\beta(\mathbb{T}^d)$ with $\beta \ge 0$ and $d \in \mathbb{N}$, a hyperbolic cross I^d_N with $|I^d_N| < \infty$ and $N \in \mathbb{N}$ as given in* (3.1.5)*, and a reconstructing rank-1 lattice $\Lambda(\mathbf{z}, M, I^d_N)$ be given. The approximation of f by the approximated Fourier partial sum $S^\Lambda_{I^d_N} f$ leads to an approximation error that is estimated by*

$$\left\| f - S^\Lambda_{I^d_N} f \right\|_{L_\infty(\mathbb{T}^d)} \le 2N^{-\beta} \|f\|_{\mathcal{A}^\beta(\mathbb{T}^d)}. \tag{3.3.1}$$

The approximation of functions in the Hilbert spaces $\mathcal{H}^\beta(\mathbb{T}^d)$ was investigated in [Tem86, KPV15]. It was proven that for all $\beta > 1$, there exists a reconstructing rank-1 lattice generated by a vector in Korobov form $(1, z, z^2, \dots, z^{d-1})^\top \in \mathbb{Z}^d$ such that the L_2-truncation error is bounded above by

$$\left\| f - S^\Lambda_{I^d_N} f \right\|_{L_2(\mathbb{T}^d)} \le N^{-\beta} (\log N)^{(d-1)/2} \|f\|_{\mathcal{H}^\beta(\mathbb{T}^d)}.$$

A more general estimate of this error and an upper bound for the corresponding aliasing error can be found in [BKUV17, Theorem 2], where slightly different frequency sets - the so-called dyadic hyperbolic cross - are used and a component-by-component approach was applied to construct the generating vector $\mathbf{z} \in \mathbb{Z}^d$ which generally is not of Korobov form anymore. Furthermore, every dyadic hyperbolic cross is embedded in a hyperbolic cross as defined in (3.1.5), see [Vol17, Lemma 2.29], so that these error estimates are easily translated in terms of hyperbolic crosses I^d_N, see [Vol17, Theorem 2.30]. We will repeatedly use the following special case:

Theorem 3.3.3. *Let $\beta > \frac{1}{2}$, $d \in \mathbb{N}$, $f \in \mathcal{H}^\beta(\mathbb{T}^d)$, a hyperbolic cross I^d_N with $N \ge 2^{d+1}$, and a reconstructing rank-1 lattice $\Lambda(\mathbf{z}, M, I^d_N)$ be given. Then we have*

$$\left\| f - S^\Lambda_{I^d_N} f \right\|_{L_2(\mathbb{T}^d)} \le C_{d,\beta} N^{-\beta} (\log N)^{(d-1)/2} \|f\|_{\mathcal{H}^\beta(\mathbb{T}^d)} \tag{3.3.2}$$

with some constant $C_{d,\beta} := C(d, \beta) > 0$.

3.4 Algorithms on the torus

3.4.1 Efficient evaluation and reconstruction of trignometric polynomials

The algorithms in [Käm14b, Algorithm 3.1 and 3.2] describe how to efficiently evaluate any high-dimensional trigonometric polynomial such as the approximated Fourier series $S^\Lambda_I f$, and how to reconstruct the approximated Fourier coefficients $\hat{f}^\Lambda_{\mathbf{k}}, \mathbf{k} \in I$ given in (3.2.5), with a single one-dimensional fast Fourier transform. Both procedures are denoted as matrix-vector-products of the form

$$\mathbf{f} = \mathbf{F}\hat{\mathbf{f}} \quad \text{and} \quad \hat{\mathbf{f}} = M^{-1}\mathbf{F}^*\mathbf{f} \tag{3.4.1}$$

with $\mathbf{f} := (f(\mathbf{x}_j))_{j=0}^{M-1}$ for $\mathbf{x}_j \in \Lambda(\mathbf{z}, M)$, $\hat{\mathbf{f}} := (\hat{f}_{\mathbf{k}})_{\mathbf{k}\in I}$ and the Fourier matrices $\mathbf{F}$ and $\mathbf{F}^*$ given by

$$\mathbf{F} := \left(\mathrm{e}^{2\pi \mathrm{i}\mathbf{k}\cdot\mathbf{x}_j}\right)_{\mathbf{x}_j\in\Lambda(\mathbf{z},M),\,\mathbf{k}\in I} \in \mathbb{C}^{M\times|I|}, \quad \mathbf{F}^* = \left(\mathrm{e}^{-2\pi \mathrm{i}\mathbf{k}\cdot\mathbf{x}_j}\right)_{\mathbf{k}\in I,\,\mathbf{x}_j\in\Lambda(\mathbf{z},M)} \in \mathbb{C}^{|I|\times M}. \tag{3.4.2}$$

3.4.1.1 Evaluation of trigonometric polynomials

Given a frequency set $I \subset \mathbb{Z}^d$ of finite cardinality $|I| < \infty$, we consider the multivariate trigonometric polynomial $f \in \Pi_I$ as in (3.1.2) with Fourier coefficients $\hat{f}_{\mathbf{k}}$. The evaluation of f at lattice points $\mathbf{x}_j \in \Lambda(\mathbf{z}, M)$ simplifies to

$$f(\mathbf{x}_j) = \sum_{\mathbf{k}\in I} \hat{f}_{\mathbf{k}}\, \mathrm{e}^{2\pi \mathrm{i}\mathbf{k}\cdot\mathbf{x}_j} = \sum_{\ell=0}^{M-1} \left(\sum_{\substack{\mathbf{k}\in I,\\ \mathbf{k}\cdot\mathbf{z}\equiv\ell \,(\bmod M)}} \hat{f}_{\mathbf{k}} \right) \mathrm{e}^{2\pi \mathrm{i}\ell\frac{j}{M}} = \sum_{\ell=0}^{M-1} \hat{g}_\ell\, \mathrm{e}^{2\pi \mathrm{i}\ell\frac{j}{M}}, \tag{3.4.3}$$

Algorithm 3.4.1 Evaluation at rank-1 lattice

Input:	$M \in \mathbb{N}$	lattice size of $\Lambda(\mathbf{z}, M)$
	$\mathbf{z} \in \mathbb{Z}^d$	generating vector of $\Lambda(\mathbf{z}, M)$
	$I \subset \mathbb{Z}^d$	frequency set of finite cardinality
	$\hat{\mathbf{f}} = \left(\hat{f}_{\mathbf{k}}\right)_{\mathbf{k}\in I}$	Fourier coefficients of $f \in \Pi_I$

$\hat{\mathbf{g}} = (0)_{\ell=0}^{M-1}$
for each $\mathbf{k} \in I$ **do**
  $\hat{g}_{\mathbf{k}\cdot\mathbf{z} \bmod M} = \hat{g}_{\mathbf{k}\cdot\mathbf{z} \bmod M} + \hat{f}_{\mathbf{k}}$
end for
$\mathbf{f} = \mathrm{iFFT\_1D}(\hat{\mathbf{g}})$
$\mathbf{f} = M\mathbf{f}$

Output:	$\mathbf{f} = \mathbf{F}\hat{\mathbf{f}} = (f(\mathbf{x}_j))_{j=0}^{M-1}$	function values of $f \in \Pi_I$

Algorithm 3.4.2 Reconstruction from sampling values along a transformed reconstructing rank-1 lattice

Input:	$I \subset \mathbb{Z}^d$	frequency set of finite cardinality
	$M \in \mathbb{N}$	lattice size of $\Lambda(\mathbf{z}, M, I)$
	$\mathbf{z} \in \mathbb{Z}^d$	generating vector of $\Lambda(\mathbf{z}, M, I)$
	$\mathbf{f} = (f(\mathbf{x}_j))_{j=0}^{M-1}$	function values of $f \in \Pi_I$

$\hat{\mathbf{g}} = \mathrm{FFT\_1D}(\mathbf{f})$
for each $\mathbf{k} \in I$ **do**
  $\hat{f}_{\mathbf{k}} = \frac{1}{M}\hat{g}_{\mathbf{k}\cdot\mathbf{z} \bmod M}$
end for

Output:	$\hat{\mathbf{f}} = M^{-1}\mathbf{F}^*\mathbf{f} = \left(\hat{f}^{\Lambda}_{\mathbf{k}}\right)_{\mathbf{k}\in I}$	approximated Fourier coefficients supported on I

with

$$\hat{g}_\ell = \sum_{\substack{\mathbf{k}\in I,\\ \mathbf{k}\cdot\mathbf{z}\equiv\ell \,(\bmod M)}} \hat{f}_{\mathbf{k}}.$$

In total, the evaluation of such a function is realized by simply pre-computing $(\hat{g}_\ell)_{\ell=0}^{M-1}$ and applying a one-dimensional inverse fast Fourier transform, see Algorithm 3.4.1.

3.4.1.2 Reconstruction of trigonometric polynomials

For the reconstruction of a multivariate trigonometric polynomial $f \in \Pi_I$ as in (3.1.2) from lattice points $\mathbf{x}_j \in \Lambda(\mathbf{z}, M, I)$, we utilize the exact integration property (3.2.4) and the fact that we have

$$\sum_{j=0}^{M-1} \left(\mathrm{e}^{2\pi\mathrm{i}\frac{(\mathbf{k}-\mathbf{h})\cdot\mathbf{z}}{M}}\right)^j = \begin{cases} M & \text{for } \mathbf{k}\cdot\mathbf{z} \equiv \mathbf{k}\cdot\mathbf{h} \,(\mathrm{mod} M), \\ 0 & \text{otherwise,} \end{cases} \tag{3.4.4}$$

and $\mathbf{F}^*\mathbf{F} = M\mathbf{I}$ with $\mathbf{I} \in \mathbb{C}^{|I|\times|I|}$ being the identity matrix. For the reconstruction of the Fourier coefficients $\hat{h}_{\mathbf{k}}$ we use a single one-dimensional fast Fourier transform. The entries of the resulting vector $(\hat{g}_\ell)_{\ell=0}^{M-1}$ are renumbered by means of the unique inverse mapping $\mathbf{k} \mapsto \mathbf{k}\cdot\mathbf{z} \bmod M$, see Algorithm 3.4.2.

3.4.2 Multiple rank-1 lattices

Under mild assumptions it was shown in Lemma 3.3.1 that it is possible to generate a reconstructing rank-1 lattice $\Lambda(\mathbf{z}, M, I)$ with some frequency set $I \subset \mathbb{Z}^d$ of finite cardinality $|I| < \infty$ and with the lattice size M being bounded by $|I| \leq M \leq |I|^2$. Usually, the lattice size M is close to $|I|^2$ and therefore still pretty large, despite the independency on the dimension d. To overcome this limitation it was suggested in [Käm18, Käm19] to use *multiple rank-1 lattices* that are a union of s rank-1 lattices

$$\Lambda(\mathbf{z}_1, M_1, \ldots, \mathbf{z}_s, M_s) := \bigcup_{j=1,\ldots,s} \Lambda(\mathbf{z}_j, M_j). \tag{3.4.5}$$

Then it is possible to determine a reconstructing sampling set for multivariate trigonometric polynomials in Π_I supported on the given frequency set I, with a probability of at least $1-\delta_s$, where we have constants $C_1, C_2 > 0$ and

$$\delta_s = C_1 \, \mathrm{e}^{-C_2 s}$$

as an upper bound on the probability that the approach fails. In [Käm19] it was proven that the upper bound on the lattice size improves to

$$M \leq C|I| \log |I| \tag{3.4.6}$$

for these particular reconstructing lattices.

3.4.3 Sparse fast Fourier transform

A major problem in reconstructing multivariate trigonometric polynomials

$$\sum_{\mathbf{k} \in I} \hat{f}_{\mathbf{k}} \, \mathrm{e}^{2\pi \mathrm{i} \mathbf{k} \cdot \mathbf{x}}, \quad \mathbf{x} \in \mathbb{T}^d,$$

is to choose a suitable frequency set $I \subset \mathbb{Z}^d$, which depends on the size and distribution of the Fourier coefficients $\hat{f}_{\mathbf{k}}$. For example, if f is an element of the Wiener algebra $\mathcal{A}(\mathbb{T}^d)$ given in (3.1.6), then the largest Fourier coefficients are located along the coordinate axis and form a hyperbolic cross I_N^d as in (3.1.5). Without any additional information on f or the Fourier coefficients $\hat{f}_{\mathbf{k}}$, it is generally not possible to immediately know which frequencies $\mathbf{k}$ belong to the largest Fourier coefficients $\hat{f}_{\mathbf{k}}$. There is the danger of picking frequency sets that do not include all of the largest Fourier coefficients, and choosing larger frequency sets in order to catch all the large Fourier coefficients will cause a significant increase in computation time in higher dimensions.

Alternatively, we find dimension incremental algorithms in [Vol15, PV16] that reconstruct sparse multivariate trigonometric polynomials with an unknown support in a frequency domain $I \subset \mathbb{Z}^d$ – the sparse fast Fourier transforms (sparse FFT). Based on the component-by-component construction of rank-1 lattices, the approach of [PV16, Algorithm 1 and Algorithm 2] describes a dimension incremental construction of a frequency set $I \subset \mathbb{Z}^d$ belonging to the approximately $|I|$ largest Fourier coefficients. For such a construction the initial search space is restricted to a full grid $[-N, N]^d \cap \mathbb{Z}^d$ of refinement $N \in \mathbb{N}$ and it is assumed that the cardinality of the support of the multivariate trigonometric polynomial is bounded by a sparsity $s \in \mathbb{N}$. Eventually, we end up with up to s non-zero Fourier coefficients $\hat{f}_{\mathbf{k}}$ of the initially given function f.

Furthermore, these techniques were adapted for multiple rank-1 lattices [KPV20, KKV20] and also found application for solving ordinary differential equations [BKP20].

3.5 Discrete approximation errors

We discretize the L_∞-error in Theorem 3.3.2 and the L_2-error appearing in Theorem 3.3.3 in order to evaluate numerical tests on the upper approximation error bounds. In both cases we use the sample data vector $\mathbf{f} := (f(\mathbf{x}_j))_{j=0}^{M-1}$ with rank-1 lattice nodes $\mathbf{x}_j \in \Lambda(\mathbf{z}, M, I)$ and apply Algorithm 3.4.2, which yields the vector of approximated Fourier coefficients $\hat{\mathbf{f}} = (\hat{f}_{\mathbf{k}})_{\mathbf{k}\in I} = M^{-1}\mathbf{F}^*\mathbf{f}$, so that we can form the approximated Fourier partial sum $S_I^\Lambda f$.

We provide arguments on the number M of samples that are theoretically needed to obtain accurate approximated error norms. However, for practical purposes these numbers are unnecessarily large, so that we resort to a smaller but reasonably large number of randomized sampling points in our numerical tests later on.

3.5.1 The ℓ_∞-approximation error

For the discretization of the L_∞-error in Theorem 3.3.2 we utilize combinatorial arguments from [DTU18] to cover the torus $\mathbb{T}^d \simeq \left[-\frac{1}{2}, \frac{1}{2}\right]^d$ by a large enough number of ε-balls. In a Banach space X the unit ball is defined as $B_X := \{x \in X : \|x\|_X \leq 1\}$. A ball with radius $\varepsilon > 0$ centered at y in a Banach space X is denoted by $B_X(y, \varepsilon) := \{x \in X : \|y - x\|_X \leq \varepsilon\}$. For a compact set S we define the *n-th entropy number*, $n \in \mathbb{N}$ as

$$\varepsilon_n(S, X) := \inf \left\{ \varepsilon > 0 : \exists y_1, \ldots, y_{2^n} \in X : S \subseteq \bigcup_{j=1}^{2^n} B_X(y_j, \varepsilon) \right\},$$

which quantifies the smallest possible radius ε of at most 2^n balls that cover the set S entirely. In [DTU18, Corollary 6.1.2] it states that for any d-dimensional Banach space X it holds

$$\varepsilon_n(B_X, X) \leq 3(2^{-\frac{n}{d}}),$$

which is applicable to the torus by choosing $X = \ell_\infty^d$ with the unit ball $B_{\ell_\infty^d} \simeq \mathbb{T}^d \simeq \left[-\frac{1}{2}, \frac{1}{2}\right)^d$. In order to discretize the L_∞-error in Theorem 3.3.2 of a d-dimensional function $f \in \mathcal{C}(\mathbb{T}^d)$ we define the *relative discrete ℓ_∞-approximation error*

$$\varepsilon_\infty^M(f, \{\mathbf{x}_j\}_{j=1}^M) := \frac{\max_{j\in\{0,\ldots,M-1\}} \left|f(\mathbf{x}_j) - S_I^\Lambda f(\mathbf{x}_j)\right|}{\max_{j\in\{0,\ldots,M-1\}} |f(\mathbf{x}_j)|}, \quad \mathbf{x}_j \in \left[-\frac{1}{2}, \frac{1}{2}\right]^d. \tag{3.5.1}$$

By choosing the sampling points $\mathbf{x}_j$ to be the center points of the ε-balls $B_{\ell_\infty^d}(\mathbf{x}_j, \varepsilon)$, the entropy number $\varepsilon_n(\mathbb{T}^d, \ell_\infty^d)$ provides a lower bound for the number M of ε-balls to cover the whole domain of f. Hence, if we want the entropy number $\varepsilon_n(\mathbb{T}^d, \ell_\infty^d)$ to be smaller than some threshold $\delta > 0$, we need a large enough number $M = 2^n$ of ε-balls to cover the whole domain of f, where

$$n > d \log_2 \left(\frac{3}{\delta}\right). \tag{3.5.2}$$

In practice, we want to sample f at random points, e.g. uniformly distributed nodes $\mathbf{x}_j \sim \mathcal{U}\left(-\frac{1}{2}, \frac{1}{2}\right)$, where $\mathcal{U}\left(\left[-\frac{1}{2}, \frac{1}{2}\right]^d\right)$ denotes the continuous uniform distribution on the cube $\left[-\frac{1}{2}, \frac{1}{2}\right]^d$. If we have a covering of the domain of f and we randomly sample f at a point $\mathbf{y}_0$ within an ε-ball $B_X(\mathbf{y}, \varepsilon)$ and f is at least Lipschitz continuous, then $\|f(\mathbf{y}) - f(\mathbf{y}_0)\|_{L_\infty(\mathbb{T}^d)} \leq$

$L\|\mathbf{y}-\mathbf{y}_0\|_{L_\infty(\mathbb{T}^d)} \le L\varepsilon$ with some constant $L \ge 0$. So, even if we sample somewhere close to the center points $\mathbf{y}$ within an ε-ball $B_X(\mathbf{y},\varepsilon)$, the discrete ℓ_∞-approximation error ε_∞^M is bounded from above by $C\varepsilon_\infty^M$ with some constant $C = C(L,d) > 0$. In total, the above arguments show that the L_∞-approximation error $\left\|f - S_I^\Lambda f\right\|_{L_\infty(\mathbb{T}^d)}$ is discretized well enough by the ℓ_∞^d- approximation error $\left\|f - S_I^\Lambda f\right\|_{\ell_\infty^d}$ if the number M of random function evaluations $\{f(\mathbf{x}_j)\}_{j=1}^M$ is large enough.

3.5.2 The ℓ_2-approximation error

For the discretization of the L_2-approximation error in Theorem 3.3.3, we make use of the Hoeffding's inequality [CZ07, Proposition 3.5]:

Lemma 3.5.1. *Let $f \in L_2(\mathbb{T}^d)$ and $\{\xi_j := f(X_j)^2\}_{j=1}^M$ with X_j being independent random variables in a probability space $(\mathcal{Z},\varrho)$ with means $\mu := \mathbb{E}(\xi_j) = \int_{\left[-\frac{1}{2},\frac{1}{2}\right]^d} f(x_j)^2 \,\mathrm{d}\varrho(x_j)$ satisfying $|\xi_j(z)-\mu| \le K$ for each $j \in \{1,\dots,M\}$ and almost all $z \in \mathcal{Z}$. For every $\varepsilon > 0$ it holds*

$$\mathbb{P}\left(\frac{1}{M}\sum_{j=1}^M \xi_j - \mu > \varepsilon\right) \le \exp\left(-\frac{M\varepsilon^2}{2K^2}\right).$$

Hence, if we want the probability in the previous lemma to be smaller than some $\delta > 0$ for a fixed $\varepsilon > 0$, then we need a large enough number of sampling points $M = M(\varepsilon)$ with

$$M > 2K^2 \log\left(\frac{1}{\delta}\right)\frac{1}{\varepsilon^2}, \tag{3.5.3}$$

so that

$$\left\|f - S_I^\Lambda f\right\|_{L_2(\mathbb{T}^d)}^2 \approx \frac{1}{M}\sum_{j=0}^{M-1}\left|f(\mathbf{x}_j) - S_I^\Lambda f(\mathbf{x}_j)\right|^2$$

for uniformly distributed sampling nodes $\mathbf{x}_j \sim \mathcal{U}\left(\left[-\frac{1}{2},\frac{1}{2}\right]^d\right)$. Finally, we define the *relative discrete ℓ_2-approximation error* as

$$\varepsilon_2^M(f,\{\mathbf{x}_j\}_{j=1}^M) := \frac{\sum_{j=0}^{M-1}\left|f(\mathbf{x}_j) - S_I^\Lambda f(\mathbf{x}_j)\right|^2}{\sum_{j=0}^{M-1}|f(\mathbf{x}_j)|^2}, \tag{3.5.4}$$

where the nodes $\mathbf{x}_j \in \left[-\frac{1}{2},\frac{1}{2}\right]^d$ may be generated randomly.

Remark 3.5.2. *By Parseval's equation we have*

$$\begin{aligned}\left\|f - S_I^\Lambda f\right\|_{L_2(\mathbb{T}^d)}^2 &= \sum_{\mathbf{k}\in\mathbb{Z}^d}|\hat{f}_\mathbf{k} - \hat{f}_\mathbf{k}^\Lambda|^2 = \sum_{\mathbf{k}\in\mathbb{Z}^d\setminus I}|\hat{f}_\mathbf{k}|^2 + \sum_{\mathbf{k}\in I}|\hat{f}_\mathbf{k} - \hat{f}_\mathbf{k}^\Lambda|^2 \\ &= \|f\|_{L_2(\mathbb{T}^d)}^2 + \sum_{\mathbf{k}\in I}\left(|\hat{f}_\mathbf{k} - \hat{f}_\mathbf{k}^\Lambda|^2 - |\hat{f}_\mathbf{k}|^2\right).\end{aligned}$$

So, if the Fourier coefficients $\hat{f}_\mathbf{k}, \mathbf{k} \in I_N^d$ are known, we can evaluate the L_2-approximation error if we use Algorithm 3.4.2 to reconstruct the approximated Fourier coefficients $\hat{f}_\mathbf{k}^\Lambda$. However, our considered functions will be too complicated to calculate the exact Fourier coefficients. □

Remark 3.5.3. *The lower bounds* (3.5.2) *and* (3.5.3) *on the number of random sampling points M are worst case bounds to theoretically ensure that the discrete approximation errors ε_∞^M and ε_2^M are below a fixed threshold $\delta > 0$ with high probability. For practical purposes such as for high dimensional numerical experiments, these lower bounds are unnecessarily large. We will use a smaller but still reasonable large number of sampling points in our numerical tests.* □

Random sample generation

The previous arguments on the discretization of the L_∞-error in Theorem 3.3.2 and the L_2-error appearing in Theorem 3.3.3 were based on uniformly distributed sampling nodes $x_j \sim \mathcal{U}\left(\left[-\frac{1}{2}, \frac{1}{2}\right]\right), j \in \{1, \ldots, M\}$. But, in higher dimensions $d \geq 5$, the straight-forward evaluation of the errors ε_∞^M and ε_2^M ends up being quite time-consuming, even for only $M = 10^6$ or $M = 10^7$ nodes.

Therefore, we make use of the dimension-independent efficiency of Algorithm 3.4.1 and simulate a uniform distribution with a set of different rank-1 lattices. We generate ten random rank-1 lattices $\{\Lambda(\mathbf{z}_{r_1}, M_{r_1}), \ldots, \Lambda(\mathbf{z}_{r_{10}}, M_{r_{10}})\}$ with $M_{\text{total}} = \sum_{j=1}^{10} M_{r_j}$ and evaluate the approximated Fourier sums $S_{I_N^d}^{\Lambda} f$ in the discrete approximation errors

$$\varepsilon_\infty^{M_{\text{total}}}(f) \quad \text{and} \quad \varepsilon_2^{M_{\text{total}}}(f) \tag{3.5.5}$$

in (3.5.1) and (3.5.4) with the efficient Algorithm 3.4.1. We try to avoid the evaluation at the same rank-1 lattice $\Lambda(\mathbf{z}, M, I), \mathbf{z} = (z_1, z_2, \ldots, z_d)^\top \in \mathbb{Z}^d$ that is initially used to reconstruct the approximated Fourier coefficients $\hat{f}_{\mathbf{k}}^{\Lambda}$. So, for all $j \in \{1, \ldots, d\}$ we generate $\mathbf{z}_{r_j} := (1, z_2^{r_j}, \ldots, z_d^{r_j})^\top$ with $z_i^{r_j} \sim z_d + \mathcal{U}\{1, z_d\}, i \in \{2, \ldots, d\}$, where $\mathcal{U}\{1, z_d\}$ denotes the discrete uniform distribution on the integers $\{1, 2, \ldots, z_d\}$, and $M_{r_j} \sim \lceil \frac{M}{2} \rceil + 2\mathcal{U}\{1, 2M\} + 1$. These distribution choices make it unlikely that we generate the original rank-1 lattice and we most likely sample at ten completely different rank-1 lattices. Furthermore, it is ensured that the ten random rank-1 lattices are not arbitrarily large.

Chapter 4

Torus-to-$\mathbb{R}^d$ transformation mappings

We introduce the notation of torus-to-$\mathbb{R}^d$ mappings $\psi = (\psi_1, \ldots, \psi_d) : \left(-\frac{1}{2}, \frac{1}{2}\right)^d \to \mathbb{R}^d$ and prove a set of conditions on the transformations ψ for a given function space $L_2(\mathbb{R}^d, \omega) \cap H^m_{\text{mix}}(\mathbb{R}^d)$ such that we obtain a bounded periodization mapping of the form

$$L_2(\mathbb{R}^d, \omega) \cap H^m_{\text{mix}}(\mathbb{R}^d) \ni h \mapsto h(\psi(\cdot)) \sqrt{\omega(\psi(\cdot)) \prod_{j=1}^{d} \psi_j'(\cdot)} \in \mathcal{H}^m(\mathbb{T}^d).$$

This allows us to freely apply the variety of approximation techniques for smooth periodic function on the torus $\mathbb{T}^d$ from Chapter 3 and transfer the orthonormality of the Fourier system, important upper approximation error bounds and the efficient algorithms based on rank-1 lattices by means of the inverse torus-to-$\mathbb{R}^d$ transformation ψ^{-1} to the considered non-periodic function class defined on $\mathbb{R}^d$. Parts of the content in this chapter were already published in [NP20].

In Section 4.1 we define increasing and invertible torus-to-$\mathbb{R}^d$ transformations ψ, cf. (4.1.1), and fix the notation of the density function ϱ as the derivative of the inverse of a torus-to-$\mathbb{R}^d$ transformation.

Then in Section 4.2 we list and compare important examples of torus-to-$\mathbb{R}^d$ transformations.

Afterwards in Section 4.3 we investigate the structure of weighted exponential functions $\left\{\sqrt{\frac{\varrho(\cdot)}{\omega(\cdot)}}\, \mathrm{e}^{2\pi \mathrm{i} \mathbf{k} \cdot \psi^{-1}(\cdot)}\right\}_{\mathbf{k} \in \mathbb{Z}^d}$, cf. (4.3.2), that form an orthonormal system in the weighted $L_2(\mathbb{R}^d, \omega)$-function space and will often be refered to as the *transformed Fourier system*.

In Section 4.4 we discuss - at first in one dimension - the periodization approach via torus-to-$\mathbb{R}$ transformations, that map functions $h \in L_2(\mathbb{R}, \omega)$ onto functions $f \in L_2(\mathbb{T})$ of the form $f(x) := h(\psi(x)) \sqrt{\omega(\psi(x))\, \psi'(x)}$, so that $\|h\|_{L_2(\mathbb{R},\omega)} = \|f\|_{L_2(\mathbb{T})}$. Then, we assume additional smoothness so that a given function h is additionally in the Sobolev space $H^m(\mathbb{R})$, cf. (2.0.8). We prove the major Theorem 4.4.1 - with its multivariate analogue in Theorem 4.4.2 - in which we provide a set of sufficient L_∞-conditions on the torus-to-$\mathbb{R}$ transformations ψ and the measure functions ω for which the periodized function f inherits the smoothness from h so that it is an element of the Sobolev space $\mathcal{H}^m(\mathbb{T})$.

In Section 4.5 we prove weighted upper $L_\infty\left(\mathbb{R}^d, \sqrt{\frac{\omega}{\varrho}}\right)$- and $L_2\left(\mathbb{R}^d, \omega\right)$-approximation error bounds based on the worst case upper $L_\infty\left(\mathbb{T}^d\right)$- and $L_2\left(\mathbb{T}^d\right)$-approximation estimates from Section 3.5.

In Section 4.6 we begin to consider parameterized torus-to-$\mathbb{R}^d$ transformations $\psi(\cdot, \boldsymbol{\eta})$ and measure functions $\omega(\cdot, \boldsymbol{\mu})$ with $\boldsymbol{\eta}, \boldsymbol{\mu} \in \mathbb{R}_+^d$. We adapt the Algorithms 3.4.1 and 3.4.2 by incorporating the inverse torus-to-$\mathbb{R}^d$ transformation $\psi^{-1}(\cdot, \boldsymbol{\eta})$ and compare some transformed rank-1 lattices $\Lambda_{\psi(\cdot,\boldsymbol{\eta})}(\mathbf{z}, M)$.

Section 4.7 we consider a parameterized Gaussian measure function $\omega(\cdot, \boldsymbol{\mu})$ as well as a Gaussian function h, cf. (4.7.2) and (4.7.1) and discuss the application of the parameterized error function transformation (4.7.3). Based on the L_∞-conditions (4.4.9) in Theorem 4.4.2 we calculate worst case lower parameter bounds for which the transformed functions f are in $\mathcal{H}^m(\mathbb{T})$ with $m \in \{0, 1, 2, 3\}$. We calculate the discrete approximations errors $\varepsilon_2^M(h, \{\mathbf{y}_j\}_{j=1}^M)$ and $\varepsilon_\infty^M(h, \{\mathbf{y}_j\}_{j=1}^M)$ given in (4.6.2) in dimensions $d \in \{1, 2\}$ with single rank-1 lattice methods. For dimensions $d \geq 4$ we switch to multiple rank-1 lattices and again compare the difference in the approximation errors when switching the frequency set from a hyperbolic cross I_N^4 to a scaled ℓ_1^4-ball $I_N^{\ell_1^4}$. Finally, for dimension $d = 8$ we again use the sparse FFT algorithm and highlight the power of the dimension incremental construction of suitable frequency sets.

In Section 4.8 we summarize the approximation results of the previous two numeric sections.

4.1 Torus-to-$\mathbb{R}^d$ transformations

Following the notation of [NP20, Section 3.1], we call a mapping

$$\psi : \left(-\frac{1}{2}, \frac{1}{2}\right) \to \mathbb{R} \quad \text{with} \quad \lim_{x \to \pm\frac{1}{2}} \psi(x) = \pm\infty \tag{4.1.1}$$

a *torus-to-$\mathbb{R}$ transformation* if it is continuously differentiable and increasing. The inverse transformation is also continuously differentiable, increasing and is denoted by $\psi^{-1} : \mathbb{R} \to (-\frac{1}{2}, \frac{1}{2})$ in the sense of $y = \psi(x) \Leftrightarrow x = \psi^{-1}(y)$ with $\psi^{-1}(y) \to \pm\frac{1}{2}$ as $y \to \pm\infty$. We call the derivative of the inverse transformation the *density function ϱ of ψ*, which is a non-negative $L_1(\mathbb{R}^d)$-function, given by

$$\varrho(y) := (\psi^{-1})'(y) = \frac{1}{\psi'(\psi^{-1}(y))}.$$

In multiple dimensions we put

$$\psi(\mathbf{x}) := (\psi_1(x_1), \ldots, \psi_d(x_d))^\top$$

with $\mathbf{x} \in (-\frac{1}{2}, \frac{1}{2})^d$ and call them *torus-to-$\mathbb{R}^d$ transformations*, where we may use different transformations ψ_j in each coordinate $j \in \{1, \ldots, d\}$. The corresponding multivariate inverse transformation is denoted by $\psi^{-1}(\mathbf{y}) := (\psi_1^{-1}(y_1), \ldots, \psi_d^{-1}(y_d))^\top$ and the density is given by

$$\varrho(\mathbf{y}) := \prod_{j=1}^d \varrho_j(y_j), \quad \mathbf{y} \in \mathbb{R}^d. \tag{4.1.2}$$

Later on, we consider families of parameterized torus-to-$\mathbb{R}^d$ transformations

$$\psi(\mathbf{x}, \boldsymbol{\eta}) := (\psi_1(x_1, \eta_1), \ldots, \psi_d(x_d, \eta_d))^\top \tag{4.1.3}$$

with $\boldsymbol{\eta} = (\eta_1, \dots, \eta_d)^\top \in \mathbb{R}_+^d$. We only consider parametrizations for which the transformation ψ, its inverse ψ^{-1} and the density function ϱ fit into the given definitions above despite being impacted by the parameter $\boldsymbol{\eta}$. In (4.7.3), we will use parameterized torus-to-$\mathbb{R}^d$ transformations of the form

$$\psi(\mathbf{x}, \boldsymbol{\eta}) := \boldsymbol{\eta} \cdot \psi(\mathbf{x}) \tag{4.1.4}$$

with $\boldsymbol{\eta} \in (0, \infty)^d$, which is a kind of parameterization that is also used in [KPPW20]. As the transformations are going to be composed with functions defined on $\mathbb{R}^d$, the parameter $\boldsymbol{\eta}$ may impact the smoothness of the resulting transformed functions, which we will discuss in depth later on.

Remark 4.1.1. *For now, we omit the parameter in the notation for simplicity and proceed to just write $\psi(\cdot)$ until we actually consider particular parameterized families of the form* (4.1.3) *or* (4.1.4). □

4.2 Exemplary transformations

We list some feasible univariate transformations ψ with either an exponential or an algebraic density function ϱ, some of which were suggested in the literature, see e.g.,[Boy00, Section 17.6], [STW11, Section 7.5], [Ste93, Example 4.2.8 and 4.2.9] or [NP20]. For now, with Remark 4.1.1 in mind, we list these transformations for simplicity in their univariate non-parameterized form with $\eta = 1$ and $\psi(x) = \psi(x, 1)$.

Let $x \in (-\frac{1}{2}, \frac{1}{2})$ and $y \in \mathbb{R}$. We are particularly interested in the following transformations:

- *error function (torus-to-$\mathbb{R}$) transformation*:

$$\begin{aligned} \psi(x) &= \operatorname{erf}^{-1}(2x), \quad \psi'(x) = \sqrt{\pi}\, \mathrm{e}^{(\operatorname{erf}^{-1}(2x))^2} \\ \psi^{-1}(y) &= \frac{1}{2} \operatorname{erf}(y), \quad \varrho(y) = \frac{1}{\sqrt{\pi}} \mathrm{e}^{-y^2} \end{aligned} \tag{4.2.1}$$

  with the error function

$$\operatorname{erf}(x) = \frac{1}{\sqrt{\pi}} \int_{-x}^{x} \mathrm{e}^{-t^2}\, \mathrm{d}t, \quad x \in \mathbb{R}, \tag{4.2.2}$$

  and $\operatorname{erf}^{-1}(\cdot)$ denoting the inverse error function

- *logarithmic (torus-to-$\mathbb{R}$) transformation*:

$$\begin{aligned} \psi(x) &= \frac{1}{2} \log\left(\frac{1+2x}{1-2x}\right) = \tanh^{-1}(2x), \quad \psi'(x) = \frac{2}{1-4x^2}, \\ \psi^{-1}(y) &= \frac{1}{2}\left(\frac{\mathrm{e}^{2y}-1}{\mathrm{e}^{2y}+1}\right) = \frac{1}{2}\tanh(y), \quad \varrho(y) = \frac{2\mathrm{e}^{2y}}{(\mathrm{e}^{2y}+1)^2} \end{aligned} \tag{4.2.3}$$

- *algebraic (torus-to-$\mathbb{R}$) transformation*:

$$\begin{aligned} \psi(x) &= \frac{2x}{(1-4x^2)^{\frac{1}{2}}}, \quad \psi'(x) = \frac{2}{(1-4x^2)^{\frac{3}{2}}}, \\ \psi^{-1}(y) &= \frac{y}{2(1+y^2)^{\frac{1}{2}}}, \quad \varrho(y) = \frac{1}{2(1+y^2)^{\frac{3}{2}}} \end{aligned} \tag{4.2.4}$$

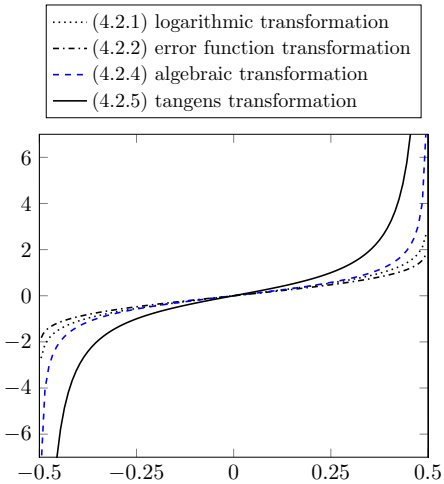

Figure 4.2.1: Plots of exemplary transformations (4.2.1)-(4.2.5).

- *tangent (torus-to-$\mathbb{R}$) transformation*:

$$\psi(x) = \tan(\pi x), \quad \psi'(x) = \frac{\pi}{\cos^2(\pi x)} \tag{4.2.5}$$
$$\psi^{-1}(y) = \frac{1}{\pi}\arctan(y), \quad \varrho(y) = \frac{1}{\pi}\left(\frac{1}{1+y^2}\right)$$

For a side-by-side comparison of their individual slope see Figure 4.2.1.

We will define so-called *torus-to-cube* transformations in (5.1.1) that are defined in a similar fashion as the torus-to-$\mathbb{R}$ transformations (4.1.1). A specific type of a torus-to-cube transformation will be induced by torus-to-$\mathbb{R}$ transformations. In particular, the error function logarithmic and the logarithmic (torus-to-$\mathbb{R}$) transformation (4.2.1) and (4.2.3) induce the the error function and the logarithmic (torus-to-cube) transformation (5.2.2) and (5.2.1). The center pieces of these names are only denoted in their original definition to emphasize that there are two different error function and two different logarithmic transformations. Usually, we omit the specification if a transformation maps to $\mathbb{R}$ or the cube as it is clear from the context about which one is used.

4.3 Weighted Hilbert spaces on $\mathbb{R}^d$

We consider families of parameterized integrable measure functions $\omega(\cdot, \boldsymbol{\mu}), \boldsymbol{\mu} \in \mathbb{R}^d_+$ of the form

$$\omega(\mathbf{y}, \boldsymbol{\mu}) := \prod_{j=1}^{d} \omega_j(y_j, \mu_j), \quad \omega_j(y_j, \mu_j) \in \mathcal{C}_0(\mathbb{R}), \tag{4.3.1}$$

such that for any given torus-to-$\mathbb{R}^d$ transformation $\psi(\cdot, \boldsymbol{\eta}), \boldsymbol{\eta} \in \mathbb{R}^d_+$ as in (4.1.3) we have

$$\omega(\psi_j(\cdot, \eta_j), \mu_j)\psi'(\cdot, \eta_j) \in \mathcal{C}_0\left(\left[-\frac{1}{2}, \frac{1}{2}\right]\right) \quad \text{with} \quad \omega\left(\psi_j\left(\pm\frac{1}{2}, \eta_j\right), \mu_j\right)\psi'\left(\pm\frac{1}{2}, \eta_j\right) := 0.$$

By putting $y_j = \psi_j(x_j, \eta_j) \in \mathbb{R}, x_j \in \left[-\frac{1}{2}, \frac{1}{2}\right]$, this property is equivalently stated as $\frac{\omega(\cdot,\mu_j)}{\varrho(\cdot,\eta_j)} \in \mathcal{C}_0(\mathbb{R})$. Consequentially, the transformed Fourier system in (4.3.2) will always be an unbounded system.

For now, we remain in the univariate case and we simplify the notation of the transformation, the weight function, and all related functions by omitting any parameter and write $\psi(\cdot), \omega(\cdot)$, etc. We describe the structure of the univariate weighted $L_2(\mathbb{R}, \omega)$-function spaces as defined in (2.0.7). The transformed Fourier system $\{\varphi_k\}_{k\in\mathbb{Z}}$ of weighted exponential functions

$$\varphi_k(y) := \sqrt{\frac{\varrho(y)}{\omega(y)}}\, \mathrm{e}^{2\pi \mathrm{i} k \psi^{-1}(y)}, \quad y \in \mathbb{R}, \tag{4.3.2}$$

forms an orthonormal system with respect to the scalar product

$$(h_1, h_2)_{L_2(\mathbb{R},\omega)} := \int_{\mathbb{R}} h_1(y)\, \overline{h_2(y)}\, \omega(y)\, \mathrm{d}y \tag{4.3.3}$$

and for $k_1, k_2 \in \mathbb{Z}$ we have

$$(\varphi_{k_1}, \varphi_{k_2})_{L_2(\mathbb{R},\omega)} = \delta_{k_1,k_2}.$$

The weighted scalar product (4.3.3) induces the norm

$$\|h\|_{L_2(\mathbb{R},\omega)} := \sqrt{(h,h)_{L_2(\mathbb{R},\omega)}}$$

and we have Fourier coefficients of the form

$$\hat{h}_k := (h, \varphi_k)_{L_2(\mathbb{R},\omega)} = \int_{\mathbb{R}} h(y)\, \sqrt{\varrho(y)\, \omega(y)}\, \mathrm{e}^{-2\pi \mathrm{i} k \psi^{-1}(y)}\, \mathrm{d}y, \tag{4.3.4}$$

as well as the respective Fourier partial sum for $I \subset \mathbb{Z}$ given by

$$S_I h(y) := \sum_{k\in I} \hat{h}_k\, \varphi_k(y). \tag{4.3.5}$$

Example 4.3.1. • *For the error function transformation* (4.2.1) *with the density* $\varrho(y) = \frac{1}{\sqrt{\pi}}\, \mathrm{e}^{-y^2}$ *and the Gaussian measure function*

$$\omega(y, \mu) = \frac{1}{\sqrt{\pi}} \mathrm{e}^{-\mu^2 y^2}, \quad \mu \in \mathbb{R}, \tag{4.3.6}$$

the orthonormal functions φ_k *as in* (4.3.2) *are of the form*

$$\varphi_k(y) = \mathrm{e}^{\frac{1}{2}(\mu^2-1)y^2 + \pi \mathrm{i} k\, \mathrm{erf}(y)}, \tag{4.3.7}$$

with graphs of their real and imaginary parts for $\mu = \sqrt{2}$ *and* $k = 0, 1, 2, 3$ *shown in Figure* (4.3.1). *The corresponding weighted scalar product* (4.3.3) *reads as*

$$(h_1, h_2)_{L_2(\mathbb{R},\omega(\cdot,\mu))} = \frac{1}{\sqrt{\pi}} \int_{\mathbb{R}} \mathrm{e}^{-\mu^2 y^2}\, h_1(y)\, \overline{h_2(y)}\, \mathrm{d}y.$$

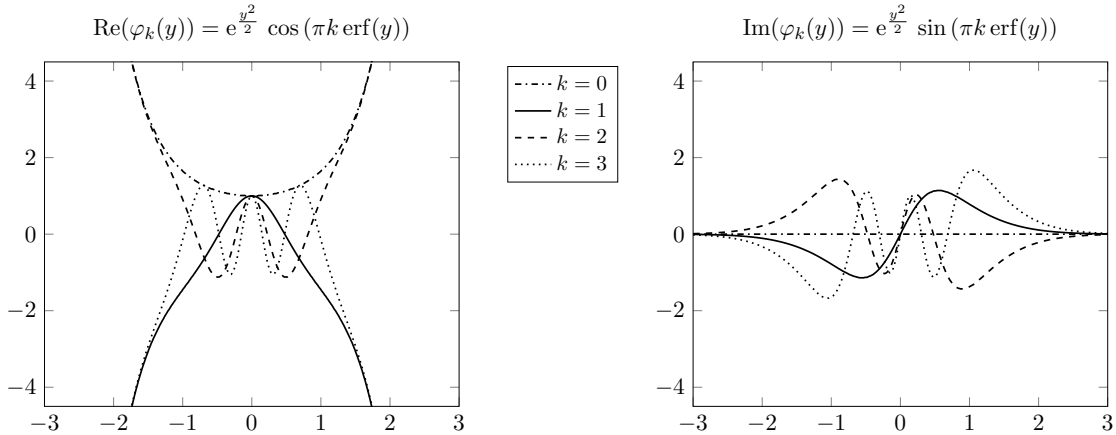

Figure 4.3.1: Real and imaginary part of the weighted exponential functions φ_k in (4.3.7) for $k = 0, 1, 2, 3$ and the fixed parameter $\mu = \sqrt{2}$.

4.4 Smoothness properties of transformed functions

In this section we characterize the smoothness properties of functions $h \in L_2(\mathbb{R}^d, \omega)$ and of their corresponding transformed versions on the torus $\mathbb{T}^d$ after the application of a torus-to-$\mathbb{R}^d$ transformation ψ given in (4.1.1). We propose specific sufficient conditions for ψ and ω such that the transformed functions are in $\mathcal{H}^m(\mathbb{T}^d)$ with $m \in \mathbb{N}_0$. These conditions are stated for both univariate and multivariate functions. Afterwards, we utilize the embedding $\mathcal{H}^{\beta+\lambda}(\mathbb{T}^d) \hookrightarrow \mathcal{A}^\beta(\mathbb{T}^d)$ in (3.1.9) for $\lambda = 1$ to discuss high-dimensional approximation problems, in which we apply fast Fourier approximation methods based on rank-1 lattices. Throughout this section we still omit the parameters $\boldsymbol{\eta}, \boldsymbol{\mu} \in \mathbb{R}_+^d$ in the notation of the torus-to-$\mathbb{R}^d$ transformations ψ and the measure functions ω.

For now we remain in the univariate case. Given a class of functions $h \in L_2(\mathbb{R}, \omega)$ with a measure function $\omega \in \mathcal{C}_0(\mathbb{R})$, we consider a torus-to-$\mathbb{R}$ transformation $y = \psi(x)$ as defined in (4.1.1), such that $\omega(\psi(x))\psi'(x) \in \mathbb{T}$, in order to transform any such function h into a function $f \in L_2(\mathbb{T})$ of the form

$$f(x) := h(\psi(x)) \sqrt{\omega(\psi(x))\, \psi'(x)}, \quad x \in \mathbb{T}, \tag{4.4.1}$$

for which we have the identity

$$\|h\|^2_{L_2(\mathbb{R},\omega)} = \int_{\mathbb{R}} |h(y)|^2 \, \omega(y) \, \mathrm{d}y = \int_{\mathbb{T}} |h(\psi(x))|^2 \, \omega(\psi(x)) \, \psi'(x) \, \mathrm{d}x = \|f\|^2_{L_2(\mathbb{T})}.$$

This is illustrated schematically in Figure 4.4.1.

Generally, it is rather difficult to check if such a transformed function f is in $\mathcal{H}^m(\mathbb{T})$ for some fixed $m \in \mathbb{N}_0$ by calculating the Sobolev norm $\|f\|_{\mathcal{H}^m(\mathbb{T})}$. We propose a set of sufficient conditions such that $f \in \mathcal{H}^m(\mathbb{T})$ with $m \in \mathbb{N}_0$, that utilize the product structure of the functions f in (4.4.1) and eliminate the necessity to be able to calculate either the exact Fourier coefficients $\hat{f}_k$ or the L_2-norms of various derivatives of f appearing in the equivalent Sobolev norm $\|f\|_{H^m(\mathbb{T})}$. When we use parameterized families of torus-to-$\mathbb{R}$ transformations $\psi(\cdot, \eta)$ and families of measure functions $\omega(\cdot, \mu)$, we will calculate how large the parameters $\eta, \mu \in \mathbb{R}_+$ have to be in order to preserve the fixed degree of smoothness m when transforming $h \in L_2(\mathbb{R}, \omega(\cdot, \mu)) \cap H^m(\mathbb{R})$ into $f \in \mathcal{H}^m(\mathbb{T})$ via $\psi(\cdot, \eta)$.

$$\begin{tikzcd}
\mathbb{T} \simeq [-\frac{1}{2}, \frac{1}{2}) \quad \supset \quad (-\frac{1}{2}, \frac{1}{2}) \arrow[r, shift left, "\psi"] \arrow[dr, "L_2(\mathbb{T}) \ni h(\psi(x))\sqrt{\omega(\psi(x))\psi'(x)} =: f(x)"'] & \mathbb{R} \arrow[l, shift left, "\psi^{-1}"] \arrow[d, "h(y) \in L_2(\mathbb{R},\omega)"] \\
& \mathbb{C}
\end{tikzcd}$$

Figure 4.4.1: Scheme of the relation between the given function $h \in L_2(\mathbb{R}^d, \omega)$ and the periodization $f \in L_2(\mathbb{T})$ resulting from applying the torus-to-$\mathbb{R}$ transformation ψ.

Now, we propose a set of sufficient univariate conditions such that we obtain smooth transformed function $f \in \mathcal{H}^m(\mathbb{T})$.

Theorem 4.4.1 ([NP20, Theorem 3.4])**.** *Let $m \in \mathbb{N}_0$, a $h \in L_2(\mathbb{R}, \omega) \cap H^m(\mathbb{R})$ with a measure function $\omega \in \mathcal{C}_0^m(\mathbb{R})$ be given. Considering a torus-to-$\mathbb{R}$ transformation $\psi \in \mathcal{C}^m((-\frac{1}{2}, \frac{1}{2}))$ with the density function $\varrho \in \mathcal{C}_0^m(\mathbb{R})$, if for all $n \in \{0, 1, \ldots, m\}$ the condition*

$$\max_{k=0,\ldots,n} \left\| \left(\sqrt{(\omega \circ \psi)\, \psi'} \right)^{(n-k)} (\cdot)\, \psi'(\cdot)^{\max(-\frac{1}{2}, 2k-\frac{3}{2})} \right\|_{L_\infty(\mathbb{T})} < \infty$$

holds, then the transformation operator

$$\begin{aligned} T : L_2(\mathbb{R}, \omega) \cap \mathrm{H}^m(\mathbb{R}) &\to \mathcal{H}^m(\mathbb{T}) \\ h &\mapsto h(\psi(\cdot))\sqrt{\omega(\psi(\cdot))\psi'(\cdot)} =: f(\cdot) \end{aligned}$$

is bounded, where f of the form (4.4.1)*.*

Proof. For $h \in L_2(\mathbb{R}, \omega) \cap H^m(\mathbb{R})$ with $m \in \mathbb{N}_0$ and a torus-to-$\mathbb{R}$ transformation ψ as defined in (4.1.1) we consider the transformed function f of the form (4.4.1). We apply the generalized Leibniz rule (2.0.1) to the Sobolev norm of f, which leads to

$$\begin{aligned} \|f\|^2_{\mathcal{H}^m(\mathbb{T})} \sim \|f\|^2_{H^m(\mathbb{T})} &= \sum_{n=0}^{m} \|f^{(n)}(\cdot)\|^2_{L_2(\mathbb{T})} \\ &\leq \sum_{n=0}^{m} \left(\sum_{k=0}^{n} \binom{n}{k} \left\| (h \circ \psi)^{(k)}(\cdot) \left(\sqrt{(\omega \circ \psi)\, \psi'} \right)^{(n-k)} (\cdot) \right\|_{L_2(\mathbb{T})} \right)^2 . \end{aligned} \tag{4.4.2}$$

We leave $h \circ \psi$ in the term corresponding to $k = 0$ untouched for now. For $k \in \{1, \ldots, m\}$ we apply the Faá di Bruno formula (2.0.2) to the k-th derivative of the composition of functions h and ψ, and provide an upper estimate for the appearing Bell polynomials (2.0.3). By differentiating both sides of $\psi^{-1}(\psi(x)) = x$ we obtain

$$\psi'(x) = \frac{1}{\varrho(\psi(x))}, \qquad \psi^{(2)}(x) = -\frac{\varrho'(\psi(x))\psi'(x)}{\varrho(\psi(x))^2} = -\varrho'(\psi(x))\psi'(x)^3$$

and we observe that for $k \in \mathbb{N}$

$$\frac{\mathrm{d}}{\mathrm{d}x} \left[(\psi')^k \right](x) = k\psi'(x)^{k-1}\psi^{(2)}(x) = -k\psi'(x)^{k+2}\varrho'(\psi(x)). \tag{4.4.3}$$

Consequently, the k-th derivative of ψ can be expressed soley in terms of powers of ψ' and the first $(k-1)$ derivatives of ϱ by repeated insertion of the expression of $\psi^{(2)}$. Formula (4.4.3) implies that the highest appearing power of ψ' increases by 2 with each differentiation, which we indeed observe for the next two derivatives given by

$$\psi^{(3)}(x) = \psi'(x)^5 \left(-\frac{\varrho^{(2)}(\psi(x))}{\psi'(x)} + 3\varrho'(\psi(x)) \right),$$
$$\psi^{(4)}(x) = \psi'(x)^7 \left(-\frac{\varrho^{(3)}(\psi(x))}{\psi'(x)^2} + \frac{4\varrho^{(2)}(\psi(x))\varrho'(\psi(x)) + 6\varrho'(\psi(x))}{\psi'(x)} - 15\varrho'(\psi(x))^3 \right).$$

We note that each derivative of ψ is bounded, based on the fact that ϱ is by definition in $\mathcal{C}_0(\mathbb{R})$. Hence, $\varrho \circ \psi = 1/\psi' \in \mathcal{C}(\mathbb{T})$ and any power of $1/\psi'$ is also bounded. Additionally, we assumed that the first k derivatives of ϱ are in $\mathcal{C}_0(\mathbb{R})$, too. Therefore, with constants $C_k > 0$ and $C > 0$, for all $k \in \mathbb{N}$ we estimate

$$\left| \frac{\mathrm{d}^k}{\mathrm{d}x^k}[\psi](x) \right| \leq C_k |\psi'(x)|^{2k-1}$$

and for the Bell polynomials $B_{k,\ell}$ in (2.0.2) we estimate

$$\begin{aligned} &|B_{k,\ell}(\psi'(x), \psi^{(2)}(x), \ldots, \psi^{(k-\ell+1)}(x))| \\ &\leq C \cdot B_{k,\ell}(|\psi'(x)|, |\psi'(x)|^3, \ldots, |\psi'(x)|^{2(k-\ell+1)-1}). \end{aligned} \tag{4.4.4}$$

The Bell polynomials were defined according to the rules to partition a number $k \in \mathbb{N}$ into a sum of $\ell \in \{1, 2, \ldots, k\}$ natural numbers $j_1, \ldots, j_\ell \in \mathbb{N}$, that are given by

$$\begin{aligned} j_1 + j_2 + j_3 + \ldots + j_{k-\ell+1} &= \ell, \\ j_1 + 2j_2 + 3j_3 + \ldots + (k-\ell+1)j_{k-\ell+1} &= k. \end{aligned}$$

By substracting the first rule from two times the second rule we obtain

$$j_1 + 3j_2 + 5j_3 + \ldots + (2(k-\ell+1)-1)j_{k-\ell+1} = 2k - \ell$$

which reveals, that the highest power of $|\psi'|$ in the upper estimate of (4.4.4) is $2k-1$ and appears for $\ell = 1$. By extracting $|\psi'(x)|^{2k-1}$ from each $B_{k,\ell}$ the remaining polynomials consist only of powers of $1/\psi'$, which are all bounded. Hence, in (4.4.4) we estimate further and obtain

$$\begin{aligned} &|B_{k,\ell}(\psi'(x), \psi^{(2)}(x), \ldots, \psi^{(k-\ell+1)}(x))| \\ &\leq C \left| \psi'(x)^{2k-1} \frac{B_{k,\ell}(|\psi'(x)|, |\psi'(x)|^3, \ldots, |\psi'(x)|^{2(k-\ell+1)-1})}{\psi'(x)^{2k-1}} \right| \\ &\leq C' \left| \psi'(x)^{2k-1} \right| \end{aligned} \tag{4.4.5}$$

with constants $C, C' > 0$.

Now, for any n we investigate the L_2-norms in the previous estimate (4.4.2) of the Sobolev norm. For $k = 0$ we insert a productive one term, estimate the second half of the inital

integrand and apply a change of variables to obtain

$$\begin{aligned}
&\left\| (h\circ\psi)(\cdot)\left(\sqrt{(\omega\circ\psi)\,\psi'}\right)^{(n)}(\cdot)\right\|_{L_2(\mathbb{T})}\\
&=\left(\int_{-\frac12}^{\frac12}|h(\psi(x))|^2\,\psi'(x)\,\psi'(x)^{-1}\left(\left(\sqrt{(\omega\circ\psi)\,\psi'}\right)^{(n)}(x)\right)^2\,\mathrm{d}x\right)^{\frac12}\\
&\le\left(\int_{-\frac12}^{\frac12}|h(\psi(x))|^2\,\psi'(x)\left(\left\|\psi'(\cdot)^{-\frac12}\left(\sqrt{(\omega\circ\psi)\,\psi'}\right)^{(n)}(\cdot)\right\|_{L_\infty(\mathbb{T})}\right)^2\,\mathrm{d}x\right)^{\frac12}\\
&=\left\|\psi'(\cdot)^{-\frac12}\left(\sqrt{(\omega\circ\psi)\,\psi'}\right)^{(n)}(\cdot)\right\|_{L_\infty(\mathbb{T})}\left(\int_{-\infty}^{\infty}|h(y)|^2\,\mathrm{d}y\right)^{\frac12}.
\end{aligned}$$

For $k>0$ we utilize the upper bound (4.4.5) and estimate in a similar fashion that

$$\begin{aligned}
&\left\|(h\circ\psi)^{(k)}(\cdot)\left(\sqrt{(\omega\circ\psi)\,\psi'}\right)^{(n-k)}(\cdot)\right\|_{L_2(\mathbb{T})}\\
&=\left(\int_{-\frac12}^{\frac12}\left|(h\circ\psi)^{(k)}(x)\right|^2\psi'(x)\,\psi'(x)^{-1}\left(\left(\sqrt{(\omega\circ\psi)\,\psi'}\right)^{(n-k)}(x)\right)^2\,\mathrm{d}x\right)^{\frac12}\\
&\le\left\|\left(\sqrt{(\omega\circ\psi)\,\psi'}\right)^{(n-k)}(\cdot)\,\psi'(\cdot)^{2k-\frac32}\right\|_{L_\infty(\mathbb{T})}\left(\int_{-\frac12}^{\frac12}\left|\sum_{\ell=1}^{k}h^{(\ell)}(\psi(x))\right|^2\psi'(x)\,\mathrm{d}x\right)^{\frac12}\\
&=\left\|\left(\sqrt{(\omega\circ\psi)\,\psi'}\right)^{(n-k)}(\cdot)\,\psi'(\cdot)^{2k-\frac32}\right\|_{L_\infty(\mathbb{T})}\sum_{\ell=1}^{k}\left\|h^{(\ell)}(\cdot)\right\|_{L_2(\mathbb{R})}.
\end{aligned}$$

Hence, for arbitrary $k\in\mathbb{N}_0$ we have

$$\begin{aligned}
&\left\|(h\circ\psi)^{(k)}(\cdot)\left(\sqrt{(\omega\circ\psi)\,\psi'}\right)^{(n-k)}(\cdot)\right\|_{L_2(\mathbb{T})}\\
&\le\left\|\left(\sqrt{(\omega\circ\psi)\,\psi'}\right)^{(n-k)}(\cdot)\,\psi'(\cdot)^{\max(-\frac12,2k-\frac32)}\right\|_{L_\infty(\mathbb{T})}\sum_{\ell=0}^{k}\left\|h^{(\ell)}(\cdot)\right\|_{L_2(\mathbb{R})}.
\end{aligned}\tag{4.4.6}$$

Finally, by inserting (4.4.6) into (4.4.2) we obtain

$$\begin{aligned}
&\|f\|_{H^m(\mathbb{T})}\\
&\le\left(\sum_{n=0}^{m}\left(\sum_{k=0}^{n}\binom{n}{k}\left\|(h\circ\psi)^{(k)}(\cdot)\left(\sqrt{(\omega\circ\psi)\,\psi'}\right)^{(n-k)}(\cdot)\right\|_{L_2(\mathbb{T})}\right)^2\right)^{\frac12}\\
&\lesssim\left(\sum_{n=0}^{m}\left(\max_{k=0,\dots,n}\left\|\left(\sqrt{(\omega\circ\psi)\,\psi'}\right)^{(n-k)}(\cdot)\,\psi'(\cdot)^{\max(-\frac12,2k-\frac32)}\right\|_{L_\infty(\mathbb{T})}(n+1)\|h\|_{H^n(\mathbb{R})}\right)^2\right)^{\frac12}\\
&\lesssim\max_{n=0,\dots,m}\left(\max_{k=0,\dots,n}\left\|\left(\sqrt{(\omega\circ\psi)\,\psi'}\right)^{(n-k)}(\cdot)\,\psi'(\cdot)^{\max(-\frac12,2k-\frac32)}\right\|_{L_\infty(\mathbb{T})}\right)(m+1)^{\frac32}\|h\|_{H^m(\mathbb{R})},
\end{aligned}$$

which is by assumption a finite upper bound. ■

Next, we prove the multivariate version of Theorem 4.4.1.

Similarly to (4.4.1), a class of functions $h \in L_2(\mathbb{R}^d, \omega)$ with a product measure function $\omega(\mathbf{y}) = \prod_{\ell=1}^d \omega_\ell(y_\ell), \omega_\ell \in \mathcal{C}_0(\mathbb{R})$ as in (4.3.1) is given. We consider a multivariate torus-to-$\mathbb{R}^d$ transformation $\mathbf{y} = \psi(\mathbf{x})$ as defined in (4.1.3), such that $\omega_\ell(\psi_\ell(x_\ell))\psi'_\ell(x_\ell) \in \mathbb{T}$, in order to transform any such function h into a function $f \in L_2(\mathbb{T}^d)$ of the form

$$f(\mathbf{x}) = h(\psi_1(x_1), \dots, \psi_d(x_d)) \prod_{\ell=1}^d \sqrt{\omega_\ell(\psi_\ell(x_\ell))\psi'_\ell(x_\ell)}, \quad \mathbf{x} \in \mathbb{T}^d, \tag{4.4.7}$$

for which we have the identity

$$\begin{aligned} \|h\|^2_{L_2(\mathbb{R}^d,\omega)} &= \int_{\mathbb{R}^d} |h(\mathbf{y})|^2 \, \omega(\mathbf{y}) \, \mathrm{d}\mathbf{y} \\ &= \int_{\mathbb{T}^d} |(h \circ \psi)(\mathbf{x})|^2 \, (\omega \circ \psi)(\mathbf{x}) \prod_{\ell=1}^d \psi'_\ell(x_\ell) \, \mathrm{d}\mathbf{x} = \|f\|^2_{L_2(\mathbb{T}^d)}. \end{aligned} \tag{4.4.8}$$

Again, we derive a set of sufficient L_∞-conditions on the torus-to-$\mathbb{R}^d$ transformation ψ and the product weight ω for an $h \in L_2(\mathbb{R}^d, \omega) \cap H^m_{\text{mix}}(\mathbb{R}^d)$ to be transformed by ψ into an $f \in \mathcal{H}^m(\mathbb{T}^d)$ of form (4.4.7).

Theorem 4.4.2 ([NP20, Theorem 3.5])**.** *Let $m \in \mathbb{N}_0$, a $h \in L_2(\mathbb{R}^d, \omega) \cap H^m(\mathbb{R}^d)$ with a multivariate measure function $\omega(\mathbf{y}) = \prod_{\ell=1}^d \omega_\ell(y_\ell)$ with $\omega_\ell \in \mathcal{C}_0(\mathbb{R})$ for all $\ell \in \{1, \dots, d\}$ be given. Considering a torus-to-$\mathbb{R}^d$ transformation $\psi = (\psi_1, \dots, \psi_d)^\top \in \mathcal{C}^m((-\frac{1}{2}, \frac{1}{2}))$ with the density function $\varrho(\mathbf{y}) = \prod_{\ell=1}^d \varrho_\ell(y_\ell) \in \mathcal{C}^m_0(\mathbb{R}^d)$, if for all multi-indices $\mathbf{m} = (m_1, \dots, m_d)^\top \in \mathbb{N}_0^d, \|\mathbf{m}\|_{\ell^d_\infty} \le m$ and $\ell \in \{1, ldots, d\}$ the condition*

$$\max_{j_\ell = 0, \dots, m_\ell} \left\| \left(\sqrt{(\omega_\ell \circ \psi_\ell)\psi'_\ell} \right)^{(m_\ell - j_\ell)} (\cdot) \, \psi'_\ell(\cdot)^{\max(-\frac{1}{2}, 2j_\ell - \frac{3}{2})} \right\|_{L_\infty(\mathbb{T})} < \infty \tag{4.4.9}$$

holds, then the transformation operator

$$\begin{aligned} T : L_2(\mathbb{R}^d, \omega) \cap \mathrm{H}^m(\mathbb{R}^d) &\to \mathcal{H}^m(\mathbb{T}^d) \\ h &\mapsto h(\psi(\cdot)) \prod_{\ell=1}^d \sqrt{\omega_\ell(\psi_\ell(\cdot))\psi'_\ell(\cdot)} =: f(\cdot) \end{aligned}$$

is bounded, where f of the form (4.4.7)*.*

Proof. For $h \in L_2(\mathbb{R}^d, \omega) \cap H^m_{\text{mix}}(\mathbb{R}^d)$ with $m \in \mathbb{N}_0$ and a torus-to-$\mathbb{R}^d$ transformation ψ as defined in (4.1.3) we consider the transformed function f as given in (4.4.7). Let $\mathbf{m} = (m_1, \dots, m_d)^\top \in \mathbb{N}_0^d$ be any multi-index with $\|\mathbf{m}\|_{\ell^d_\infty} \le m$. We have

$$\|D^{\mathbf{m}}[f](\cdot)\|_{L_2(\mathbb{T}^d)} = \left(\int_{\mathbb{T}^d} \left| D^{\mathbf{m}} \left[(h \circ \psi) \prod_{k=1}^d \sqrt{(\omega_k \circ \psi_k)\psi'_k} \right] (\mathbf{x}) \right|^2 \mathrm{d}\mathbf{x} \right)^{\frac{1}{2}}. \tag{4.4.10}$$

The product form of the measure function ω allows the componentwise application of the Leibniz formula (4.4.2), so that we estimate

$$\begin{aligned} &D^{\mathbf{m}} \left[(h \circ \psi) \prod_{k=1}^d \sqrt{(\omega_k \circ \psi_k)\psi'_k} \right] (\mathbf{x}) \\ &\le \sum_{j_1=0}^{m_1} \dots \sum_{j_d=0}^{m_d} D^{(j_1,\dots,j_d)}[h \circ \psi](\mathbf{x}) \, D^{(m_1-j_1,\dots,m_d-j_d)} \left[\prod_{k=1}^d \sqrt{(\omega_k \circ \psi_k)\psi'_k} \right] (\mathbf{x}). \end{aligned} \tag{4.4.11}$$

Next, we apply the Faá di Bruno formula (2.0.2) to each univariate j_k-th derivative of $h \circ \psi$ occurring in the term $D^{(j_1,\dots,j_d)}[h \circ \psi](\mathbf{x})$ in (4.4.11). For all $\ell \in \{1,\dots,d\}$ we put $B_{j_\ell,i_\ell}(\psi_\ell(x_\ell)) := B_{j_\ell,i_\ell}(\psi_\ell'(x_\ell),\dots,\psi_\ell^{(j_\ell-i_\ell+1)}(x_\ell))$ and we have

$$D^{(0,\dots,0,j_\ell,0,\dots,0)}[h \circ \psi](\mathbf{x}) = \begin{cases} h(\psi(\mathbf{x})) & : j_\ell = 0, \\ \displaystyle\sum_{i_\ell=1}^{j_\ell} D^{(0,\dots,0,i_\ell,0,\dots,0)}[h](\psi(\mathbf{x}))B_{j_\ell,i_\ell}(\psi_\ell(x_\ell)) & : j_\ell \in \mathbb{N}. \end{cases} \tag{4.4.12}$$

We combine the norm $\|D^{\mathbf{m}}[f](\mathbf{x})\|_{L_2(\mathbb{T}^d)}$ in (4.4.10) with the expression resulting from applying the Leibniz formula to $D^{\mathbf{m}}[f]$ in (5.4.7) and the subsequent application of the Faá di Bruno formula in (4.4.12). We estimate

$$\begin{aligned} \|D^{\mathbf{m}}[f](\mathbf{x})\|_{L_2(\mathbb{T}^d)} \lesssim \sum_{j_1=0,\dots,j_d=0}^{m_1,\dots,m_d} \sum_{i_1=1,\dots,i_d=1}^{j_1,\dots,j_d} \Bigg(\int_{\mathbb{T}^d} |D^{(i_1,\dots,i_d)}[h](\psi(\mathbf{x}))|^2 \prod_{\ell=1}^d |B_{j_\ell,i_\ell}(\psi_\ell(x_\ell))|^2 \times \\ \times \left| D^{(m_1-j_1,\dots,m_d-j_d)} \left[\prod_{k=1}^d \sqrt{(\omega_k \circ \psi_k)\psi_k'} \right](\mathbf{x}) \right|^2 \mathrm{d}\mathbf{x} \Bigg)^{\frac{1}{2}}. \end{aligned} \tag{4.4.13}$$

Within this multivariate integral we estimate each coordinate separately with the univariate arguments of the previous proof by fixing all but one coordinate one after another. Recalling the arguments in (4.4.5), if all appearing derivatives of ψ_ℓ are in $\mathcal{C}\left(\left(-\frac{1}{2},\frac{1}{2}\right)\right)$ and the corresponding derivatives of the density ϱ_ℓ are in $\mathcal{C}_0(\mathbb{R})$ then for all Bell polynomials B_{j_ℓ,i_ℓ} with $j_\ell \geq 1$ appearing in (4.4.12) and (4.4.13) there is some constant $C > 0$ so that we can estimate

$$|B_{j_\ell,i_\ell}(\psi_\ell'(x_\ell),\psi_\ell^{(2)}(x_\ell),\dots,\psi_\ell^{(j_\ell-i_\ell+1)}(x_\ell))| \leq C|\psi_\ell'(x_\ell)|^{2j_\ell-1}.$$

For each coordinate $\ell \in \{1,\dots,d\}$ we seperate the summand for $j_\ell = 0$ from the summands corresponding to $j_\ell \in \{1,\dots,d\}$ insert a productive one $1 = \psi_\ell'(x_\ell)\frac{1}{\psi_\ell'(x_\ell)}$ and estimate as in (4.4.6). Applying these arguments for $\ell = 1$ to (4.4.13) yields

$$\begin{aligned} &\|D^{\mathbf{m}}[f](\cdot)\|_{L_2(\mathbb{T}^d)} \\ &\lesssim \max_{j_1=0,\dots,m_1} \left\| \left(\sqrt{(\omega_1 \circ \psi_1)\psi_1'} \right)^{(m_1-j_1)} (\cdot)\, \psi_1'(\cdot)^{\max(-\frac{1}{2},2j_1-\frac{3}{2})} \right\|_{L_\infty(\mathbb{T})} \times \\ &\quad \times \sum_{j_2=0,\dots,j_d=0}^{m_2,\dots,m_d} \sum_{i_2=1,\dots,i_d=1}^{j_2,\dots,j_d} \Bigg(\int_{\mathbb{T}^{d-1}} \int_{\mathbb{T}} |D^{(i_1,\dots,i_d)}[h](\psi(x_1),\dots,\psi_d(x_d))|^2 \psi_1'(x_1)\,\mathrm{d}x_1 \times \\ &\quad \times \prod_{\ell=2}^d |B_{j_\ell,i_\ell}(\psi_\ell(x_\ell))|^2 \left| D^{(m_2-j_2,\dots,m_d-j_d)} \left[\prod_{k=2}^d \sqrt{(\omega_k \circ \psi_k)\psi_k'} \right](x_2,\dots,x_d) \right|^2 \mathrm{d}(x_2,\dots,x_d) \Bigg)^{\frac{1}{2}}. \end{aligned}$$

and after repeating this process for $\ell \in \{2, \dots, d\}$ and applying the inverse transformations $x_\ell = \psi_\ell^{-1}(y_\ell)$ for all $\ell \in \{1, \dots, d\}$ we have estimated

$$\lesssim \prod_{\ell=1}^{d} \max_{j_\ell=0,\dots,m_\ell} \left\| \left(\sqrt{(\omega_\ell \circ \psi_\ell)\psi_\ell'} \right)^{(m_\ell - j_\ell)} (\cdot)\, \psi_\ell'(\cdot)^{\max(-\frac{1}{2}, 2j_\ell - \frac{3}{2})} \right\|_{L_\infty(\mathbb{T})} \times$$

$$\times \sum_{j_1=0,\dots,j_d=0}^{m_1,\dots,m_d} \sum_{i_1=1,\dots,i_d=1}^{j_1,\dots,j_d} \left(\int_{\mathbb{T}^d} |D^{(i_1,\dots,i_d)}[h](\psi_1(x_1), \dots, \psi_d(x_d))|^2 \prod_{\ell=1}^{d} \psi_\ell'(x_\ell)\, \mathrm{d}\mathbf{x} \right)^{\frac{1}{2}}$$

$$\leq \prod_{\ell=1}^{d} \max_{j_\ell=0,\dots,m_\ell} \left\| \left(\sqrt{(\omega_\ell \circ \psi_\ell)\psi_\ell'} \right)^{(m_\ell - j_\ell)} (\cdot)\, \psi_\ell'(\cdot)^{\max(-\frac{1}{2}, 2j_\ell - \frac{3}{2})} \right\|_{L_\infty(\mathbb{T})} \sum_{j_1=0,\dots,j_d=0}^{m_1,\dots,m_d} \|h\|_{H^j_{\mathrm{mix}}(\mathbb{R}^d)},$$

with $j = \max\{j_1, \dots, j_d\}$ in the last estimate. The previous estimate is valid for all multi-indices $\mathbf{m} = (m_1, \dots, m_d)^\top \in \mathbb{N}_0^d$ with $\|\mathbf{m}\|_{\ell_\infty^d} \leq m$, so that we finally estimate

$$\|f\|_{\mathcal{H}^m(\mathbb{T}^d)} \sim \left(\sum_{\|\mathbf{m}\|_{\ell_\infty^d} \leq m} \|D^{\mathbf{m}}[f](\cdot)\|^2_{L_2(\mathbb{T}^d)} \right)^{\frac{1}{2}} = \left(\sum_{m_1=0,\dots,m_d=0}^{m,\dots,m} \|D^{\mathbf{m}}[f](\cdot)\|^2_{L_2(\mathbb{T}^d)} \right)^{\frac{1}{2}}$$

$$\lesssim \prod_{\ell=1}^{d} \max_{m_\ell=0,\dots,m} \left(\max_{j_\ell=0,\dots,m_\ell} \left\| \left(\sqrt{(\omega_\ell \circ \psi_\ell)\psi_\ell'} \right)^{(m_\ell - j_\ell)} (\cdot)\, \psi_\ell'(\cdot)^{\max(-\frac{1}{2}, 2j_\ell - \frac{3}{2})} \right\|_{L_\infty(\mathbb{T})} \right) \times$$

$$\times (m+1)^d \|h\|_{H^m_{\mathrm{mix}}(\mathbb{R}^d)},$$

which is finite by assumption. ■

In the following we establish two specific approximation error bounds for functions defined on $\mathbb{R}^d$ based on the approximation error bounds on the torus $\mathbb{T}^d$ that we recalled in Theorems 3.3.2 and 3.3.3. The corresponding proofs rely heavily on the previously introduced sufficient conditions in Theorem 4.4.2 which guarantee that functions $h \in L_2(\mathbb{R}^d, \omega) \cap H^m_{\mathrm{mix}}(\mathbb{R}^d)$ are transformed into Sobolev functions of dominating mixed smoothness on $\mathbb{T}^d$ of the form (4.4.7) by torus-to-$\mathbb{R}^d$ transformations $\psi : (-\frac{1}{2}, \frac{1}{2})^d \to \mathbb{R}^d$ as given in (4.1.3).

4.5 Approximation of transformed functions

Based on the definition of a rank-1 lattice $\Lambda(\mathbf{z}, M)$ in (3.2.2), we define a *transformed rank-1 lattice* as

$$\Lambda_\psi(\mathbf{z}, M) := \{\mathbf{y}_j := \psi(\mathbf{x}_j) : \mathbf{x}_j \in \Lambda(\mathbf{z}, M), j = 0, \dots, M-1\}. \tag{4.5.1}$$

A *transformed reconstructing rank-1 lattice* is denoted by $\Lambda_\psi(\mathbf{z}, M, I)$. Based on the orthonormal functions φ_k given in (4.3.2) we put

$$\varphi_{\mathbf{k}}(\mathbf{y}) := \prod_{j=1}^{d} \varphi_{k_j}(y_j), \quad \mathbf{k} \in \mathbb{Z}^d, \tag{4.5.2}$$

which form an orthonormal system with respect to the multivariate weighted $L_2(\mathbb{R}^d, \omega)$-scalar product , so that

$$(h_1, h_2)_{L_2(\mathbb{R}^d, \omega)} := \int_{\mathbb{R}^d} h_1(\mathbf{y})\, \overline{h_2(\mathbf{y})} \prod_{j=1}^{d} \omega_j(y_j)\, \mathrm{d}\mathbf{y} \tag{4.5.3}$$

and for all $\mathbf{k}_1, \mathbf{k}_2 \in \mathbb{Z}^d$ we have

$$(\varphi_{\mathbf{k}_1}, \varphi_{\mathbf{k}_2})_{L_2(\mathbb{R}^d,\omega)} = \delta_{\mathbf{k}_1,\mathbf{k}_2}.$$

The multivariate Fourier coefficients $\hat{h}_{\mathbf{k}}$ are naturally given by

$$\hat{h}_{\mathbf{k}} = (h, \varphi_{\mathbf{k}})_{L_2(\mathbb{R}^d,\omega)}. \tag{4.5.4}$$

As in (4.3.5), we define the multivariate Fourier partial sum for any $I \subset \mathbb{Z}^d$ as

$$S_I h(\mathbf{y}) := \sum_{\mathbf{k}\in I} \hat{h}_{\mathbf{k}}\, \varphi_{\mathbf{k}}(\mathbf{y}).$$

Suppose $f \in L_2(\mathbb{T}^d)$. For each $I \subset \mathbb{Z}^d$ the system $\{\varphi_{\mathbf{k}}\}_{\mathbf{k}\in I}$ spans the space of transformed trigonometric functions on $\mathbb{R}^d$

$$\Pi_{I,\psi} = \operatorname{span}\left\{ \sqrt{\frac{\varrho(\cdot)}{\omega(\cdot)}}\, \mathrm{e}^{2\pi \mathrm{i}\mathbf{k}\cdot\psi^{-1}(\cdot)} : \mathbf{k} \in I \right\}. \tag{4.5.5}$$

As in (3.2.4), for transformed trigonometric functions $h \in \Pi_{I,\psi}$ on $\mathbb{R}^d$, transformed lattice nodes $\mathbf{y}_j \in \Lambda_\psi(\mathbf{z}, M, I)$ and all $\mathbf{k} \in I$, we have the exact integration property of the form

$$\begin{aligned}\hat{h}_{\mathbf{k}} &= \int_{\mathbb{R}^d} h(\mathbf{y})\, \sqrt{\varrho(\mathbf{y})\,\omega(\mathbf{y})}\, \mathrm{e}^{-2\pi\mathrm{i}\mathbf{k}\cdot\psi^{-1}(\mathbf{y})}\, \mathrm{d}y = \int_{\mathbb{T}^d} f(\mathbf{x})\, \mathrm{e}^{-2\pi\mathrm{i}\mathbf{k}\cdot\mathbf{x}}\, \mathrm{d}\mathbf{x} \\ &= \frac{1}{M}\sum_{j=0}^{M-1} f(\mathbf{x}_j)\, \mathrm{e}^{-2\pi\mathrm{i}\mathbf{k}\cdot\mathbf{x}_j} = \frac{1}{M}\sum_{j=0}^{M-1} h(\mathbf{y}_j)\, \sqrt{\frac{\varrho(\mathbf{y}_j)}{\omega(\mathbf{y}_j)}}\, \mathrm{e}^{-2\pi\mathrm{i}\mathbf{k}\cdot\psi^{-1}(\mathbf{y}_j)} = \hat{h}^{\Lambda}_{\mathbf{k}}.\end{aligned} \tag{4.5.6}$$

Generally, for functions $h \in L_2(\mathbb{R}^d, \omega) \cap H^m_{\mathrm{mix}}(\mathbb{R}^d)$ the multivariate approximated Fourier coefficients of the form

$$\hat{h}^{\Lambda}_{\mathbf{k}} := \frac{1}{M}\sum_{j=0}^{M-1} h(\mathbf{y}_j)\, \sqrt{\frac{\varrho(\mathbf{y}_j)}{\omega(\mathbf{y}_j)}}\, \mathrm{e}^{-2\pi\mathrm{i}\mathbf{k}\cdot\psi^{-1}(\mathbf{y}_j)} = \frac{1}{M}\sum_{j=0}^{M-1} h(\mathbf{y}_j)\, \overline{\varphi_{\mathbf{k}}(\mathbf{y}_j)} \tag{4.5.7}$$

approximate the multivariate Fourier coefficients $\hat{h}_{\mathbf{k}}$. Finally, the multivariate version of the approximated Fourier partial sum is given by

$$S^{\Lambda}_I h(\mathbf{y}) := \sum_{\mathbf{k}\in I} \hat{h}^{\Lambda}_{\mathbf{k}}\, \varphi_{\mathbf{k}}(\mathbf{y}). \tag{4.5.8}$$

Finally, we introduce the analogue of the Hilbert space $\mathcal{H}^\beta(\mathbb{T}^d)$ given in (3.1.7) on $\mathbb{R}^d$. We define the space of weighted $L_2\left(\mathbb{R}^d, \omega\right)$-functions with square summable Fourier coefficients $\hat{h}_{\mathbf{k}}$ given in (4.5.4) by

$$\begin{aligned}\mathcal{H}^\beta\left(\mathbb{R}^d, \omega\right) &:= \left\{ h \in L_2\left(\mathbb{R}^d, \omega\right) : \|h\|_{\mathcal{H}^\beta(\mathbb{R}^d,\omega)} < \infty \right\}, \\ \|h\|_{\mathcal{H}^\beta(\mathbb{R}^d,\omega)} &:= \left(\sum_{\mathbf{k}\in\mathbb{Z}^d} \mathrm{w}_{\mathrm{hc}}(\mathbf{k})^{2\beta} |\hat{h}_{\mathbf{k}}|^2 \right)^{\frac{1}{2}}.\end{aligned}$$

4.5.1 L_2-approximation error

Similarly, based on the $L_2(\mathbb{T}^d)$-approximation error bound (3.3.2) and the conditions proposed in Theorem 4.4.2 we prove an upper bound for the approximation error $\left\|h - S^{\Lambda}_{I^d_N} h\right\|$ in terms of a weighted L_2-norm on $\mathbb{R}^d$.

Theorem 4.5.1 ([NP20, Theorem 3.7])**.** *Let $d \in \mathbb{N}$, $m \in \mathbb{N}$, a hyperbolic cross I^d_N with $N \geq 2^{d+1}$ and a reconstructing rank-1 lattice $\Lambda(\mathbf{z}, M, I^d_N)$ and an $h \in L_2(\mathbb{R}^d, \omega) \cap H^m(\mathbb{R}^d)$ with a multivariate measure function $\omega(\mathbf{y}) = \prod_{\ell=1}^d \omega_\ell(y_\ell)$ with $\omega_\ell \in \mathcal{C}_0(\mathbb{R})$ for all $\ell \in \{1, \dots, d\}$ be given. We consider a ψ as in (4.1.3) with its corresponding density function ϱ as in (4.1.2) for all multi-indices $\mathbf{m} = (m_1, \dots, m_d)^\top \in \mathbb{N}_0^d$, $\|\mathbf{m}\|_{\ell^d_\infty} \leq m$ and $\ell \in \{1, ldots, d\}$ the condition*

$$\max_{j_\ell=0,\dots,m_\ell} \left\| \left(\sqrt{(\omega_\ell \circ \psi_\ell)\psi'_\ell} \right)^{(m_\ell - j_\ell)} (\cdot)\, \psi'_\ell(\cdot)^{\max(-\frac{1}{2}, 2j_\ell - \frac{3}{2})} \right\|_{L_\infty(\mathbb{T})} < \infty$$

holds.

Then there is an approximation error estimate of the form

$$\left\|h - S^{\Lambda}_{I^d_N} h\right\|_{L_2\left(\mathbb{R}^d, \omega\right)} \lesssim N^{-m} (\log N)^{(d-1)/2} \|h\|_{\mathcal{H}^m(\mathbb{R}^d, \omega)}.$$

Proof. Let $m \in \mathbb{N}, d \in \mathbb{N}$ and let $h \in L_2(\mathbb{R}^d, \omega) \cap H^m_{\text{mix}}(\mathbb{R}^d)$. By assumption are the criteria in Theorem 4.4.2 fulfilled and the transformed function f of the form (4.4.7) is in $\mathcal{H}^m(\mathbb{T}^d)$ and has a continuous representative because of the inclusion $\mathcal{H}^m(\mathbb{T}^d) \hookrightarrow \mathcal{C}(\mathbb{T}^d)$ in (3.1.9). For $f \in \mathcal{H}^m(\mathbb{T}^d) \cap \mathcal{C}(\mathbb{T}^d)$ Theorem 3.3.3 yields the approximation error bound of the form

$$\left\|f - S^{\Lambda}_{I^d_N} f\right\|_{L_2(\mathbb{T}^d)} \leq C_{d,\beta} N^{-\beta} (\log N)^{(d-1)/2} \|f\|_{\mathcal{H}^\beta(\mathbb{T}^d)} \tag{4.5.9}$$

with some constant $C_{d,\beta} := C(d, \beta) > 0$. With the inverse torus-to-$\mathbb{R}^d$ transformation $\boldsymbol{x} = \psi^{-1}(\boldsymbol{y})$ we have

$$\hat{h}_{\mathbf{k}} = (h, \varphi_{\mathbf{k}})_{L_2\left(\mathbb{R}^d, \omega\right)} = (f, \mathrm{e}^{2\pi \mathrm{i} \mathbf{k} \cdot})_{L_2(\mathbb{T}^d)} = \hat{f}_{\mathbf{k}},$$

and

$$\|h\|^2_{\mathcal{H}^m(\mathbb{R}^d, \omega)} = \sum_{\mathbf{k} \in \mathbb{Z}^d} \mathrm{w}_{\mathrm{hc}}(\mathbf{k})^{2m} |\hat{h}_{\mathbf{k}}|^2 = \sum_{\mathbf{k} \in \mathbb{Z}^d} \mathrm{w}_{\mathrm{hc}}(\mathbf{k})^{2m} |\hat{f}_{\mathbf{k}}|^2 = \|f\|^2_{\mathcal{H}^m(\mathbb{T}^d)}$$

as in (4.5.12), as well as

$$\left\|h - S_{I^d_N} h\right\|^2_{L_2\left(\mathbb{R}^d, \omega\right)} = \int_{\mathbb{R}^d} \left| h(\mathbf{y}) - \sum_{\mathbf{k} \in I^d_N} \hat{h}_{\mathbf{k}}\, \varphi_{\mathbf{k}}(\mathbf{y}) \right|^2 \omega(\boldsymbol{y})\, \mathrm{d}\mathbf{y} = \left\|f - S_{I^d_N} f\right\|^2_{L_2(\mathbb{T}^d)} \tag{4.5.10}$$

and

$$\left\|h - S^{\Lambda}_{I^d_N} h\right\|_{L_2\left(\mathbb{R}^d, \omega\right)} = \left\|f - S^{\Lambda}_{I^d_N} f\right\|_{L_2(\mathbb{T}^d)}.$$

In total, by combining (4.5.10), (4.5.9), and (4.5.12) we estimated for $f \in \mathcal{H}^m(\mathbb{T}^d) \cap \mathcal{C}(\mathbb{T}^d)$ that the approximation error can be bounded by

$$\begin{aligned} \left\|h - S^{\Lambda}_{I^d_N} h\right\|_{L_2\left(\mathbb{R}^d, \omega\right)} = \left\|f - S^{\Lambda}_{I^d_N} f\right\|_{L_2(\mathbb{T}^d)} &\lesssim C_{d,\beta} N^{-\beta} (\log N)^{(d-1)/2} \|f\|_{\mathcal{H}^\beta(\mathbb{T}^d)} \\ &= C_{d,\beta} N^{-\beta} (\log N)^{(d-1)/2} \|h\|_{\mathcal{H}^m(\mathbb{R}^d, \omega)} < \infty \end{aligned}$$

with some constant $C_{d,\beta} > 0$. ∎

Finally, let us recap the results of this section. We've seen that under the assumptions of Theorem 4.5.2, a function $h \in L_2\left(\mathbb{R}^d, \omega\right) \cap H^m_{\text{mix}}\left(\mathbb{R}^d\right)$ is transformed into a smooth function $f \in \mathcal{H}^m\left(\mathbb{R}^d, \omega\right)$ of the form (4.4.7) and its L_∞-approximation error decays with the rate

$$\left\| f - S^\Lambda_{I^d_N} f \right\|_{L_\infty\left(\mathbb{T}^d\right)} = \left\| h - S^\Lambda_{I^d_N} h \right\|_{L_\infty\left(\mathbb{R}^d, \sqrt{\frac{\omega}{\varrho}}\right)} \lesssim N^{-m+\lambda} \to 0$$

for $N \to \infty$ (or equivalently for $|I^d_N| \to \infty$) and with $\lambda > \frac{1}{2}$. Under the same assumptions we've then shown in Theorem 4.5.1 that the L_2-approximation error is bounded by

$$\left\| f - S^\Lambda_{I^d_N} f \right\|_{L_2\left(\mathbb{T}^d\right)} = \left\| h - S^\Lambda_{I^d_N} h \right\|_{L_2\left(\mathbb{R}^d, \omega\right)} \lesssim N^{-m} (\log N)^{(d-1)/2} \to 0$$

for $N \to \infty$.

4.5.2 L_∞-approximation error

Based on the $L_\infty(\mathbb{T}^d)$-approximation error bound (3.3.1) and the conditions proposed in Theorem 4.4.2 we prove a similar upper bound for the approximation error $\left\| h - S^\Lambda_{I^d_N} h \right\|$ in terms of a weighted L_∞-norm on $\mathbb{R}^d$.

Theorem 4.5.2 ([NP20, Theorem 3.6])**.** *Let $d \in \mathbb{N}$, $m \in \mathbb{N}$, a hyperbolic cross I^d_N with $N \geq 2^{d+1}$ and a reconstructing rank-1 lattice $\Lambda(\mathbf{z}, M, I^d_N)$ and an $h \in L_2(\mathbb{R}^d, \omega) \cap H^m(\mathbb{R}^d)$ with a multivariate measure function $\omega(\mathbf{y}) = \prod_{\ell=1}^d \omega_\ell(y_\ell)$ with $\omega_\ell \in \mathcal{C}_0(\mathbb{R})$ for all $\ell \in \{1, \dots, d\}$ be given. We consider a ψ as in (4.1.3) with its corresponding density function ϱ as in (4.1.2) for all multi-indices $\mathbf{m} = (m_1, \dots, m_d)^\top \in \mathbb{N}^d_0$, $\|\mathbf{m}\|_{\ell^d_\infty} \leq m$ and $\ell \in \{1, ldots, d\}$ the condition*

$$\max_{j_\ell = 0, \dots, m_\ell} \left\| \left(\sqrt{(\omega_\ell \circ \psi_\ell)\psi'_\ell} \right)^{(m_\ell - j_\ell)} (\cdot)\, \psi'_\ell(\cdot)^{\max(-\frac{1}{2}, 2j_\ell - \frac{3}{2})} \right\|_{L_\infty(\mathbb{T})} < \infty$$

holds.

Then there is an approximation error estimate of the form

$$\left\| h - S^\Lambda_{I^d_N} h \right\|_{L_\infty\left(\mathbb{R}^d, \sqrt{\frac{\omega}{\varrho}}\right)} \lesssim N^{-m+\lambda} \|h\|_{\mathcal{H}^m(\mathbb{R}^d, \omega)}.$$

Proof. Let $m \in \mathbb{N}, d \in \mathbb{N}$ and let $h \in L_2(\mathbb{R}^d, \omega) \cap H^m_{\text{mix}}(\mathbb{R}^d)$. By assumption, Theorem 4.4.2 is applicable, so that the transformed function f of the form (4.4.7) is in $\mathcal{H}^m(\mathbb{T}^d)$ and f has a continuous representative because of the inclusion $\mathcal{H}^m(\mathbb{T}^d) \hookrightarrow \mathcal{A}^{m-\lambda}(\mathbb{T}^d) \hookrightarrow \mathcal{C}(\mathbb{T}^d)$ with $\lambda > \frac{1}{2}$ as in (3.1.9). Hence, for $f \in \mathcal{A}^{m-\lambda}(\mathbb{T}^d) \cap \mathcal{C}(\mathbb{T}^d)$ we have the approximation error bound

$$\left\| f - S^\Lambda_{I^d_N} f \right\|_{L_\infty(\mathbb{T}^d)} \leq 2N^{-m+\lambda} \|f\|_{\mathcal{A}^{m-\lambda}(\mathbb{T}^d)} \tag{4.5.11}$$

as stated in Theorem 3.3.2. With the inverse torus-to-$\mathbb{R}^d$ transformation $\mathbf{x} = \psi^{-1}(\mathbf{y})$ we have

$$\hat{h}_\mathbf{k} = (h, \varphi_\mathbf{k})_{L_2\left(\mathbb{R}^d, \omega\right)} = (f, \mathrm{e}^{2\pi \mathrm{i} \mathbf{k} \cdot})_{L_2(\mathbb{T}^d)} = \hat{f}_\mathbf{k}$$

and

$$\|h\|^2_{\mathcal{H}^m(\mathbb{R}^d, \omega)} = \sum_{\mathbf{k} \in \mathbb{Z}^d} \mathrm{w}_{\mathrm{hc}}(\mathbf{k})^{2m} |\hat{h}_\mathbf{k}|^2 = \sum_{\mathbf{k} \in \mathbb{Z}^d} \mathrm{w}_{\mathrm{hc}}(\mathbf{k})^{2m} |\hat{f}_\mathbf{k}|^2 = \|f\|^2_{\mathcal{H}^m(\mathbb{T}^d)}, \tag{4.5.12}$$

as well as

$$\begin{aligned}
\left\| h - S_{I_N^d} h \right\|_{L_\infty\left(\mathbb{R}^d, \sqrt{\frac{\omega}{\varrho}}\right)} &= \operatorname{ess\,sup}_{\mathbf{y}\in\mathbb{R}^d} \left| \sqrt{\frac{\omega(\mathbf{y})}{\varrho(\mathbf{y})}} \left(h(\mathbf{y}) - \sum_{\mathbf{k}\in I_N^d} \hat{h}_{\mathbf{k}}\, \varphi_{\mathbf{k}}(\mathbf{y}) \right) \right| \\
&= \operatorname{ess\,sup}_{\mathbf{y}\in\mathbb{R}^d} \left| h(\mathbf{y}) \sqrt{\frac{\omega(\mathbf{y})}{\varrho(\mathbf{y})}} - \sum_{\mathbf{k}\in I_N^d} \hat{h}_{\mathbf{k}}\, \mathrm{e}^{2\pi \mathrm{i}\mathbf{k}\cdot\psi^{-1}(\mathbf{y})} \right| \\
&= \operatorname{ess\,sup}_{\mathbf{x}\in\mathbb{T}^d} \left| h(\psi(\mathbf{x})) \sqrt{\omega(\psi(\mathbf{x})) \prod_{j=1}^d \psi_j'(x_j)} - \sum_{\mathbf{k}\in I_N^d} \hat{h}_{\mathbf{k}}\, \mathrm{e}^{2\pi \mathrm{i}\mathbf{k}\cdot\mathbf{x}} \right| \\
&= \left\| f - S_{I_N^d} f \right\|_{L_\infty(\mathbb{T}^d)}
\end{aligned}$$

and

$$\left\| h - S_{I_N^d}^{\Lambda} h \right\|_{L_\infty\left(\mathbb{R}^d, \sqrt{\frac{\omega}{\varrho}}\right)} = \left\| f - S_{I_N^d}^{\Lambda} f \right\|_{L_\infty(\mathbb{T}^d)}. \tag{4.5.13}$$

In total, by combining (4.5.13), (4.5.11), (3.1.10), and (4.5.12) we estimated for $f \in \mathcal{H}^m(\mathbb{T}^d) \cap \mathcal{C}(\mathbb{T}^d)$ that the approximation error can be bounded by

$$\begin{aligned}
\left\| h - S_{I_N^d}^{\Lambda} h \right\|_{L_\infty\left(\mathbb{R}^d, \sqrt{\frac{\omega}{\varrho}}\right)} &= \left\| f - S_{I_N^d}^{\Lambda} f \right\|_{L_\infty(\mathbb{T}^d)} \le 2N^{-m+\lambda} \|f\|_{\mathcal{A}^{m-\lambda}(\mathbb{T}^d)} \\
&\le 2C_{d,\lambda} N^{-m+\lambda} \|f\|_{\mathcal{H}^m(\mathbb{T}^d)} = 2C_{d,\lambda} N^{-m+\lambda} \|h\|_{\mathcal{H}^m(\mathbb{R}^d,\omega)} < \infty
\end{aligned}$$

with $\lambda > \frac{1}{2}$ and some constant $C_{d,\lambda} > 1$. ■

4.6 Fast algorithms and discrete approximation errors on $\mathbb{R}^d$

In this chapter we start denoting the parameters $\boldsymbol{\eta}, \boldsymbol{\mu} \in \mathbb{R}_+^d$. Families of multivariate measure functions are denoted by $\omega(\cdot, \boldsymbol{\mu})$ as in (4.3.1) and families of torus-to-$\mathbb{R}^d$ transformations as in (4.1.3) are denoted by $\psi(\cdot, \boldsymbol{\eta})$.

For the evaluation of transformed multivariate trigonometric functions $h \in \Pi_{I,\psi(\cdot,\boldsymbol{\eta})}$ on $\mathbb{R}^d$ as in (4.5.5) such as the approximated Fourier series $S_I^{\Lambda} h$, and for the reconstruction of the approximated Fourier coefficients $\hat{h}_{\mathbf{k}}^{\Lambda}$ as in (4.5.7), we follow [NP20, Section 4] and outline the necessary adjustments within the efficient algorithms described in [Käm14b, Algorithm 3.1 and 3.2] that were recalled in Algorithms 3.4.1 and 3.4.2. Similarly to (3.4.1) and (3.4.2), for $\boldsymbol{\eta}, \boldsymbol{\mu} \in \mathbb{R}_+^d$ we form transformed Fourier matrices $\mathbf{F}_R$ and $\mathbf{F}_R^*$ given by

$$\begin{aligned}
\mathbf{F}_R &:= \left(\mathrm{e}^{2\pi \mathrm{i}\mathbf{k}\cdot\psi^{-1}(\mathbf{y}_j,\boldsymbol{\eta})} \right)_{\mathbf{y}_j\in\Lambda_{\psi(\cdot,\boldsymbol{\eta})}(\mathbf{z},M),\, \mathbf{k}\in I} \in \mathbb{C}^{M\times|I|}, \\
\mathbf{F}_R^* &= \left(\mathrm{e}^{-2\pi \mathrm{i}\mathbf{k}\cdot\psi^{-1}(\mathbf{y}_j,\boldsymbol{\eta})} \right)_{\mathbf{k}\in I,\, \mathbf{y}_j\in\Lambda_{\psi(\cdot,\boldsymbol{\eta})}(\mathbf{z},M)} \in \mathbb{C}^{|I|\times M}
\end{aligned}$$

as well as $\mathbf{h} := \left(h(\mathbf{y}_j) \sqrt{\frac{\omega(\mathbf{y}_j,\boldsymbol{\mu})}{\varrho(\mathbf{y}_j,\boldsymbol{\eta})}} \right)_{j=0}^{M-1}$ for $\mathbf{y}_j \in \Lambda_{\psi(\cdot,\boldsymbol{\eta})}(\mathbf{z}, M)$, $\hat{\mathbf{h}} := (\hat{h}_{\mathbf{k}})_{\mathbf{k}\in I}$ with some frequency set $I \subset \mathbb{Z}^d$ of finite cardinality $|I| < \infty$, so that we have matrix-vector-products of the form

$$\mathbf{h} = \mathbf{F}_R \hat{\mathbf{h}} \quad \text{and} \quad \hat{\mathbf{h}} = M^{-1} \mathbf{F}_R^* \mathbf{h}$$

A function $h \in L_2(\mathbb{R}^d, \omega) \cap H^m_{\text{mix}}(\mathbb{R}^d)$ is transformed by a torus-to-$\mathbb{R}^d$ transformation $\mathbf{y}_j = \psi(\mathbf{x}_j, \boldsymbol{\eta}), \mathbf{x}_j = (x_1^j, \dots, x_d^j)^\top$ into a periodic function f on the torus $\mathbb{T}^d$ of the form (4.4.7). The resulting samples are given by

$$h(\mathbf{y}_j)\sqrt{\frac{\omega(\mathbf{y}_j, \boldsymbol{\mu})}{\varrho(\mathbf{y}_j, \boldsymbol{\eta})}} = h(\psi(\mathbf{x}_j, \boldsymbol{\eta}))\sqrt{\omega(\psi(\mathbf{x}_j, \boldsymbol{\eta}), \boldsymbol{\mu}) \prod_{k=1}^{d} \psi_k'(x_k^j, \eta_k)} = f(\mathbf{x}_j, \boldsymbol{\eta}, \boldsymbol{\mu})$$

and

$$\sqrt{\frac{\omega(\mathbf{y}_j, \boldsymbol{\mu})}{\varrho(\mathbf{y}_j, \boldsymbol{\eta})}} S_I^\Lambda h(\mathbf{y}_j) = S_I^\Lambda f(\mathbf{x}_j, \boldsymbol{\eta}, \boldsymbol{\mu}) \tag{4.6.1}$$

with the parameters $\boldsymbol{\eta}, \boldsymbol{\mu} \in \mathbb{R}_+^d$.

So, we now put the coefficient vector $\hat{\mathbf{h}} = \left(\hat{h}_{\mathbf{k}}\right)_{\mathbf{k}\in I}$ into Algorithm 3.4.1 and obtain the function values $\mathbf{h} = \mathbf{F}_R\hat{\mathbf{h}} = \left(h(\mathbf{y}_j)\sqrt{\frac{\omega(\mathbf{y}_j,\boldsymbol{\mu})}{\varrho(\mathbf{y}_j,\boldsymbol{\eta})}}\right)_{j=0}^{M-1}$ as the output, while the simplification idea (3.4.3) of the Fourier partial sum remains the same. Conversely, we put the function values $\mathbf{h} = \left(h(\mathbf{y}_j)\sqrt{\frac{\omega(\mathbf{y}_j,\boldsymbol{\mu})}{\varrho(\mathbf{y}_j,\boldsymbol{\eta})}}\right)_{j=0}^{M-1}$ into Algorithm 3.4.2 observe that the orthogonality property (3.4.4) as well as the subsequent arguments remain the same, so that we obtain the coeffcients $\hat{\mathbf{h}} = M^{-1}\mathbf{F}_R^*\mathbf{h} = \left(\hat{h}_{\mathbf{k}}\right)_{\mathbf{k}\in I}$.

Remark 4.6.1. *We identify the torus with different cubes. We consider $\mathbb{T}^d \simeq [0,1)^d$ when defining rank-1 lattices $\Lambda(\mathbf{z}, M)$ in (3.2.2). However, we consider $\mathbb{T}^d \simeq [-\frac{1}{2}, \frac{1}{2})^d$ when applying a torus-to-$\mathbb{R}^d$ transformation ψ to a rank-1 lattice. In this process, we reassign all lattice points $\mathbf{x}_j \in \Lambda(\mathbf{z}, M)$ via*

$$\mathbf{x}_j \mapsto \left(\left(\mathbf{x}_j + \frac{\mathbf{1}}{2}\right) \bmod \mathbf{1}\right) - \frac{\mathbf{1}}{2}$$

for all $j = 0, \dots, M-1$.

We already showcased in Figure 4.2.1 that the definition of ψ in (4.1.1) allows a range of functions with different slopes. Now, in Figure 4.6.1 we show different two-dimensional transformed rank-1 lattices $\Lambda_{\psi(\cdot,\boldsymbol{\eta})}(\mathbf{z}, M)$ as defined in (4.5.1), generated by $\mathbf{z} = (1,3)^\top$ and $M = 31$. We compare the lattices transformed by the the algebraic transformation (4.2.4) and the error function transformation (4.2.1) of the form (4.1.4) with the parameter vector $\boldsymbol{\eta} = \mathbf{1}$. The graphs in the center and on the right of Figure 4.6.1 reveal that the algebraic transformation causes a wider spread of the lattice nodes close to the center, whereas the slope of the error function transformation increases hugely towards the boundary points which we only notice for larger values M and finer lattices with more nodes closer to the boundary of the cube $(-\frac{1}{2}, \frac{1}{2})^2$. □

On a similar note, the discrete approximation errors ε_2^M and ε_∞^M as defined in (3.5.1) and (3.5.4) are slightly adjusted in the sense of the transformed approximation error bounds of Theorems 4.5.2 and 4.5.1. Under certain assumptions we've shown in (4.5.13), (4.5.10) and

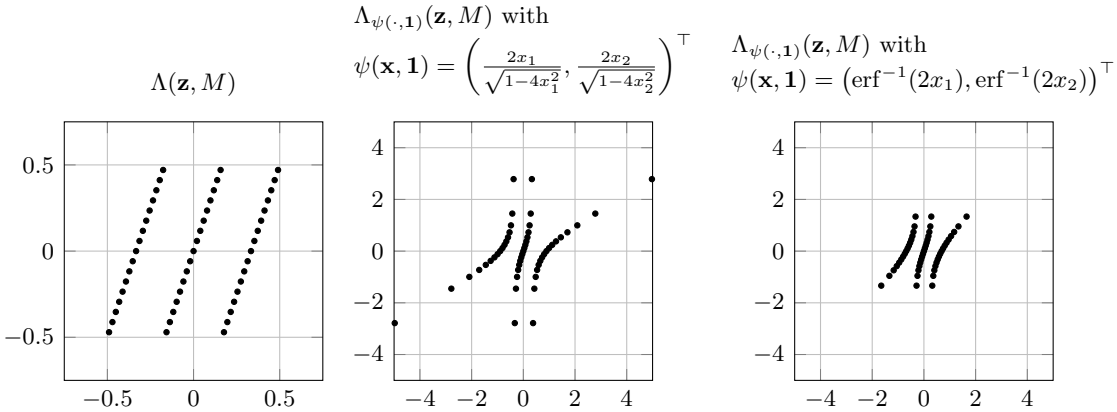

Figure 4.6.1: A two-dimensional lattice $\Lambda(\mathbf{z}, M)$ with $\mathbf{z} = (1, 3)^\top, M = 31$ on the left and the resulting transformed lattice $\Lambda_{\psi(\cdot,\boldsymbol{\eta})}(\mathbf{z}, M)$ for the algebraic transformation in the center and for the error function transformation on the right of the parameter form (4.1.4) and both used with $\boldsymbol{\eta} = \mathbf{1}$.

(4.6.1) that we have

$$\varepsilon_2^M(h, \{\mathbf{y}_j\}_{j=1}^M) \approx \frac{\left\|h - S_I^\Lambda h\right\|_{L_2(\mathbb{R}^d,\omega)}^2}{\|h\|_{L_2(\mathbb{R}^d,\omega)}^2} = \frac{\left\|f - S_I^\Lambda f\right\|_{L_2(\mathbb{T}^d)}^2}{\|f\|_{L_2(\mathbb{T}^d)}^2} \approx \varepsilon_2^M(f, \{\mathbf{x}_j\}_{j=1}^M), \tag{4.6.2}$$

$$\varepsilon_\infty^M(h, \{\mathbf{y}_j\}_{j=1}^M) \approx \frac{\left\|h - S_I^\Lambda h\right\|_{L_\infty\left(\mathbb{R}^d,\sqrt{\frac{\omega}{\varrho}}\right)}}{\|h\|_{L_\infty\left(\mathbb{R}^d,\sqrt{\frac{\omega}{\varrho}}\right)}} = \frac{\left\|f - S_I^\Lambda f\right\|_{L_\infty(\mathbb{T}^d)}}{\|f\|_{L_\infty(\mathbb{T}^d)}} \approx \varepsilon_\infty^M(h, \{\mathbf{x}_j\}_{j=1}^M).$$

4.7 Numerics for the error function transformation

Let the multivariate version of the Gaussian measure function (4.3.6), reading as

$$\omega(\mathbf{y}, \boldsymbol{\mu}) = \frac{1}{\pi^{\frac{d}{2}}} \prod_{\ell=1}^d \mathrm{e}^{-\mu_\ell^2 y_\ell^2}, \quad \mu_\ell \neq 0 \text{ for all } \ell \in \{1, \dots, d\}, \tag{4.7.1}$$

and the $L_2(\mathbb{R}^d, \omega(\cdot, \boldsymbol{\mu}))$-function

$$h(\mathbf{y}) = \prod_{\ell=1}^d \frac{\mathrm{e}^{y_\ell}}{1 + \mathrm{e}^{y_\ell}} \tag{4.7.2}$$

be given. We consider the parameterized error function transformation $\psi(\cdot, \boldsymbol{\eta}), \boldsymbol{\eta} \in \mathbb{R}_+^d$ with the univariate components of the form $\psi_j(x_j, \eta_j) = \eta_j \psi_j(x_j), x_j \in (-\frac{1}{2}, \frac{1}{2})$ and the ψ_j as in (4.2.1), which now reads as

$$\psi_j(x_j, \eta_j) = \eta_j \,\mathrm{erf}^{-1}(2x_j), \quad \psi_j'(x_j, \eta_j) = \eta_j \sqrt{\pi}\, \mathrm{e}^{(\mathrm{erf}^{-1}(2x_j))^2} \tag{4.7.3}$$

$$\psi^{-1}(y_j, \eta_j) = \frac{1}{2} \,\mathrm{erf}\left(\frac{y_j}{\eta_j}\right), \quad \varrho(y_j, \eta_j) = \frac{1}{\sqrt{\pi \eta_j^2}}\, \mathrm{e}^{-\left(\frac{y_j}{\eta_j}\right)^2}.$$

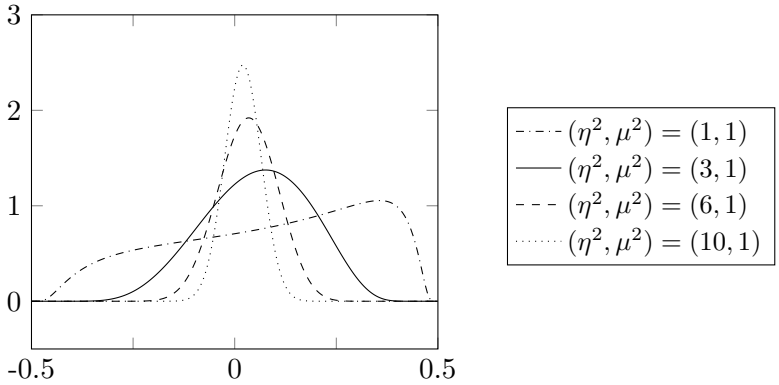

Figure 4.7.1: Plots of the univariate transformed Gaussian function f as in (4.7.4) for various combinations of the parameter η with fixed $\mu = 1$, the Gaussian measure function ω (4.7.1) and the parameterized error function transformation (4.7.3).

We have the orthonormal system $\{\varphi_{\mathbf{k}}\}_{\mathbf{k}\in\mathbb{Z}^d}$ as in (4.5.2) with the univariate components $(\varphi_{k_j})_{j=1}^d$ as in (4.3.2), that are of the form

$$\varphi_{k_j}(y_j, \eta_j, \mu_j) = \frac{1}{\eta_j}\, \mathrm{e}^{\frac{1}{2}(\mu_j^2 - \frac{1}{\eta_j^2})y_j^2 + \pi \mathrm{i} k_j \operatorname{erf}\left(\frac{y_j}{\eta_j}\right)}.$$

The Fourier coefficients $\hat{h}_{\mathbf{k}}$ of an arbitrary function $h \in L_2(\mathbb{R}^d, \omega(\cdot, \boldsymbol{\mu}))$ are of the form

$$\begin{aligned}
\hat{h}_{\mathbf{k}} := (h, \varphi_{\mathbf{k}})_{L_2(\mathbb{R}^d, \omega(\cdot, \boldsymbol{\mu}))} &= \int_{\mathbb{R}^d} h(\mathbf{y})\, \overline{\varphi_{\mathbf{k}}(\mathbf{y}, \boldsymbol{\eta}, \boldsymbol{\mu})}\, \omega(\mathbf{y}, \boldsymbol{\mu})\, \mathrm{d}\mathbf{y} \\
&= \int_{\mathbb{R}^d} h(\mathbf{y}) \prod_{j=1}^d \frac{1}{\eta_j}\, \mathrm{e}^{\frac{1}{2}(\mu_j^2 - \frac{1}{\eta_j^2})y_j^2 - \pi \mathrm{i} k_j \operatorname{erf}\left(\frac{y_j}{\eta_j}\right)} \frac{1}{\sqrt{\pi}}\, \mathrm{e}^{-\mu_j^2 y_j^2}\, \mathrm{d}\mathbf{y} \\
&= \pi^{-\frac{d}{2}} \prod_{j=1}^d \frac{1}{\eta_j} \int_{\mathbb{R}^d} h(\mathbf{y}) \prod_{j=1}^d \mathrm{e}^{-\pi \mathrm{i} k_j \operatorname{erf}\left(\frac{y_j}{\eta_j}\right)}\, \mathrm{e}^{-\frac{1}{2}(\mu_j^2 + \frac{1}{\eta_j^2})y_j^2}\, \mathrm{d}\mathbf{y}.
\end{aligned}$$

The considered function h in (4.7.2), the Gaussian measure function (4.7.1) and the error function transformation (4.7.3) yield transformed functions f in the sense of (4.4.7) of the form

$$\begin{aligned}
f(\mathbf{x}, \boldsymbol{\eta}, \boldsymbol{\mu}) &= h(\psi_1(x_1, \eta_1), \ldots, \psi_d(x_d, \eta_d)) \prod_{j=1}^d \sqrt{\omega_j(\psi_j(x_j, \eta_j), \mu_j)\, \psi_j'(x_j, \eta_j)} \\
&= \prod_{j=1}^d \eta_j^{\frac{1}{2}}\, \mathrm{e}^{\frac{1}{2}\left(1 - \eta_j^2 - \mu_j^2 \eta_j^2\right)\operatorname{erf}^{-1}(2x_j)^2}. \qquad (4.7.4)
\end{aligned}$$

In Figure 4.7.1 we have a side-by-side comparison of the graphs of these transformed functions in $d = 1$ for fixed $\eta = 1$ with various parameters $1 \le \mu^2 \le 10$.

We proceed to determine the values $\boldsymbol{\eta}, \boldsymbol{\mu} \in \mathbb{R}_+^d$ for which $f(\cdot, \boldsymbol{\eta}, \boldsymbol{\mu})$ as in (4.7.4) is element of $\mathcal{H}^m(\mathbb{T}^d)$ by checking the conditions (4.4.9) of Theorem 4.4.2. First of all, for all $\eta_1, \ldots, \eta_d > 0$ we observe that the univariate components $\psi_1, \ldots, \psi_d$ of the error function transformation $\psi(\cdot, \boldsymbol{\eta})$ in (4.7.3) are transformations in the sense of (4.1.1) by being increasing, continuously

differentiable and invertible functions. Furthermore, for all $\ell \in \{1, \dots, d\}$ it is easy to check that its first three derivatives of all $\psi_j(\cdot, \eta_j)$ are in fact continuous on $(-\frac{1}{2}, \frac{1}{2})$ for $\eta_j > 0$ and that the first three derivatives of $\varrho_j(\cdot, \eta_j)$ are in $\mathcal{C}_0(\mathbb{R})$ for all $0 < \eta_j \in \mathbb{R}$. Finally, we check the L_∞-conditions (4.4.9) in Theorem 4.4.2 for $m \in \{0, 1, 2, 3\}$. We suppose that for $\ell \in \{1, \dots, d\}$ we have $m = m_\ell$ and need to check that the appearing $L_\infty(\mathbb{T})$-norms are finite for all $j_\ell \in \{0, \dots, m\}$:

- Let $m = 0$. The $L_\infty(\mathbb{T})$-norm of
$$\sqrt{\omega(\psi(x, \eta), \mu)} = \pi^{-\frac{1}{4}} \mathrm{e}^{-\frac{1}{2}\eta^2\mu^2 \operatorname{erf}^{-1}(2x)^2}$$
is finite for $\eta^2\mu^2 \geq 0$.

- Let $m = 1$. We have to check two conditions. For $j_\ell = 0$ the $L_\infty(\mathbb{T})$-norm of
$$\begin{aligned}&\frac{\partial}{\partial x_\ell}\left[\sqrt{\omega_\ell(\psi_\ell(x_\ell, \eta_\ell), \mu_\ell)\, \psi_\ell'(x_\ell, \eta_\ell)}\right] \psi_\ell'(x_\ell, \eta_\ell)^{-\frac{1}{2}} \\ &= \pi^{\frac{1}{4}} \frac{\eta_\ell^2 - \mu_\ell^2}{\eta_\ell^2} \operatorname{erf}^{-1}(2x_\ell)\, \mathrm{e}^{-\frac{1}{2}(\eta_\ell^2\mu_\ell^2 - 2)\operatorname{erf}^{-1}(2x_\ell)^2}\end{aligned}$$
is finite for $\eta_\ell^2\mu_\ell^2 > 2$. For $j_\ell = 1$ the $L_\infty(\mathbb{T})$-norm of
$$\sqrt{\omega_\ell(\psi_\ell(x_\ell, \eta_\ell), \mu_\ell)\, \psi_\ell'(x_\ell, \eta_\ell)}\, (\psi_\ell'(x_\ell, \eta_\ell))^{\frac{1}{2}} = \pi^{\frac{1}{4}} \mathrm{e}^{-\frac{1}{2}(\mu_\ell^2\eta_\ell^2 - 2)(\operatorname{erf}^{-1}(2x_\ell)^2}$$
is finite if the exponent is negative or zero, which is the case for $\eta_\ell^2\mu_\ell^2 \geq 2$.

- Let $m = 2$. We check three conditions. For $j_\ell = 0$ the $L_\infty(\mathbb{T})$-norm of
$$\frac{\partial^2}{\partial x_\ell^2}\left[\sqrt{\omega_\ell(\psi_\ell(x_\ell, \eta_\ell), \mu_\ell)\, \psi_\ell'(x_\ell, \eta_\ell)}\right] \psi_\ell'(x_\ell, \eta_\ell)^{-\frac{1}{2}}$$
is finite for all $\eta_\ell^2\mu_\ell^2 > 4$. For $j_\ell = 1$ the $L_\infty(\mathbb{T})$-norm of
$$\frac{\partial}{\partial x_\ell}\left[\sqrt{\omega_\ell(\psi_\ell(x_\ell, \eta_\ell), \mu_\ell)\, \psi_\ell'(x_\ell, \eta_\ell)}\right] \psi_\ell'(x_\ell, \eta_\ell)^{\frac{1}{2}}$$
is finite for all $\eta_\ell^2\mu_\ell^2 > 4$. For $j_\ell = 2$ the $L_\infty(\mathbb{T})$-norm of
$$\sqrt{\omega_\ell(\psi_\ell(x_\ell, \eta_\ell), \mu_\ell)\, \psi_\ell'(x_\ell, \eta_\ell)}\, (\psi_\ell'(x_\ell, \eta_\ell))^{\frac{5}{2}}$$
is finite for all $\eta_\ell^2\mu_\ell^2 \geq 6$.

- For $m = 3$ the individual conditions for $k \in \{0, 1, 2, 3\}$ are finite in case of $\eta_\ell^2\mu_\ell^2 > 6$, $\eta_\ell^2\mu_\ell^2 > 6$, $\eta_\ell^2\mu_\ell^2 > 8$ and $\eta_\ell^2\mu_\ell^2 \geq 10$ respectively. Hence, we need $\eta_\ell^2\mu_\ell^2 \geq 10$ in order to have $f \in H^3_{\mathrm{mix}}(\mathbb{T}^d) \sim \mathcal{H}^3(\mathbb{T}^d)$.

In total, for $j \in \{1, \dots, d\}$ we have
$$f \in \begin{cases} L_2(\mathbb{T}^d) & \text{for} \quad \eta_j^2\mu_j^2 \geq 0, \\ \mathcal{H}^1(\mathbb{T}^d) & \text{for} \quad \eta_j^2\mu_j^2 > 2, \\ \mathcal{H}^2(\mathbb{T}^d) & \text{for} \quad \eta_j^2\mu_j^2 \geq 6, \\ \mathcal{H}^3(\mathbb{T}^d) & \text{for} \quad \eta_j^2\mu_j^2 \geq 10. \end{cases} \tag{4.7.5}$$

For numerical tests, we start with single rank-1 methods in dimensions $d \in \{1, 2\}$, switch to multiple rank-1 methods in dimension $d = 4$ and finally use the sparse FFT and an unknown frequency set in dimensions $d \geq 4$.

(4.7.3) erf transf. $\psi(\cdot,\eta)$	bounds by Thm. 4.5.1 and 4.5.2 ε_2^M	ε_∞^M	Numerical observation ε_2^M	ε_∞^M
$\eta^2 = 1$			$N^{-0.5}$	N^0
$\eta^2 = 3$	N^{-1}	N^0	$N^{-1.4}$	$N^{-0.9}$
$\eta^2 = 6$	N^{-2}	N^{-1}	$N^{-2.7}$	$N^{-2.2}$
$\eta^2 = 10$	N^{-3}	N^{-2}	$N^{-4.5}$	N^{-4}

Table 4.7.1: The observed decay rates of the discrete approximation errors $\varepsilon_2^M(h,\{\mathbf{y}_j\}_{j=1}^M)$ and $\varepsilon_\infty^M(h,\{\mathbf{y}_j\}_{j=1}^M)$ as given in (4.6.2) in comparison with the upper bounds proposed in Theorems 4.5.2 and 4.5.1 when h is the univariate function in (4.7.2).

4.7.1 Single rank-1 lattices in dimension $d = 1$

Next, we discuss the application of the weighted $L_2(\mathbb{R}^d)$-approximation error bound in Theorem 4.5.1 and the weighted $L_\infty(\mathbb{R}^d)$-approximation error bound in Theorem 4.5.2 for $d = 1$ with the given function h in (4.7.2), the Gaussian measure function (4.7.1), the parameterized error function transformation (4.7.3) and the resulting transformed functions f of the form in (4.7.4).

Let a reconstructing rank-1 lattice $\Lambda(\mathbf{z}, M, I_N^1)$ with $N \geq 1$ be given. In (4.7.5) we already evaluated the sufficient conditions proposed in Theorem 4.4.2, yielding lower bounds for $\eta, \mu \in \mathbb{R}_+$ such that $f \in \mathcal{H}^m(\mathbb{T})$ for $m \in \{0,1,2,3\}$. We fix $\lambda = 1$ and for $m \in \mathbb{N}$ we choose $\mu, \eta \in \mathbb{R}_+$ such that $f \in \mathcal{H}^m(\mathbb{T}) \hookrightarrow \mathcal{A}^{m-1}(\mathbb{T})$ as in (3.1.9). Theorems 4.5.1 and 4.5.2 provide worst case upper bounds for both discrete approximations errors $\varepsilon_2^M(h,\{\mathbf{y}_j\}_{j=1}^M)$ and $\varepsilon_\infty^M(h,\{\mathbf{y}_j\}_{j=1}^M)$ of the form

$$\varepsilon_2^M(h,\{\mathbf{y}_j\}_{j=1}^M) \approx \left\| h - S_{I_N^d}^\Lambda h \right\|_{L_2\left(\mathbb{R}^d,\omega\right)} \lesssim N^{-m},$$

$$\text{and} \quad \varepsilon_\infty^M(h,\{\mathbf{y}_j\}_{j=1}^M) \approx \left\| h - S_{I_N^d}^\Lambda h \right\|_{L_\infty\left(\mathbb{R}^d,\sqrt{\frac{\omega}{\varrho}}\right)} \lesssim N^{-m+1}$$

which are valid if the corresponding transformed function f is in $\mathcal{H}^m(\mathbb{T}), m \geq 1$, which is the case for all parameters $\eta^2\mu^2 > 2$ as calculated in (4.7.5). We list these worst case upper bounds in Table 4.7.1 for $\mu = 1$ accordingly.

For $N \in \{1,\ldots,100\}$, $\mu = 1$ and $\eta \in \{1,\sqrt{3},\sqrt{6},\sqrt{10}\}$ we generate ten random rank-1 lattices as described in (3.5.5), so that the discrete approximation errors are evaluated at $M \approx 1.5 \cdot 10^4$ random nodes in $\left(-\frac{1}{2},\frac{1}{2}\right)$. Additionally, for each η we repeat the calculations five times and plot the averages of the errors. As shown in Figure 4.7.2, the decay rates of both approximation errors increase significantly if the parameter η is chosen large enough. In Table 4.7.1 we also list the exact approximation errors obtained in the numerical tests.

Remark 4.7.1. *The evaluated error are measured in weighted $L_2(\mathbb{R},\omega)$- and $L_\infty\left(\mathbb{R},\sqrt{\frac{\omega}{\varrho}}\right)$-norms, where the parameter μ of the measure function $\omega(\cdot,\mu)$ is fixed and the parameter η in the transformation $\psi(\cdot,\eta)$ is varied. Therefore, on one hand, the error plots on the left hand side of Figure 4.7.2 are comparable to each other as they are based on the same norm. On the other hand, the error plots on the right hand side of the same Figure are based on different norms due to the variation of the transformations $\psi(\cdot,\eta)$ and their densities $\varrho(\cdot,\eta)$. But for simplicity we still show them in one figure.*

The same remark has to be made about the plots for dimension $d = 2$ in Figure 4.7.3 and $d = 7$ in Figure 4.7.7. □

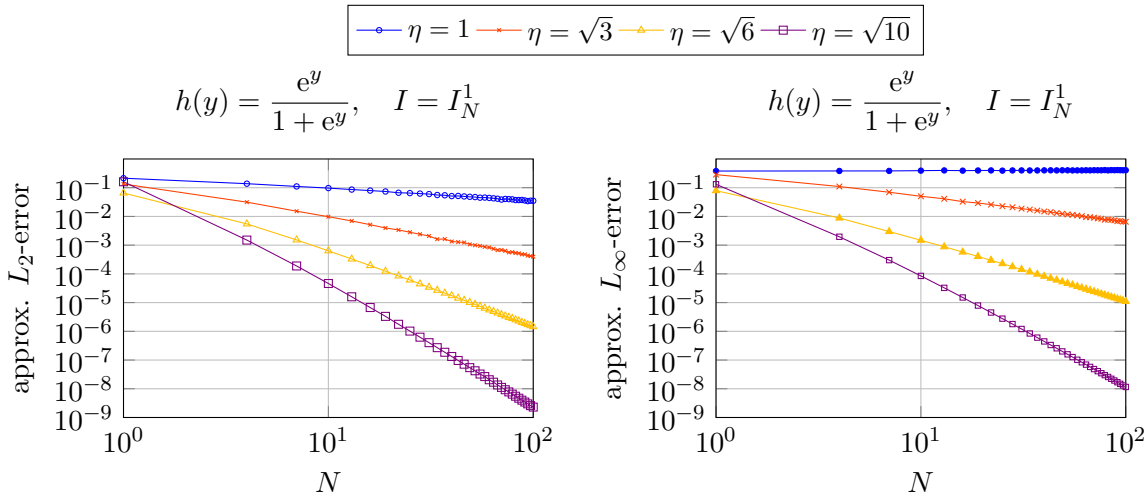

Figure 4.7.2: Comparison of the approximated errors $\varepsilon_2^M(h, \{\mathbf{y}_j\}_{j=1}^M)$ and $\varepsilon_\infty^M(h, \{\mathbf{y}_j\}_{j=1}^M)$ at $12.000 \leq M \leq 18.000$ random samples of the univariate function (4.7.2) combined with the error function transformation $\psi(\cdot, \eta)$ in (4.7.3) for $\eta \in \{1, \sqrt{3}, \sqrt{10}, \sqrt{16}\}$.

4.7.2 Single rank-1 lattices in dimension $d = 2$

Next, we discuss the application of the $L_2(\mathbb{R}^d)$-approximation error bound in Theorem 4.5.1 and the $L_\infty(\mathbb{R}^d)$-approximation error bound in Theorem 4.5.2 for $d = 2$ with the measure function (4.7.1), the given function in (4.7.2), the parameterized error function transformation (4.7.3) and the resulting transformed functions f given in (4.7.4).

Let a reconstructing rank-1 lattice $\Lambda(\mathbf{z}, M, I_N^2)$ with $N \geq 1$ be given. In (4.7.5) we already evaluated the sufficient conditions proposed in Theorem 4.4.2, yielding lower bounds for $\boldsymbol{\mu}, \boldsymbol{\eta} \in \mathbb{R}_+^2$ such that $f \in \mathcal{H}^m(\mathbb{T}^2)$ for $m \in \{0, 1, 2, 3\}$. We fix $\lambda = 1$ and for $m \in \mathbb{N}$ we choose $\boldsymbol{\mu}, \boldsymbol{\eta} \in \mathbb{R}_+^2$ such that $f \in \mathcal{H}^m(\mathbb{T}^2) \hookrightarrow \mathcal{A}^{m-1}(\mathbb{T}^2)$ as in (3.1.9). According to Theorems 4.5.1 and 4.5.2, the discrete approximation errors as given in (4.6.2) are bounded from above by

$$\varepsilon_2^M(h, \{\mathbf{y}_j\}_{j=1}^M) \lesssim \begin{cases} N^{-1}(\log N)^{\frac{1}{2}} & \text{for} \quad \eta_\ell^2 \mu_\ell^2 > 2, \\ N^{-2}(\log N)^{\frac{1}{2}} & \text{for} \quad \eta_\ell^2 \mu_\ell^2 \geq 6, \\ N^{-3}(\log N)^{\frac{1}{2}} & \text{for} \quad \eta_\ell^2 \mu_\ell^2 \geq 10, \end{cases} \tag{4.7.6}$$

and

$$\varepsilon_\infty^M(h, \{\mathbf{y}_j\}_{j=1}^M) \lesssim \begin{cases} N^{0} & \text{for} \quad \eta_\ell^2 \mu_\ell^2 > 2, \\ N^{-1} & \text{for} \quad \eta_\ell^2 \mu_\ell^2 \geq 6, \\ N^{-2} & \text{for} \quad \eta_\ell^2 \mu_\ell^2 \geq 10, \end{cases} \tag{4.7.7}$$

for sufficiently large numbers of random points $M \in \mathbb{N}$, $\ell \in \{1, \ldots, d\}$.

For $N \in \{1, \ldots, 100\}$, $\boldsymbol{\mu} = \mathbf{1}$ and $\boldsymbol{\eta} \in \{\mathbf{1}, \sqrt{\mathbf{3}}, \sqrt{\mathbf{6}}, \sqrt{\mathbf{10}}\}$ we generate ten random rank-1 lattices as described in (3.5.5), so that the discrete approximation errors are evaluated at $M \approx 10^5$ random nodes in $\left(-\frac{1}{2}, \frac{1}{2}\right)^2$. Additionally, for each $\boldsymbol{\eta}$ we repeat the calculations five times and plot the averages of the errors. As shown in Figure 4.7.3, the decay rates of both approximation errors increase significantly if the parameters $\boldsymbol{\eta}$ are chosen large enough.

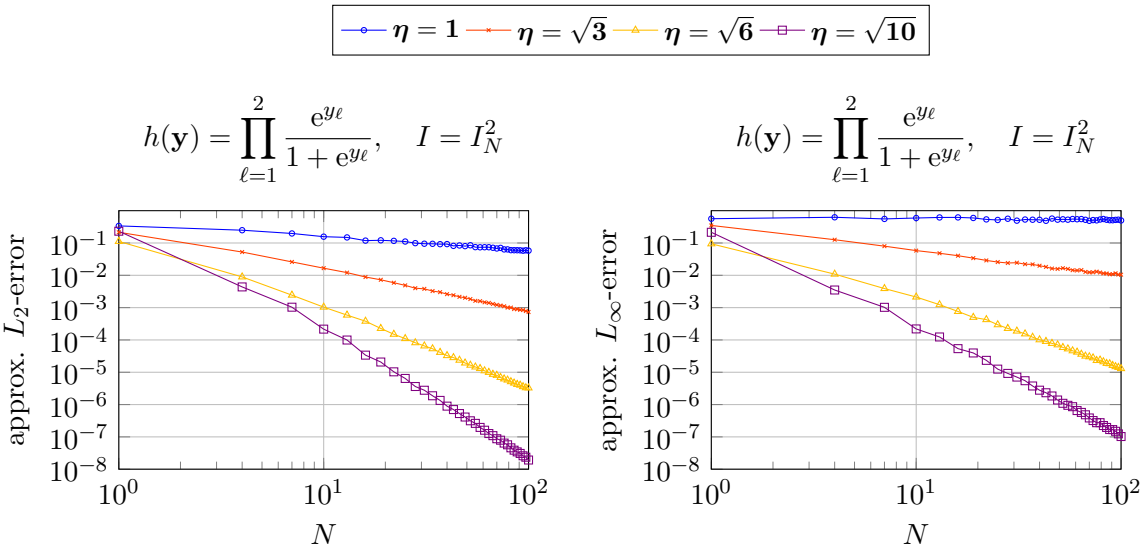

Figure 4.7.3: Comparison of $\varepsilon_2^M(h, \{\mathbf{y}_j\}_{j=1}^M)$ and $\varepsilon_\infty^M(h, \{\mathbf{y}_j\}_{j=1}^M)$ at $100.000 \leq M \leq 150.000$ random samples of function (4.7.2) in dimension $d = 2$ combined with the error function transformation $\psi(\cdot, \boldsymbol{\eta})$ in (4.7.3) for $\boldsymbol{\eta} \in \{\mathbf{1}, \sqrt{\mathbf{3}}, \sqrt{\mathbf{6}}, \sqrt{\mathbf{10}}\}$.

4.7.3 Multiple rank-1 lattices in dimension $d = 4$

In this section, we apply the techniques of multiple rank-1 lattices [Käm18]. We recalled in (3.4.5) that a multiple rank-1 lattice is a union of up to $t \in \mathbb{N}$ single rank-1 lattices $\Lambda(\mathbf{z}_j, M_j), j \in \{1, \ldots, t\}$. The previously outlined periodization approach is incorporated easily. After choosing a torus-to-$\mathbb{R}^d$ transformation $\psi(\cdot, \boldsymbol{\eta}), \boldsymbol{\eta} \in \mathbb{R}_+^d$ as in (4.1.1), we define a *transformed multiple rank-1 lattice* as the union of t transformed rank-1 lattices

$$\Lambda_{\psi(\cdot,\boldsymbol{\eta})}(\mathbf{z}_1, M_1, \ldots, \mathbf{z}_t, M_t) := \bigcup_{j=1,\ldots,t} \Lambda_{\psi(\cdot,\boldsymbol{\eta})}(\mathbf{z}_j, M_j). \tag{4.7.8}$$

In particular, we utilize [Käm19, Algorithm 6] on h at a transformed multiple rank-1 lattice to efficiently reconstruct the approximated Fourier coefficients $\hat{h}_{\mathbf{k}}^{\Lambda}$. This approach has two major advantages. On one hand, we don't need to construct the generating vector $\mathbf{z}$ via component-by-component construction methods, which generally takes quite some time. On the other hand, the upper bound on the lattice size decreases significantly, as pointed out in (3.4.6), which makes it easier to investigate higher dimensional problems.

For $N \in \{1, \ldots, 30\}$, $\boldsymbol{\mu} = \mathbf{1}$ and $\boldsymbol{\eta} \in \{\mathbf{1}, \sqrt{\mathbf{3}}, \sqrt{\mathbf{6}}, \sqrt{\mathbf{10}}\}$ we initialize [Käm19, Algorithm 6] with the parameters $c = 2, n = 4$ and $\delta = \frac{1}{2}$ to efficiently reconstruct the approximated Fourier coefficients $\hat{h}_{\mathbf{k}}^{\Lambda}$ by means of a transformed multiple rank-1 lattice as in (4.7.8) and to form the approximated Fourier partial sum $S_I^{\Lambda} h$. Afterwards, we generate ten random rank-1 lattices as described in (3.5.5), so that the discrete approximation errors are evaluated at $M \approx 5.3 \cdot 10^6$ random nodes in $\left(-\frac{1}{2}, \frac{1}{2}\right)^2$. Additionally, for each $\boldsymbol{\eta}$ we repeat the calculations five times and plot the averages of the errors.

As shown in Figure 4.7.4, the decay rates of both approximation errors increase significantly if the parameters $\boldsymbol{\eta}$ are chosen large enough. However, as in the previous example, for large $\boldsymbol{\eta}$ we obtain step-like error plots in the top row of Figure 4.7.4, which indicates that the largest Fourier coefficients of h are not primarily located around the coordinate axis. At the same time, the hyperbolic cross I_N^4 is defined in such a way that an increase

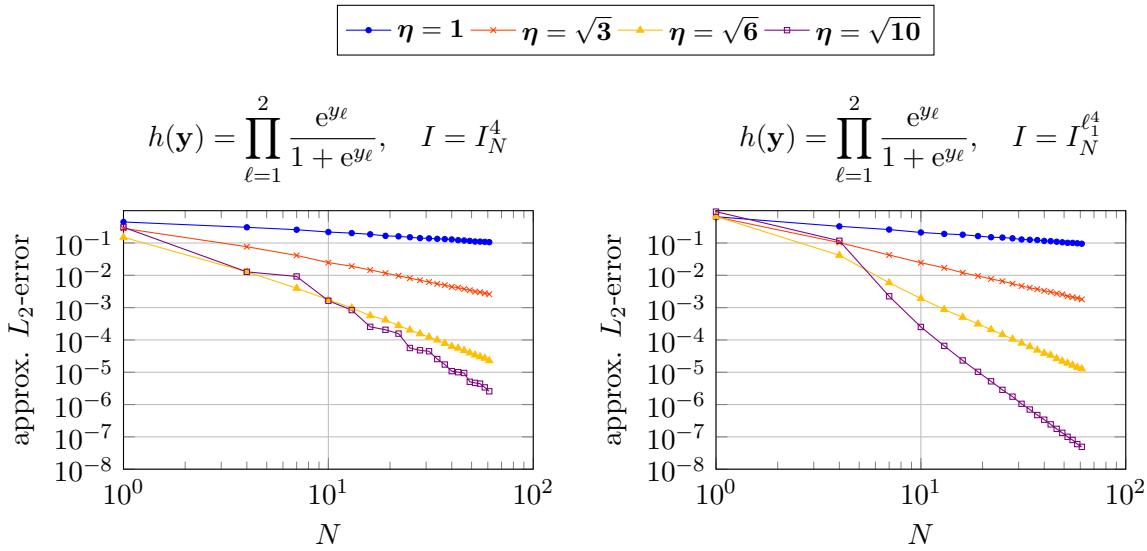

Figure 4.7.4: Comparison of $\varepsilon_2^M(h, \{\mathbf{y}_j\}_{j=1}^M)$ at $4.0 \cdot 10^7 \leq M \leq 6.6 \cdot 10^7$ random samples of function (4.7.2) in dimension $d = 4$ combined with the error function transformation $\psi(\cdot, \boldsymbol{\eta})$ in (4.7.3) for $\boldsymbol{\eta} \in \{\mathbf{1}, \sqrt{\mathbf{3}}, \sqrt{\mathbf{6}}, \sqrt{\mathbf{10}}\}$, for the hyperbolic cross I_N^4 (left) and the scaled ℓ_1^4-ball $I_N^{\ell_1^4}$ (right).

from N to $N+1$ primarily adds frequencies along the coordinate axis. Hence, even tough the proposed decay behavior in (4.7.6) is still obtained, the results suggest that there are more suitable choices for frequency sets in this setup. Therefore, we repeat the same tests for the scaled four-dimensional ℓ_1^4-unit ball $I_N^{\ell_1^4}$ and obtain much smoother error plots in the bottom row of Figure 4.7.4. But, it has to emphasized that the ℓ_1^4-unit ball contains a lot more frequencies than a hyperbolic cross I_N^d for the same $N \in \mathbb{N}$, which results a significantly longer computation time.

4.7.4 Suitable frequency sets in up to dimension $d = 7$

The previous numerical tests for single and multiple rank-1 lattices revealed that it is easy to create examples in which certain combinations of a given function $h \in L_2(\mathbb{R}^d, \omega(\cdot, \boldsymbol{\mu}))$, a measure function $\omega(\cdot, \boldsymbol{\mu})$ and a torus-to-$\mathbb{R}^d$ transformation $\psi(\cdot, \boldsymbol{\eta})$ lead to transformed functions $f = f(\cdot, \boldsymbol{\eta}, \boldsymbol{\mu})$ as in (4.4.7), for which a hyperbolic cross I_N^d might not be the best choice for a frequency set as the frequencies $\mathbf{k}$ belonging to the largest Fourier coefficients $\hat{h}_{\mathbf{k}}$ supposedly are not clustering along the coordinate axis. Generally, we do not have the exact values of the Fourier coefficients $\hat{h}_{\mathbf{k}}$, so that we must guess an optimal choice for an initially given frequency set. Alternatively, we use a dimension incremental construction method [Vol15, PV16] that reconstructs sparse multivariate trigonometric polynomials p with an unknown support in a frequency domain $I \subset \mathbb{Z}^d$. Based on the component-by-component construction of rank-1 lattices, the approach of [PV16, Algorithm 1 and Algorithm 2] determines the $s \in \mathbb{N}$ approximately largest Fourier coefficients $\hat{p}_{\mathbf{k}}$ within a fixed search space $[-N, N]^d \cap \mathbb{Z}^d$ with $N \in \mathbb{N}$ and $s \ll (2N+1)^d$. We adapt these algorithms for transformed reconstructing rank-1 lattices $\Lambda_{\psi(\cdot,\boldsymbol{\eta})}(\mathbf{z}, M, I)$ by again calculating the relative discretized approximation errors $\varepsilon_2^M(h, \{\mathbf{y}_j\}_{j=1}^M)$ and $\varepsilon_\infty^M(h, \{\mathbf{y}_j\}_{j=1}^M)$ with samples $\left(h(\mathbf{y}_j)\sqrt{\frac{\omega(\mathbf{y}_j,\boldsymbol{\mu})}{\varrho(\mathbf{y}_j,\boldsymbol{\eta})}}\right)_{j=0}^{M-1}$

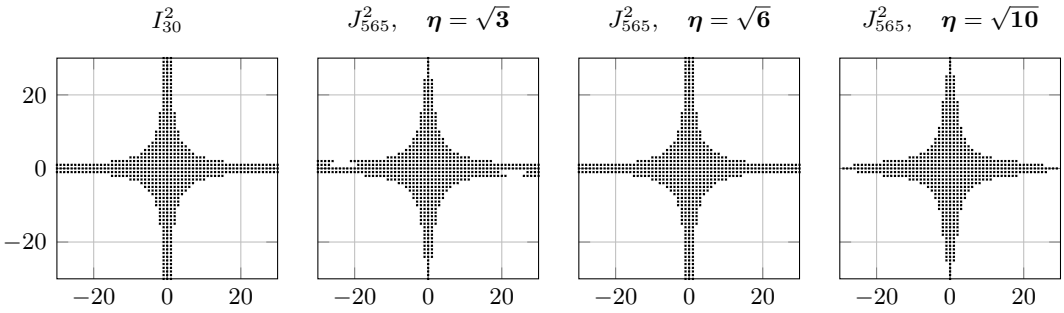

Figure 4.7.5: The two-dimensional hyperbolic cross I_{30}^2 and the sparse frequency set J_s^d with sparsity $s = |I_{30}^2| = 565$ generated by a dimension incremental construction approach for the parameterized error function transformation $\psi(\cdot, \boldsymbol{\eta})$ as in (4.7.3) with $\boldsymbol{\eta} \in \{\sqrt{\mathbf{3}}, \sqrt{\mathbf{6}}, \sqrt{\mathbf{10}}\}$.

and $\left(\sqrt{\frac{\omega(\mathbf{y}_j,\boldsymbol{\mu})}{\varrho(\mathbf{y}_j,\boldsymbol{\eta})}}\, S_I^{\Lambda} h(\mathbf{y}_j)\right)_{j=0}^{M-1}$ but use an unknown frequency set I with cardinality $s = |I_N^d|$ that was constructed via a dimensional incremental construction method as outlined above.

We remain in the initial setup of using the Gaussian function h as in (4.7.2), the Gaussian measure function (4.7.1) and the error function transformation (4.7.3). In dimension $d = 2$, we compare the hyperbolic cross I_{30}^2 with the frequency set J_s^d of cardinality $s = |I_{30}^2| = 565$ that is constructed in a dimension incremental way. The error plots in Figure 4.7.4 caused suspicion that larger parameter choices, the largest Fourier coefficients of the transformed functions (4.7.4) cluster less along the coordinate axis like a hyperbolic cross. Figure 4.7.5 shows that the frequencies belonging to the largest Fourier coefficients vary depending on the the parameter $\boldsymbol{\eta}$ and might be an indication as to why the approximation errors with respect to the two-dimensional ℓ_1^2-unit ball, shown on the right of Figure 4.7.4, are so much better than when a hyperbolic cross is used on the left of Figure 4.7.4.

Finally, we apply the sparse FFT algorithm [PV16, Algorithm 2] to have an efficient fast Fourier transformation in combination with a suitable and sparse frequency set J_s^d for the transformed function (4.7.4). Again, let $d = 4, N \in \{1, \ldots, 60\}, \boldsymbol{\mu} = \mathbf{1}$ and $\boldsymbol{\eta} \in \{\mathbf{1}, \mathbf{3}, \mathbf{6}, \mathbf{10}\}$. On the left of Figure 4.7.6, we show the results from using multiple rank-1 lattices with the given hyperbolic cross sets I_N^4 from Figure 4.7.4, but this time the cardinalities of the hyperbolic crosses $|I_N^4|$ are used on the x-axis. On the right of Figure 4.7.6 are the approximation errors $\varepsilon_\infty^M(h)$ and $\varepsilon_2^M(h)$ that are the result from applying the algorithm called 'a2r1l' in [Vol15] and use the cardinality of the hyperbolic cross I_N^4 as the sparsity parameter 'sparsity_s' $= s = |I_N^4|$. As it turns out, the sparse FFT algorithm yields the initially proposed error decay behavior (4.7.6), in which an increase of the parameter $\boldsymbol{\eta}$ causes a much faster approximation error decay. Additionally, the computation speed of the sparse FFT method is slightly slower than the multiple rank-1 method with a fixed hyperbolic cross frequency set, but also much faster than the multiple rank-1 method with a fixed ℓ_1^d-unit ball. So, the sparse FFT algorithms trades off a bit computation speed in order to automatically construct a suitable frequency set for the initially given function. We repeat this test for dimension $d = 7$ for $N \in \{1, \ldots, 17\}$ as shown in Figure 4.7.7.

4.8 Summary of the numerics on $\mathbb{R}^d$

We presented the approximation results of the transformed Fourier system (4.5.2) for the error function transformation (4.7.3) in up to dimension $d = 7$. Numerical tests highlighted

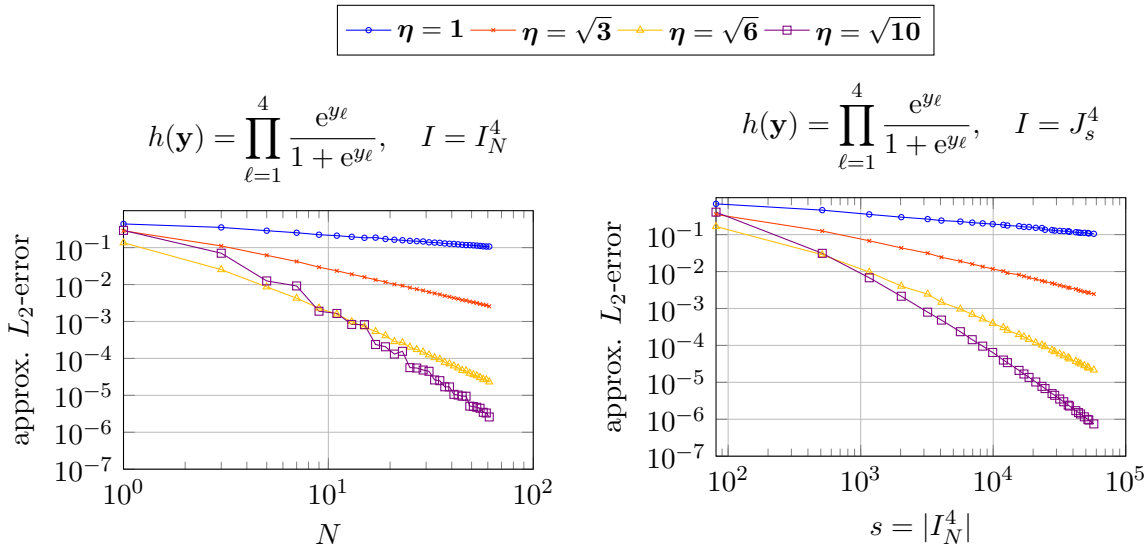

Figure 4.7.6: Comparison of $\varepsilon_2^M(h, \{\mathbf{y}_j\}_{j=1}^M)$ at $4.0 \cdot 10^6 \leq M \leq 6.6 \cdot 10^6$ random samples of function (4.7.2) in dimension $d = 4$ combined with the error function transformation $\psi(\cdot, \boldsymbol{\eta})$ in (4.7.3) for $\boldsymbol{\eta} \in \{\mathbf{1}, \sqrt{\mathbf{3}}, \sqrt{\mathbf{6}}, \sqrt{\mathbf{10}}\}$ and for the hyperbolic cross I_N^4 (top) and the constructed sparse index set $J^4_{|I_N^4|}$ (bottom).

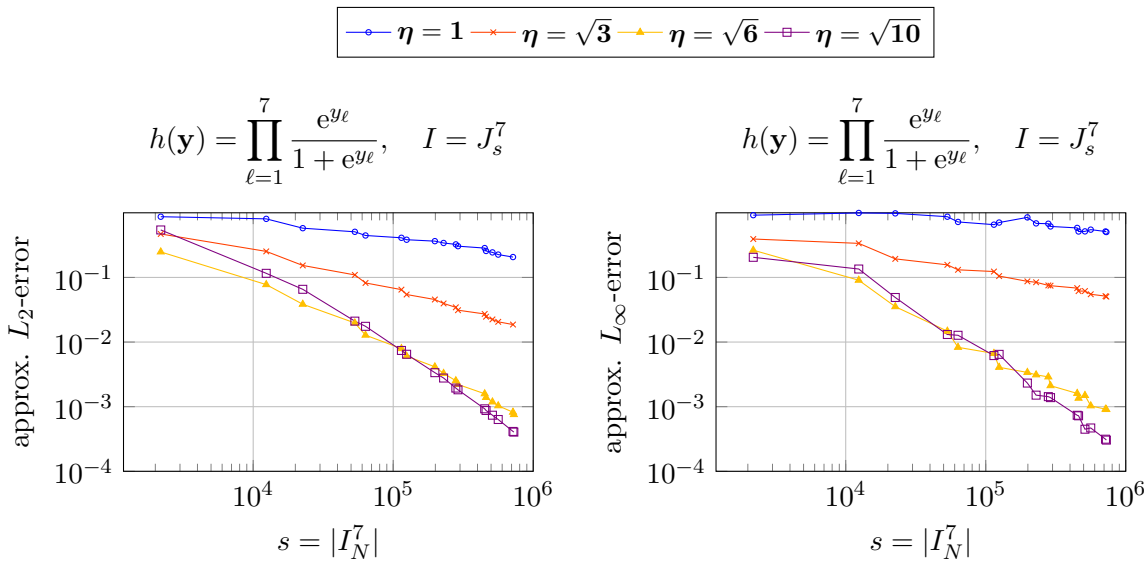

Figure 4.7.7: Comparison of $\varepsilon_2^M(h, \{\mathbf{y}_j\}_{j=1}^M)$ and $\varepsilon_\infty^M(h, \{\mathbf{y}_j\}_{j=1}^M)$ in dimension $d = 7$ of function (4.7.2) for the error function transformation $\psi(\cdot, \boldsymbol{\eta})$ in (4.7.3) for $\boldsymbol{\eta} \in \{\mathbf{1}, \sqrt{\mathbf{3}}, \sqrt{\mathbf{6}}, \sqrt{\mathbf{10}}\}$ with the sparse index set $J^d_{|I_N^d|}$.

certain limitations of the presented periodization strategy to transform functions from the function space $L_2(\mathbb{R}^d, \omega(\cdot, \boldsymbol{\mu})) \cap \mathcal{H}^m(\mathbb{R}^d)$ into smooth functions in $\mathcal{H}^m(\mathbb{T}^d)$ via a torus-to-$\mathbb{R}^d$ transformation $\psi(\cdot, \boldsymbol{\eta}), \boldsymbol{\eta} \in \mathbb{R}_+^d$ as defined in (4.1.3). In lower dimensions $d \in \{1, 2\}$, we observed good approximation results with the Fourier approach based on a single rank-1 lattice. For higher dimensions $d \geq 4$, we switched to the more efficient Fourier approach based on multiple rank-1 lattices to save on computation time and on the number of necessary sam-

pling nodes. The combination of working in a high dimension $d \in \mathbb{N}$ and having large enough parameters $\boldsymbol{\eta}, \boldsymbol{\mu} \in \mathbb{R}_+^d$ smoothened the given functions so much that they are essentially 0 near the boundary points of their domain, so that the hyperbolic cross frequency sets (3.1.5) started to contain a significant number of Fourier coefficients that are (almost) zero, which lowered the quality of the approximations. Therefore, we switched to a dimension incremental construction to determine the frequencies belonging to the largest Fourier coefficients within a fixed search space before each approximation, which again improved the approximation results for a slight increase in computation time.

We observed, that even though the L_∞-conditions (4.4.9) on $\psi(\cdot, \boldsymbol{\eta})$ and $\omega(\cdot, \boldsymbol{\mu})$ in Theorem 4.4.2 are rather easy to check, the resulting parameter bounds for $\boldsymbol{\eta}$ and $\boldsymbol{\mu}$ are worst case bounds and are more or less optimal, which has to be checked individually in any specific example. On a similar note, the upper approximation error bounds of Theorems 4.5.1 and 4.5.2 are worst case upper bounds, too, so that the constants appearing after the estimates may have some bad growth behavior for certain combinations of $\psi(\cdot, \boldsymbol{\eta})$ and $\omega(\cdot, \boldsymbol{\mu})$, potentially causing the problematic preasymptotical behavior that we observed in higher dimensions.

Besides studying the structure and growth behavior of the constants in the error estimates, it might be helpful to extend the impact of the measure function $\omega(\cdot, \boldsymbol{\mu})$. For example in [Suz20] an approximation approach is presented in which each derivative of h is weighted by an algebraic or exponential weight before being evaluated in some norm.

Chapter 5

Torus-to-cube transformation mappings

We introduce the notation of torus-to-cube mappings ${}_{\square}\psi : \left[-\frac{1}{2}, \frac{1}{2}\right]^d \to \left[-\frac{1}{2}, \frac{1}{2}\right]^d$ and prove a set of conditions on the transformation ${}_{\square}\psi$ and the involved function spaces for which we obtain a bounded mapping of the form

$$L_2\left(\left[-\frac{1}{2}, \frac{1}{2}\right]^d, \omega\right) \cap \mathcal{C}^m_{\text{mix}}\left(\left[-\frac{1}{2}, \frac{1}{2}\right]^d\right) \ni h \mapsto h({}_{\square}\psi(\cdot)) \sqrt{\omega({}_{\square}\psi(\cdot)) \prod_{j=1}^{d} {}_{\square}\psi'_j(\cdot)} \in \mathcal{H}^m(\mathbb{T}^d).$$

Then, we are able to apply the various approximation techniques for smooth periodic function on the torus $\mathbb{T}^d$ from Chapter 3 and transfer the orthonormality of the Fourier system, important upper approximation error bounds and the efficient Algorithms based on rank-1 lattices by means of the inverse torus-to-cube transformation ${}_{\square}\psi^{-1}$ to the considered non-periodic function class defined on $\left[-\frac{1}{2}, \frac{1}{2}\right]^d$. Parts of the content in this chapter were already published in [NP21a, NP21b].

In Section 5.1 we define invertible torus-to-cube transformations ${}_{\square}\psi$, cf. (5.1.1), and we fix the notation of the density function ${}_{\square}\varrho$ as the derivative of the inverse of a torus-to-cube transformation. We're mainly interested in classes of torus-to-cube transformations ${}_{\square}\psi$ that are induced by torus-to-$\mathbb{R}$ transformations ψ and are of the form ${}_{\square}\psi(\cdot, \eta) = \psi^{-1}(\eta\, \psi(x)), \eta \in \mathbb{R}_+$, cf. (5.1.4).

In Section 5.2 we list some examples of torus-to-cube transformations ${}_{\square}\psi$, some of which are induced by torus-to-$\mathbb{R}$ transformations ψ. We also show examples of torus-to-$\mathbb{R}$ transformations ψ for which the composition $\psi^{-1}(\eta\, \psi(x))$ is not a torus-to-cube transformation ${}_{\square}\psi$ as defined in (5.1.4).

In Section 5.3 we consider measure functions $\omega(\cdot, \mu), \mu \in \mathbb{R}_+$. We investigate the structure of weighted exponential functions $\left\{\sqrt{\frac{{}_{\square}\varrho(\cdot,\eta)}{\omega(\cdot,\mu)}}\, \mathrm{e}^{2\pi \mathrm{i} k\, {}_{\square}\psi^{-1}(\cdot,\eta)}\right\}_{k\in\mathbb{Z}}$, cf. (5.3.2), that form an orthonormal system in the weighted $L_2\left(\left[-\frac{1}{2}, \frac{1}{2}\right]^d, \omega(\cdot, \mu)\right)$-function space.

In Section 5.4 we switch to parameter free notation and discuss the periodization approach via torus-to-cube transformations ${}_{\square}\psi$, that map functions $h \in L_2\left(\left[-\frac{1}{2}, \frac{1}{2}\right], \omega\right)$ onto functions $f \in L_2(\mathbb{T})$ of the form $f(x) := h({}_{\square}\psi(x)) \sqrt{\omega({}_{\square}\psi(x))\, {}_{\square}\psi'(x)}$, so that $\|h\|_{L_2\left(\left[-\frac{1}{2}, \frac{1}{2}\right], \omega\right)} = \|f\|_{L_2(\mathbb{T})}$. Afterwards, we assume more smoothness so that the given function h is also in the Sobolev space $H^m\left(\left[-\frac{1}{2}, \frac{1}{2}\right]\right)$, cf. (5.5.8). We prove the major Theorem 5.4.1 - with the multivariate version in Theorem 5.4.2 - in which we state a set of sufficient L_∞-conditions on the torus-

to-cube transformations ${}_{\square}\psi$ and the measure functions ω for which the periodized function f inherits the smoothness from h so that it is an element of the Sobolev space $\mathcal{H}^m(\mathbb{T})$.

In Section 5.5 we prove weighted upper $L_2\left(\left[-\frac{1}{2},\frac{1}{2}\right]^d,\omega\right)$- and $L_\infty\left(\left[-\frac{1}{2},\frac{1}{2}\right]^d,\sqrt{\frac{\omega}{{}_{\square}\varrho}}\right)$-approximation error bounds that are based on the worst case upper $L_2\left(\mathbb{T}^d\right)$- and $L_\infty\left(\mathbb{T}^d\right)$-approximation estimates from Section 3.5.

In Section 5.6 we again denote the torus-to-cube transformations ${}_{\square}\psi(\cdot,\boldsymbol{\eta})$ and measure functions $\omega(\cdot,\boldsymbol{\mu})$ with $\boldsymbol{\eta},\boldsymbol{\mu}\in\mathbb{R}_+^d$ in their parameterized form. We adapt the two algorithms 3.4.1 and 3.4.2 by incorporating the inverse torus-to-cube transformation ${}_{\square}\psi^{-1}(\cdot,\boldsymbol{\eta})$ and compare some transformed rank-1 lattices $\Lambda_{{}_{\square}\psi(\cdot,\boldsymbol{\eta})}(\mathbf{z},M)$.

In Section 5.7 we reflect on some classical orthonormal systems used for the approximation of functions defined on the cube $\left[-\frac{1}{2},\frac{1}{2}\right]^d$. Af first we define the half-periodic cosine system (5.7.1) which uses tent-transformed rank-1 lattice points (5.7.3) as samples in order to reduce the approximation of a function by its cosine partial sum to an FFT. Analogously, we define the Chebyshev polynomials (5.7.6) which use Chebyshev transformed rank-1 lattice sampling nodes (5.7.9) to reduce the approximation of a function by its Chebyshev partial sum to an FFT, too. We note that neither of these two transformations are torus-to-cube transformations. Nevertheless, we showcase that the transformed Fourier system from Section 5.3 provides a generalized framework for orthonormal systems. Inserting the Chebyshev transformation into the weighted exponential functions (5.3.2) yields again the Chebyshev system (5.7.1).

In Section 5.8 we discuss the obtained numerical results. We consider a constant measure function $\omega\equiv 1$ and apply the logarithmic torus-to-cube transformation (5.2.1) and the error function torus-to-cube transformation (5.2.2), as well as the sine transformation (5.2.3) to the transformed Fourier system (5.3.2). For these transformations we obtain that the periodized functions $f=f(\cdot,\boldsymbol{\eta})$ are in $\mathcal{H}^m(\mathbb{T}^d)$ if $\eta_j>2m+1, j\in\{1,\dots,d\}$. We compare the approximation quality of these specific transformed Fourier systems for varying values of $\boldsymbol{\eta}$ with the cosine and Chebyshev system from Section 5.8 and measure the discrete approximation errors $\varepsilon_2^M(h,\{\mathbf{y}_j\}_{j=1}^M)$ and $\varepsilon_\infty^M(h,\{\mathbf{y}_j\}_{j=1}^M)$ as given in (5.6.2). At first, we consider the tensored first order B-spline cutout B_1 in (5.8.4). As it turns out, even though some of the actual decay rates are the same, for certain parameter values $\eta_j>1$ the error function transformation yields by far the best approximation errors in up to dimension $d=7$. Secondly, we consider the tensored second order B-spline cutout B_2 in (5.8.5). In this example, there are parameter values for which the error function transformed Fourier system provides similar approximation errors as the Chebyshev system in low dimensions $d\le 4$. However, for dimension $d=7$ the Chebyshev system yields by far the best approximation results. Finally, we showcase one example in which the adapted sparse FFT algorithm once again shows it is strengths by improving the approximation errors of a 7-dimensional test function because of the dimension incremental construction of an initially unknown frequency set $I\subset\mathbb{Z}^d$ in reasonable time.

In Section 5.9 we summarize the obtained approximation results of the previous two numerical examples.

5.1 Torus-to-cube transformations

Following [NP21a, Section 3], a *torus-to-cube transformation* is defined as a mapping

$$ {}_{\square}\psi : \left[-\frac{1}{2}, \frac{1}{2}\right] \to \left[-\frac{1}{2}, \frac{1}{2}\right] \quad \text{with} \quad \lim_{x \to \pm\frac{1}{2}} {}_{\square}\psi(x) = \pm\frac{1}{2}, \tag{5.1.1} $$

that is continuously differentiable, increasing and ${}_{\square}\psi' \in \mathcal{C}_0\left(\left[-\frac{1}{2}, \frac{1}{2}\right]\right)$. Its inverse transformation is also continuously differentiable, increasing and is denoted by ${}_{\square}\psi^{-1} : [-\frac{1}{2}, \frac{1}{2}] \to [-\frac{1}{2}, \frac{1}{2}]$ in the sense of $y = {}_{\square}\psi(x) \Leftrightarrow x = {}_{\square}\psi^{-1}(y)$ with ${}_{\square}\psi^{-1}(y) \to \pm\frac{1}{2}$ as $y \to \pm\frac{1}{2}$. We call the first derivative of the inverse transformation the *density function* ${}_{\square}\varrho$ *of* ${}_{\square}\psi$, which is given by

$$ {}_{\square}\varrho(y) := ({}_{\square}\psi^{-1})'(y) = \frac{1}{{}_{\square}\psi'({}_{\square}\psi^{-1}(y))} $$

and for which

$$ \int_{-\frac{1}{2}}^{\frac{1}{2}} {}_{\square}\varrho(y)\,\mathrm{d}y = 1 $$

holds. In multiple dimensions we put

$$ {}_{\square}\psi(\mathbf{x}) := ({}_{\square}\psi_1(x_1), \ldots, {}_{\square}\psi_d(x_d))^\top \tag{5.1.2} $$

with $\mathbf{x} \in [-\frac{1}{2}, \frac{1}{2}]^d$ and we may use different univariate torus-to-cube transformations ${}_{\square}\psi_j$ in each coordinate $j \in \{1, \ldots, d\}$. The multivariate inverse transformation is denoted by ${}_{\square}\psi^{-1}(\mathbf{y}) := ({}_{\square}\psi_1^{-1}(y_1), \ldots, {}_{\square}\psi_d^{-1}(y_d))^\top$ and the density is given by

$$ {}_{\square}\varrho(\mathbf{y}) := \prod_{j=1}^{d} {}_{\square}\varrho_j(y_j), \quad \mathbf{y} \in \left[-\frac{1}{2}, \frac{1}{2}\right]^d. \tag{5.1.3} $$

We introduce a particular class of parameterized torus-to-cube transformations as defined in (5.1.1) that are based on torus-to-$\mathbb{R}$ transformations $\psi : (-\frac{1}{2}, \frac{1}{2}) \to \mathbb{R}$ with $\psi(x) \to \pm\infty$ for $x \to \pm\frac{1}{2}$ that are defined in (4.1.1). We obtain parameterized torus-to-cube transformations ${}_{\square}\psi(\cdot, \eta) : [-\frac{1}{2}, \frac{1}{2}] \to [-\frac{1}{2}, \frac{1}{2}]$ with $\eta \in \mathbb{R}_+$ by putting

$$ {}_{\square}\psi(x, \eta) := \begin{cases} \psi^{-1}(\eta\,\psi(x)) & \text{for} \quad x \in \left(-\frac{1}{2}, \frac{1}{2}\right), \\ \pm\frac{1}{2} & \text{for} \quad x = \pm\frac{1}{2}. \end{cases} \tag{5.1.4} $$

These transformations form a subset of all torus-to-cube transformations and are in a natural way continuously differentiable and increasing. Their first derivative, inverse transformation and density function are given by

$$ \begin{aligned} {}_{\square}\psi'(x, \eta) &:= \frac{\partial}{\partial x}[{}_{\square}\psi](x, \eta), \\ {}_{\square}\psi^{-1}(y, \eta) &:= \psi^{-1}\left(\frac{1}{\eta}\,\psi(y)\right) = {}_{\square}\psi\left(y, \frac{1}{\eta}\right), \\ {}_{\square}\varrho(y, \eta) &:= \frac{\partial}{\partial x}[{}_{\square}\psi^{-1}](x, \eta) = {}_{\square}\psi'\left(y, \frac{1}{\eta}\right). \end{aligned} $$

The multivariate torus-to-cube transformation ${}_{\square}\psi(\cdot, \boldsymbol{\eta})$, its inverse ${}_{\square}\psi^{-1}(\cdot, \boldsymbol{\eta})$ and density function ${}_{\square}\varrho(\cdot, \boldsymbol{\eta})$ with $\boldsymbol{\eta} \in \mathbb{R}_+^d$ are simply the parameterized versions of (5.1.2) and (5.1.3) and share the same properties.

5.2 Exemplary transformations

Among the torus-to-$\mathbb{R}$ transformations (4.1.1), we consider the logarithmic (torus-to-$\mathbb{R}$) transformation (4.2.3) and the error function (torus-to-$\mathbb{R}$) transformation (4.2.1). Both induce a parameterized torus-to-cube transformation ${}_{\square}\psi(\cdot,\eta)$ with $\eta \in \mathbb{R}_+$ as in (5.1.4), so that for $x, y \in [-\frac{1}{2}, \frac{1}{2}]$ we obtain the following torus-to-cube transformations:

- *logarithmic (torus-to-cube) transformation*:

$$
\begin{aligned}
{}_{\square}\psi(x,\eta) &= \frac{1}{2}\tanh(\eta \operatorname{arctanh}(2x)) = \frac{1}{2}\frac{(1+2x)^{\eta}-(1-2x)^{\eta}}{(1+2x)^{\eta}+(1-2x)^{\eta}},\\
{}_{\square}\psi'(x,\eta) &= \frac{4\eta(1-4x^2)^{\eta-1}}{((1+2x)^{\eta}+(1-2x)^{\eta})^2},
\end{aligned}
\tag{5.2.1}
$$

  and we observe that $\lim_{x\to\pm\frac{1}{2}} {}_{\square}\psi'(x,\eta) = 0$ for $\eta > 1$.

- *error function (torus-to-cube) transformation*:

$$
{}_{\square}\psi(x,\eta) = \frac{1}{2}\operatorname{erf}(\eta \operatorname{erf}^{-1}(2x)), \quad {}_{\square}\psi'(x,\eta) = \eta\, \mathrm{e}^{(1-\eta^2)(\operatorname{erf}^{-1}(2x))^2}
\tag{5.2.2}
$$

  with the error function $\operatorname{erf}(\cdot)$ as given in (4.2.2), and erf^{-1} denoting the inverse error function. Again, we observe that $\lim_{x\to\pm\frac{1}{2}} {}_{\square}\psi'(x,\eta) = 0$ for $\eta > 1$.

We provide an example for a torus-to-cube transformation as defined in (5.1.1) that is not induced by a torus-to-$\mathbb{R}$ transformation:

- *sine transformation*:

$$
\begin{aligned}
{}_{\square}\psi(x) &= \frac{1}{2}\sin(\pi x), & {}_{\square}\psi'(x) &= \frac{\pi}{2}\cos(\pi x),\\
{}_{\square}\psi^{-1}(y) &= \frac{1}{\pi}\arcsin(2y), & {}_{\square}\varrho(y) &= \frac{1}{\pi}\frac{1}{\sqrt{1-4y^2}}.
\end{aligned}
\tag{5.2.3}
$$

Parameterized sine transformation variants have also been considered in [Sid93, AP16]. Later on, we compare the limited smoothening effect of the sine transformation on any given function $h \in L_2\left(\left[-\frac{1}{2}, \frac{1}{2}\right], \omega\right) \cap \mathcal{C}^m_{\text{mix}}\left(\left[-\frac{1}{2}, \frac{1}{2}\right]\right)$ with the logarithmic transformation (5.2.1) and the error function transformation (5.2.2), for which we can achieve different degrees of smoothness, depending on how large the parameter $\eta \in \mathbb{R}_+$ is chosen. In Figure 5.2.1 we compare the transformation mapping, its inverse and their derivatives of the logarithmic transformation (5.2.1) for $\eta \in \{2, 4\}$ and the sine transformation (5.2.3).

For the rest of this section, we omit to point out that the logarithmic and error function transformations given in (5.2.1) and (5.2.2) map onto the cube. The extended name only has the purpose to highlight that the logarithmic and the error function transformations (5.2.1) and (5.2.2) are different from their torus-to-$\mathbb{R}$ counterparts in (4.2.3) and (4.2.1), that induced the torus-to-cube transformations above.

Remark 5.2.1. *The algebraic and the tangent torus-to-$\mathbb{R}$ transformation given by*

$$\psi(x) = \frac{2x}{(1-4x^2)^{\frac{1}{2}}} \quad \text{and} \quad \psi(x) = \tan(\pi x),$$

are examples of torus-to-$\mathbb{R}$ transformations that fail to induce a torus-to-cube transformation. Composing these ψ with their inverse ψ^{-1} as in (5.1.4), we obtain the combined algebraic transformation

$${}_{\square}\psi(x,\eta) = \frac{\eta\, x}{(1+4x^2(\eta^2-1))^{\frac{1}{2}}}, \quad {}_{\square}\psi'(x,\eta) = \eta\left(\frac{1}{1+4x^2(\eta^2-1)}\right)^{\frac{3}{2}}$$

and we observe that

$$\lim_{x\to\pm\frac{1}{2}} {}_{\square}\psi'(x,\eta) = \frac{1}{\eta^2},$$

as well as the combined tangent transformation

$${}_{\square}\psi(x,\eta) = \frac{1}{\pi}\arctan(\eta\tan(\pi x)), \quad {}_{\square}\psi'(x,\eta) = \frac{1}{\pi}\frac{\eta}{\cos^2(\pi x)+\eta^2\sin^2(\pi x)},$$

for which we similarly obtain that

$$\lim_{x\to\pm\frac{1}{2}} {}_{\square}\psi'(x,\eta) = \frac{1}{\eta}.$$

These transformations are continuously differentiable and increasing, but their first derivatives are not equal to 0 at their boundary bounds. □

5.3 Weighted Hilbert spaces on the cube

We consider families of parameterized integrable measure functions $\omega(\cdot,\boldsymbol{\mu}), \boldsymbol{\mu}\in\mathbb{R}^d_+$ of the form

$$\omega(\mathbf{y},\boldsymbol{\mu}) := \prod_{j=1}^{d}\omega_j(y_j,\mu_j), \quad \mathbf{y}\in\left[-\frac{1}{2},\frac{1}{2}\right]^d, \boldsymbol{\mu}\in\mathbb{R}^d_+, \tag{5.3.1}$$

such that for any given torus-to-cube transformation ${}_{\square}\psi(\cdot,\boldsymbol{\eta})$ as in (5.1.2) we have

$$\omega({}_{\square}\psi_j(\cdot,\eta_j),\mu_j)\,{}_{\square}\psi'(\cdot,\eta_j)\in\mathcal{C}_0\left(\left[-\frac{1}{2},\frac{1}{2}\right]\right).$$

For now, we remain in the univariate setting and simplify the notation of the transformation, the measure function, and all related functions by omitting any parameter and write ${}_{\square}\psi(\cdot),\omega(\cdot)$, etc. The transformed Fourier system $\{\varphi_k\}_{k\in\mathbb{Z}}$ of weighted exponential functions

$$\varphi_k(y) := \sqrt{\frac{{}_{\square}\varrho(y)}{\omega(y)}}\,\mathrm{e}^{2\pi\mathrm{i}k\,{}_{\square}\psi^{-1}(y)}, \quad y\in\left[-\frac{1}{2},\frac{1}{2}\right] \tag{5.3.2}$$

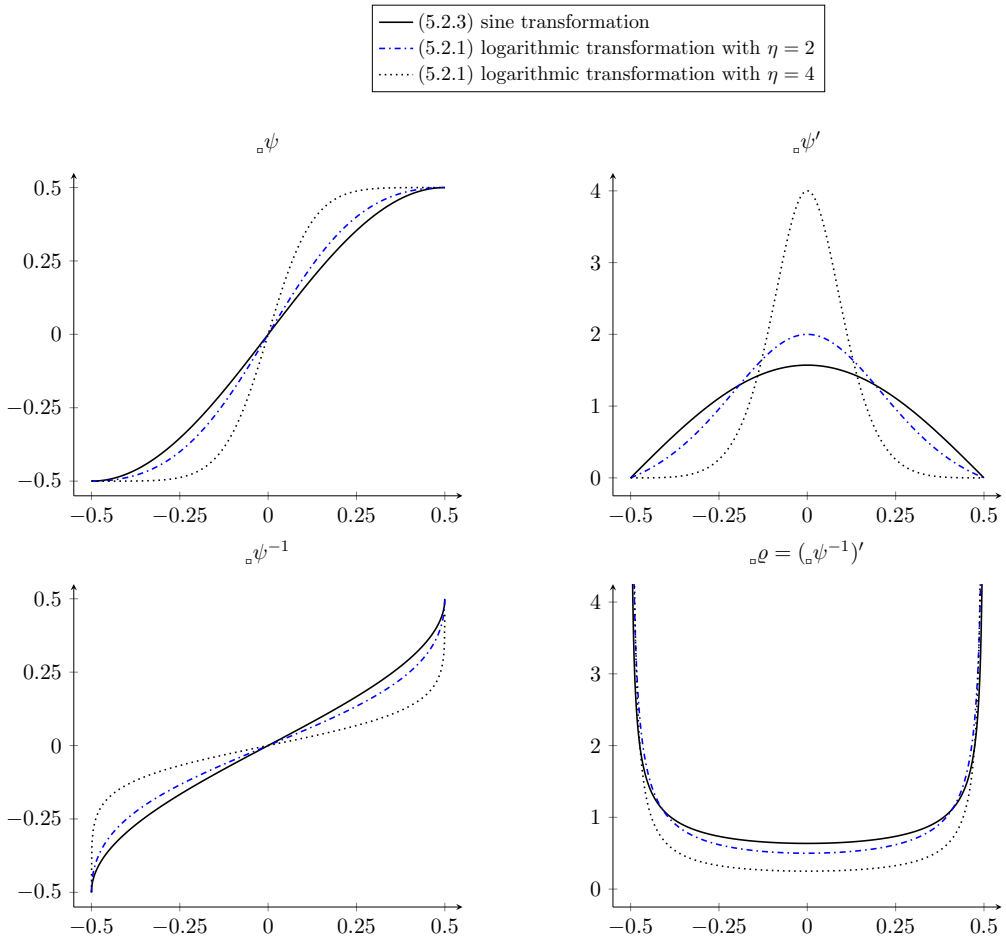

Figure 5.2.1: Comparison of the logarithmic transformation (5.2.1) with $\eta \in \{2, 4\}$ and the sine transformation (5.2.3).

forms an orthonormal system with respect to the scalar product

$$(h_1, h_2)_{L_2([-\frac{1}{2},\frac{1}{2}],\omega)} := \int_{-\frac{1}{2}}^{\frac{1}{2}} h_1(y)\,\overline{h_2(y)}\,\omega(y)\,\mathrm{d}y, \tag{5.3.3}$$

so that we have

$$(\varphi_{k_1}, \varphi_{k_2})_{L_2([-\frac{1}{2},\frac{1}{2}],\omega)} = \delta_{k_1,k_2}, \quad k_1, k_2 \in \mathbb{Z}.$$

The weighted scalar product (5.3.3) induces the norm

$$\|h\|_{L_2([-\frac{1}{2},\frac{1}{2}],\omega)} := \sqrt{(h,h)_{L_2([-\frac{1}{2},\frac{1}{2}],\omega)}}.$$

In a natural way we have Fourier coefficients of the form

$$\hat{h}_k := (h, \varphi_k)_{L_2([-\frac{1}{2},\frac{1}{2}],\omega)} = \int_{-\frac{1}{2}}^{\frac{1}{2}} h(y)\,\sqrt{_{\square}\varrho(y)\,\omega(y)}\,\mathrm{e}^{-2\pi \mathrm{i} k\,_{\square}\psi^{-1}(y)}\,\mathrm{d}y, \tag{5.3.4}$$

as well as the respective Fourier partial sum for $I \subset \mathbb{Z}$ given by

$$S_I h(y) := \sum_{k \in I} \hat{h}_k\,\varphi_k(y). \tag{5.3.5}$$

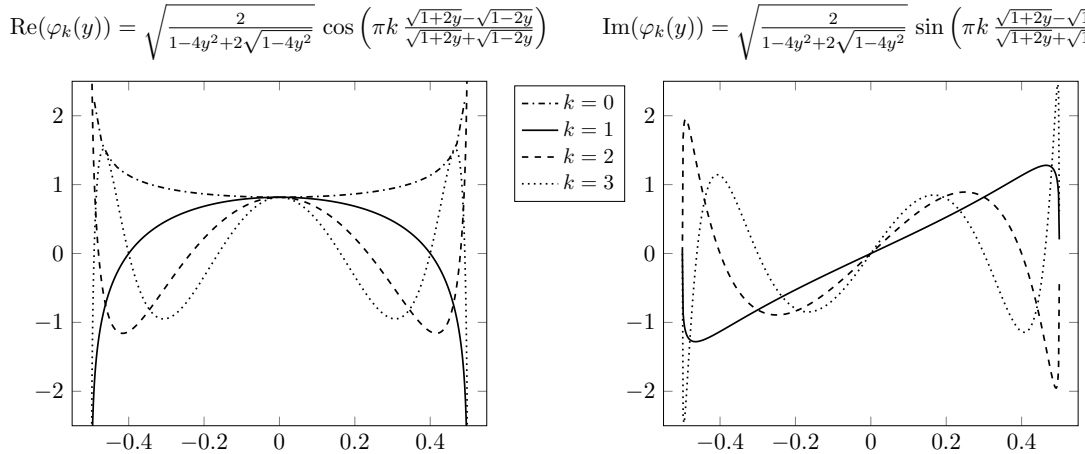

Figure 5.3.1: Real and imaginary part of the weighted exponential functions φ_k in (5.3.6) for $k = 0, 1, 2, 3$ and the fixed parameters $\eta = \mu = 2$.

Example 5.3.1. *We consider the constant measure function $\omega(y) = \omega(y, \mu) \equiv 1$.*

- *For $\eta = 2$, the logarithmic transformation* (5.2.1) *and its density function simplify to*

$$ {}_{\square}\psi(x, 2) = \frac{2x}{1 - 4x^2}, \quad \textit{and} \quad {}_{\square}\varrho(y, 2) = \frac{2}{1 - 4y^2 + 2\sqrt{1 - 4y^2}}. $$

  The orthonormal functions φ_k as in (5.3.2) *are of the form*

$$ \varphi_k(y) = \sqrt{\frac{2}{1 - 4y^2 + 2\sqrt{1 - 4y^2}}}\, \mathrm{e}^{\pi \mathrm{i} k\, \frac{\sqrt{1+2x}-\sqrt{1-2x}}{\sqrt{1+2x}+\sqrt{1-2x}}}. \tag{5.3.6} $$

  The graphs of their real and imaginary parts of these φ_k are shown for $k = 0, 1, 2, 3$ in Figure 5.3.1.

- *For the sine transformation* (5.2.3)*, the orthonormal functions φ_k as in* (5.3.2) *are of the form*

$$ \varphi_k(y) = \sqrt{\frac{1}{\sqrt{1 - 4y^2}}}\, \mathrm{e}^{2\mathrm{i} k \arcsin(2y)}, \tag{5.3.7} $$

  with graphs of their real and imaginary parts for $k = 0, 1, 2, 3$ shown in Figure 5.3.2.

5.4 Smoothness properties of transformed functions

We investigate the smoothness properties of functions $h \in L_2\left(\left[-\frac{1}{2}, \frac{1}{2}\right]^d, \omega\right)$ and of their corresponding transformed versions on the torus $\mathbb{T}^d$ after the application of a torus-to-cube transformation ${}_{\square}\psi$ as defined in (5.1.4). We also discuss the possibility to continuously extend the derivatives of these transformed functions f to the torus $\mathbb{T}^d$. Eventually, we propose specific sufficient conditions for ${}_{\square}\psi$ and ω such that a transformed function f is in the Sobolev space $\mathcal{H}^m\left(\mathbb{T}^d\right), m \in \mathbb{N}_0$. These conditions are stated for both univariate and multivariate

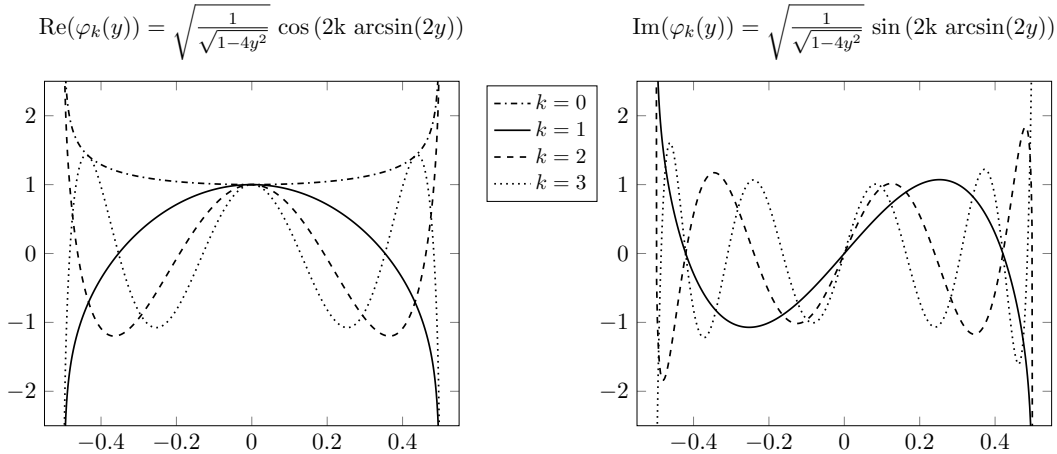

Figure 5.3.2: Real and imaginary part of the weighted exponential functions φ_k in (5.3.7) for $k = 0, 1, 2, 3$.

$$\begin{tikzcd}
\left[-\frac{1}{2}, \frac{1}{2}\right] \arrow[rr, shift left, "\psi(x)"] \arrow[dr, "L_2(\mathbb{T}) \ni h(\psi(x))\sqrt{\omega(\psi(x))\psi'(x)} =: f(x)"'] & & \left[-\frac{1}{2}, \frac{1}{2}\right] \arrow[ll, shift left, "\psi^{-1}(y)"] \arrow[dl, "h(y) \in L_2\left(\left[-\frac{1}{2}, \frac{1}{2}\right], \omega\right)"] \\
& \mathbb{C} &
\end{tikzcd}$$

Figure 5.4.1: Scheme of the relation between f and h caused by a transformation ${}_{\square}\psi$.

functions. Afterwards, we utilize the embedding $\mathcal{H}^{\beta+\lambda}(\mathbb{T}^d) \hookrightarrow \mathcal{A}^{\beta}(\mathbb{T}^d)$ in (3.1.9) for all $\lambda > \frac{1}{2}$ to discuss high-dimensional approximation problems, in which we apply fast Fourier approximation methods based on rank-1 lattices. Throughout this section we still omit the parameters $\boldsymbol{\eta}, \boldsymbol{\mu} \in \mathbb{R}_+^d$ in the notation of the torus-to-cube transformations ${}_{\square}\psi$ and of the measure functions ω.

For now, we consider univariate transformed functions $f \in L_2(\mathbb{T})$ of the form

$$f(x) := h({}_{\square}\psi(x)) \sqrt{\omega({}_{\square}\psi(x))\, {}_{\square}\psi'(x)}, \quad x \in \mathbb{T}, \tag{5.4.1}$$

that are the result of applying a torus-to-cube transformation $y = {}_{\square}\psi(x)$ as defined in (5.1.1) to a given function $h \in L_2\left(\left[-\frac{1}{2}, \frac{1}{2}\right], \omega\right)$ so that we have the identity

$$\|h\|^2_{L_2\left(\left[-\frac{1}{2}, \frac{1}{2}\right], \omega\right)} = \int_{-\frac{1}{2}}^{\frac{1}{2}} |h(y)|^2\, \omega(y)\, \mathrm{d}y = \int_{-\frac{1}{2}}^{\frac{1}{2}} |h({}_{\square}\psi(x))|^2\, \omega({}_{\square}\psi(x))\, {}_{\square}\psi'(x)\, \mathrm{d}x = \|f\|^2_{L_2(\mathbb{T})}.$$

This is illustrated schematically in Figure 5.4.1.

Generally, it is rather difficult to check if such transformed functions f are elements of $H^m\left(\left[-\frac{1}{2}, \frac{1}{2}\right]\right)$ for some fixed $m \in \mathbb{N}_0$ by calculating the Sobolev norm $\|f\|_{H^m\left(\left[-\frac{1}{2}, \frac{1}{2}\right]\right)}$. We propose a set of sufficient conditions such that $f \in H^m\left(\left[-\frac{1}{2}, \frac{1}{2}\right]\right)$ with $m \in \mathbb{N}_0$, that utilize the product structure of the functions f in (5.4.1) and eliminate the necessity to be able to calculate either the Fourier coefficients $\hat{f}_k$ or the L_2-norms of various derivatives

of f appearing in the equivalent Sobolev norm $\|f\|_{H^m(\mathbb{T})}$. Once we consider parameterized families of torus-to-cube transformations ${}_{\square}\psi(\cdot,\eta)$ and families of measure functions $\omega(\cdot,\mu)$, we will calculate how large the parameters $\eta,\mu\in\mathbb{R}_+$ have to be in order to preserve the fixed degree of smoothness m when transforming $h\in L_2\left(\left[-\frac{1}{2},\frac{1}{2}\right],\omega\right)\cap\mathcal{C}^m\left(\left[-\frac{1}{2},\frac{1}{2}\right]\right)$ into $f\in H^m\left(\left[-\frac{1}{2},\frac{1}{2}\right]\right)$ via ${}_{\square}\psi(\cdot,\eta)$. In general, by additionally assuming a certain vanishing behavior of the derivatives of the transformed measure function $\sqrt{(\omega({}_{\square}\psi(\cdot))\,{}_{\square}\psi'(\cdot)}$ the transformed functions f are continuously extendable to the torus $\mathbb{T}$ and we finally have smooth transformed functions $f\in\mathcal{H}^m(\mathbb{T})$ due to the norm equivalence (3.1.8).

Now, we propose a set of sufficient univariate conditions such that we obtain smooth transformed functions $f\in\mathcal{H}^m(\mathbb{T})$.

Theorem 5.4.1 ([NP21a, Theorem 3])**.** *Let $m\in\mathbb{N}_0$, an $h\in L_2\left(\left[-\frac{1}{2},\frac{1}{2}\right],\omega\right)\cap\mathcal{C}^m\left(\left[-\frac{1}{2},\frac{1}{2}\right]\right)$, a torus-to-cube transformation ${}_{\square}\psi$ and the resulting transformed function f of the form* (5.4.1) *be given.*

We have $f\in\mathcal{H}^m(\mathbb{T})$ if for all $n=0,1,\dots,m$ we have

$$ {}_{\square}\psi\in\mathcal{C}^m\left(\left[-\frac{1}{2},\frac{1}{2}\right]\right)\quad\text{and}\quad\left(\sqrt{(\omega\circ{}_{\square}\psi)\,{}_{\square}\psi'}\right)^{(n)}\in\mathcal{C}_0\left(\left[-\frac{1}{2},\frac{1}{2}\right]\right). \tag{5.4.2}$$

Proof. For $h\in L_2\left(\left[-\frac{1}{2},\frac{1}{2}\right],\omega\right)\cap\mathcal{C}^m\left(\left[-\frac{1}{2},\frac{1}{2}\right]\right)$ with $m\in\mathbb{N}_0$ and a torus-to-cube transformation ${}_{\square}\psi$ as defined in (5.1.1), we consider the transformed function f as given in (5.4.1). We apply the generalized Leibniz rule (2.0.1) to the Sobolev norm of f, which leads to

$$\begin{aligned}\|f\|^2_{H^m([-\frac{1}{2},\frac{1}{2}])}&=\sum_{n=0}^m\|f^{(n)}(\cdot)\|^2_{L_2([-\frac{1}{2},\frac{1}{2}])}\\&\le\sum_{n=0}^m\left(\sum_{k=0}^n\binom{n}{k}\left\|(h\circ{}_{\square}\psi)^{(k)}(\cdot)\left(\sqrt{(\omega\circ{}_{\square}\psi)\,{}_{\square}\psi'}\right)^{(n-k)}(\cdot)\right\|_{L_2([-\frac{1}{2},\frac{1}{2}])}\right)^2.\end{aligned} \tag{5.4.3}$$

In the term corresponding to $k=0$ we leave the composition $h\circ{}_{\square}\psi$ untouched for now. For $k=1,\dots,m$ we apply the Faá di Bruno formula (2.0.2) to the k-th derivative of the composition $h\circ{}_{\square}\psi$ and estimate

$$\|f\|^2_{H^m([-\frac{1}{2},\frac{1}{2}])}\lesssim\sum_{n=0}^m\left(\sum_{k=0}^n\left\|\sum_{\ell=1}^k h^{(\ell)}({}_{\square}\psi(\cdot))B_{k,\ell}({}_{\square}\psi(\cdot))\left(\sqrt{(\omega\circ{}_{\square}\psi)\,{}_{\square}\psi'}\right)^{(n-k)}(\cdot)\right\|_{L_2([-\frac{1}{2},\frac{1}{2}])}\right)^2$$

where we used the simplified notation $B_{k,\ell}({}_{\square}\psi(x)):=B_{k,\ell}({}_{\square}\psi'(x),\dots,{}_{\square}\psi^{(k-\ell+1)}(x))$ for the Bell polynomial $B_{k,\ell}$ given in (2.0.3). All derivatives of ${}_{\square}\psi$ are bounded on the interval $[-\frac{1}{2},\frac{1}{2}]$ by assumption, so that each Bell polynomial $B_{k,\ell}$ is bounded, too. It was also assumed that h is m-times continuously differentiable. Hence, the appearing L_2-norms are estimated by their respective L_∞-norms, so that

$$\begin{aligned}&\left\|\sum_{\ell=1}^k h^{(\ell)}({}_{\square}\psi(\cdot))B_{k,\ell}({}_{\square}\psi(\cdot))\left(\sqrt{(\omega\circ{}_{\square}\psi)\,{}_{\square}\psi'}\right)^{(n-k)}(\cdot)\right\|_{L_2([-\frac{1}{2},\frac{1}{2}])}\\&\lesssim\sum_{\ell=1}^k\left\|\left(\sqrt{(\omega\circ{}_{\square}\psi)\,{}_{\square}\psi'}\right)^{(n-k)}(\cdot)\right\|_{L_\infty([-\frac{1}{2},\frac{1}{2}])}.\end{aligned}$$

Consequentially, the norm $\|f\|_{H^m([-\frac{1}{2},\frac{1}{2}])}$ is finite, if the first m derivatives of $\sqrt{(\omega({}_{\square}\psi(\cdot))\ {}_{\square}\psi'(\cdot)}$ have a finite L_∞-norm. We also assumed that the first m derivatives of $\sqrt{(\omega({}_{\square}\psi(\cdot))\ {}_{\square}\psi'(\cdot)}$ vanish at the boundary points, which implies that the first m derivatives of the transformed function f vanish at the boundary points, too. Hence, $f \in H^m(\mathbb{T}) \sim \mathcal{H}^m(\mathbb{T})$ due to the norm equivalence (3.1.8). ■

Next, we prove the multivariate version of Theorem 5.4.1. Similarly to (5.4.1), we consider multivariate transformed functions $f \in L_2\left(\left[-\frac{1}{2},\frac{1}{2}\right]^d\right)$ of the form

$$f(\mathbf{x}) = h({}_{\square}\psi_1(x_1),\dots,{}_{\square}\psi_d(x_d)) \prod_{k=1}^{d} \sqrt{\omega_k({}_{\square}\psi_k(x_k))\,{}_{\square}\psi_k'(x_k)}, \quad \mathbf{x} \in \mathbb{T}^d, \tag{5.4.4}$$

that are the result of applying a torus-to-cube transformation $\mathbf{y} = {}_{\square}\psi(\mathbf{x})$ as defined in (5.1.2) to a function $h \in L_2\left(\left[-\frac{1}{2},\frac{1}{2}\right]^d,\omega\right)$ with a product weight ω as in (5.3.1). For these we have the identity

$$\begin{aligned}\|h\|^2_{L_2\left(\left[-\frac{1}{2},\frac{1}{2}\right]^d,\omega\right)} &= \int_{\left[-\frac{1}{2},\frac{1}{2}\right]^d} |h(\mathbf{y})|^2\omega(\mathbf{y})\,\mathrm{d}\mathbf{y}\\ &= \int_{\mathbb{T}^d} |(h\circ{}_{\square}\psi)(\mathbf{x})|^2(\omega\circ{}_{\square}\psi)(\mathbf{x})\prod_{j=1}^{d}{}_{\square}\psi_j'(x_j)\,\mathrm{d}\mathbf{x} = \|f\|^2_{L_2(\mathbb{T}^d)}.\end{aligned}$$

Again, we derive a set of sufficient L_∞-conditions on the torus-to-cube transformation ${}_{\square}\psi$ and the product weight ω for an $h \in L_2\left(\left[-\frac{1}{2},\frac{1}{2}\right]^d,\omega\right) \cap \mathcal{C}^m_{\mathrm{mix}}\left(\left[-\frac{1}{2},\frac{1}{2}\right]^d\right)$ to be transformed by ${}_{\square}\psi$ into an $f \in \mathcal{H}^m\left(\mathbb{T}^d\right)$ of form (5.4.4).

Theorem 5.4.2 ([NP21a, Theorem 4])**.** *Let $d \in \mathbb{N}$, $m \in \mathbb{N}_0$, a d-variate torus-to-cube transformation ${}_{\square}\psi$, an $h \in L_2\left(\left[-\frac{1}{2},\frac{1}{2}\right]^d,\omega\right) \cap \mathcal{C}^m_{\mathrm{mix}}\left(\left[-\frac{1}{2},\frac{1}{2}\right]^d\right)$ and the corresponding transformed functions f of the form* (5.4.4) *be given.*

We have $f \in \mathcal{H}^m\left(\mathbb{T}^d\right)$ if for all multi-indices $\mathbf{m} \in \mathbb{N}_0^d$, $\|\mathbf{m}\|_{\ell^d_\infty} \le m$, we have

$${}_{\square}\psi \in \mathcal{C}^m_{\mathrm{mix}}\left(\left[-\frac{1}{2},\frac{1}{2}\right]^d\right) \quad \textit{and} \quad D^{\boldsymbol{m}}\left[\prod_{k=1}^{d}\sqrt{(\omega_k\circ{}_{\square}\psi_k)\,{}_{\square}\psi_k'}\right] \in \mathcal{C}_0\left(\left[-\frac{1}{2},\frac{1}{2}\right]^d\right). \tag{5.4.5}$$

Proof. For $h \in L_2\left(\left[-\frac{1}{2},\frac{1}{2}\right]^d,\omega\right) \cap \mathcal{C}^m_{\mathrm{mix}}\left(\left[-\frac{1}{2},\frac{1}{2}\right]^d\right)$ with $m \in \mathbb{N}_0$ and a multivariate torus-to-cube transformation ${}_{\square}\psi$ as defined in (5.1.2) we consider the transformed function f as given in (5.4.4).

At first we verify that $f \in H^m_{\mathrm{mix}}\left(\left[-\frac{1}{2},\frac{1}{2}\right]^d\right)$, so for all multi-indices $\mathbf{m} \in \mathbb{N}_0^d$ with $\|\mathbf{m}\|_{\ell^d_\infty} \le m$ we have to show that $\|D^{\mathbf{m}}[f]\|_{L_2\left(\left[-\frac{1}{2},\frac{1}{2}\right]^d\right)} < \infty$. For a multivariate transformed function f of the form (5.4.4) we have

$$\|D^{\mathbf{m}}[f](\mathbf{x})\|^2_{L_2\left(\left[-\frac{1}{2},\frac{1}{2}\right]^d\right)} = \int_{\left[-\frac{1}{2},\frac{1}{2}\right]^d}\left|D^{\mathbf{m}}\left[(h\circ{}_{\square}\psi)\prod_{k=1}^{d}\sqrt{(\omega_k\circ{}_{\square}\psi_k)\,{}_{\square}\psi_k'}\right](\mathbf{x})\right|^2\mathrm{d}\mathbf{x}. \tag{5.4.6}$$

Utilizing the product measure function in the transformed function f in (5.4.4), we apply the Leibniz formula (5.4.3) componentwise and estimate

$$\begin{aligned} &D^{\mathbf{m}}\left[(h\circ {}_{\square}\psi)\prod_{k=1}^{d}\sqrt{(\omega_k\circ {}_{\square}\psi_k)\,{}_{\square}\psi_k'}\right](\mathbf{x}) \\ &\leq \sum_{j_1=0}^{m_1}\cdots\sum_{j_d=0}^{m_d} D^{(j_1,\dots,j_d)}[h\circ {}_{\square}\psi](\mathbf{x})\, D^{(m_1-j_1,\dots,m_d-j_d)}\left[\prod_{k=1}^{d}\sqrt{(\omega_k\circ {}_{\square}\psi_k)\,{}_{\square}\psi_k'}\right](\mathbf{x}). \end{aligned} \tag{5.4.7}$$

Next, we apply the Faá di Bruno formula (2.0.2) to each univariate j_ℓ-th derivative occurring in the term $D^{(j_1,\dots,j_d)}[h\circ {}_{\square}\psi](\mathbf{x})$ in (5.4.7). For all $\ell=1,\dots,d$ we put $B_{j_\ell,i_\ell}({}_{\square}\psi_\ell(x_\ell)) := B_{j_\ell,i_\ell}({}_{\square}\psi_\ell'(x_\ell),\dots,{}_{\square}\psi_\ell^{(j_\ell-i_\ell+1)}(x_\ell))$ and we have

$$D^{(0,\dots,0,j_\ell,0,\dots,0)}[h\circ {}_{\square}\psi](\mathbf{x}) = \begin{cases} h({}_{\square}\psi(\mathbf{x})) & \text{for } j_\ell=0, \\ \displaystyle\sum_{i_\ell=1}^{j_\ell} D^{(0,\dots,0,i_\ell,0,\dots,0)}[h]({}_{\square}\psi(\mathbf{x}))B_{j_\ell,i_\ell}({}_{\square}\psi_\ell(x_\ell)) & \text{for } j_\ell\in\mathbb{N}. \end{cases} \tag{5.4.8}$$

After combining (5.4.6), (5.4.7) and (5.4.8), we estimate the occurring summands by their L_2-norm, after these norms are estimated by their L_∞-norm and finally we utilize the boundedness of the Bell polynomials B_{j_ℓ,i_ℓ} as well as the assumption that h is a $\mathcal{C}^m_{\text{mix}}$-function, so that we end up with

$$\begin{aligned} &\|D^{\mathbf{m}}[f](\mathbf{x})\|_{L_2\left(\left[-\frac{1}{2},\frac{1}{2}\right]^d\right)} \\ &\lesssim \sum_{j_1=0,\dots,j_d=0}^{m_1,\dots,m_d}\ \sum_{i_1=1,\dots,i_d=1}^{j_1,\dots,j_d}\left(\int_{\left[-\frac{1}{2},\frac{1}{2}\right]^d}|D^{(i_1,\dots,i_d)}[h]({}_{\square}\psi(\mathbf{x}))|^2\times\right. \\ &\quad\left.\times\prod_{\ell=1}^{d}|B_{j_\ell,i_\ell}({}_{\square}\psi_\ell(x_\ell))|^2\left|D^{(m_1-j_1,\dots,m_d-j_d)}\left[\prod_{k=1}^{d}\sqrt{(\omega_k\circ {}_{\square}\psi_k)\,{}_{\square}\psi_k'}\right](\mathbf{x})\right|^2\,\mathrm{d}\mathbf{x}\right)^{\frac{1}{2}} \\ &\lesssim \sum_{j_1=0,\dots,j_d=0}^{m_1,\dots,m_d}\left\|D^{(m_1-j_1,\dots,m_d-j_d)}\left[\prod_{k=1}^{d}\sqrt{(\omega_k\circ {}_{\square}\psi_k)\,{}_{\square}\psi_k'}\right](\cdot)\right\|_{L_\infty\left(\left[-\frac{1}{2},\frac{1}{2}\right]^d\right)}. \end{aligned}$$

By assumption, the derivatives $D^{\mathbf{m}}\left[\prod_{k=1}^{d}\sqrt{(\omega_k\circ {}_{\square}\psi_k)\,{}_{\square}\psi_k'}\right]$ vanish towards the boundary points of their domains for all $\mathbf{m}\in\mathbb{N}_0^d, \|\mathbf{m}\|_{\ell_\infty^d}\leq m$. Thus, the derivatives $D^{\mathbf{m}}[f]$ of the transformed function f vanish at their boundary points, too, and f is in $\mathcal{H}^m\left(\mathbb{T}^d\right)$ due to the equivalence (3.1.8). ■

We establish two specific approximation error bounds for functions defined on the cube $\left[-\frac{1}{2},\frac{1}{2}\right]^d$ based on the approximation error bounds on the torus $\mathbb{T}^d$ that we recalled in Theorems 3.3.2 and 3.3.3. The corresponding proofs rely heavily on the previously introduced sufficient conditions in Theorem 5.4.2 which guarantee that functions $h\in L_2\left(\left[-\frac{1}{2},\frac{1}{2}\right]^d,\omega\right)\cap\mathcal{C}^m_{\text{mix}}\left(\left[-\frac{1}{2},\frac{1}{2}\right]^d\right)$ are transformed into Sobolev functions of dominating mixed smoothness on $\mathbb{T}^d$ of the form (5.4.4) by multivariate torus-to-cube transformations ${}_{\square}\psi:\left[-\frac{1}{2},\frac{1}{2}\right]^d\to\left[-\frac{1}{2},\frac{1}{2}\right]^d$ as given in (5.1.2).

5.5 Approximation of transformed functions

Based on the definition of a rank-1 lattice $\Lambda(\mathbf{z}, M)$ in (3.2.2), we define a *transformed rank*-1 *lattice* as

$$\Lambda_{\square\psi}(\mathbf{z}, M) := \{\mathbf{y}_j := {}_{\square}\psi(\mathbf{x}_j) : \mathbf{x}_j \in \Lambda(\mathbf{z}, M), j = 0, \ldots, M-1\}. \tag{5.5.1}$$

A *transformed reconstructing rank*-1 *lattice* is denoted by $\Lambda_{\square\psi}(\mathbf{z}, M, I)$. Based on the univariate orthonormal functions φ_k given in (5.3.2) we put

$$\varphi_{\mathbf{k}}(\mathbf{y}) := \prod_{j=1}^{d} \varphi_{k_j}(y_j), \quad \mathbf{k} \in \mathbb{Z}^d, \tag{5.5.2}$$

forming an orthonormal system with respect to the multivariate weighted $L_2\left(\left[-\frac{1}{2}, \frac{1}{2}\right]^d, \omega\right)$-scalar product, so that

$$(h_1, h_2)_{L_2\left(\left[-\frac{1}{2},\frac{1}{2}\right]^d,\omega\right)} := \int_{\left[-\frac{1}{2},\frac{1}{2}\right]^d} h_1(\mathbf{y})\, \overline{h_2(\mathbf{y})} \prod_{j=1}^{d} \omega_j(y_j)\, \mathrm{d}\mathbf{y} \tag{5.5.3}$$

and for all $\mathbf{k}_1, \mathbf{k}_2 \in \mathbb{Z}^d$ we have

$$(\varphi_{\mathbf{k}_1}, \varphi_{\mathbf{k}_2})_{L_2\left(\left[-\frac{1}{2},\frac{1}{2}\right]^d,\omega\right)} = \delta_{\mathbf{k}_1,\mathbf{k}_2}.$$

The multivariate Fourier coefficients $\hat{h}_{\mathbf{k}}$ are naturally given by

$$\hat{h}_{\mathbf{k}} := (h, \varphi_{\mathbf{k}})_{L_2\left(\left[-\frac{1}{2},\frac{1}{2}\right]^d,\omega\right)}. \tag{5.5.4}$$

The multivariate Fourier partial sum for any $I \subset \mathbb{Z}^d$ is defined as

$$S_I h(\mathbf{y}) := \sum_{\mathbf{k}\in I} \hat{h}_{\mathbf{k}}\, \varphi_{\mathbf{k}}(\mathbf{y}).$$

Suppose $f \in L_2\left(\mathbb{T}^d\right)$. For each $I \subset \mathbb{Z}^d$ the system $\{\varphi_{\mathbf{k}}\}_{\mathbf{k}\in I}$ spans the space of transformed trigonometric functions on the cube

$$\Pi_{I,\square\psi} := \operatorname{span}\left\{\sqrt{\frac{{}_{\square}\varrho(\cdot)}{\omega(\cdot)}}\, \mathrm{e}^{2\pi\mathrm{i}\mathbf{k}\cdot{}_{\square}\psi^{-1}(\cdot)} : \mathbf{k} \in I\right\}. \tag{5.5.5}$$

As in (3.2.4), for any transformed trigonometric functions on the cube $h \in \Pi_{I,\square\psi}$, transformed lattice nodes $\mathbf{y}_j \in \Lambda_{\square\psi}(\mathbf{z}, M, I)$ and all $\mathbf{k} \in I$, we have the exact integration property of the form

$$\begin{aligned}\hat{h}_{\mathbf{k}} &= \int_{\left[-\frac{1}{2},\frac{1}{2}\right]^d} h(\mathbf{y})\, \sqrt{{}_{\square}\varrho(\mathbf{y})\, \omega(\mathbf{y})}\, \mathrm{e}^{-2\pi\mathrm{i}\mathbf{k}\cdot{}_{\square}\psi^{-1}(\mathbf{y})}\, \mathrm{d}\mathbf{y} = \int_{\mathbb{T}^d} f(\mathbf{x})\, \mathrm{e}^{-2\pi\mathrm{i}\mathbf{k}\cdot\mathbf{x}}\, \mathrm{d}\mathbf{x} \\ &= \frac{1}{M}\sum_{j=0}^{M-1} f(\mathbf{x}_j)\, \mathrm{e}^{-2\pi\mathrm{i}\mathbf{k}\cdot\mathbf{x}_j} = \frac{1}{M}\sum_{j=0}^{M-1} h(\mathbf{y}_j) \sqrt{\frac{\omega(\mathbf{y}_j)}{{}_{\square}\varrho(\mathbf{y}_j)}}\, \mathrm{e}^{-2\pi\mathrm{i}\mathbf{k}\cdot{}_{\square}\psi^{-1}(\mathbf{y}_j)} = \hat{h}^{\Lambda}_{\mathbf{k}}.\end{aligned} \tag{5.5.6}$$

For an arbitrary function $h \in L_2\left(\left[-\frac{1}{2},\frac{1}{2}\right]^d,\omega\right) \cap \mathcal{C}^m_{\text{mix}}\left(\left[-\frac{1}{2},\frac{1}{2}\right]^d\right)$ we lose the former mentioned exactness and have multivariate approximated transformed Fourier coefficients of the form

$$\hat{h}^{\Lambda}_{\mathbf{k}} := \frac{1}{M}\sum_{j=0}^{M-1} h(\mathbf{y}_j)\sqrt{\frac{\omega(\mathbf{y}_j)}{{}_{\square}\varrho(\mathbf{y}_j)}}\,\mathrm{e}^{-2\pi\mathrm{i}\mathbf{k}\cdot{}_{\square}\psi^{-1}(\mathbf{y}_j)} = \frac{1}{M}\sum_{j=0}^{M-1}\frac{\omega(\mathbf{y}_j)}{{}_{\square}\varrho(\mathbf{y}_j)}\,h(\mathbf{y}_j)\,\overline{\varphi_{\mathbf{k}}(\mathbf{y}_j)}$$

that only approximate the multivariate Fourier coefficients $\hat{h}_{\mathbf{k}}$. Finally, the multivariate version of the approximated Fourier partial sum is given by

$$S^{\Lambda}_{I} h(\mathbf{y}) := \sum_{\mathbf{k}\in I} \hat{h}^{\Lambda}_{\mathbf{k}}\,\varphi_{\mathbf{k}}(\mathbf{y}). \tag{5.5.7}$$

Finally, we introduce the analogue of the Hilbert space $\mathcal{H}^{\beta}(\mathbb{T}^d), \beta \geq 0$ given in (3.1.7) on the cube $\left[-\frac{1}{2},\frac{1}{2}\right]^d$. We define the space of weighted $L_2\left(\left[-\frac{1}{2},\frac{1}{2}\right]^d,\omega\right)$-functions with square summable Fourier coefficients $\hat{h}_{\mathbf{k}}$ given in (5.5.4) by

$$\mathcal{H}^{\beta}\left(\left[-\tfrac{1}{2},\tfrac{1}{2}\right]^d,\omega\right) := \left\{h \in L_2\left(\left[-\tfrac{1}{2},\tfrac{1}{2}\right]^d,\omega\right) : \|h\|_{\mathcal{H}^{\beta}\left(\left[-\frac{1}{2},\frac{1}{2}\right]^d,\omega\right)} < \infty\right\}, \tag{5.5.8}$$

$$\|h\|_{\mathcal{H}^{\beta}\left(\left[-\frac{1}{2},\frac{1}{2}\right]^d,\omega\right)} := \left(\sum_{\mathbf{k}\in\mathbb{Z}^d} \mathrm{w}_{\mathrm{hc}}(\mathbf{k})^{2\beta}|\hat{h}_{\mathbf{k}}|^2\right)^{\frac{1}{2}}.$$

Analogously, the counterpart to the space $\mathcal{A}^{\beta}(\mathbb{T}^d), \beta \geq 0$ as in (3.1.6) is given on the cube $\left[-\frac{1}{2},\frac{1}{2}\right]^d$ by

$$\mathcal{A}^{\beta}\left(\left[-\tfrac{1}{2},\tfrac{1}{2}\right]^d,\omega\right) := \left\{h \in L_1\left(\left[-\tfrac{1}{2},\tfrac{1}{2}\right]^d,\omega\right) : \|h\|_{\mathcal{A}^{\beta}\left(\left[-\frac{1}{2},\frac{1}{2}\right]^d,\omega\right)} < \infty\right\}, \tag{5.5.9}$$

$$\|h\|_{\mathcal{A}^{\beta}\left(\left[-\frac{1}{2},\frac{1}{2}\right]^d,\omega\right)} := \sum_{\mathbf{k}\in\mathbb{Z}^d} \mathrm{w}_{\mathrm{hc}}(\mathbf{k})^{\beta}|\hat{h}_{\mathbf{k}}|.$$

5.5.1 L_∞-approximation error

Based on the $L_\infty(\mathbb{T}^d)$-approximation error bound (3.3.1) and the conditions proposed in Theorem 5.4.2 we prove a similar upper bound for the approximation error $\left\|h - S^{\Lambda}_{I^d_N} h\right\|$ in terms of a weighted L_∞-norm on $\left[-\frac{1}{2},\frac{1}{2}\right]^d$.

Theorem 5.5.1 ([NP21a, Theorem 5])**.** *Let $d \in \mathbb{N}$, $m \in \mathbb{N}$, a hyperbolic cross I^d_N with $N \geq 2^{d+1}$ and a reconstructing rank-1 lattice $\Lambda(\mathbf{z}, M, I^d_N)$ be given. Let $h \in L_2\left(\left[-\frac{1}{2},\frac{1}{2}\right]^d,\omega\right) \cap \mathcal{C}^m_{\text{mix}}\left(\left[-\frac{1}{2},\frac{1}{2}\right]^d\right)$ with ω as in (5.3.1), ${}_{\square}\psi$ as in (5.1.2), and let $\lambda > \frac{1}{2}$. For all multi-indices $\mathbf{m} = (m_1,\ldots,m_d)^{\top} \in \mathbb{N}^d_0$ with $\|\mathbf{m}\|_{\ell^d_\infty} \leq m$ we assume that*

$${}_{\square}\psi \in \mathcal{C}^m_{\text{mix}}\left(\left[-\frac{1}{2},\frac{1}{2}\right]^d\right) \quad \textit{and} \quad D^{\mathbf{m}}\left[\prod_{\ell=1}^{d}\sqrt{(\omega_\ell \circ {}_{\square}\psi_\ell)\,{}_{\square}\psi'_\ell}\right] \in \mathcal{C}_0\left(\left[-\frac{1}{2},\frac{1}{2}\right]^d\right).$$

Then there is an approximation error estimate of the form

$$\left\|h - S^{\Lambda}_{I^d_N} h\right\|_{L_\infty\left(\left[-\frac{1}{2},\frac{1}{2}\right]^d,\sqrt{\frac{\omega}{{}_{\square}\varrho}}\right)} \lesssim N^{-m+\lambda}\|h\|_{\mathcal{H}^m\left(\left[-\frac{1}{2},\frac{1}{2}\right]^d,\omega\right)}.$$

Proof. Let $d \in \mathbb{N}, m \in \mathbb{N}$ and $h \in L_2\left(\left[-\frac{1}{2},\frac{1}{2}\right]^d, \omega\right) \cap \mathcal{C}^m_{\text{mix}}\left(\left[-\frac{1}{2},\frac{1}{2}\right]^d\right)$. By assumption, the criteria of Theorem 5.4.2 are fulfilled and the transformed function f of the form (5.4.4) is $\mathcal{H}^m(\mathbb{T}^d)$ and has a continuous representative, because for $\lambda > \frac{1}{2}$ there is the inclusion $\mathcal{H}^m(\mathbb{T}^d) \hookrightarrow \mathcal{A}^{m-\lambda}(\mathbb{T}^d) \hookrightarrow \mathcal{C}(\mathbb{T}^d)$ as in (3.1.9). Hence, for $f \in \mathcal{A}^{m-\lambda}(\mathbb{T}^d) \cap \mathcal{C}(\mathbb{T}^d)$ we have the approximation error bound

$$\left\| f - S^{\Lambda}_{I^d_N} f \right\|_{L_\infty(\mathbb{T}^d)} \leq 2N^{-m+\lambda} \|f\|_{\mathcal{A}^{m-\lambda}(\mathbb{T}^d)} \tag{5.5.10}$$

as stated in Theorem 3.3.2. With the inverse torus-to-cube transformation $\mathbf{x} = {}_{\square}\psi^{-1}(\mathbf{y})$ we have

$$\hat{h}_{\mathbf{k}} = (h, \varphi_{\mathbf{k}})_{L_2\left(\left[-\frac{1}{2},\frac{1}{2}\right]^d,\omega\right)} = (f, \mathrm{e}^{2\pi \mathrm{i}\mathbf{k}(\cdot)})_{L_2(\mathbb{T}^d)} = \hat{f}_{\mathbf{k}}$$

and

$$\|h\|^2_{\mathcal{H}^m\left(\left[-\frac{1}{2},\frac{1}{2}\right]^d,\omega\right)} = \sum_{\mathbf{k}\in\mathbb{Z}^d} \mathrm{w}_{\mathrm{hc}}(\mathbf{k})^{2m} |\hat{h}_{\mathbf{k}}|^2 = \sum_{\mathbf{k}\in\mathbb{Z}^d} \mathrm{w}_{\mathrm{hc}}(\mathbf{k})^{2m} |\hat{f}_{\mathbf{k}}|^2 = \|f\|^2_{\mathcal{H}^m(\mathbb{T}^d)}, \tag{5.5.11}$$

as well as

$$\begin{aligned}
\left\| h - S_{I^d_N} h \right\|_{L_\infty\left(\left[-\frac{1}{2},\frac{1}{2}\right]^d, \sqrt{\frac{\omega}{{}_{\square}\varrho}}\right)} &= \operatorname{esssup}_{\mathbf{y}\in\left[-\frac{1}{2},\frac{1}{2}\right]^d} \left| \sqrt{\frac{\omega(\mathbf{y})}{{}_{\square}\varrho(\mathbf{y})}} \left(h(\mathbf{y}) - \sum_{\mathbf{k}\in I^d_N} \hat{h}_{\mathbf{k}}\, \varphi_{\mathbf{k}}(\mathbf{y}) \right) \right| \\
&= \operatorname{esssup}_{\mathbf{y}\in\left[-\frac{1}{2},\frac{1}{2}\right]^d} \left| h(\mathbf{y}) \sqrt{\frac{\omega(\mathbf{y})}{{}_{\square}\varrho(\mathbf{y})}} - \sum_{\mathbf{k}\in I^d_N} \hat{h}_{\mathbf{k}}\, \mathrm{e}^{2\pi\mathrm{i}\mathbf{k}\cdot {}_{\square}\psi^{-1}(\mathbf{y})} \right| \\
&= \operatorname{esssup}_{\mathbf{x}\in\mathbb{T}^d} \left| h({}_{\square}\psi(\mathbf{x})) \sqrt{\omega({}_{\square}\psi(\mathbf{x})) \prod_{j=1}^d {}_{\square}\psi'_j(x_j)} - \sum_{\mathbf{k}\in I^d_N} \hat{h}_{\mathbf{k}}\, \mathrm{e}^{2\pi\mathrm{i}\mathbf{k}\cdot\mathbf{x}} \right| \\
&= \left\| f - S_{I^d_N} f \right\|_{L_\infty(\mathbb{T}^d)}
\end{aligned}$$

and

$$\left\| h - S^{\Lambda}_{I^d_N} h \right\|_{L_\infty\left(\left[-\frac{1}{2},\frac{1}{2}\right]^d, \sqrt{\frac{\omega}{{}_{\square}\varrho}}\right)} = \left\| f - S^{\Lambda}_{I^d_N} f \right\|_{L_\infty(\mathbb{T}^d)}. \tag{5.5.12}$$

In total, by combining (5.5.12), (5.5.10), (3.1.10) and (5.5.11) we estimate for the function $f \in \mathcal{H}^m(\mathbb{T}^d) \cap \mathcal{C}(\mathbb{T}^d)$ that

$$\begin{aligned}
\left\| h - S^{\Lambda}_{I^d_N} h \right\|_{L_\infty\left(\left[-\frac{1}{2},\frac{1}{2}\right]^d, \sqrt{\frac{\omega}{{}_{\square}\varrho}}\right)} &= \left\| f - S^{\Lambda}_{I^d_N} f \right\|_{L_\infty(\mathbb{T}^d)} \\
&\leq 2N^{-m+\lambda} \|f\|_{\mathcal{A}^{m-\lambda}(\mathbb{T}^d)} \\
&\leq 2\, C_{d,\lambda} N^{-m+\lambda} \|f\|_{\mathcal{H}^m(\mathbb{T}^d)} \\
&= 2\, C_{d,\lambda} N^{-m+\lambda} \|h\|_{\mathcal{H}^m\left(\left[-\frac{1}{2},\frac{1}{2}\right]^d,\omega\right)} < \infty
\end{aligned}$$

with $\lambda > \frac{1}{2}$ and some constant $C_{d,\lambda} > 1$. ■

5.5.2 L_2-approximation error

Based on the $L_2(\mathbb{T}^d)$-approximation error bound (3.3.2) and the conditions proposed in Theorem 5.4.2 we prove an upper bound for the approximation error $\left\|h - S^{\Lambda}_{I^d_N} h\right\|$ in terms of a weighted L_2-norm on $\left[-\frac{1}{2}, \frac{1}{2}\right]^d$.

Theorem 5.5.2 ([NP21a, Theorem 6])**.** *Let $d \in \mathbb{N}$, $m \in \mathbb{N}$, a hyperbolic cross I^d_N with $N \geq 2^{d+1}$ and a reconstructing rank-1 lattice $\Lambda(\mathbf{z}, M, I^d_N)$ be given. Let $h \in L_2\left(\left[-\frac{1}{2}, \frac{1}{2}\right]^d, \omega\right) \cap \mathcal{C}^m_{\mathrm{mix}}\left(\left[-\frac{1}{2}, \frac{1}{2}\right]^d\right)$ with ω as in (5.3.1) and ${}_{\square}\psi$ as in (5.1.2). For all multi-indices $\mathbf{m} = (m_1, \ldots, m_d)^\top \in \mathbb{N}^d_0$ with $\|\mathbf{m}\|_{\ell^d_\infty} \leq m$ we assume that*

$$ {}_{\square}\psi \in \mathcal{C}^m_{\mathrm{mix}}\left(\left[-\frac{1}{2}, \frac{1}{2}\right]^d\right) \quad \text{and} \quad D^{\mathbf{m}}\left[\prod_{\ell=1}^{d} \sqrt{(\omega_\ell \circ {}_{\square}\psi_\ell)\, {}_{\square}\psi'_\ell}\right] \in \mathcal{C}_0\left(\left[-\frac{1}{2}, \frac{1}{2}\right]^d\right). $$

Then there is an approximation error estimate of the form

$$ \left\|h - S^{\Lambda}_{I^d_N} h\right\|_{L_2\left(\left[-\frac{1}{2}, \frac{1}{2}\right]^d, \omega\right)} \lesssim N^{-m} (\log N)^{(d-1)/2} \|h\|_{\mathcal{H}^m\left(\left[-\frac{1}{2}, \frac{1}{2}\right]^d, \omega\right)}. $$

Proof. Let $m \in \mathbb{N}, d \in \mathbb{N}$ and $h \in L_2\left(\left[-\frac{1}{2}, \frac{1}{2}\right]^d, \omega\right) \cap \mathcal{C}^m_{\mathrm{mix}}\left(\left[-\frac{1}{2}, \frac{1}{2}\right]^d\right)$. By assumption are the criteria of Theorem 5.4.2 fulfilled and the transformed function f of the form (5.4.4) is in $\mathcal{H}^m(\mathbb{T}^d)$ and has a continuous representative because of the inclusion $\mathcal{H}^m(\mathbb{T}^d) \hookrightarrow \mathcal{C}(\mathbb{T}^d)$ as in (3.1.9). For $f \in \mathcal{H}^m(\mathbb{T}^d) \cap \mathcal{C}(\mathbb{T}^d)$ Theorem 3.3.3 yields the approximation error bound of the form

$$ \left\|f - S^{\Lambda}_{I^d_N} f\right\|_{L_2(\mathbb{T}^d)} \leq C_{d,\beta} N^{-\beta} (\log N)^{(d-1)/2} \|f\|_{\mathcal{H}^\beta(\mathbb{T}^d)} \tag{5.5.13} $$

with some constant $C_{d,\beta} := C(d, \beta) > 0$. With the inverse torus-to-cube transformation $\boldsymbol{x} = {}_{\square}\psi^{-1}(\boldsymbol{y})$ we have

$$ \hat{h}_{\mathbf{k}} = (h, \varphi_{\mathbf{k}})_{L_2\left(\left[-\frac{1}{2}, \frac{1}{2}\right]^d, \omega\right)} = (f, \mathrm{e}^{2\pi \mathrm{i} \mathbf{k} \cdot})_{L_2(\mathbb{T}^d)} = \hat{f}_{\mathbf{k}}, $$

and

$$ \|h\|^2_{\mathcal{H}^m\left(\left[-\frac{1}{2}, \frac{1}{2}\right]^d, \omega\right)} = \sum_{\mathbf{k} \in \mathbb{Z}^d} \mathrm{w}_{\mathrm{hc}}(\mathbf{k})^{2m} |\hat{h}_{\mathbf{k}}|^2 = \sum_{\mathbf{k} \in \mathbb{Z}^d} \mathrm{w}_{\mathrm{hc}}(\mathbf{k})^{2m} |\hat{f}_{\mathbf{k}}|^2 = \|f\|^2_{\mathcal{H}^m(\mathbb{T}^d)} $$

as in (5.5.11), as well as

$$ \left\|h - S_{I^d_N} h\right\|^2_{L_2\left(\left[-\frac{1}{2}, \frac{1}{2}\right]^d, \omega\right)} = \int_{\left[-\frac{1}{2}, \frac{1}{2}\right]^d} \left| h(\mathbf{y}) - \sum_{\mathbf{k} \in I^d_N} \hat{h}_{\mathbf{k}}\, \varphi_{\mathbf{k}}(\mathbf{y}) \right|^2 \omega(\mathbf{y})\, \mathrm{d}\mathbf{y} = \left\|f - S_{I^d_N} f\right\|^2_{L_2(\mathbb{T}^d)} \tag{5.5.14} $$

and

$$ \left\|h - S^{\Lambda}_{I^d_N} h\right\|_{L_2\left(\left[-\frac{1}{2}, \frac{1}{2}\right]^d, \omega\right)} = \left\|f - S^{\Lambda}_{I^d_N} f\right\|_{L_2(\mathbb{T}^d)}. $$

In total, by combining (5.5.14), (5.5.13), and (5.5.11) we estimate for $f \in \mathcal{H}^m(\mathbb{T}^d) \cap \mathcal{C}(\mathbb{T}^d)$ that

$$\begin{aligned}\left\|h - S^{\Lambda}_{I^d_N} h\right\|_{L_2\left(\left[-\frac{1}{2},\frac{1}{2}\right]^d,\omega\right)} &= \left\|f - S^{\Lambda}_{I^d_N} f\right\|_{L_2(\mathbb{T}^d)} \\ &\lesssim C_{d,\beta} N^{-\beta} (\log N)^{(d-1)/2} \|f\|_{\mathcal{H}^\beta(\mathbb{T}^d)} \\ &= C_{d,\beta} N^{-\beta} (\log N)^{(d-1)/2} \|h\|_{\mathcal{H}^m\left(\left[-\frac{1}{2},\frac{1}{2}\right]^d,\omega\right)} < \infty\end{aligned}$$

with some constant $C_{d,\beta} > 0$. ■

Finally, let us recap the results of this section. We've seen that under the assumptions of Theorem 5.5.1, a function $h \in L_2\left(\left[-\frac{1}{2},\frac{1}{2}\right]^d,\omega\right) \cap \mathcal{C}^m_{\text{mix}}\left(\left[-\frac{1}{2},\frac{1}{2}\right]^d\right)$ is transformed into a smooth function $f \in \mathcal{H}^m\left(\left[-\frac{1}{2},\frac{1}{2}\right]^d,\omega\right)$ of the form (5.4.4) and its L_∞-approximation error decays with the rate

$$\left\|f - S^{\Lambda}_{I^d_N} f\right\|_{L_\infty(\mathbb{T}^d)} = \left\|h - S^{\Lambda}_{I^d_N} h\right\|_{L_\infty\left(\left[-\frac{1}{2},\frac{1}{2}\right]^d,\sqrt{\frac{\omega}{{}_\square\varrho}}\right)} \lesssim N^{-m+\lambda} \to 0$$

for $N \to \infty$ (or equivalently for $|I^d_N| \to \infty$) and with $\lambda > \frac{1}{2}$. Under the same assumptions we've then shown in Theorem 5.5.2 that the L_2-approximation error is bounded by

$$\left\|f - S^{\Lambda}_{I^d_N} f\right\|_{L_2(\mathbb{T}^d)} = \left\|h - S^{\Lambda}_{I^d_N} h\right\|_{L_2\left(\left[-\frac{1}{2},\frac{1}{2}\right]^d,\omega\right)} \lesssim N^{-m} (\log N)^{(d-1)/2} \to 0$$

for $N \to \infty$.

5.6 Fast algorithms and discrete approximation errors on the cube

In this section we start denoting the parameters $\boldsymbol{\eta}, \boldsymbol{\mu} \in \mathbb{R}^d_+$. Families of multivariate measure functions are denoted by $\omega(\cdot, \boldsymbol{\mu})$ as in (5.3.1) and families of multivariate torus-to-cube transformations as in (5.1.2) are denoted by ${}_\square\psi(\cdot, \boldsymbol{\eta})$.

For the evaluation of transformed multivariate trigonometric functions on the cube $h \in \Pi_{I,{}_\square\psi(\cdot,\boldsymbol{\eta})}$ as in (5.5.5) such as the approximated Fourier series $S^{\Lambda}_I h$, and for the reconstruction of the approximated Fourier coefficients $\hat{h}^{\Lambda}_{\mathbf{k}}$ as in (5.5.7), we follow [NP21a, Section 4] and outline the necessary adjustments within the efficient algorithms described in [Käm14b, Algorithm 3.1 and 3.2] that were recalled in Algorithms 3.4.1 and 3.4.2. Similarly to (3.4.1) and (3.4.2), for $\boldsymbol{\eta}, \boldsymbol{\mu} \in \mathbb{R}^d_+$ we form transformed Fourier matrices $\mathbf{F}_{\text{cube}}$ and $\mathbf{F}^*_{\text{cube}}$ given by

$$\begin{aligned}\mathbf{F}_{\text{cube}} &:= \left(\mathrm{e}^{2\pi \mathrm{i}\mathbf{k}\cdot{}_\square\psi^{-1}(\mathbf{y}_j,\boldsymbol{\eta})}\right)_{\mathbf{y}_j \in \Lambda_{{}_\square\psi(\cdot,\boldsymbol{\eta})}(\mathbf{z},M),\, \mathbf{k}\in I} \in \mathbb{C}^{M\times|I|}, \\ \mathbf{F}^*_{\text{cube}} &= \left(\mathrm{e}^{-2\pi \mathrm{i}\mathbf{k}\cdot{}_\square\psi^{-1}(\mathbf{y}_j,\boldsymbol{\eta})}\right)_{\mathbf{k}\in I,\, \mathbf{y}_j \in \Lambda_{{}_\square\psi(\cdot,\boldsymbol{\eta})}(\mathbf{z},M)} \in \mathbb{C}^{|I|\times M},\end{aligned}$$

as well as $\mathbf{h} := \left(h(\mathbf{y}_j)\sqrt{\frac{\omega(\mathbf{y}_j,\boldsymbol{\mu})}{{}_\square\varrho(\mathbf{y}_j,\boldsymbol{\eta})}}\right)_{j=0,\dots,M-1}$ for $\mathbf{y}_j \in \Lambda_{{}_\square\psi(\cdot,\boldsymbol{\eta})}(\mathbf{z},M)$, $\hat{\mathbf{h}} := (\hat{h}_{\mathbf{k}})_{\mathbf{k}\in I}$ with some frequency set $I \subset \mathbb{Z}^d$ of finite cardinality $|I| < \infty$, so that we have matrix-vector-products of the form

$$\mathbf{h} = \mathbf{F}_{\text{cube}}\hat{\mathbf{h}} \quad \text{and} \quad \hat{\mathbf{h}} = M^{-1}\mathbf{F}^*_{\text{cube}}\mathbf{h}$$

We transform a function $h \in L_2\left(\left[-\frac{1}{2},\frac{1}{2}\right]^d,\omega\right) \cap \mathcal{C}^m_{\text{mix}}\left(\left[-\frac{1}{2},\frac{1}{2}\right]^d\right)$ by a torus-to-cube transformation ${}_{\square}\psi(\mathbf{x}_j,\boldsymbol{\eta}) = \mathbf{y}_j, \mathbf{x}_j = (x_1^j,\ldots,x_d^j)^\top$ into a periodic function f on the torus $\mathbb{T}^d$ of the form (5.4.4). The resulting samples are given by

$$h(\mathbf{y}_j)\sqrt{\frac{\omega(\mathbf{y}_j,\boldsymbol{\mu})}{{}_{\square}\varrho(\mathbf{y}_j,\boldsymbol{\eta})}} = h({}_{\square}\psi(\mathbf{x}_j,\boldsymbol{\eta}))\sqrt{\omega({}_{\square}\psi(\mathbf{x}_j,\boldsymbol{\eta}),\boldsymbol{\mu})\prod_{k=1}^d {}_{\square}\psi'_k(x_k^j,\eta_k)} = f(\mathbf{x}_j,\boldsymbol{\eta},\boldsymbol{\mu})$$

and

$$\sqrt{\frac{\omega(\mathbf{y}_j,\boldsymbol{\mu})}{{}_{\square}\varrho(\mathbf{y}_j,\boldsymbol{\eta})}}S_I^\Lambda h(\mathbf{y}_j) = S_I^\Lambda f(\mathbf{x}_j,\boldsymbol{\eta},\boldsymbol{\mu}) \tag{5.6.1}$$

with the parameters $\boldsymbol{\eta},\boldsymbol{\mu} \in \mathbb{R}_+^d$.

By putting the coefficient vector $\hat{\mathbf{h}} = \left(\hat{h}_{\mathbf{k}}\right)_{\mathbf{k}\in I}$ into Algorithm 3.4.1, we obtain the function values $\mathbf{h} = \mathbf{F}_{\text{cube}}\hat{\mathbf{h}} = \left(h(\mathbf{y}_j)\sqrt{\frac{\omega(\mathbf{y}_j,\boldsymbol{\mu})}{{}_{\square}\varrho(\mathbf{y}_j,\boldsymbol{\eta})}}\right)_{j=0}^{M-1}$ as the output, while the regrouping idea (3.4.3) in the Fourier partial sum remains the same, so that we can rewrite the initial d-variate discrete Fourier transform into a 1-dimensional one. Conversely, we put the function values $\mathbf{h} = \left(h(\mathbf{y}_j)\sqrt{\frac{\omega(\mathbf{y}_j,\boldsymbol{\mu})}{{}_{\square}\varrho(\mathbf{y}_j,\boldsymbol{\eta})}}\right)_{j=0}^{M-1}$ into Algorithm 3.4.2 and observe that the orthogonality property (3.4.4) as well as the subsequent arguments remain the same, so that we obtain the coeffcients $\hat{\mathbf{h}} = M^{-1}\mathbf{F}^*_{\text{cube}}\mathbf{h} = \left(\hat{h}_{\mathbf{k}}\right)_{\mathbf{k}\in I}$.

Remark 5.6.1. *We identify the torus with different cubes. We consider $\mathbb{T}^d \simeq [0,1)^d$ when defining rank-1 lattices $\Lambda(\mathbf{z},M)$ in (3.2.2). However, we consider $\mathbb{T}^d \simeq [-\frac{1}{2},\frac{1}{2})^d$ when applying a torus-to-cube transformation ${}_{\square}\psi$ to a rank-1 lattice. In this process, we reassign all lattice points $\mathbf{x}_j \in \Lambda(\mathbf{z},M)$ via*

$$\mathbf{x}_j \mapsto \left(\left(\mathbf{x}_j + \frac{\mathbf{1}}{2}\right) \bmod \mathbf{1}\right) - \frac{\mathbf{1}}{2}$$

for all $j = 0,\ldots,M-1$. For example, in one dimension this reassignment projects the nodes $(0,\frac{1}{9},\frac{2}{9},\frac{3}{9},\frac{4}{9},\frac{5}{9},\frac{6}{9},\frac{7}{9},\frac{8}{9})^\top$ onto the nodes $(0,\frac{1}{9},\frac{2}{9},\frac{3}{9},\frac{4}{9},-\frac{4}{9},-\frac{3}{9},-\frac{2}{9},-\frac{1}{9})^\top$.

We already showcased in Figure 5.2.1 that the definition of ${}_{\square}\psi$ in (5.1.1) allows a variety of functions with different slopes. Now, in Figure 5.6.1 we show different two-dimensional transformed rank-1 lattices $\Lambda_{{}_{\square}\psi(\cdot,\boldsymbol{\eta})}(\mathbf{z},M)$ as defined in (5.5.1), generated by $\mathbf{z} = (1,7)^\top$ and $M = 150$. We compare the lattices transformed by the sine transformation (5.2.3) and the logarithmic transformation (5.2.1) with the parameter vector $\boldsymbol{\eta} = \mathbf{3}$ with the lattices transformed by the tent transformation (5.7.2) and the Chebyshev transformation (5.7.8). □

On a similar note, the discrete approximation errors $\varepsilon_2^M(h,\{\mathbf{y}_j\}_{j=1}^M)$ and $\varepsilon_\infty^M(h,\{\mathbf{y}_j\}_{j=1}^M)$ as defined in (3.5.1) and (3.5.4) are slightly adjusted in the sense of the transformed approximation error bounds of Theorems 5.5.1 and 5.5.2. Under certain assumptions we've shown

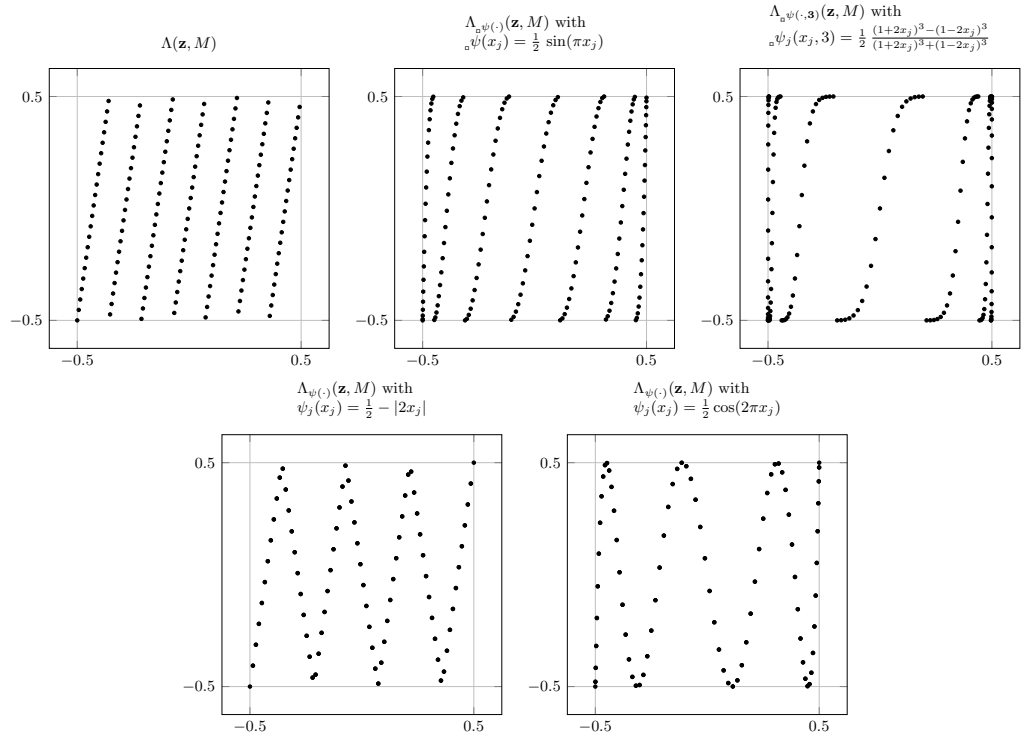

Figure 5.6.1: The two-dimensional lattice $\Lambda(\mathbf{z}, M)$ with $\mathbf{z} = (1, 7)^\top, M = 150$ (top-left), the transformed lattice the sine transformation (5.2.3) (top-center), the logarithmic transformation (5.2.1) (top-right) with $\boldsymbol{\eta} = \mathbf{3}$, the tent transformation (5.7.2) (bottom-left) and the Chebyshev transformation (5.7.8) (bottom-right).

in (5.5.12), (5.5.14) and (5.6.1) that we have

$$\begin{aligned}
\varepsilon_2^M(h, \{\mathbf{y}_j\}_{j=1}^M) &\approx \frac{\left\|h - S_I^\Lambda h\right\|^2_{L_2\left(\left[-\frac{1}{2},\frac{1}{2}\right]^d,\omega\right)}}{\|h\|^2_{L_2\left(\left[-\frac{1}{2},\frac{1}{2}\right]^d,\omega\right)}} = \frac{\left\|f - S_I^\Lambda f\right\|^2_{L_2(\mathbb{T}^d)}}{\|f\|^2_{L_2(\mathbb{T}^d)}} \approx \varepsilon_2^M(f, \{\mathbf{x}_j\}_{j=1}^M), \\
\varepsilon_\infty^M(h, \{\mathbf{y}_j\}_{j=1}^M) &\approx \frac{\left\|h - S_I^\Lambda h\right\|_{L_\infty\left(\left[-\frac{1}{2},\frac{1}{2}\right]^d,\sqrt{\frac{\omega}{{}_\square\varrho}}\right)}}{\|h\|_{L_\infty\left(\left[-\frac{1}{2},\frac{1}{2}\right]^d,\sqrt{\frac{\omega}{{}_\square\varrho}}\right)}} = \frac{\left\|f - S_I^\Lambda f\right\|_{L_\infty(\mathbb{T}^d)}}{\|f\|_{L_\infty(\mathbb{T}^d)}} \approx \varepsilon_\infty^M(f, \{\mathbf{x}_j\}_{j=1}^M).
\end{aligned} \tag{5.6.2}$$

5.7 Half-periodic cosine and Chebyshev approximation

In this section we reflect on the half-periodic cosine functions as well as the Chebyshev polynomials are classical orthonormal system used for the approximation of non-periodic functions on the cube $\left[-\frac{1}{2}, \frac{1}{2}\right]^d$. Both systems can be discretized with suitably chosen transformed reconstructing rank-1 lattices in such a way that the Algorithms 3.4.1 and 3.4.2 for the fast evaluation and reconstruction of multivariate trigonometric polynomials are applicable [PV15, SNC16, KMNN21, NP21b]. We recall the definitions of both systems, their respective transformations mappings ψ and how they inherit the exact integration property (3.2.3) of the Fourier system (3.1.1). Additionally, we showcase the connection of the Cheby-

shev system with the previously introduced general framework of the transformed Fourier systems (5.3.2). Afterwards, we compare all the considered orthonormal systems on the cube $\left[-\frac{1}{2},\frac{1}{2}\right]^d$, the involved scalar product measure functions and transformations mappings, in order to in particular highlight the fact that both the tent-transformation (5.7.2) used for the cosine system and the Chebyshev transformation (5.7.8) used in the Chebyshev system are not torus-to-cube transformations as in (5.1.2).

5.7.1 Cosine approximation with tent-transformed sampling nodes

The half-periodic cosine system is defined on the cube $\mathbf{x} = (x_1, \ldots, x_d)^\top \in \left[-\frac{1}{2},\frac{1}{2}\right]^d$ as

$$\left\{ \lambda_{\mathbf{k}}(\mathbf{x}) := \sqrt{2}^{\|\mathbf{k}\|_0} \prod_{j=1}^{d} \cos\left(\pi k_j \left(x_j + \frac{1}{2}\right)\right) \right\}_{\mathbf{k}\in I}, \quad I \subset \mathbb{N}_0^d \tag{5.7.1}$$

and was investigated in [Adc10, Adc11, SNC16], has been used as a comparison to certain worst-case errors in weighted Korobov spaces of smooth periodic functions [CKNS16] and was considered in the context of various reproducing kernel Hilbert spaces [DNP14, IKP18].

Remark 5.7.1. *In [IN08, AIN12] it is pointed out that the univariate version of system* (5.7.1) *can be rewritten by the transformation $t = 2x$ into the equivalent system*

$$\left\{ \frac{1}{\sqrt{2}}, \cos(k\pi t), \sin\left(\left(k - \frac{1}{2}\right)\pi t\right) \right\}_{k=1,\ldots,N}, \quad t \in [-1,1],$$

whose corresponding coefficients decay one order faster than the classical Fourier coefficients. This modified Fourier system is extended to the multivariate setting [IN09] and was also enhanced by the polynomial subtraction method [HIN11]. □

The cosine system (5.7.1) is orthonormal with respect to the scalar product

$$(h_1, h_2)_{L_2\left(\left[-\frac{1}{2},\frac{1}{2}\right]^d\right)} := \int_{\left[-\frac{1}{2},\frac{1}{2}\right]^d} h_1(\mathbf{y})\, \overline{h_2(\mathbf{y})}\, \mathrm{d}\mathbf{y},$$

so that for $\mathbf{k}_1, \mathbf{k}_2 \in \mathbb{Z}^d$ we have

$$(\lambda_{\mathbf{k}_1}, \lambda_{\mathbf{k}_2})_{L_2\left(\left[-\frac{1}{2},\frac{1}{2}\right]^d,\omega\right)} := \delta_{\mathbf{k}_1,\mathbf{k}_2}.$$

For $\mathbf{k} \in \mathbb{Z}^d$ the cosine coefficient of a function $h \in L_2\left(\left[-\frac{1}{2},\frac{1}{2}\right]^d\right)$ is naturally defined as $\hat{h}_{\mathbf{k}}^{\cos} := (h, \lambda_{\mathbf{k}})_{L_2\left(\left[-\frac{1}{2},\frac{1}{2}\right]^d\right)}$ and for $I \subset \mathbb{Z}^d$ the corresponding cosine partial sum is given by $S_I h(\mathbf{x}) := \sum_{\mathbf{k}\in I} \hat{h}_{\mathbf{k}}^{\cos} \lambda_{\mathbf{k}}(\mathbf{x})$. We transfer the crucial properties of the Fourier system (3.1.1) via the tent transformation

$$\psi(\mathbf{x}) := (\psi_1(x_1), \ldots, \psi_d(x_d))^\top, \quad \psi_j(x_j) = \begin{cases} \frac{1}{2} + 2x_j & \text{for } -\frac{1}{2} \le x_j < 0, \\ \frac{1}{2} - 2x_j & \text{for } 0 \le x_j \le \frac{1}{2}, \end{cases} \tag{5.7.2}$$

which is not a torus-to-cube transformation as defined in (5.1.1). We have sampling nodes in the tent-transformed rank-1 lattice $\Lambda_\psi(\mathbf{z}, M)$ defined as

$$\Lambda_\psi(\mathbf{z}, M) := \left\{ \mathbf{y}_j^{\cos} := \psi(\mathbf{x}_j) : \mathbf{x}_j \in \Lambda(\mathbf{z}, M), j = 0, \ldots, M-1 \right\}. \tag{5.7.3}$$

and we have a reconstructing tent-transformed rank-1 lattice $\Lambda_\psi(\mathbf{z}, M, I)$ if the underlying rank-1 lattice is a reconstructing one. Recalling the definition of difference sets $\mathcal{D}(I)$ in (3.2.1), multivariate trigonometric polynomials $h(\cdot), h(\cdot)\,\lambda_{\mathbf{k}}(\cdot) \in \Pi_{\mathcal{D}(I)}$ supported on $\mathbf{k} \in I \subset \mathbb{N}_0^d$ inherit the exact integration property (3.2.3), because with the tent transformation as in (5.7.2) and transformed nodes $\mathbf{y}_j^{\cos} = \psi(\mathbf{x}_j) \in \Lambda_\psi(\mathbf{z}, M, I)$ with $\mathbf{x}_j = (x_1^j, \ldots, x_d^j)^\top \in \Lambda(\mathbf{z}, M, I)$ we have

$$\begin{aligned}
\hat{h}_{\mathbf{k}}^{\cos} = \int_{\left[-\frac{1}{2},\frac{1}{2}\right]^d} h(\mathbf{y})\,\lambda_{\mathbf{k}}(\mathbf{y})\,\mathrm{d}\mathbf{y} &= \sqrt{2}^{\|\mathbf{k}\|_0} \int_{\mathbb{T}^d} h(\psi(\mathbf{x})) \prod_{\ell=1}^{d} \cos(2\pi k_\ell x_\ell)\,\mathrm{d}\mathbf{x} \\
&= \frac{\sqrt{2}^{\|\mathbf{k}\|_0}}{2^d} \int_{\mathbb{T}^d} h(\psi(\mathbf{x}))\,\left(\mathrm{e}^{2\pi\mathrm{i}\mathbf{k}\cdot\mathbf{x}} + \mathrm{e}^{-2\pi\mathrm{i}\mathbf{k}\cdot\mathbf{x}}\right)\,\mathrm{d}\mathbf{x} \\
&= \frac{\sqrt{2}^{\|\mathbf{k}\|_0}}{2^d} \frac{1}{M} \sum_{j=0}^{M-1} h(\psi(\mathbf{x}_j))\,\left(\mathrm{e}^{2\pi\mathrm{i}\mathbf{k}\cdot\mathbf{x}_j} + \mathrm{e}^{-2\pi\mathrm{i}\mathbf{k}\cdot\mathbf{x}_j}\right) \\
&= \sqrt{2}^{\|\mathbf{k}\|_0} \frac{1}{M} \sum_{j=0}^{M-1} h(\psi(\mathbf{x}_j)) \prod_{\ell=1}^{d} \cos(2\pi k_\ell x_\ell^j) \\
&= \frac{1}{M} \sum_{j=0}^{M-1} h(\mathbf{y}_j^{\cos})\,\lambda_{\mathbf{k}}(\mathbf{y}_j^{\cos}).
\end{aligned}$$

For an arbitrary function $h \in \mathcal{C}\left(\left[-\frac{1}{2},\frac{1}{2}\right]^d\right)$, we lose the former mentioned exactness and define the *approximated cosine coefficients* $\hat{h}_{\mathbf{k}}^{\cos,\Lambda}$ of the form

$$\hat{h}_{\mathbf{k}}^{\cos} \approx \hat{h}_{\mathbf{k}}^{\cos,\Lambda} := \frac{1}{M} \sum_{j=0}^{M-1} h(\mathbf{y}_j^{\cos})\,\lambda_{\mathbf{k}}(\mathbf{y}_j^{\cos}), \quad \mathbf{y}_j^{\cos} \in \Lambda_\psi(\mathbf{z}, M, I),$$

leading to the *approximated cosine partial sum* $S_I^\Lambda h$ given by

$$S_I h(\mathbf{x}) \approx S_I^\Lambda h(\mathbf{x}) := \sum_{\mathbf{k}\in I} \hat{h}_{\mathbf{k}}^{\cos,\Lambda}\,\lambda_{\mathbf{k}}(\mathbf{x}). \tag{5.7.4}$$

Accordingly, the discrete approximation errors $\varepsilon_2^M(h, \{\mathbf{y}_j\}_{j=1}^M)$ and $\varepsilon_\infty^M(h, \{\mathbf{y}_j\}_{j=1}^M)$ given in (5.6.2) are evaluated with respect to the approximated cosine partial sum in (5.7.4). The discretization with respect to the tent-transformed lattice points (5.7.9) leads to matrix-vector-notation of the form

$$\mathbf{h}_{\cos} := \left(h(\mathbf{y}_j^{\cos})\right)_{j=0}^{M-1}, \quad \mathbf{C} := \left(\lambda_{\mathbf{k}}\left(\mathbf{y}_j^{\cos}\right)\right)_{j=0,\mathbf{k}\in I}^{M-1}.$$

Both the evaluation of h and the reconstruction of the approximated cosine coefficients $\hat{\mathbf{h}} := \left\{\hat{h}_{\mathbf{k}}^{\cos,\Lambda}\right\}_{\mathbf{k}\in I_{\cos}}$ are realized by solving the systems

$$\mathbf{h}_{\cos} = \mathbf{C}\hat{\mathbf{h}}. \quad \text{and} \quad \hat{\mathbf{h}} = \frac{1}{M}\mathbf{C}^*\mathbf{h}_{\cos}. \tag{5.7.5}$$

Fast algorithms for the computation of both systems follow the same core ideas as the Algorithms 3.4.1 and 3.4.2 for the Fourier system (3.4.1), because the cosine system at tent-transformed sampling nodes can be rewritten as a Fourier system sampled at equispaced points. Therefore, specific regrouping of the cosine coefficients allows the computation of the d-dimensional matrix-vector-operation (5.7.5) by a single (inverse) FFT. We just have to incorporate that the frequency sets $I_N^d \cap \mathbb{N}_0^d$ are now restricted to the first orthant, which is outlined in [SNC16, KMNN21].

5.7.2 Chebyshev approximation

For $\mathbf{x} = (x_1, \ldots, x_d)^\top \in \left[-\frac{1}{2}, \frac{1}{2}\right]^d$ and a finite frequency set $\mathbf{k} = (k_1, \ldots, k_d)^\top \in I \subset \mathbb{N}_0^d$, we consider the Chebyshev system

$$\left\{ T_{\mathbf{k}}(\mathbf{x}) := \sqrt{2}^{\|\mathbf{k}\|_0} \prod_{\ell=1}^{d} \cos\left(k_\ell \arccos(2x_\ell)\right) \right\}_{\mathbf{k}\in I}, \tag{5.7.6}$$

that is orthonormal with respect to the weighted scalar product

$$(h_1, h_2)_{L_2\left(\left[-\frac{1}{2},\frac{1}{2}\right]^d,\omega\right)} = \int_{\left[-\frac{1}{2},\frac{1}{2}\right]^d} h_1(\mathbf{x})\, \overline{h_2(\mathbf{x})}\, \omega(\mathbf{x})\, \mathrm{d}\mathbf{x}, \quad \omega(\mathbf{x}) := \prod_{j=1}^{d} \frac{2}{\pi\sqrt{1-4x_j^2}}, \tag{5.7.7}$$

so that for $\mathbf{k}_1, \mathbf{k}_2 \in \mathbb{Z}^d$ we have

$$(T_{\mathbf{k}_1}, T_{\mathbf{k}_2})_{L_2\left(\left[-\frac{1}{2},\frac{1}{2}\right]^d,\omega\right)} := \delta_{\mathbf{k}_1,\mathbf{k}_2}.$$

The *Chebyshev coefficients* of a function $h \in L_2\left(\left[-\frac{1}{2}, \frac{1}{2}\right]^d, \omega\right)$ are naturally defined as $\hat{h}_{\mathbf{k}}^{\mathrm{cheb}} := (h, T_{\mathbf{k}})_{L_2\left(\left[-\frac{1}{2},\frac{1}{2}\right]^d,\omega\right)}, \mathbf{k} \in \mathbb{Z}^d$ and for $I \subset \mathbb{Z}^d$ the corresponding Chebyshev partial sum is given by $S_I h(\mathbf{x}) := \sum_{\mathbf{k}\in I} \hat{h}_{\mathbf{k}}^{\mathrm{cheb}} T_{\mathbf{k}}(\mathbf{x})$. We transfer some properties of the Fourier system (3.1.1) via the *Chebyshev transformation*

$$\begin{aligned} \psi(\mathbf{x}) &:= (\psi_1(x_1), \ldots, \psi_d(x_d))^\top, \\ \psi_j(x_j) &:= \frac{1}{2}\cos(2\pi x_j), \quad x_j \in \left[-\frac{1}{2}, \frac{1}{2}\right], \end{aligned} \tag{5.7.8}$$

which is not a torus-to-cube transformation as defined in (5.1.1). We have sampling nodes in the Chebyshev-transformed rank-1 lattice $\Lambda_\psi(\mathbf{z}, M)$ defined as

$$\Lambda_\psi(\mathbf{z}, M) := \left\{ \mathbf{y}_j^{\mathrm{cheb}} := \psi(\mathbf{x}_j) : \mathbf{x}_j \in \Lambda(\mathbf{z}, M), j = 0, \ldots, M-1 \right\} \tag{5.7.9}$$

and we have a reconstructing Chebyshev-transformed rank-1 lattice $\Lambda_\psi(\mathbf{z}, M, I)$ if the underlying rank-1 lattice is a reconstructing one. We note that the Chebyshev-transformed sampling nodes are fundamentally connected to Padua points and Lissajous curves, as well as certain interpolation methods that are based on [BCD+06, DE17]. Recalling the definition of difference sets $\mathcal{D}(I)$ in (3.2.1), multivariate trigonometric polynomials $h(\cdot), h(\cdot)\, T_{\mathbf{k}}(\cdot) \in \Pi_{\mathcal{D}(I)}$ supported on $\mathbf{k} \in I \subset \mathbb{N}_0^d$ inherit the exact integration property (3.2.3), because with the Chebyshev transformation ψ as in (5.7.8) and transformed nodes $\mathbf{y}_j^{\mathrm{cheb}} = \psi(\mathbf{x}_j) \in \Lambda_\psi(\mathbf{z}, M, I)$

with $\mathbf{x}_j = (x_1^j, \dots, x_d^j)^\top \in \Lambda(\mathbf{z}, M, I)$ we have

$$\begin{aligned}
\hat{h}_{\mathbf{k}}^{\mathrm{cheb}} = \int_{\left[-\frac{1}{2},\frac{1}{2}\right]^d} h(\mathbf{y})\, T_{\mathbf{k}}(\mathbf{y})\, \omega(\mathbf{y})\, \mathrm{d}\mathbf{y} &= \sqrt{2}^{\|\mathbf{k}\|_0} \int_{\mathbb{T}^d} h(\psi(\mathbf{x})) \prod_{\ell=1}^{d} \cos(2\pi k_\ell x_\ell)\, \mathrm{d}\mathbf{x} \\
&= \frac{\sqrt{2}^{\|\mathbf{k}\|_0}}{2^d} \int_{\mathbb{T}^d} h(\psi(\mathbf{x})) \left(\mathrm{e}^{2\pi \mathrm{i}\mathbf{k}\cdot\mathbf{x}} + \mathrm{e}^{-2\pi \mathrm{i}\mathbf{k}\cdot\mathbf{x}}\right) \mathrm{d}\mathbf{x} \\
&= \frac{\sqrt{2}^{\|\mathbf{k}\|_0}}{2^d} \frac{1}{M} \sum_{j=0}^{M-1} h(\psi(\mathbf{x}_j)) \left(\mathrm{e}^{2\pi \mathrm{i}\mathbf{k}\cdot\mathbf{x}_j} + \mathrm{e}^{-2\pi \mathrm{i}\mathbf{k}\cdot\mathbf{x}_j}\right) \\
&= \sqrt{2}^{\|\mathbf{k}\|_0} \frac{1}{M} \sum_{j=0}^{M-1} h(\psi(\mathbf{x}_j)) \prod_{\ell=1}^{d} \cos(2\pi k_\ell x_\ell^j) \\
&= \frac{1}{M} \sum_{j=0}^{M-1} h(\mathbf{y}_j^{\mathrm{cheb}})\, T_{\mathbf{k}}(\mathbf{y}_j^{\mathrm{cheb}}).
\end{aligned}$$

For an arbitrary function $h \in L\left(\left[-\frac{1}{2},\frac{1}{2}\right]^d, \omega\right) \cap \mathcal{C}\left(\left[-\frac{1}{2},\frac{1}{2}\right]^d\right)$, we lose the former mentioned exactness and define the *approximated Chebyshev coefficients* $\hat{h}_{\mathbf{k}}^{\mathrm{cheb},\Lambda}$ of the form

$$\hat{h}_{\mathbf{k}}^{\mathrm{cheb}} \approx \hat{h}_{\mathbf{k}}^{\mathrm{cheb},\Lambda} := \frac{1}{M} \sum_{j=0}^{M-1} h(\mathbf{y}_j^{\mathrm{cheb}})\, T_{\mathbf{k}}(\mathbf{y}_j^{\mathrm{cheb}}), \quad \mathbf{y}_j^{\mathrm{cheb}} \in \Lambda_\psi(\mathbf{z}, M, I),$$

leading to the *approximated Chebyshev partial sum* $S_I^\Lambda h$ given by

$$S_I h(\mathbf{x}) \approx S_I^\Lambda h(\mathbf{x}) := \sum_{\mathbf{k}\in I} \hat{h}_{\mathbf{k}}^{\mathrm{cheb},\Lambda}\, T_{\mathbf{k}}(\mathbf{x}). \tag{5.7.10}$$

Accordingly, the discrete approximation errors $\varepsilon_\infty^M(h)$ and $\varepsilon_2^M(h)$ given in (5.6.2) are evaluated with respect to the approximated Chebyshev partial sum in (5.7.10). The discretization with respect to the tent-transformed lattice points (5.7.9) leads to matrix-vector-notation of the form

$$\mathbf{h}_{\mathrm{cheb}} := \left(h(\mathbf{y}_j^{\mathrm{cheb}})\right)_{j=0}^{M-1}, \quad \mathbf{T} := \left(T_{\mathbf{k}}(\mathbf{y}_j^{\mathrm{cheb}})\right)_{j=0,\mathbf{k}\in I}^{M-1}.$$

The evaluation of h as well as the reconstruction of the approximated Chebyshev coefficients $\hat{\mathbf{h}} := \left(\hat{h}_{\mathbf{k}}^{\mathrm{cheb},\Lambda}\right)_{\mathbf{k}\in I}$ of h are realized by solving the systems

$$\mathbf{h}_{\mathrm{cheb}} = \mathbf{T}\hat{\mathbf{h}} \quad \text{and} \quad \hat{\mathbf{h}} = \frac{1}{M}\mathbf{T}^*\mathbf{h}_{\mathrm{cheb}}. \tag{5.7.11}$$

Fast algorithms for the computation of both systems follow the same core ideas as the Algorithms 3.4.1 and 3.4.2 for the Fourier system (3.4.1), because the Chebyshev system at tent-transformed sampling nodes can be rewritten as a Fourier system sampled at equispaced points. Therefore, specific regrouping of the Chebyshev coefficients allows the computation of the d-dimensional matrix-vector-operation (5.7.5) by a single (inverse) FFT. We just have to incorporate that the frequency sets $I_N^d \cap \mathbb{N}_0^d$ are now restricted to the first orthant, which is outlined in [PV15, SNC16, KMNN21].

Remark 5.7.2. *The Chebyshev system* (5.7.6) *is the result of a minimally adjusted version of the classical derivation of the Chebyshev polynomials by a cosine periodization strategy [PPST18, p. 312 ff.].*

We consider the domain $\left[-\frac{1}{2},\frac{1}{2}\right]$ *and any continuous function* $h:\left[-\frac{1}{2},\frac{1}{2}\right]\to\mathbb{R}$. *The change of variable* $\frac{1}{2}\cos(2\pi\cdot):\mathbb{R}\to\left[-\frac{1}{2},\frac{1}{2}\right]$, *that is invertible when restricted to the interval* $\left[0,\frac{1}{2}\right]$, *yields the even 1-periodic function* $f(\cdot):=h\left(\frac{1}{2}\cos(2\pi\cdot)\right):\mathbb{T}\simeq\left[-\frac{1}{2},\frac{1}{2}\right)\to\mathbb{R}$ *so that* $f(x)=f(-x)$ *holds. Therefore, the Fourier coefficients of* f *can be written as*

$$\hat{f}_k:=\int_{-\frac{1}{2}}^{\frac{1}{2}}f(x)\,\mathrm{e}^{-2\pi k\mathrm{i}x}\,\mathrm{d}x=\int_{-\frac{1}{2}}^{\frac{1}{2}}f(x)\cos(2\pi kx)\,\mathrm{d}x=2\int_{0}^{\frac{1}{2}}f(x)\cos(2\pi kx)\,\mathrm{d}x.$$

On the same note, f *can be expressed by a cosine series of the form*

$$f(x)=\sum_{k=-\infty}^{\infty}\hat{f}_k\,\mathrm{e}^{2\pi k\mathrm{i}x}=\hat{f}_0+2\sum_{k=1}^{\infty}\hat{f}_k\cos(2\pi kx).$$

By reverting the initial change of variable via $\frac{\arccos(2\cdot)}{2\pi}:\left[-\frac{1}{2},\frac{1}{2}\right]\to\left[0,\frac{1}{2}\right]$, *we obtain the expression*

$$\begin{aligned}h(y)&=\hat{h}_0+2\sum_{k=1}^{\infty}\hat{h}_k\cos(k\arccos(2y)),\\ \hat{h}_k&=2\int_{-\frac{1}{2}}^{\frac{1}{2}}h(y)\cos(k\arccos(2y))\frac{2}{\pi\sqrt{1-4y^2}}\,\mathrm{d}y,\end{aligned}$$

so that $\hat{f}_k=\hat{h}_k$ *and we derived the orthogonal Chebyshev polynomials* $\cos(k\arccos(2\cdot)):\left[-\frac{1}{2},\frac{1}{2}\right]\to[0,1]$. *Additional scaling yields the orthonormal system* (5.7.6) *with respect to the weighted scalar product* (5.7.7). □

Remark 5.7.3. *For any univariate torus-to-*$\mathbb{R}$ *transformation* $\psi:\left(-\frac{1}{2},\frac{1}{2}\right)\to\mathbb{R}$ *as in* (4.1.1), *the first derivative* ψ' *is by definition diverging towards their boundary points, so that its density* ϱ *is converging to* 0 *at its boundary points. Therefore, it is necessary to consider a measure function* ω *that counteracts the boundary singularities of* ψ' *in order to obtain a bounded periodized function as in* (4.4.1) *of the form* $h(\psi(\cdot))\sqrt{\omega(\psi(\cdot))\,\psi'(\cdot)}$ *after applying a torus-to-*$\mathbb{R}$ *transformations* ψ *to a given function* $h\in L_2(\mathbb{R},\omega)$.

In contrast, torus-to-cube transformations ${}_{\square}\psi$ *are defined in* (5.1.1) *in such a way that the roles of* ${}_{\square}\psi'$ *and* ${}_{\square}\varrho$ *are switched. Hence,* ${}_{\square}\psi'$ *already causes transformed functions to be* 0 *at their boundary points, which is why we later on resort to constant measure functions* $\omega\equiv1$ *in our numerical tests. Nevertheless, it is generally feasible to consider a non-constant measure function* ω *as long as it does not counteract* ${}_{\square}\psi'$ *and causes singularities. Furthermore, the transformed Fourier systems* $\{\varphi_k\}_{k\in\mathbb{Z}}$ *as in* (5.3.2) *and* (5.5.2) *and the corresponding* $L_2\left(\left[-\frac{1}{2},\frac{1}{2}\right],\omega\right)$*-scalar product given in* (5.3.3) *and* (5.5.3) *are intended to be a generalize the Chebyshev system* (5.7.6) *and its deduction idea that we recalled in Remark 5.7.2.*

To show the connection of the transformed Fourier framework with the Chebyshev system, we put the Chebyshev transformation (5.7.8) *into the transformed Fourier system* (5.3.2) *despite the fact that it is not a torus-to-cube transformation as in* (5.1.1). *We consider a hyperbolic cross* I_N^1 *as defined in* (3.1.5). *For* $x,y\in\left[-\frac{1}{2},\frac{1}{2}\right]$ *we choose* ψ *to be the Chebyshev transformation* (5.7.8) *of the form* $\psi(x)=\frac{1}{2}\cos(2\pi x)$, *with the inverse* $\psi^{-1}(y)=\frac{\arccos(2y)}{2\pi}$ *and*

orthonormal system $\{\varphi_k(x)\}_{k\in I}$	scalar product weight ω	sampling transformation	frequency set I
$\sqrt{2}^{\lVert k\rVert_0}\cos\left(\pi k\left(x+\frac{1}{2}\right)\right)$	1	$\psi(x)=\begin{cases}\frac{1}{2}+2x & \text{for } -\frac{1}{2}\le x<0,\\ \frac{1}{2}-2x & \text{for } 0\le x\le\frac{1}{2}.\end{cases}$	$I_N^1\cap\mathbb{N}_0$
$\sqrt{2}^{\lVert k\rVert_0}\cos\left(k\arccos(2x)\right)$	$\frac{1}{\pi\sqrt{1-4x^2}}$	$\psi(x)=\frac{1}{2}\cos\left(2\pi x\right)$	$I_N^1\cap\mathbb{N}_0$
$\sqrt{\frac{{}_{\square}\varrho(x,\eta)}{\omega(x,\mu)}}\,\mathrm{e}^{2\pi\mathrm{i}k\,{}_{\square}\psi^{-1}(x,\eta)}$	$\omega(x,\mu)$	${}_{\square}\psi(x,\eta)$ as in (5.1.1)	I_N^1

Table 5.7.1: Comparison of the univariate orthonormal system, sampling sets and frequency sets from the Chebyshev, Cosine and transformed Fourier approximation methods.

the density $\varrho(y)=\frac{1}{\pi\sqrt{1-4y^2}}$. *By putting* $\omega(y)=\varrho(y)$, *the transformed Fourier system* (5.3.2) *turns into*

$$\varphi_k(y)=\mathrm{e}^{\mathrm{i}k\arccos(2y)}=\cos(k\arccos(2y))+\mathrm{i}\sin(k\arccos(2y)),\quad k\in\{-N,\dots,N\},\tag{5.7.12}$$

and by combining the positive and negative frequencies we obtain

$$\varphi_k(y)=\begin{cases}1 & \textit{for}\quad k=0,\\ 2\cos(k\arccos(2y)) & \textit{for}\quad k\in\{1,2,\dots,N\},\end{cases}$$

which is orthogonal with respect to the $L_2\left(\left[-\frac{1}{2},\frac{1}{2}\right],\omega\right)$*-scalar product with* $\omega(y)=\frac{1}{\pi\sqrt{1-4y^2}}$. *With some additional scaling we obtain the orthonormal Chebyshev system* (5.7.6). □

5.7.3 Comparison of the orthonormal systems

The previously presented approximation approaches are based on very different orthonormal systems and use differently transformed sampling sets, which is summarized in dimension $d=1$ in Table 5.7.1 with the definition of the hyperbolic cross $I_N^1=\{-N,\dots,N\}, N\in\mathbb{N}$ provided in (3.1.5).

Applying the univariate tent-transformation ψ in (5.7.2) to a sampling set of equispaced nodes in $\left[-\frac{1}{2},\frac{1}{2}\right]$ can be interpreted as mirroring a given function $h\in\mathcal{C}^k\left(\left[-\frac{1}{2},\frac{1}{2}\right]\right), k\in\mathbb{N}$ at its right boundary point and approximating the resulting continuous periodic function $h\circ\psi\in\mathcal{C}(\mathbb{T})$ by means of a 1-periodic cosine system. Similarly, the Chebyshev-transformation (5.7.8) mirrors the original function $h\in L_2\left(\left[-\frac{1}{2},\frac{1}{2}\right],\frac{2}{\pi\sqrt{1-4(\cdot)^2}}\right)\cap\mathcal{C}^k\left(\left[-\frac{1}{2},\frac{1}{2}\right]\right), k\in\mathbb{N}$ at its right boundary point. But, the Chebyshev transformation (5.7.8) is a $\mathcal{C}^\infty(\mathbb{T})$-function, so that it is capable of preserving a high order of smoothness and we obtain transformed function $h\circ\psi\in\mathcal{C}^k(\mathbb{T})$. Parametrized torus-to-cube transformations ${}_{\square}\psi(\cdot,\eta)$ as in (5.1.4) adapt this periodization approach by mirroring the original function $h\in L_2\left(\left[-\frac{1}{2},\frac{1}{2}\right],\omega\right)\cap\mathcal{C}^k\left(\left[-\frac{1}{2},\frac{1}{2}\right]\right), k\in\mathbb{N}$ into an even, continuous and periodic function, but this time the involved parameter $\eta\in\mathbb{R}_+$ controls the smoothening effect on the periodized function, see [NP21a], which we discussed earlier in Theorems 5.4.1 and 5.4.2.

In Figure 5.7.1 we provide a side-by-side comparison of all the previously mentioned transformation mappings. In particular, the center and right plot of Figure 5.7.1 showcase the effect of the parameter η. For larger η we obtain transformations ${}_{\square}\psi(\cdot,\eta)$ that converge faster, their first derivatives ${}_{\square}\psi'(\cdot,\eta)$ decay more rapidly towards 0 and their densities ${}_{\square}\varrho(\cdot,\eta)$

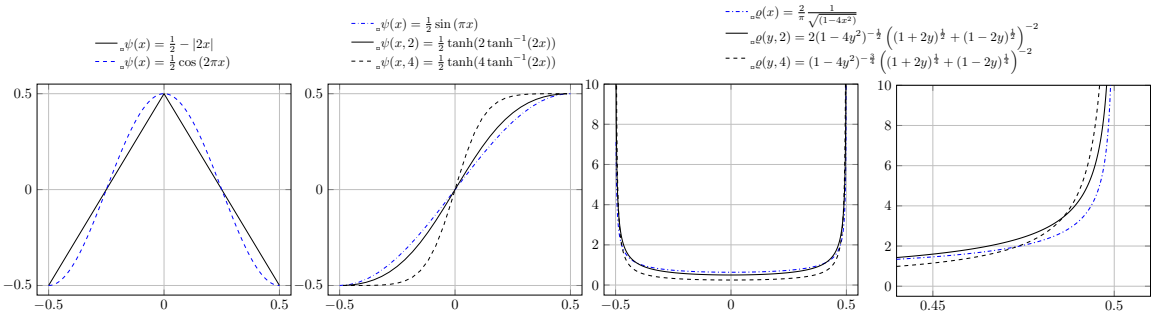

Figure 5.7.1: Left: The tent-transformation (5.7.2) and the Chebyshev-transformation (5.7.8). Center and right: The parameterized logarithmic transformation (5.2.1) in comparison with the sine transformation (5.2.3), as well as their respective density functions $_{\square}\varrho(\cdot,\eta), \eta \in \{2,4\}$.

diverge faster close to their boundary points $\{-\frac{1}{2}, \frac{1}{2}\}$. Furthermore, the transformed Fourier system is based on an integer frequency set in $\mathbb{Z}$, such as the hyperbolic cross I_N^1, in contrast to both the cosine and the Chebyshev systems that work with non-negative frequencies in $\mathbb{N}_0$.

5.8 Numerics on the cube

In this section, we approximate a given function $h \in L_2\left(\left[-\frac{1}{2}, \frac{1}{2}\right]^d, \omega\right) \cap \mathcal{C}^m_{\text{mix}}\left(\left[-\frac{1}{2}, \frac{1}{2}\right]^d\right)$ by the approximated transformed Fourier partial sum given in (5.5.7), as well as by the Chebyshev and cosine partial sums $S_I^{\Lambda} h$ given in (5.7.4) and (5.7.10). For the transformed Fourier system we apply the parameterized logarithmic and the error function torus-to-cube transformations (5.2.1) and (5.2.2), as well as the sine transformation (5.2.3).

For now, we consider the constant measure function $\omega \equiv 1$, so that the transformed functions in the sense of (5.4.4) are of the form

$$f(\mathbf{x}, \boldsymbol{\eta}) = h(_{\square}\psi(\mathbf{x}, \boldsymbol{\eta})) \prod_{j=1}^{d} \sqrt{_{\square}\psi_j'(x_j, \eta_j)}. \tag{5.8.1}$$

Suppose h to be in $\mathcal{C}^{\infty}\left(\left[-\frac{1}{2}, \frac{1}{2}\right]^d\right)$. We determine the values $\eta_j \in \mathbb{R}_+, j \in \{1, \dots, d\}$ for which the $f(\cdot, \boldsymbol{\eta})$ in (5.8.1) are an element of $\mathcal{H}^m(\mathbb{T}^d)$ by investigating the smoothness conditions (5.4.2) in Theorem 5.4.1. First of all, we need $\eta_j > 1$ to have torus-to-cube transformations $_{\square}\psi(\cdot, \boldsymbol{\eta})$ of the form (5.1.1). Due to the constant measure function, checking conditions (5.4.2) for a given $m \in \mathbb{N}_0$ simplifies to the task of determining the values $\eta_j \in \mathbb{R}_+$ for which we have

$$\left\| \left(\sqrt{_{\square}\psi_j'(\cdot, \eta_j)} \right)^{(k)} (\cdot) \right\|_{L_\infty\left(\left[-\frac{1}{2}, \frac{1}{2}\right]\right)} < \infty,$$

as well as

$$\left(\sqrt{_{\square}\psi_j'(x_j, \eta_j)} \right)^{(k)} (x_j) \to 0 \quad \text{for} \quad |x_j| \to \frac{1}{2}$$

for all $k \in \{0, \dots, m\}$. We obtain the following:

- For $m = 0$ we already mentioned in (5.2.1) that the functions ${}_{\square}\psi_j'(\cdot, \eta_j)$ are finite for $\eta_j \geq 1$ and converge to 0 at the boundary points $\pm\frac{1}{2}$ for $\eta_j > 1$.
- For natural degrees of smoothness m the m-th derivative of $\sqrt{{}_{\square}\psi_j'(\cdot, \eta_j)}$ is in $\mathcal{C}_0\left(\left[-\frac{1}{2}, \frac{1}{2}\right]\right)$ if $\eta_j > 2m + 1$.
- For values $2m+1 < \eta_j < 2m+3$ the $(m+1)$-th and all higher derivatives of $\sqrt{{}_{\square}\psi_j'(\cdot, \eta_j)}$ are unbounded and in case of $\eta_j = 2m + 3$ they are bounded but not $\mathcal{C}_0\left(\left[-\frac{1}{2}, \frac{1}{2}\right]\right)$.

In total, we have for $j \in \{1, \ldots, d\}$ that

$$f \in \begin{cases} L_2(\mathbb{T}^d) & \text{for} \quad \eta_j > 1, \\ \mathcal{H}^m(\mathbb{T}^d) & \text{for} \quad \eta_j > 2m + 1, \end{cases} \tag{5.8.2}$$

for the logarithmic and the error function torus-to-cube transformations (5.2.1) and (5.2.2). In later references to this conclusion we summarize relations such as $\eta_j > 3$ for $j \in \{1, \ldots, d\}$ by using the bold notation $\boldsymbol{\eta} > \mathbf{3}$ instead.

Switching to the sine transformation (5.2.3) leads to a transformed function f as given in (5.4.4) of the form

$$\begin{aligned} f(\mathbf{x}) &= h({}_{\square}\psi(\mathbf{x})) \prod_{j=1}^{d} \sqrt{{}_{\square}\psi_j'(x_j)} \\ &= h\left(\frac{1}{2}\sin(\pi\mathbf{x})\right) \prod_{j=1}^{d} \sqrt{\frac{\pi}{2}\cos(\pi x_j)} \in \mathcal{H}^0(\mathbb{T}^d) = L_2(\mathbb{T}^d), \end{aligned} \tag{5.8.3}$$

for which we can not achieve any higher order of Sobolev smoothness according to Theorem 5.4.2, because all derivatives of all $\sqrt{{}_{\square}\psi_j'(\circ)}$ are unbounded.

5.8.1 Approximation of a first-order B-spline in dimensions $d \in \{1, 2, 4, 7\}$

We define a shifted, scaled and dilated B-spline of first order as

$$B_1(x) := \begin{cases} 2x + \frac{1}{2} & \text{for } -\frac{1}{2} \leq x < \frac{1}{4}, \\ -2x + \frac{3}{2} & \text{for } \frac{1}{4} \leq x \leq \frac{1}{2}, \end{cases}$$

and refer to it as the B_1-*cutout* that is depicted in Figure 5.8.1 and was also considered in [PV15, NP21a]. The continuous B_1-cutout is an element of $\mathcal{H}^{\frac{3}{2}-\varepsilon}\left(\left[-\frac{1}{2}, \frac{1}{2}\right]\right)$ for any $\varepsilon > 0$, which is due to the fact that the Fourier coefficients $\hat{h}_k = (B_1, \mathrm{e}^{2\pi \mathrm{i} k(\cdot)})_{L_2([-\frac{1}{2}, \frac{1}{2}])}$ decay like $|k|^{-2}$ for $k \to \pm\infty$. Considering a constant measure function $\omega \equiv 1$, so that $\mathcal{H}^\beta\left(\left[-\frac{1}{2}, \frac{1}{2}\right], \omega\right) = \mathcal{H}^\beta\left(\left[-\frac{1}{2}, \frac{1}{2}\right]\right)$, the $\|\cdot\|_{\mathcal{H}^\beta([-\frac{1}{2}, \frac{1}{2}])}$-norm given in (5.5.8) of the B_1-cutout is finite if

$$\|B_1\|^2_{\mathcal{H}^\beta([-\frac{1}{2}, \frac{1}{2}])} = \sum_{k \in \mathbb{Z}} \mathrm{w_{hc}}(k)^{2\beta} |\hat{h}_k|^2 = \sum_{k \in \mathbb{Z}} \max\{1, |k|\}^{2\beta} \frac{1}{|k|^4} < \infty,$$

which is the case for

$$|k|^{2\beta-2} \leq k^{-(1+\varepsilon)} \Leftrightarrow \beta \leq \frac{3}{2} - \varepsilon, \quad \varepsilon > 0.$$

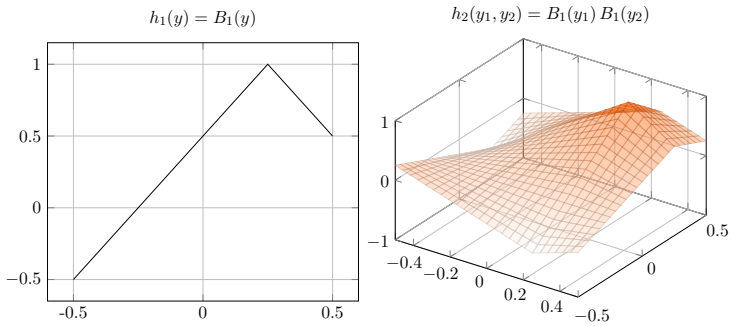

Figure 5.8.1: The univariate B_1-cutout $h_1(x) = B_1(x)$ and the two-dimensional tensored B_1-cutout $h_2(x_1, x_2) = B_1(x_1)\, B_1(x_2)$.

An analogue argument shows that we also have $B_1 \in \mathcal{A}^{1-\varepsilon}\left(\left[-\frac{1}{2}, \frac{1}{2}\right]\right)$ for any $\varepsilon > 0$. We consider a constant measure function, so that $\mathcal{A}^{\beta}\left(\left[-\frac{1}{2}, \frac{1}{2}\right], \omega\right) = \mathcal{A}^{\beta}\left(\left[-\frac{1}{2}, \frac{1}{2}\right]\right)$ as defined in (5.5.9), and the $\|\cdot\|_{\mathcal{A}^{\beta}\left(\left[-\frac{1}{2}, \frac{1}{2}\right]\right)}$-norm of the B_1-cutout is finite if

$$\|B_1\|_{\mathcal{A}^{\beta}\left(\left[-\frac{1}{2}, \frac{1}{2}\right]\right)} = \sum_{k \in \mathbb{Z}} \mathrm{w}_{\mathrm{hc}}(k)^{\beta} |\hat{h}_k| = \sum_{k \in \mathbb{Z}} \max\{1, |k|\}^{\beta} \frac{1}{|k|^2} < \infty,$$

which is the case for

$$|k|^{\beta-2} \leq k^{-(1+\varepsilon)} \Leftrightarrow \beta \leq 1 - \varepsilon, \quad \varepsilon > 0.$$

The tensored B_1-cutout is given by

$$h(\mathbf{x}) = \prod_{j=1}^{d} B_1(x_j) \tag{5.8.4}$$

and will be approximated by the transformed Fourier, cosine and Chebyshev partial sums $S_I^{\Lambda} h$ given in (5.5.7), (5.7.4) and (5.7.10). Consequentially, we have $h \in \mathcal{H}^{\frac{3}{2}-\varepsilon}\left(\left[-\frac{1}{2}, \frac{1}{2}\right]^d\right)$ and by Theorem 5.4.2 the maximum integer degree of Sobolev smoothness m that can be preserved by any torus-to-cube transformation ${}_{\square}\psi$ is limited to $m = 1$, where the sine transformation restricts it even more as we saw in (5.8.3).

We discuss the application of the weighted $L_\infty\left(\left[-\frac{1}{2}, \frac{1}{2}\right]^d\right)$-approximation error bound in Theorem 5.5.1 and the weighted $L_2\left(\left[-\frac{1}{2}, \frac{1}{2}\right]^d\right)$-approximation error bound in Theorem 5.5.2 for dimensions $d \in \{1, 2, 4, 7\}$ with the function h as the tensored first-order B-spline cutout in (5.8.4), a constant measure function, the logarithmic transformation (5.2.1), the error function transformation (5.2.2), the sine transformation (5.2.3) and the resulting transformed functions f of the form (5.8.1). We compare the results with the approximation of h by the cosine system (5.7.1) and the Chebyshev system (5.7.6). Accordingly, we use the hyperbolic frequency set I_N^d as defined in (3.1.5) for all considered transformed Fourier systems, but only consider the non-negative frequencies of a hyperbolic cross $I_N^d \cap \mathbb{N}_0^d$ for the Chebyshev and cosine approximation.

For each transformed system, we generate ten random rank-1 lattices as described in (3.5.5). We repeat the calculations five times and plot the averages of the errors in Figure 5.8.2. In each dimension we consider the parameters $\boldsymbol{\eta} \in \{\mathbf{1.75}, \mathbf{2}, \mathbf{2.5}\}$. We use

$N \in \{1, \dots, 140\}$ for $d = 1$, $N \in \{1, \dots, 80\}$ for $d = 2$, $N \in \{1, \dots, 50\}$ for $d = 4$ and $N \in \{1, \dots, 30\}$ for $d = 7$. In dimensions $d \geq 4$ we initialize [Käm19, Algorithm 6] with the parameters $c = 2, n = 4$ and $\delta = \frac{1}{2}$ to efficiently reconstruct the approximated Fourier coefficients $\hat{h}^{\Lambda}_{\mathbf{k}}$ by means of a transformed multiple rank-1 lattice as in (4.7.8) and to form the approximated Fourier partial sum $S^{\Lambda}_{I} h$, whereas in dimensions $d \in \{1, 2\}$ we apply Algorithm 3.4.2 based on a single rank-1 lattice as outlined in (5.6.1).

The discrete approximation errors $\varepsilon^M_2(h, \{\mathbf{y}_j\}_{j=1}^M)$ and $\varepsilon^M_\infty(h, \{\mathbf{y}_j\}_{j=1}^M)$ as given in (5.6.2) reveal slightly different behaviors for the various approximation systems with increasing dimensions. We begin with the discussion of the error $\varepsilon^M_\infty(h, \{\mathbf{y}_j\}_{j=1}^M)$. In dimension $d = 1$ only the sine transformed Fourier system stands out by providing the worst error, whereas the other systems provide a similar error, with the error function Fourier system being the best. In dimension $d = 2$ the sine transformed Fourier system improves by being better than the Chebyshev system, and the error function Fourier system remains the best. In dimension $d = 4$ the errors diverge significantly for the first time. The Chebyshev system is now clearly the worst, followed by the cosine and logarithmically transformed Fourier system. This time, the sine transformed Fourier system is as good as the error function Fourier system. Finally, in dimension $d = 7$ the results are very similar to the ones in dimension $d = 4$, but the sine transformed Fourier system turned out to be even better than the error function Fourier system. We note, that we tested a variety of parameters $\boldsymbol{\eta} \in \mathbb{R}^d_+$ and settled on $\boldsymbol{\eta} = \mathbf{1.75}$ for the error function Fourier system as well as on $\boldsymbol{\eta} = \mathbf{2.5}$ for the logarithmically transformed Fourier system because they produced the best approximation results.

For the ℓ_2-approximation error $\varepsilon^M_2(h, \{\mathbf{y}_j\}_{j=1}^M)$, the results show the major difference that the error function Fourier system yields the best errors in each dimension. Apart from that, the other approximations behave quite similar throughout the increasing dimensions. In particular, the cosine and Chebyshev systems yield identical errors in dimensions $d \in \{1, 2\}$ and the cosine system turns out be slightly better in dimensions $d \in \{4, 7\}$. The logarithmically transformed Fourier system is better than both of them in all dimensions. The error function Fourier system turns out to be the best system throughout all dimensions. Finally, the sine transformed Fourier system is again the worst one in dimension $d \in \{1, 2\}$, but it becomes the second best of the considered systems in higher dimensions $d \geq 4$.

But it has to be emphasized that the tensored B_1-cutout (5.8.4) is transformed into a function $f \in \mathcal{H}^0(\mathbb{T}^d)$ of the form (5.4.4) for all considered torus-to-cube transformations ${}_{\square}\psi(\cdot, \boldsymbol{\eta})$ with these parameter choices according to (5.8.2) and (5.8.3). Therefore, the weighted L_∞-approximation error provided in Theorem 5.5.1 and the weighted L_2-approximation error bound in Theorem 5.5.2 are not applicable as f would have to be at least an $\mathcal{H}^1(\mathbb{T}^d)$-function. Consequentially, Table 5.8.1 only lists the numerically observed decay rates for $d = 1$.

Next, we have a look at the error decay rates of $\varepsilon^M_2(h, \{\mathbf{y}_j\}_{j=1}^M)$ and $\varepsilon^M_\infty(h, \{\mathbf{y}_j\}_{j=1}^M)$ for the univariate case $d = 1$ that were numerically observed. In this specific setup, h is still the continuous first-order B-spline cutout given in (5.8.4) that is both in $\mathcal{A}^{1-\varepsilon}\left(\left[-\frac{1}{2}, \frac{1}{2}\right]\right)$ and in $\mathcal{H}^{\frac{3}{2}-\varepsilon}\left(\left[-\frac{1}{2}, \frac{1}{2}\right]\right)$. Hence, theoretically we can achieve at most $\varepsilon^M_2(h, \{\mathbf{y}_j\}_{j=1}^M) \lesssim N^{-\frac{3}{2}+\varepsilon}$ and $\varepsilon^M_\infty(h, \{\mathbf{y}_j\}_{j=1}^M) \lesssim N^{-1+\varepsilon}$ for any $\varepsilon > 0$ when approximating h with respect to any transformed Fourier system. As it turns out, we achieve these decay rates numerically for both errors when using the cosine and the Chebyshev system and are furthermore able to match these rates with the transformed Fourier system when considering the logarithmic transformation with $\eta = 2.5$ and the error function transformation with $\eta = 1.75$. On the other hand, the sine transformed and the logarithmically transformed Fourier system with $\eta = 2$ lose half an order in both error decay observations. In total, we observe that some

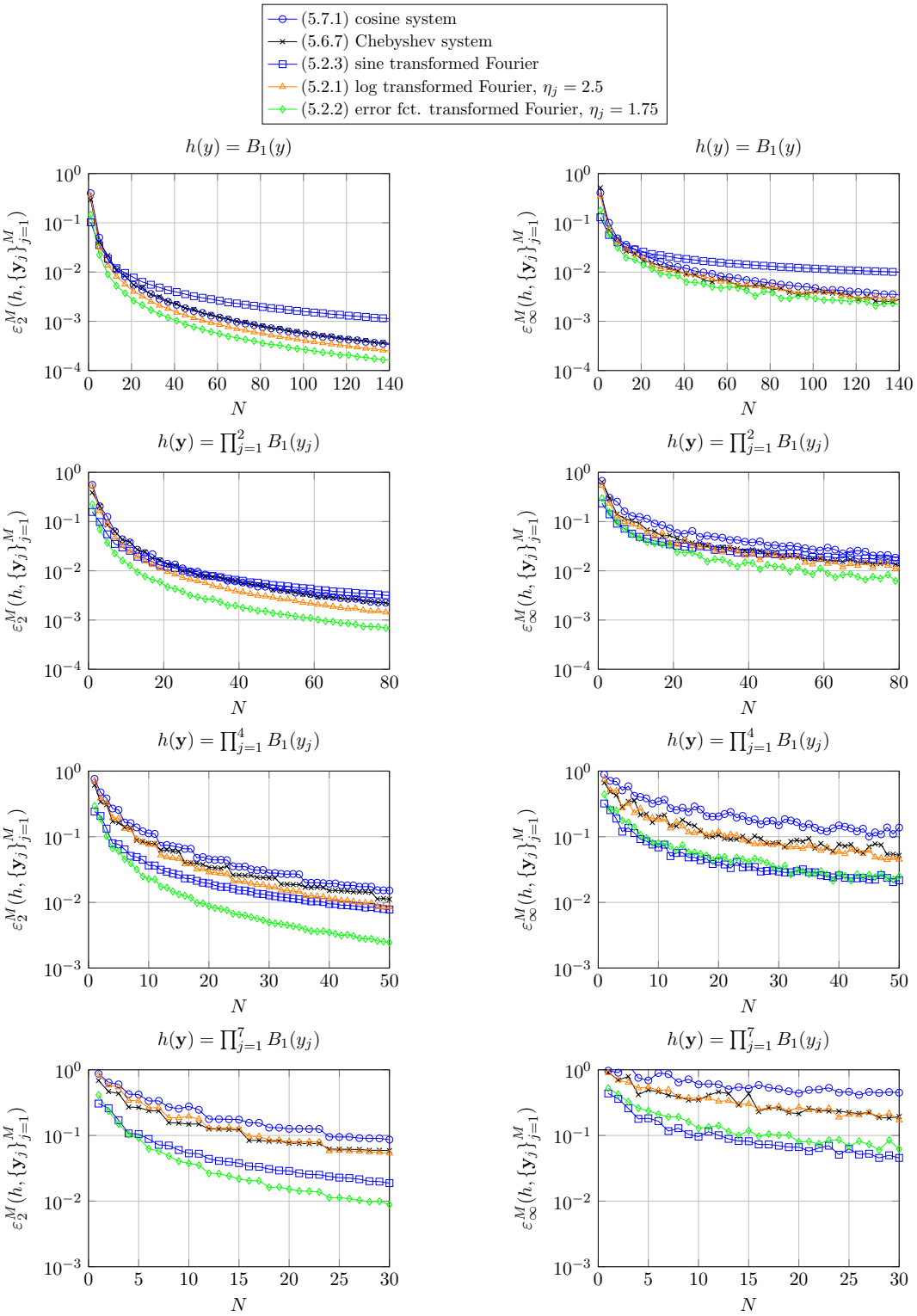

Figure 5.8.2: Comparison of $\varepsilon_2^M(h, \{\mathbf{y}_j\}_{j=1}^M)$ and $\varepsilon_\infty^M(h, \{\mathbf{y}_j\}_{j=1}^M)$ of the tensored first-order B-spline (5.8.4) approximated by various orthonormal systems in dimensions $d \in \{1, 2, 4, 7\}$.

transformed Fourier systems are able to achieve the same decay rates as the Chebyshev system, when we use parameterized torus-to-cube transformations ${}_{\square}\psi(\cdot, \eta)$ and pick a large

transformation	Numerical observation ε_2^M	ε_∞^M
(5.7.1) cosine system	$N^{-\frac{3}{2}}$	N^{-1}
(5.7.6) Chebyshev system	$N^{-\frac{3}{2}}$	N^{-1}
(5.2.3) sine transf. Fourier	N^{-1}	$N^{-\frac{1}{2}}$
(5.2.1) log transf. Fourier, $\eta = 2$	N^{-1}	$N^{-\frac{1}{2}}$
(5.2.1) log transf. Fourier, $\eta = 2.5$	$N^{-\frac{3}{2}}$	N^{-1}
(5.2.2) error fct. transf. Fourier, $\eta = 1.75$	$N^{-\frac{3}{2}}$	N^{-1}

Table 5.8.1: The observed decay rates of the discrete approximation errors $\varepsilon_2^M(h, \{\mathbf{y}_j\}_{j=1}^M)$ and $\varepsilon_\infty^M(h, \{\mathbf{y}_j\}_{j=1}^M)$ as given in (5.6.2) when h is the univariate first order B-spline cutout B_1 as defined in (5.8.4).

enough parameter $\eta \in \mathbb{R}_+$. The results are summarized in Table 5.8.1.

It is particularly interesting to observe that the sine transformed Fourier system has the slowest decay rate of all considered orthonormal system, while it yields the best or second best approximation errors in Figure 5.8.2. In total, the obtained error decay rates emphasize that the smoothness properties (5.8.2) only provide worst case lower parameter bounds.

5.8.2 Approximation of a second-order B-spline in dimensions $d \in \{1, 2, 4, 7\}$

We define a shifted, scaled and dilated B-spline of second order as

$$B_2(x) := \begin{cases} -x^2 - x + \frac{1}{2} & \text{for } -\frac{1}{2} \le x < 0, \\ \frac{x^2}{2} - x + \frac{1}{2} & \text{for } 0 \le x \le \frac{1}{2}, \end{cases}$$

and call it B_2-*cutout*, that is depicted in Figure 5.8.3 and was also considered in [PV15, NP21b]. The continuous B_2-cutout is an element of $\mathcal{H}^{\frac{5}{2}-\varepsilon}\left(\left[-\frac{1}{2}, \frac{1}{2}\right]\right)$ for any $\varepsilon > 0$, which is due to the fact that the Fourier coefficients $\hat{h}_k = (B_2, \mathrm{e}^{2\pi \mathrm{i} k(\cdot)})_{L_2([-\frac{1}{2},\frac{1}{2}])}$ decay like $|k|^{-3}$ for $k \to \pm\infty$. Considering a constant measure function $\omega \equiv 1$, so that $\mathcal{H}^\beta\left(\left[-\frac{1}{2}, \frac{1}{2}\right]^d, \omega\right) = \mathcal{H}^\beta\left(\left[-\frac{1}{2}, \frac{1}{2}\right]^d\right)$, the $\|\cdot\|_{\mathcal{H}^\beta\left(\left[-\frac{1}{2},\frac{1}{2}\right]^d\right)}$-norm, given in (5.5.8), of the B_2-cutout is finite if

$$\|B_2\|^2_{\mathcal{H}^\beta\left(\left[-\frac{1}{2},\frac{1}{2}\right]^d\right)} = \sum_{k\in\mathbb{Z}} \mathrm{w_{hc}}(k)^{2\beta} |\hat{h}_k|^2 = \sum_{k\in\mathbb{Z}} \max\{1, |k|\}^{2\beta} \frac{1}{|k|^6} < \infty,$$

which is the case for

$$|k|^{2\beta-6} \le k^{-(1+\varepsilon)} \Leftrightarrow \beta \le \frac{5}{2} - \varepsilon, \quad \varepsilon > 0.$$

An analogue argument shows that we also have $B_2 \in \mathcal{A}^{2-\varepsilon}\left(\left[-\frac{1}{2}, \frac{1}{2}\right]\right)$ for any $\varepsilon > 0$. We consider a constant measure function $\omega \equiv 1$, so that $\mathcal{A}^\beta\left(\left[-\frac{1}{2}, \frac{1}{2}\right]^d, \omega\right) = \mathcal{A}^\beta\left(\left[-\frac{1}{2}, \frac{1}{2}\right]^d\right)$ as defined in (5.5.9), and the $\|\cdot\|_{\mathcal{A}^\beta\left(\left[-\frac{1}{2},\frac{1}{2}\right]^d\right)}$-norm of the B_2-cutout is finite if

$$\|B_2\|_{\mathcal{A}^\beta\left(\left[-\frac{1}{2},\frac{1}{2}\right]^d\right)} = \sum_{k\in\mathbb{Z}} \mathrm{w_{hc}}(k)^{\beta} |\hat{h}_k| = \sum_{k\in\mathbb{Z}} \max\{1, |k|\}^{\beta} \frac{1}{|k|^2} < \infty,$$

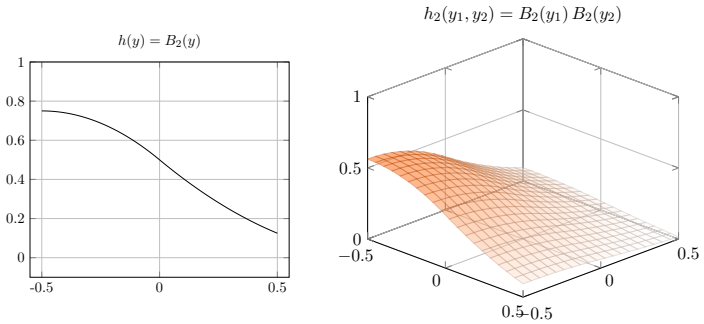

Figure 5.8.3: The univariate B_2-cutout $h_1(x) = B_2(x)$ and the two-dimensional tensored B_2-cutout $h_2(x_1, x_2) = B_2(x_1)\, B_2(x_2)$.

which is the case for

$$|k|^{\beta-3} \leq k^{-(1+\varepsilon)} \Leftrightarrow \beta \leq 2 - \varepsilon, \quad \varepsilon > 0.$$

The tensored B_2-cutout is given by

$$h(\mathbf{x}) = \prod_{j=1}^{d} B_2(x_j) \tag{5.8.5}$$

and will be approximated by the transformed Fourier, cosine and Chebyshev partial sums $S_I^\Lambda h$ given in (5.5.7), (5.7.4) and (5.7.10). Consequentially, we have $h \in \mathcal{H}^{\frac{5}{2}-\varepsilon}\left(\left[-\frac{1}{2}, \frac{1}{2}\right]^d\right)$ and by Theorem 5.4.2 the maximum integer degree of Sobolev smoothness m that can be preserved by any torus-to-cube transformation ${}_\square\psi$ is limited to $m = 2$, where the sine transformation restricts it even more as we saw in (5.8.3).

We discuss the application of the weighted $L_\infty\left(\left[-\frac{1}{2}, \frac{1}{2}\right]^d\right)$-approximation error bound in Theorem 5.5.1 and the weighted $L_2\left(\left[-\frac{1}{2}, \frac{1}{2}\right]^d\right)$-approximation error bound in Theorem 5.5.2 for $d \in \{1, 2, 4\}$ with the given function h in (5.8.5), a constant measure function ω, the logarithmic transformation (5.2.1), the error function transformation (5.2.2), the sine transformation (5.2.3) and the resulting transformed functions f of the form (5.8.1). We compare the results with the approximation of h by the cosine system (5.7.1) and the Chebyshev system (5.7.6). Accordingly, we use the hyperbolic frequency set I_N^d as defined in (3.1.5) for all considered transformed Fourier system, but only consider the non-negative frequencies of a hyperbolic cross $I_N^d \cap \mathbb{N}_0^d$ for the Chebyshev and cosine approximation.

For each transformed system, we generate ten random rank-1 lattices as described in (3.5.5). We repeat the calculations five times and plot the averages of the errors in Figure 5.8.4. In each dimension we consider the parameters $\boldsymbol{\eta} \in \{\mathbf{2}, \mathbf{4}\}$. We use $N \in \{1, \ldots, 140\}$ for $d = 1$, $N \in \{1, \ldots, 80\}$ for $d = 2$, $N \in \{1, \ldots, 50\}$ for $d = 4$ and $N \in \{1, \ldots, 30\}$ for $d = 7$. In dimension $d = 4$ we initialize [Käm19, Algorithm 6] with the parameters $c = 2, n = 4$ and $\delta = \frac{1}{2}$ to efficiently reconstruct the approximated Fourier coefficients $\hat{h}_{\mathbf{k}}^\Lambda$ by means of a transformed multiple rank-1 lattice as in (4.7.8) and to form the approximated Fourier partial sum $S_I^\Lambda h$, whereas in dimensions $d \in \{1, 2\}$ we apply Algorithm 3.4.2 based on a single rank-1 lattice as outlined in (5.6.1).

For both discrete approximation errors $\varepsilon_2^M(h, \{\mathbf{y}_j\}_{j=1}^M)$ and $\varepsilon_\infty^M(h, \{\mathbf{y}_j\}_{j=1}^M)$ as given in (5.6.2) we obtain a similar behavior in each dimension. In dimensions $d = 1$ and $d = 2$ we

observe the proposed behavior in (5.8.2) as the approximation errors are significantly better for $\boldsymbol{\eta} = \mathbf{4}$ than for $\boldsymbol{\eta} = \mathbf{2}$, indicating the increased smoothening effect of both the logarithmic and the error function transformation. In dimension $d = 4$, the errors for $\boldsymbol{\eta} = \mathbf{4}$ turn out to be worse than for $\boldsymbol{\eta} = \mathbf{2}$. On the other hand, the sine transformation yields the worst error decays in each dimension as we expected. The Chebyshev approximation turns out to be a solid candidate to approximate the B-spline cutout (5.8.5).

In this specific setup, we also checked the error behavior for other parameters $\boldsymbol{\eta} \in \{\mathbf{2.1}, \mathbf{2.2}, \dots, \mathbf{3.8}, \mathbf{3.9}, \mathbf{4.1}, \mathbf{4.2}, \dots, \mathbf{4.9}, \mathbf{5}\}$. As it turns out, $\boldsymbol{\eta} = \mathbf{4}$ is the best choice for the logarithmic transformation and for the error function transformation the best choice is $\boldsymbol{\eta} = \mathbf{2.5}$. However, only the error function transformation is able to match the approximation error of the Chebyshev approximation.

But it has to be emphasized that the tensored B_2-cutout (5.8.5) is transformed into a function $f \in \mathcal{H}^0(\mathbb{T}^d)$ of the form (5.4.4) for all considered torus-to-cube transformations ${}_{\square}\psi(\cdot, \boldsymbol{\eta})$ with parameters $\mathbf{1} < \boldsymbol{\eta} \leq \mathbf{3}$, and into a function $f \in \mathcal{H}^1(\mathbb{T}^d)$ for parameters $\boldsymbol{\eta} > \mathbf{3}$ according to (5.8.2) and (5.8.3). Therefore, the weighted L_∞-approximation error provided in Theorem 5.5.1 and the weighted L_2-approximation error bound in Theorem 5.5.2 are of the form

$$\varepsilon_2^M(h, \{\mathbf{y}_j\}_{j=1}^M) \approx \left\| h - S_{I_N^d}^{\Lambda} h \right\|_{L_2\left(\left[-\frac{1}{2}, \frac{1}{2}\right]^d\right)} \lesssim N^{-1} (\log N)^{(d-1)/2} \quad \text{for} \quad \boldsymbol{\eta} > \mathbf{3},$$

and

$$\varepsilon_\infty^M(h, \{\mathbf{y}_j\}_{j=1}^M) \approx \left\| h - S_{I_N^d}^{\Lambda} h \right\|_{L_\infty\left(\left[-\frac{1}{2}, \frac{1}{2}\right]^d, \sqrt{\frac{1}{{}_{\square}\varrho(\cdot, \boldsymbol{\eta})}}\right)} \lesssim N^0 \quad \text{for} \quad \boldsymbol{\eta} > \mathbf{3},$$

which is listed in Table 5.8.2 for $d = 1$, accordingly.

Again, we investigate the error decay rates of $\varepsilon_2^M(h, \{\mathbf{y}_j\}_{j=1}^M)$ and $\varepsilon_\infty^M(h, \{\mathbf{y}_j\}_{j=1}^M)$ for the univariate case $d = 1$ that were numerically observed. In this specific setup, h is still the continuous second-order B-spline cutout given in (5.8.5) that is both in $\mathcal{A}^{2-\varepsilon}\left(\left[-\frac{1}{2}, \frac{1}{2}\right]\right)$ and in $\mathcal{H}^{\frac{5}{2}-\varepsilon}\left(\left[-\frac{1}{2}, \frac{1}{2}\right]\right)$. Hence, theoretically we can achieve at most $\varepsilon_2^M(h, \{\mathbf{y}_j\}_{j=1}^M) \lesssim N^{-\frac{5}{2}+\varepsilon}$ and $\varepsilon_\infty^M(h, \{\mathbf{y}_j\}_{j=1}^M) \lesssim N^{-2+\varepsilon}$ for any $\varepsilon > 0$ when approximating h with respect to any transformed Fourier system. In contrast to the previous case with the B_1 cutout, we only achieve these decay rates numerically with the Chebyshev system and with the transformed Fourier system when considering the logarithmic transformation with $\eta \in \{2.5, 4\}$. Interestingly, the decay rates of the cosine system remain at N^{-1} and $N^{-1.5}$, respectively, even though the approximated function h gained a smoothness order. In comparison, the sine transformed Fourier system loses one and a half orders, whereas the logarithmically transformed Fourier system with $\eta = 2$ loses half an order in both error decay observations, which is slightly improved for $\eta = 4$. In total we observe that some transformed Fourier systems are able to achieve the same decay rates as the Chebyshev system, when we use parameterized torus-to-cube transformations ${}_{\square}\psi(\cdot, \eta)$ and pick a large enough parameter $\eta \in \mathbb{R}_+$. The results are summarized in Table 5.8.2.

5.8.3 Sparse frequency sets

In Figure 4.7.5 we saw that torus-to-$\mathbb{R}^d$ transformations are capable of distorting any given signal so much, that the frequency set of the periodized function changes fundamentally. For torus-to-cube transformations the same effect might occur. Therefore, we again incorporate a dimension incremental construction method [Vol15, PV16] to reconstruct a multivariate

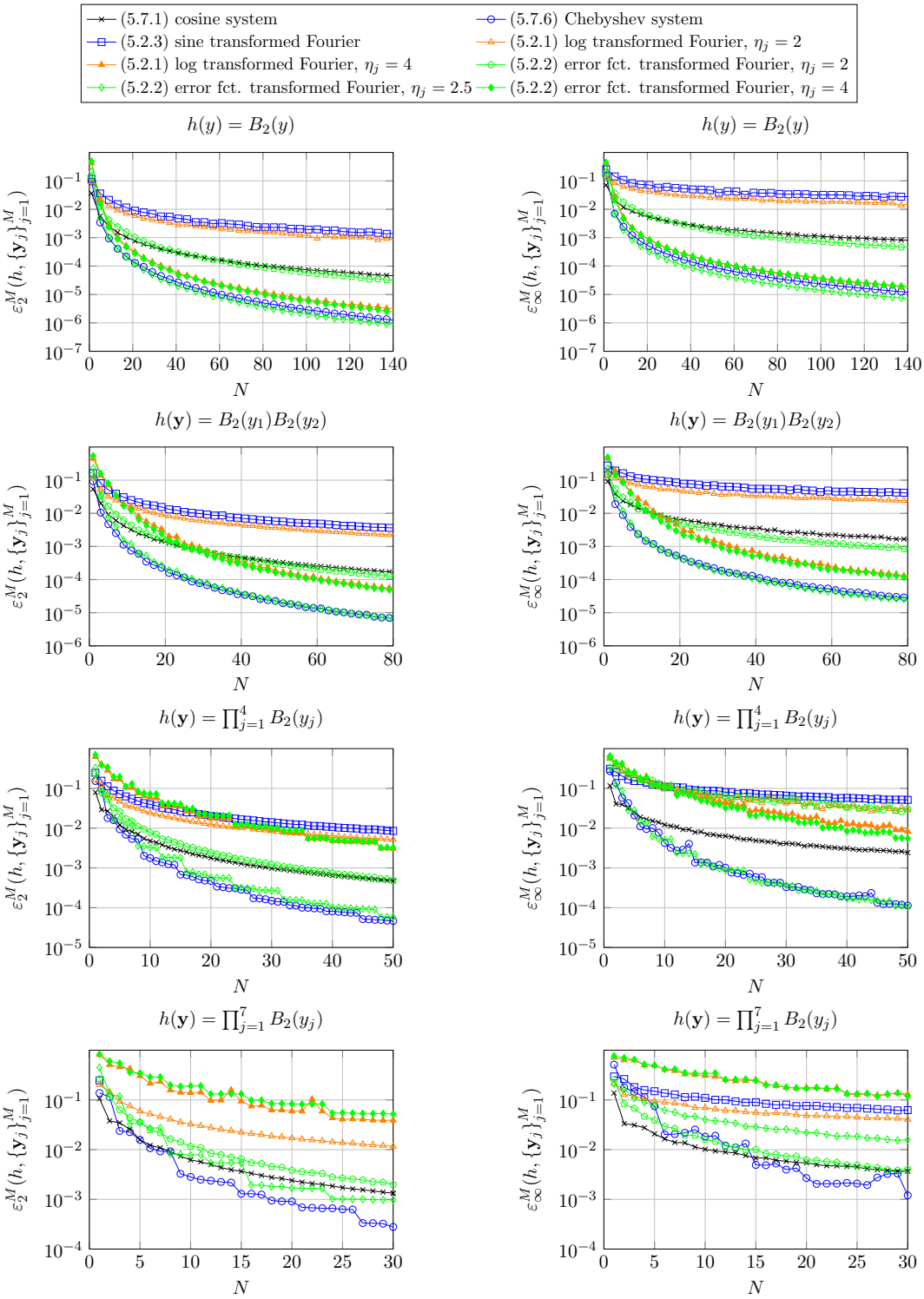

Figure 5.8.4: Comparison of $\varepsilon_2^M(h, \{\mathbf{y}_j\}_{j=1}^M)$ and $\varepsilon_\infty^M(h, \{\mathbf{y}_j\}_{j=1}^M)$ of the tensored second-order B-spline (5.8.5) approximated by various orthonormal systems in dimensions $d \in \{1, 2, 4, 7\}$.

trigonometric polynomial h with an unknown support in a frequency domain $I \subset \mathbb{Z}^d$ by some partial sum $S_I h(\cdot) = \sum_{\mathbf{k} \in I} \hat{h}_{\mathbf{k}} \, \varphi_{\mathbf{k}}(\cdot)$ with some orthonormal system $\{\varphi_{\mathbf{k}}\}_{\mathbf{k} \in I}$. As a reminder,

transformation	upper bound by Thm. 5.5.1 and Thm. 5.5.2 ε_2^M	ε_∞^M	Numerical observation ε_2^M	ε_∞^M
(5.7.1) cosine system			$N^{-1.5}$	N^{-1}
(5.7.6) Chebyshev system			$N^{-2.45}$	N^{-2}
(5.2.3) sine transf. Fourier			N^{-1}	$N^{-0.5}$
(5.2.1) log transf. Fourier, $\eta = 2$			N^{-1}	$N^{-0.5}$
(5.2.1) log transf. Fourier, $\eta = 4$	N^{-1}	N^0	$N^{-2.25}$	$N^{-1.5}$
(5.2.2) error fct. transf. Fourier, $\eta = 2$			$N^{-1.9}$	$N^{-1.4}$
(5.2.2) error fct. transf. Fourier, $\eta = 2.5$			$N^{-2.55}$	N^{-2}
(5.2.2) error fct. transf. Fourier, $\eta = 4$	N^{-1}	N^0	$N^{-2.5}$	N^{-2}

Table 5.8.2: The worst case upper bounds proposed in Theorems 5.5.1 and 5.5.2 in comparison with the observed decay rates of the discrete approximation errors $\varepsilon_2^M(h, \{\mathbf{y}_j\}_{j=1}^M)$ and $\varepsilon_\infty^M(h, \{\mathbf{y}_j\}_{j=1}^M)$ as given in (5.6.2) when h is the univariate second order B-spline cutout B_2 as defined in (5.8.5).

the approach of [PV16, Algorithm 1 and Algorithm 2] determines the $s \in \mathbb{N}$ approximately largest Fourier coefficients $\hat{p}_{\mathbf{k}}$ within a fixed search space $[-N, N]^d \cap \mathbb{Z}^d$ with $N \in \mathbb{N}$ and $s \ll (2N+1)^d$. For transformed reconstructing rank-1 lattices $\Lambda_{\square\psi(\cdot,\boldsymbol{\eta})}(\mathbf{z}, M, I)$ these algorithms are adapted by calculating the relative discretized approximation errors $\varepsilon_2^M(h, \{\mathbf{y}_j\}_{j=1}^M)$ and $\varepsilon_\infty^M(h, \{\mathbf{y}_j\}_{j=1}^M)$ with samples $\left(h(\mathbf{y}_j)\sqrt{\frac{\omega(\mathbf{y}_j,\boldsymbol{\mu})}{\square\varrho(\mathbf{y}_j,\boldsymbol{\eta})}}\right)_{j=0}^{M-1}$ and $\left(\sqrt{\frac{\omega(\mathbf{y}_j,\boldsymbol{\mu})}{\square\varrho(\mathbf{y}_j,\boldsymbol{\eta})}}\, S_I^\Lambda h(\mathbf{y}_j)\right)_{j=0}^{M-1}$ and by using an unknown frequency set $I = J_s^d$ with cardinality $s = |I_N^d|$ that was constructed via a dimensional incremental construction method as outlined above.

For this application we consider the function

$$h(\mathbf{y}) = y_1 + y_2 + y_3^2 + y_4^2 + y_5 y_6 y_7, \tag{5.8.6}$$

which indicates some structure of the underlying frequency set. We know, that the frequency set of the function $h_1(y_1, y_2) = y_1 + y_2$ is a scaled ℓ_1^2-ball, the frequency set of the function $h_2(y_3, y_4) = y_3^2 + y_4^2$ is a scaled ℓ_2^2-ball and the frequency set of the function $h_3(y_5, y_6, y_7) = y_5 y_6 y_7$ is a hyperbolic cross I_N^3. However, we will not use this information and let the dimension incremental construction method [Vol15, PV16] determine a suitable frequency set J_s^7. We consider the error function Fourier system (5.2.2) with parameters $\boldsymbol{\eta} \in \{\mathbf{2}, \mathbf{3}\}$ for both the hyperbolic cross I_N^7 and the constructed sparse frequency sets J_s^7 with $s = |I_N^7|$ for $N \in \{1, \ldots, 15\}$. The resulting ℓ_2-errors $\varepsilon_2^M(h, \{\mathbf{y}_j\}_{j=1}^M)$ in Figure 5.8.5 show, that we obtain a slightly better approximation error for $\boldsymbol{\eta} = \mathbf{2}$, whereas the error improves significantly for $\boldsymbol{\eta} = \mathbf{3}$ when using the sparse frequency set J_s^7.

5.9 Summary of the numerics on the cube

We compared the approximation results of the half-periodic cosine system (5.7.1) and Chebyshev system (5.7.6) with the transformed Fourier systems given in (5.3.2) and (5.5.2), that we derived within a specific periodization strategy to transform functions in the function space $L_2(\left[-\frac{1}{2}, \frac{1}{2}\right]^d, \omega(\cdot, \boldsymbol{\mu})) \cap \mathcal{C}_{\text{mix}}^m\left(\left[-\frac{1}{2}, \frac{1}{2}\right]^d\right)$ into smooth functions in $\mathcal{H}^m(\mathbb{T}^d)$ via a torus-to-cube transformation $_\square\psi : \left[-\frac{1}{2}, \frac{1}{2}\right]^d \to \left[-\frac{1}{2}, \frac{1}{2}\right]^d$ as given in (5.1.1). Similarly to the numerics on $\mathbb{R}^d$,

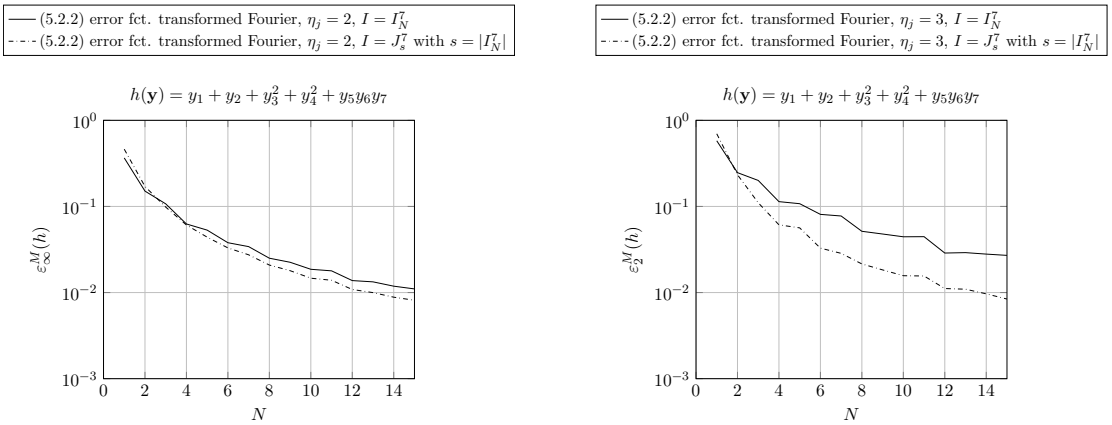

Figure 5.8.5: Comparison of $\varepsilon_2^M(h, \{\mathbf{y}_j\}_{j=1}^M)$ of the function (5.8.6) approximated by the error function Fourier systems with $\boldsymbol{\eta} = \mathbf{2}$ and $\boldsymbol{\eta} = \mathbf{3}$ for the hyperbolic cross set I_N^7 and the sparse frequency set J_s^7.

a main objective was to define variable torus-to-cube transformations ${}_{\square}\psi(\cdot, \boldsymbol{\eta}), \boldsymbol{\eta} \in \mathbb{R}_+^d$, which leads to parameterized transformed Fourier systems, and to determine the parameter values for which we obtain the best ℓ_2- and ℓ_∞-approximation results. A first experiment in up to dimension $d = 7$ with the first order B-spline cutout B_1 in (5.8.4) showed, that the error function transformation (5.2.2) is capable to induce a transformed Fourier system, which resulted in a significantly better ℓ_2-approximation error $\varepsilon_2^M(\cdot, \{\mathbf{y}_j\}_{j=1}^M)$ as defined in (5.6.2) than the Chebyshev system, as shown in Figure 5.8.2. At the same time, the ℓ_∞-approximation error $\varepsilon_\infty^M(\cdot, \{\mathbf{y}_j\}_{j=1}^M)$ as given in (5.6.2) of the Chebyshev system remained the best of all considered. A second experiment in up to dimension $d = 7$ with the smoother second order B-spline cutout B_2 in (5.8.5) showed that in lower dimensions, the transformed Fourier system induced by the error function transformation is capable to match the approximation errors of the Chebyshev system. In higher dimensions $d \geq 4$, the Chebyshev system yielded significantly better approximation results than any other considered orthonormal system. In a third test in dimension $d = 7$ with the polynomial (5.8.6), we again adapted a dimension incremental construction method to determine sparse frequency sets and indeed obtained significant improvements for the ℓ_2-approximation with the error function transformation, as showcased in Figure (5.8.5).

We observed, that even though the L_∞-conditions (5.4.5) on ${}_{\square}\psi(\cdot, \boldsymbol{\eta})$ and $\omega(\cdot, \boldsymbol{\mu})$ in Theorem 5.4.2 are rather easy to check, the resulting parameter bounds for $\boldsymbol{\eta}$ and $\boldsymbol{\mu}$ are worst case bounds and are only more or less optimal, which has to be checked individually in any specific example. On a similar note, the upper approximation error bounds of Theorems 5.5.1 and 5.5.2 are worst case upper bounds, too, so that the constants occurring in the error estimates may have some bad growth behavior for certain combinations of ${}_{\square}\psi(\cdot, \boldsymbol{\eta})$ and $\omega(\cdot, \boldsymbol{\mu})$, potentially causing some problematic decay behavior.

Even though we overall obtained that it is possible to create orthonormal systems that yield better approximation results than the Chebyshev system, the structure and growth behavior of the constants in the error estimates has to be studied more thoroughly. Also, the measure function ω needs more attention. We highlighted in (5.7.12) that the induced transformed Fourier systems are a generalization of the well-known orthonormal systems such as the Chebyshev system, but there could be other relevant orthonormal systems in which the density ${}_{\square}\varrho$ and measure function ω are not the same. Afterwards. extending the influence

of the measure function on the derivatives of h might be interesting, too.

Chapter 6

Conclusion

In this work, we consider the approximation of functions $f : \Omega \to \mathbb{C}$ define on the domains $\Omega \in \{\mathbb{T}^d, \mathbb{R}^d, \left[-\frac{1}{2}, \frac{1}{2}\right]^d\}$ by trigonometric and transformed trigonometric functions, respectively. We investigate which of the many results known from the approximation theory on the torus $\mathbb{T}^d$ can be transfered to the domains $\{\mathbb{R}^d, \left[-\frac{1}{2}, \frac{1}{2}\right]^d\}$.

We establishe invertible torus-to-$\mathbb{R}^d$ transformations $\psi(\cdot, \boldsymbol{\eta}) : \left(-\frac{1}{2}, \frac{1}{2}\right)^d \to \mathbb{R}^d, \boldsymbol{\eta} \in \mathbb{R}^d_+$ and prove conditions for which we obtaine a periodization mapping of the form

$$L_2(\mathbb{R}^d, \omega(\cdot, \boldsymbol{\mu})) \cap H^m_{\text{mix}}(\mathbb{R}^d) \ni h \mapsto f \in \mathcal{H}^m(\mathbb{T}^d)$$

with $f := h(\psi(\cdot, \boldsymbol{\eta})) \sqrt{\omega(\psi(\cdot, \boldsymbol{\eta}), \boldsymbol{\mu}) \prod_{j=1}^d \psi_j'(\cdot, \eta_j)}$, $\boldsymbol{\mu} \in \mathbb{R}^d_+$, so that $\|h\|_{L_2(\mathbb{R}^d, \omega)} = \|f\|_{L_2(\mathbb{T}^d)}$. We evaluate these periodization conditions for two specific mappings $\psi(\cdot, \boldsymbol{\eta})$ and calculate the parameter values $\boldsymbol{\eta}, \boldsymbol{\mu}$ for which the Sobolev smoothness m of the function h was preserve under the transformation $\psi(\cdot, \boldsymbol{\eta})$. By means of the inverse torus-to-$\mathbb{R}^d$ transformations $\psi^{-1}(\cdot, \boldsymbol{\eta})$ we transfer crucial properties and algorithms for the approximation of periodic functions on the torus $\mathbb{T}^d$ to the considered function class on $\mathbb{R}^d$. In particular, we prove weighted worst case upper approximation error bounds and described fast algorithms for the evaluation and reconstruction of transformed trigonometric functions on $\mathbb{R}^d$ based on transformed rank-1 lattices $\Lambda_{\psi(\cdot, \boldsymbol{\eta})}(\mathbf{z}, M)$. In numerical tests in up to dimension $d = 8$ we calculate discrete ℓ_2- and ℓ_∞-approximation errors for torus-to-$\mathbb{R}^d$ transformations of algebraic and exponential type. Both setups confirm the theoretical proposition that a sufficient increase of the parameters $\boldsymbol{\mu}, \boldsymbol{\eta}$ leads to more Sobolev smoothness being preserve by the particular torus-to-$\mathbb{R}^d$ transformation and to a faster approximation error decay. However, in higher dimensions $d \geq 4$ we face the problem that the considered periodiziation strategy distort the originally considered function h too much, resulting in the constants appearing in the error estimates to grow too fast. So, we switch to an adapted dimension incremental construction method to obtain an initially unknown optimal frequency set $I \subset \mathbb{Z}^d$ containing the largest frequencies of the periodized function. Afterwards, we apply an adapted sparse FFT algorithm for which the numerical results improve and again showcase the previously expected behavior of faster error decays for larger parameters.

Based on the insight we got from torus-to-$\mathbb{R}^d$ transformations $\psi(\cdot, \boldsymbol{\eta})$, we extend the core ideas of this periodization strategy to non-periodic signals on the cube $\left[-\frac{1}{2}, \frac{1}{2}\right]^d$ and proceeded in a similar fashion. We introduce invertible torus-to-cube transformations ${}_{\square}\psi(\cdot, \boldsymbol{\eta}) : \left[-\frac{1}{2}, \frac{1}{2}\right]^d \to \left[-\frac{1}{2}, \frac{1}{2}\right]^d$ and prove conditions for which we obtain a periodization mapping of

the form

$$L_2\left(\left[-\frac{1}{2},\frac{1}{2}\right]^d,\omega(\cdot,\boldsymbol{\mu})\right)\cap\mathcal{C}^m_{\mathrm{mix}}\left(\left[-\frac{1}{2},\frac{1}{2}\right]^d\right)\ni h\mapsto f\in\mathcal{H}^m(\mathbb{T}^d)$$

with $f := h({}_{\square}\psi(\cdot,\boldsymbol{\eta}))\sqrt{\omega({}_{\square}\psi(\cdot,\boldsymbol{\eta}),\boldsymbol{\mu})\prod_{j=1}^d {}_{\square}\psi'_j(\cdot,\eta_j)}$, so that $\|h\|_{L_2\left(\left[-\frac{1}{2},\frac{1}{2}\right]^d,\omega\right)} = \|f\|_{L_2(\mathbb{T}^d)}$. We evaluate these periodization conditions for two specific mappings ${}_{\square}\psi(\cdot,\boldsymbol{\eta})$ and calculate the parameter values $\boldsymbol{\eta},\boldsymbol{\mu}\in\mathbb{R}^d_+$ for which the Sobolev smoothness m of the function h are preserved by the transformation ${}_{\square}\psi(\cdot,\boldsymbol{\eta})$. By means of the inverse torus-to-cube transformations ${}_{\square}\psi^{-1}(\cdot,\boldsymbol{\eta})$ we adapt certain properties and fast algorithms for the approximation of periodic functions on the torus $\mathbb{T}^d$ to the considered function class on the cube $\left[-\frac{1}{2},\frac{1}{2}\right]^d$. In particular, we prove weighted worst case upper approximation error bounds and describe fast algorithms for the evaluation and reconstruction of trigonometric functions on $\left[-\frac{1}{2},\frac{1}{2}\right]^d$ based on transformed rank-1 lattices $\Lambda_{{}_{\square}\psi(\cdot,\boldsymbol{\eta})}(\mathbf{z},M)$. In multiple numerical tests in up to dimension $d=7$ we calculate discrete ℓ_2- and ℓ_∞-approximation errors for three torus-to-cube transformed Fourier systems in comparison with the classical half-periodic cosine system and the Chebyshev polynomials. As it turns out, for specific parameter choices the error function transformed Fourier system was able to match the approximation quality of the Chebyshev system, and even yielding better approximation results in some cases.

In both frameworks we observe that the parameter ranges for $\boldsymbol{\eta},\boldsymbol{\mu}\in\mathbb{R}^d_+$ are comparably coarse for our particular examples. However, the strength of our periodization approach lies in its generality as it was valid for the whole considered function spaces. Furthermore, a huge advantage is the availability of fast algorithms for the calculation of the discretized approximation errors.

Bibliography

[Adc10] B. Adcock. Modified Fourier expansions: theory, construction and applications (doctoral thesis), 2010. (Cited on page 73.)

[Adc11] B. Adcock. Convergence acceleration of modified Fourier series in one or more dimensions. *Math. Comput.*, 80(273):225–261, 2011. (Cited on page 73.)

[AH20] B. Adcock and D. Huybrechs. Frames and numerical approximation II: Generalized sampling. *J. Fourier Anal. Appl.*, 26(6):1–34, 2020. (Cited on page 7.)

[AIN12] B. Adcock, A. Iserles, and S. P. Nørsett. From high oscillation to rapid approximation II: Expansions in Birkhoff series. *IMA J. Numer. Anal.*, 32(1):105–140, 2012. (Cited on page 73.)

[AP16] B. Adcock and R. B. Platte. A mapped polynomial method for high-accuracy approximations on arbitrary grids. *SIAM J. Numer. Anal.*, 54(4):2256–2281, 2016. (Cited on page 58.)

[BCD+06] L. Bos, M. Caliari, S. De Marchi, M. Vianello, and Y. Xu. Bivariate Lagrange interpolation at the Padua points: The generating curve approach. *J. Approx. Theory*, 143(1):15–25, 2006. Special Issue on Foundations of Computational Mathematics. (Cited on page 75.)

[BDuSU16] G. Byrenheid, D. Dũng, W. Sickel, and T. Ullrich. Sampling on energy-norm based sparse grids for the optimal recovery of Sobolev type functions in H^γ. *J. Approx. Theory*, 207:207–231, 2016. (Cited on page 6.)

[Bel61] R. E. Bellman. *Adaptive control processes — A guided tour*. Princeton University Press, Princeton, New Jersey, U.S.A., 1961. (Cited on page 6.)

[BH92] M. Beckers and A. Haegemans. *Transformation of Integrands for Lattice Rules*, pages 329–340. Springer Netherlands, Dordrecht, 1992. (Cited on page 7.)

[BKP20] M. Bochmann, L. Kämmerer, and D. Potts. A sparse FFT approach for ODE with random coefficients. *Adv. Comput. Math.*, 46(5):1–21, 2020. (Cited on page 23.)

[BKUV17] G. Byrenheid, L. Kämmerer, T. Ullrich, and T. Volkmer. Tight error bounds for rank-1 lattice sampling in spaces of hybrid mixed smoothness. *Numer. Math.*, 136:993–1034, 2017. (Cited on pages 6 and 21.)

[Boy00] J. P. Boyd. *Chebyshev and Fourier Spectral Methods*. Dover Press, New York, NY, USA, second edition, 2000. (Cited on pages 7 and 29.)

[CIK21] B. Choi, M. A. Iwen, and F. Krahmer. Sparse Harmonic Transforms: A New Class of Sublinear-Time Algorithms for Learning Functions of Many Variables. *Found. Comput. Math.*, 21(2):275–329, 2021. (Cited on page 6.)

[CKN10] R. Cools, F. Y. Kuo, and D. Nuyens. Constructing lattice rules based on weighted degree of exactness and worst case error. *Computing*, 87:63–89, 2010. (Cited on pages 6 and 19.)

[CKNS16] R. Cools, F. Y. Kuo, D. Nuyens, and G. Suryanarayana. Tent-transformed lattice rules for integration and approximation of multivariate non-periodic functions. *J. Complexity*, 36:166–181, 2016. (Cited on pages 7 and 73.)

[CN04] R. Cools and D. Nuyens. Fast algorithms for component-by-component construction of rank-1 lattice rules in shift-invariant reproducing kernel Hilbert spaces. *Math. Comput.*, 75:903–920, 2004. (Cited on page 6.)

[CT65] J. W. Cooley and J. W. Tukey. An algorithm for machine calculation of complex Fourier series. *Math. Comput.*, 19:297–301, 1965. (Cited on page 6.)

[CZ07] F. Cucker and D. Zhou. *Learning Theory: An Approximation Theory Viewpoint.* Cambridge monographs on applied and computational mathematics. Cambridge University Press, 2007. (Cited on page 25.)

[DE17] P. Dencker and W. Erb. Multivariate polynomial interpolation on Lissajous-Chebyshev nodes. *J. Approx. Theory*, 219:15–45, 2017. (Cited on page 75.)

[DGSY17] J. Dick, T. Goda, K. Suzuki, and T. Yoshiki. Construction of interlaced polynomial lattice rules for infinitely differentiable functions. *Numer. Math.*, 137(2):257–288, 2017. (Cited on page 6.)

[DILP18] J. Dick, C. Irrgeher, G. Leobacher, and F. Pillichshammer. On the optimal order of integration in hermite spaces with finite smoothness. *SIAM J. Numer. Anal.*, 56(2):684–707, 2018. (Cited on page 7.)

[DKS13] J. Dick, F. Y. Kuo, and I. H. Sloan. High-dimensional integration: The quasi-Monte Carlo way. *Acta Numer.*, 22:133–288, 2013. (Cited on page 6.)

[DNP14] J. Dick, D. Nuyens, and F. Pillichshammer. Lattice rules for nonperiodic smooth integrands. *Numer. Math.*, 126:259–291, 2014. (Cited on pages 7 and 73.)

[DP21] J. Dick and F. Pillichshammer. Weighted integration over a hyperrectangle based on digital nets and sequences. *J. Comput. Appl. Math.*, 393:113509, 2021. (Cited on page 7.)

[DTU18] D. Dũng, V. N. Temlyakov, and T. Ullrich. *Hyperbolic Cross Approximation.* Advanced Courses in Mathematics – CRM Barcelona. Birkhäuser, Cham, 2018. (Cited on pages 6 and 24.)

[GD15] T. Goda and J. Dick. Construction of interlaced scrambled polynomial lattice rules of arbitrary high order. *Found. Comput. Math.*, 15(5):1245–1278, 2015. (Cited on page 6.)

[GH14] M. Griebel and J. Hamaekers. Fast discrete Fourier transform on generalized sparse grids. In J. Garcke and D. Pflüger, editors, *Sparse Grids and Applications - Munich 2012*, volume 97 of *Lect. Notes Comput. Sci. Eng.*, pages 75–107. Springer International Publishing, 2014. (Cited on page 6.)

[GH19] M. Griebel and J. Hamaekers. Generalized sparse grid interpolation based on the fast discrete Fourier transform. 2019. Submitted to Proceedings of SGA 2018. Available as INS Preprint No. 1902. (Cited on page 6.)

[GKL13] R. Golovanov, N. Kalitkin, and K. Lutskiy. Odd extension for Fourier approximation of nonperiodic functions. *Math. Models Comput. Simul.*, 5, 2013. (Cited on page 7.)

[GSY19] T. Goda, K. Suzuki, and T. Yoshiki. Lattice rules in non-periodic subspaces of Sobolev spaces. *Numer. Math.*, 141(2):399–427, 2019. (Cited on page 7.)

[HIN11] D. Huybrechs, A. Iserles, and S. Nørsett. From high oscillation to rapid approximation IV: Accelerating convergence. *IMA J. Numer. Anal.*, 31(2):442–468, 2011. (Cited on page 73.)

[IKLP15] C. Irrgeher, P. Kritzer, G. Leobacher, and F. Pillichshammer. Integration in Hermite spaces of analytic functions. *J. Complexity*, 31(3):380–404, 2015. (Cited on page 7.)

[IKP18] C. Irrgeher, P. Kritzer, and F. Pillichshammer. Integration and approximation in cosine spaces of smooth functions. *Math. Comput. Simulation*, 143:35–45, 2018. (Cited on pages 7 and 73.)

[IN08] A. Iserles and S. Nørsett. From high oscillation to rapid approximation I: Modified Fourier expansions. *IMA J. Numer. Anal.*, 28:862–887, 2008. (Cited on page 73.)

[IN09] A. Iserles and S. P. Nørsett. From high oscillation to rapid approximation III: Multivariate expansions. *IMA J. Numer. Anal.*, 29(4):882–916, 2009. (Cited on page 73.)

[Käm14a] L. Kämmerer. Reconstructing multivariate trigonometric polynomials from samples along rank-1 lattices. In G. E. Fasshauer and L. L. Schumaker, editors, *Approximation Theory XIV: San Antonio 2013*, pages 255–271. Springer International Publishing, 2014. (Cited on pages 6 and 20.)

[Käm14b] L. Kämmerer. *High Dimensional Fast Fourier Transform Based on Rank-1 Lattice Sampling*. Dissertation. Universitätsverlag Chemnitz, 2014. (Cited on pages 6, 19, 21, 42, and 70.)

[Käm18] L. Kämmerer. Multiple rank-1 lattices as sampling schemes for multivariate trigonometric polynomials. *J. Fourier Anal. Appl.*, 24:17–44, 2018. (Cited on pages 23 and 49.)

[Käm19] L. Kämmerer. Constructing spatial discretizations for sparse multivariate trigonometric polynomials that allow for a fast discrete Fourier transform. *Appl. Comput. Harmon. Anal.*, 47:702–729, 2019. (Cited on pages 6, 23, 49, 82, and 85.)

[KKV20] L. Kämmerer, F. Krahmer, and T. Volkmer. A sample efficient sparse FFT for arbitrary frequency candidate sets in high dimensions, 2020. arXiv:2006.13053 [math.NA]. (Cited on pages 6 and 23.)

[KMNN21] F. Kuo, G. Migliorati, F. Nobile, and D. Nuyens. Function integration, reconstruction and approximation using rank-1 lattices. *Math. Comp.*, 90(330):1861–1897, 2021. (Cited on pages 6, 7, 72, 74, and 76.)

[KNP18] P. Kritzer, H. Niederreiter, and F. Pillichshammer. Ian Sloan and Lattice Rules. In *Contemporary Computational Mathematics-A Celebration of the 80th Birthday of Ian Sloan*, pages 741–769. Springer, 2018. (Cited on page 6.)

[KPPW20] P. Kritzer, F. Pillichshammer, L. Plaskota, and G. W. Wasilkowski. On efficient weighted integration via a change of variables. *Numer. Math.*, 146(3):545–570, 2020. (Cited on pages 7 and 29.)

[KPV15] L. Kämmerer, D. Potts, and T. Volkmer. Approximation of multivariate periodic functions by trigonometric polynomials based on rank-1 lattice sampling. *J. Complexity*, 31:543–576, 2015. (Cited on pages 6, 19, 20, and 21.)

[KPV20] L. Kämmerer, D. Potts, and T. Volkmer. High-dimensional sparse FFT based on sampling along multiple rank-1 lattices. *Appl. Comput. Harmon. Anal.*, 51:225–257, 2020. (Cited on pages 6 and 23.)

[KSU15] T. Kühn, W. Sickel, and T. Ullrich. Approximation of mixed order Sobolev functions on the d-torus: asymptotics, preasymptotics, and d-dependence. *Constr. Approx.*, 42(3):353–398, 2015. (Cited on page 19.)

[KSW07] F. Y. Kuo, I. H. Sloan, and H. Woźniakowski. Periodization strategy may fail in high dimensions. *Numer. Algorithms*, 46(4):369–391, 2007. (Cited on page 7.)

[KU20] D. Krieg and M. Ullrich. Function values are enough for L_2-approximation. *Found. Comput. Math.*, pages 1–11, 2020. (Cited on page 6.)

[KUV19] L. Kämmerer, T. Ullrich, and T. Volkmer. Worst case recovery guarantees for least squares approximation using random samples. *ArXiv e-prints*, 2019. arXiv:1911.10111. (Cited on page 6.)

[KWW06] F. Y. Kuo, G. W. Wasilkowski, and B. J. Waterhouse. Randomly shifted lattice rules for unbounded integrands. *J. Complexity*, 22(5):630–651, 2006. (Cited on page 7.)

[Nie78] H. Niederreiter. Quasi-Monte Carlo methods and pseudo-random numbers. *B. Am. Math. Soc.*, 84:957–1041, 1978. (Cited on page 6.)

[NN17] D. T. Nguyen and D. Nuyens. Multivariate integration over $\mathbb{R}^s$ with exponential rate of convergence. *J. Comput. Appl. Math.*, 315:327–342, 2017. (Cited on page 7.)

[NP20] R. Nasdala and D. Potts. Transformed rank-1 lattices for high-dimensional approximation. *Electron. Trans. Numer. Anal.*, 53:239–282, 2020. (Cited on pages 10, 27, 28, 29, 33, 36, 40, 41, and 42.)

[NP21a] R. Nasdala and D. Potts. Efficient multivariate approximation on the cube. *Numer. Math.*, 147(2):393–429, 2021. (Cited on pages 10, 55, 57, 63, 64, 67, 69, 70, 78, and 80.)

[NP21b] R. Nasdala and D. Potts. A note on transformed Fourier systems for the approximation of non-periodic signals. *arXiv preprint arXiv:2102.00717*, 2021. (Cited on pages 10, 55, 72, and 84.)

[NUU17] V. K. Nguyen, M. Ullrich, and T. Ullrich. Change of variable in spaces of mixed smoothness and numerical integration of multivariate functions on the unit cube. *Constr. Approx.*, 46(1):69–108, 2017. (Cited on page 7.)

[NW12] E. Novak and H. Woźniakowski. *Tractability of Multivariate Problems Volume III: Standard Information for Operators.* Eur. Math. Society, EMS Tracts in Mathematics Vol 18, 2012. (Cited on page 6.)

[PPST18] G. Plonka, D. Potts, G. Steidl, and M. Tasche. *Numerical Fourier Analysis.* Applied and Numerical Harmonic Analysis. Birkhäuser, 2018. (Cited on page 77.)

[PV15] D. Potts and T. Volkmer. Fast and exact reconstruction of arbitrary multivariate algebraic polynomials in Chebyshev form. In *11th international conference on Sampling Theory and Applications (SampTA 2015)*, pages 392–396, 2015. (Cited on pages 7, 72, 76, 80, and 84.)

[PV16] D. Potts and T. Volkmer. Sparse high-dimensional FFT based on rank-1 lattice sampling. *Appl. Comput. Harmon. Anal.*, 41:713–748, 2016. (Cited on pages 6, 18, 23, 50, 51, 86, and 88.)

[Sid93] A. Sidi. A new variable transformation for numerical integration. In *Numerical integration IV*, pages 359–373. Springer, 1993. (Cited on page 58.)

[SJ94] I. H. Sloan and S. Joe. *Lattice methods for multiple integration.* Oxford Science Publications. The Clarendon Press Oxford University Press, New York, 1994. (Cited on page 6.)

[SK87] I. H. Sloan and P. J. Kachoyan. Lattice methods for multiple integration: Theory, error analysis and examples. *SIAM J. Numer. Anal.*, 24:116–128, 1987. (Cited on pages 19 and 20.)

[SNC16] G. Suryanarayana, D. Nuyens, and R. Cools. Reconstruction and collocation of a class of non-periodic functions by sampling along tent-transformed rank-1 lattices. *J. Fourier Anal. Appl.*, 22:187–214, 2016. (Cited on pages 72, 73, 74, and 76.)

[SSO83] W. E. Smith, I. H. Sloan, and A. H. Opie. Product integration over infinite intervals. I. Rules based on the zeros of Hermite polynomials. *Math. Comp.*, 40(162):519–535, 1983. (Cited on page 7.)

[ST87] H.-J. Schmeisser and H. Triebel. *Topics in Fourier analysis and function spaces*, volume 42 of *Mathematik und ihre Anwendungen in Physik und Technik*. Akademische Verlagsgesellschaft Geest & Portig K.-G., Leipzig, 1987. (Cited on pages 14 and 15.)

[Ste93] F. Stenger. *Numerical Methods Based on Sinc and Analytic Functions*, volume 20 of *Springer Series in Computational Mathematics*. Springer-Verlag New York, 1993. (Cited on page 29.)

[STW11] J. Shen, T. Tang, and L.-L. Wang. *Spectral Methods*, volume 41 of *Springer Ser. Comput. Math.* Springer-Verlag Berlin Heidelberg, Berlin, 2011. (Cited on page 29.)

[Suz20] Y. Suzuki. Applications and analysis of lattice points: Time-stepping and integration over $\mathbb{R}^d$, 2020. PhD thesis, KU Leuven. (Cited on page 53.)

[Tem86] V. N. Temlyakov. Reconstruction of periodic functions of several variables from the values at the nodes of number-theoretic nets. *Anal. Math.*, 12:287–305, 1986. In Russian. (Cited on pages 6 and 21.)

[Tem93] V. N. Temlyakov. *Approximation of periodic functions*. Computational Mathematics and Analysis Series. Nova Science Publishers Inc., Commack, NY, 1993. (Cited on page 6.)

[Ull07] T. Ullrich. Smolyak's algorithm, sparse grid approximation and periodic function spaces with dominating mixed smoothness. Dissertation, Friedrich-Schiller-Universität Jena, 2007. (Cited on page 15.)

[Vol15] T. Volkmer. sparseFFTr1l, MATLAB® toolbox for computing the sparse fast Fourier transform based on reconstructing rank-1 lattices in a dimension incremental way. `http://www.tu-chemnitz.de/~tovo/software`, 2015. (Cited on pages 6, 18, 23, 50, 51, 86, and 88.)

[Vol17] T. Volkmer. *Multivariate Approximation and High-Dimensional Sparse FFT Based on Rank-1 Lattice Sampling*. Dissertation. Universitätsverlag Chemnitz, 2017. (Cited on pages 6 and 21.)

[Vyb05] J. Vybiral. Function spaces with dominating mixed smoothness. Dissertation, Friedrich-Schiller-Universität Jena, 2005. (Cited on page 15.)

[Wei12] F. Weisz. Summability of multi-dimensional trigonometric Fourier series. *Surv. Approx. Theory*, 7:1–179, 2012. (Cited on page 18.)